

https://dspace.org/

Corrosion characteristics of steels and metallic alloys used as construction materials in plants exposed to fluorine containing acids: Corrosion characteristics of metallic alloys and steels used as construction materials in plants exposed to fluorine containing acids

Van der Merwe, Ryno

2018

https://hdl.handle.net/10539/26652

Van der Merwe, Ryno (2018) Corrosion characteristics of steels and metallic alloys used as construction materials in plants exposed to fluorine containing acids, University of the Witwatersrand, Johannesburg, <http://hdl.handle.net/10539/26652>

Downloaded from a DSpace repository. https://dspace.org/

CORROSION CHARACTERISTICS OF STEELS AND METALLIC ALLOYS USED AS CONSTRUCTION MATERIALS IN PLANTS EXPOSED TO FLUORINE CONTAINING ACIDS

Ryno van der Merwe

A dissertation submitted to the Faculty of Engineering and the Built Environment, University of the Witwatersrand, Johannesburg, in fulfilment of the requirement for the degree of Master of Science in Engineering

Johannesburg, August 2018

DECLARATION BY CANDIDATE

I, Ryno van der Merwe declare that the dissertation submitted to the degree of Master in Science at the University of the Witwatersrand, Johannesburg is my own work except where otherwise acknowledged. It is being submitted to the degree of Master of Science and has not been submitted previously at this, or any other institution of higher education.

…… ……

SIGNATURE DATE

DEDICATION

The glory belongs to God

This study is dedicated to my wife, Ruzanna and our beloved Appleseed.

ACKNOWLEDGEMENTS

I would like to express my sincere thanks to the following people for their great help and contributions towards this study:

- My supervisor, Professor Lesley Cornish for her perseverance and dedication. She set the highest standards and maintained it throughout. She is an inspiration and I am blessed to have worked with her.
- My Co-supervisor, Dr Josias van der Merwe for his calm confidence and reliability.
- Dr Snyders for his mentoring, endless support and determination to uphold the commitments made and seeing them through to the end.
- The School of Chemical and Metallurgical Engineering at Wits.
- Financial support from the DST-NRF Centre of Excellence in Strong Materials (CoE-SM) at the University of the Witwatersrand (Wits),which is funded by the Department of Science and Technology (DST) and the National Research Foundation (NRF).
- The South African Nuclear Energy Corporation Ltd. (Necsa) for time allowed for completing this study, as well as the Nuclear Materials (NM) and the Organic Fluorine Chemistry (OFC) sections within the Applied Chemistry (AC) department, in the Research and Development Division at Necsa, for the use of their facilities.
- Pelchem SOC Ltd. and specifically Mr E Valkenburgh for initiating the study, providing access to the plant and decommissioned tanks and for supplying the hydrofluoric acid and Teflon bottles that became essential to the project.
- The late Mr C Koch for his metallurgical expertise and supplying the steel and nickel alloy sheets from which the coupons were cut and which were so crucial to this project.
- Pelindaba Analytical Labs (PAL) for analytical support.
- The Advanced Materials Division at Mintek for their expertise and use of their facilities.
- Fellow postgraduate students and staff at Necsa, particularly Dr S Lötter, Dr H Besset, Mr B van der Walt and Mr J Gama.
- Mrs K Premlall at the Tshwane University of Technology for sharing her expertise on corrosion testing with me.
- My mother, Mrs K Nieman, for her encouragement and believing in me.
- My late grandmother, the late Mrs L Swanepoel for her love and guidance.

ABSTRACT

The two hydrofluoric acid (HF) storage tanks used for holding 70% technical grade HF product at the HF plant at Necsa started leaking in March 2012. An evaluation of the failure was conducted in the form of a corrosion failure analysis. It was confirmed that a higher than usual nitric acid (HNO_3) content in the technical grade HF stream changed the corrosion mechanisms typically experienced within the HF storage vessels, which then caused the tanks to fail.

Immersion type corrosion experiments were done to safely simulate the corrosive environment experienced by the mild steel, stainless steel and nickel alloys used on site, and to predict the change in corrosion rates and characteristics associated with the HNO_3 contamination in the HF production plant circuit. Since the corrosion resistance of mild steel in HF is heavily dependent on the thickness of the protective scale on the steel, a series of planned interval corrosion tests (PICTs) was done to reproduce and then examine the oxide-fluoride barrier on mild steel coupons in pure 70% HF prior to corrosion tests. These shorter PICTs were also done on the stainless steel and nickel alloys and showed that the pre-passivation step had a surface cleaning effect when exposed for only 24 h.

Eleven day corrosion tests were conducted to establish the effect of HNO_3 concentration and temperature on mild steel corrosion in 70% HF, and to determine the change in corrosion rates and mechanisms associated with HNO_3 contamination (0.1-1% HNO_3) of the downstream HF products. The corrosion was characterized by analysing the corroded coupons for mass loss, apparent corrosion rates, acid consumptions, visual observations of scale formation and pits, as well as depth profiles from scanning electron microscopy and energy dispersive spectroscopy analyses. Linear relationships were frequently observed when analysing mass losses for the coupons over time, making it possible to define corrosion rates in terms of first order reaction kinetics. The harshest corrosive condition for mild steel in HF was determined to be 1% HNO_3 in 70% HF at a constant temperature of 25ºC.

The corrosion characteristics of alloys used in the HF plant, as affected by HNO_3 impurities (in the range 50–10000 ppm) in the final HF acid product (70% Technical grade) were successfully established. Normalized SA516 Grade 70 mild steel and Monel 400 were found not adequate for use as construction materials in a plant where HNO_3 contamination was >100 ppm. However, the corrosion resistance of SS 904 L was suitable under these conditions and was recommended for

applications in HF solutions where the presence of an oxygen-containing acid (e.g. HNO_3) is consistent.

It was recommended that Alloy 31, Alloy 33 or Nirosta 4565S, with higher chromium content (>20 wt% Cr), should be considered for construction material of the HF plant when HNO_3 contamination becomes unavoidable. However, if the continued use of mild steel at the plant cannot be avoided, other inhibition strategies tailored to the selective consumption of HNO_3 in the HF product stream need to be investigated.

TABLE OF CONTENTS

PAGE

LIST OF FIGURES xi
LIST OF TABLES xix
LIST OF SYMBOLS xxiii
NOMENCLATURE xxv
CHAPTER 1 1
INTRODUCTION 1
1.1. BACKGROUND 1
1.2. PROBLEM STATEMENT 2
1.3. AIM AND OBJECTIVES 3
1.4. HYPOTHESES 4
1.5. RATIONALE 5
1.6. DISSERTATION LAYOUT 5
CHAPTER 2 7
LITERATURE REVIEW 7
2.1. HYDROFLUORIC ACID 7
2.1.1. Hydrofluoric acid production 7
2.1.2. Market for hydrofluoric acid 8
2.1.3. Metallurgical importance 9
2.2. CORROSION AND METALLURGY 9
2.2.1. Corrosion 9
2.2.2. Leaching 11
2.3. OXIDATION OF METALS 12
2.3.1. Oxygen in acid 12
2.3.2. Passivation 14
2.4. HYDROFLUORIC ACID PLANT CORROSION 16
2.4.1. Hydrofluoric acid corrosion in the international industry 16
2.4.2. Hydrofluoric acid corrosion in the South African industry 20
2.4.2.1. Corrosion failure at Pelchem 20
2.4.2.2. On site HF plant examinations 22
2.4.2.3. Use of alternative alloys 26

2.5. CORROSION OF STEEL AND OTHER METALLIC ALLOYS IN CONTAMINATED ACIDS 27
2.5.1. Mild steel corrosion in contaminated sulphuric acid 27
2.5.2. Steel and nickel alloy corrosion in contaminated nitric acid 28
2.5.3. Improved passivation in contaminated fluoride solutions 29
2.6. CONCLUSION 30
CHAPTER 3 32
CORROSION FAILURE ANALYSIS 32
3.1. INTRODUCTION 32
3.2. BACKGROUND 33
3.3. OBJECTIVES OF THE CORROSION FAILURE ANALYSIS 34
3.4. MATERIALS AND METHODOLOGY 34
3.5. RESULTS 37
3.6. DISCUSSION 40
3.7. CONCLUSIONS 41
3.8. RECOMMENDATONS 41
CHAPTER 4 42
EXPERIMENTAL PROCEDURE 42
4.1. MATERIALS 42
4.1.1. Steels and metallic alloys 42
4.1.2. Chemicals and reagents 42
4.1.3. Handling of metals 44
4.1.3.1. Material selection 44
4.1.3.2. Cutting of the coupons 44
4.1.3.3. Cleaning 47
4.2. ANALYSES 49
4.2.1. Solution samples 49
4.2.2. Solid samples 50
4.2.2.1. Mass loss 51
4.2.2.2. Apparent corrosion rate 51
4.2.2.3. Corrosion examination and observations 52
4.2.2.4. Verification of the alloy compositions 55

4.3. SAFETY CONSIDERATIONS 56
4.4. PLANNED INTERVAL CORROSION TESTS 57
4.4.1. Planned interval corrosion test methods 57
4.4.2. Effect of pre-passivation on mild steel 61
4.4.3. Effect of HF concentration on mild steel 62
4.4.4. Effect of steel and alloy composition 63
4.5. CORROSION TESTS 63
4.5.1. Corrosion test methods 63
4.5.2. Mild steel corrosion 65
4.5.2.1. Effect of nitric acid concentration 65
4.5.2.2. Effect of temperature 66
4.5.2.3. Effect on scale thickness 66
4.5.3. Nickel alloy and stainless steel corrosion 67
CHAPTER 5 69
RESULTS 69
5.1. PLANNED INTERVAL COROSION TESTS 69
5.1.1. Introduction 69
5.1.2. Effect of pre-passivation on mild steel 69
5.1.3. Effect of steel and alloy composition 90
5.2. CORROSION TESTS 103
5.2.1. Introduction 103
5.2.2. Mild steel corrosion 103
5.2.2.1. Effect of HNO_3 concentration in HF 103
5.2.2.2. Effect of temperature 105
5.2.3. Stainless steel corrosion 145
5.2.3.1. Effect of nitic acid concentration 145
5.2.4. Nickel alloy corrosion 151
5.2.4.1. Effect of nitic acid concentration 151
CHAPTER 6 159
DISCUSSION 159
6.1. PLANNED INTERVAL CORROSION TESTS 159
6.1.1. Introduction 159

6.1.2. Effect of pre-passivation on mild steel 159
6.1.3. Effect of steel and alloy composition 164
6.2. CONTINUOUS CORROSION TESTS 167
6.2.1. Introduction 167
6.2.2. Mild steel corrosion 167
6.2.2.1. Effect of nitic acid concentration 167
6.2.2.2. Effect of temperature 170
6.2.3. Stainless steel corrosion 176
6.2.3.1. Effect of nitic acid concentration 176
6.2.4. Nickel alloy corrosion 179
6.2.4.1. Effect of nitric acid concentration 179
6.2.5. Kinetics and rate constants 182
6.2.5.1. Purpose of kinetic study 182
6.2.5.2. Determining rate constants 183
6.2.6. Summary 193
6.2.7. Inhibition strategies 199
CHAPTER 7 201
CONCLUSIONS AND RECOMMENDATIONS 201
7.1. CONCLUSIONS 201
7.1.1. Evaluation of aims 201
7.1.2. Evaluation of objectives 201
7.1.2.1. Rates and mechanism of corrosion of steels and alloys 201
7.1.2.2. Inhibition strategies 203
7.2. RECOMMENDATIONS 204
REFERENCES 205
APPENDICES 214
APPENDIX A: ERROR CALCULATIONS 214
APPENDIX B: CONSIDERATIONS FOR COUPON SIZES AND DOSING HYDROFLUORIC ACID CALCULATIONS 221
APPENDIX C: PUBLICATIONS AND CONFERENCE PROCEEDINGS 224

LIST OF FIGURES

PAGE

Figure 2.1: General HF production flow sheet (Eurofluor, 2017). 7

Figure 2.2: Schematic representation of the corrosion mechanism of a steel surface in contact with an electrolyte accompanied by sub-reactions and corresponding steps (1-4) taking place during corrosion (Adapted from McEwan, 2004). 10

Figure 2.3: Schematic summary of types of metallic corrosion (Adapted from Jones (1996)). 17

Figure 2.4: (a) Corrosion in the liquid phase, and (b) in the vapour phase above HF liquid level of Monel dip tubes installed on March 2012 into Storage tanks V1460 and removed 2 weeks later due to excessive corrosion (Valkenburgh, 2012e). 23

Figure 2.5: HF storage tank loading and transportation facility located on site at Necsa. 23

Figure 2.6: (a) H_2SO_4 as-received from the supplier's tanker, and (b) H_2SO_4 from the bottom of the plant storage tanks where the impurity which settled out was predominantly $FeSO_4$ (Valkenburgh, 2012c). 25

Figure 2.7: (a) 98% Laboratory grade H_2SO_4 indicting no reaction with iron powder, and (b) H_2SO_4 from the supplier which had reacted to form a thick brown residue with the iron powder (Valkenburgh, 2012c). 25

Figure 2.8: (a) 70% technical grade HF indicating no visual reaction with iron powder, and (b) 70% industrial HF showing some visible reaction had occurred with the iron powder (Valkenburgh, 2012c). 25

Figure 3.1: Storage tanks V1460 (left) and V1461 (right) which failed on 30 May and 26 March 2012 from excessive corrosion which were removed from the plant (a), and (b) an area where it leaked even after patching. 33

Figure 3.2: Leak in V1460 approximately 300 mm from the vessel bottom due to unusual corrosion, observed (a) from outside, and (b) from inside the storage tank. 34

Figure 3.3: Inside V1460, indicating: (a) corrosion at various liquid levels, and (b) weld joint. 35

Figure 3.4: Samples cut from storage tank V1460 (Figure 3.1a) at the area where the HF leak initiated (Figure 3.2), the level of the liquid phase of the HF, is shown (also visible in Figure 3.3a)..... 36

Figure 3.5: Samples sectioned from the sheet cut from storage tank V1460 (Figure 3.4) at: (a) the point where the HF leak initiated, and (b) the area well above the liquid band. 36

Figure 3.6: Removable scale, collected from below the liquid band (point 5 in Figure 3.4) on the inside of the HF storage vessel (Figure 3.2b), for XRD analysis. 37

Figure 3.7: SEM-BSE image of a cross-section of the mild steel with corrosion, showing scale formation above the liquid band (sampled from point 4 in Figure 3.4). 38

Figure 3.8: Depth profile of the corrosion layer above the liquid band (EDS of Figure 3.7). 38

Figure 3.9: SEM-BSE image of the cross-section of mild steel with corrosion, showing scale formation in the liquid phase (sampled from point 1 in Figure 3.4). 39

Figure 3.10: Depth profile of the corrosion layer in the liquid phase (EDS of Figure 3.9). 39

Figure 3.11: XRD pattern of the corrosion products (removable scale). Unidentified peaks were marked by UI. 40

Figure 4.1: Steps for sample preparation prior to corrosion experiments and analyses. 45

Figure 4.2: Example of the original steel received from hot rolling received after sand-blasting. 45

Figure 4.3: Example of a sandblasted template made by water-jet cutting. 46

Figure 4.4: Examples of final coupons, after washing with acetone, prepared for corrosion immersion tests, with sequencing marks on the bottom edges. 46

Figure 4.5: SEM-BSE micrographs showing the original hot rolled edges of the mild steel after etching with 3% Nital. 47

Figure 4.6: Water bath with immersion cooler set-up for corrosion tests. 58

Figure 4.7: Corrosion reactor components: (a) Teflon bottle, and (b) cylindrical corrosion rack with Teflon rod to the suspend coupon. 59

Figure 4.8: Top view of a complete assembly for a planned interval corrosion test. 59

Figure 5.1: Effect of an increase in percentage HF in the corrosion solution on percentage acid consumption after 8 days of mild steel corrosion, at 25ºC. Error bars obscured by markers in some instances. 73

Figure 5.2: PCT 1: Mild steel coupons: (1) A_1 (2) A_t (3) A_{t+1} and (4) B: Row a; before, and Row b; after exposure to 40% HF, with Row c; after removal of the scale layer..... 77

Figure 5.3: PICT 3: Mild steel coupons: (1) A_1 (2) A_t (3) A_{t+1} and (4) B: Row a; before, and Row b; after exposure to 48% HF, with Row c; after removal of the scale layer..... 78

Figure 5.4: PICT 6: Mild steel coupons: (1) A_1 (2) A_t (3) A_{t+1} and (4) B: Row a; before, and Row b; after exposure to 70% HF, with Row c; after removal of the scale layer..... 79

Figure 5.5: PICT 2: Mild steel coupons: (1) A_1 (2) A_t (3) A_{t+1} and (4) B: Row a; before exposure, Row b; after pre-passivation step, Row c; after exposure to 40% HF, and Row d; after removal of the scale layer..... 81

Figure 5.6: PICT 5: Mild steel coupons: (1) A_1 (2) A_t (3) A_{t+1} and (4) B: Row a; before exposure, Row b; after pre-passivation step, Row c; after exposure to 48% HF, and Row d; after removal of the scale layer..... 82

Figure 5.7: PICT 7: Mild steel coupons: (1) A_1 (2) A_t (3) A_{t+1} and (4) B: Row a; before exposure, Row b; after pre-passivation step, Row c; after exposure to 70% HF, and Row d; after removal of the scale layer..... 83

Figure 5.8: Pit depth and distribution measurements of 2 x 2 mm of a sand-blasted mild steel surface before corrosion tests, using optical microscopy to construct: (a and b) 3D height images, (c and d) 2D height profiles and (e) contours..... 85

Figure 5.9: Pit depth and distribution measurements of 2 x 2 mm of a mild steel surface corroded in 40% HF for 8 days at 25ºC, using optical microscopy to construct: (a and b) 3D height images, (c and d) 2D height profiles and (e) contours. 86

Figure 5.10: Pit depth and distribution measurements of 2 x 2 mm of a mild steel surface corroded in 48% HF for 8 days at 25ºC, using optical microscopy to construct: (a and b) 3D height images, (c and d) 2D height profiles and (e) contours. 87

Figure 5.11: Pit depth and distribution measurements of 2 x 2 mm of a mild steel surface corroded in 70% HF for 8 days at 25ºC, using optical microscopy to construct: (a and b) 3D height images, (c and d) 2D height profiles and (e) contours. 88

Figure 5.12: Effect of HF concentration in the corrosion solution on pit mouth diameters and distribution after 8 days of mild steel corrosion, at 25ºC. 89

Figure 5.13: Effect of HF concentration in the corrosion solution on pit depth and distribution after 8 days of mild steel corrosion, at 25ºC..... 89

Figure 5.14: Effect of pre-passivation on percentage acid consumption during PICTs - comparing mild steel, stainless steel and nickel alloy corrosion in 70% HF at 25ºC. Error bars obscured by markers in some instances..... 94

Figure 5.15: PICT 10: Stainless steel coupons (SS 904 L): (1) A_1 (2) A_t (3) A_{t+1} and (4) B: Row a; before, and Row b; after exposure to 70% HF, with Row c; after removal of the scale layer. 97

Figure 5.16: PICT 8: Stainless steel coupons (SS 904 L): (1) A_1 (2) A_t (3) A_{t+1} and (4) B: Row a; before exposure, Row b; after pre-passivation step, Row c; after exposure to 70% HF, and Row d; after removal of the scale layer. 98

Figure 5.17: PICT 11: Nickel alloy (Monel 400): (1) A_1 (2) A_t (3) A_{t+1} and (4) B: Row a; before, and Row b; after exposure to 70% HF, with Row c; after removal of the scale layer. 101

Figure 5.18: PICT 9: Nickel alloy (Monel 400): (1) A_1 (2) A_t (3) A_{t+1} and (4) B): Row a; before exposure, Row b; after pre-passivation step, Row c; after exposure to 70% HF, and Row d; after removal of the scale layer. 102

Figure 5.19: HF and HNO_3 acid consumption after 11 days of mild steel corrosion, at 25ºC. Error bars obscured by markers in some instances. 111

Figure 5.20: Effect of temperature on percentage HF acid consumption after 11 days of mild steel corrosion. Error bars obscured by markers in some instances. 111

Figure 5.21: Effect of temperature on percentage HNO_3 acid consumption after 11 days of mild steel corrosion. Error bars obscured by markers in some instances. 112

Figure 5.22: CT 1: Mild steel coupons (1-7): Row a; before exposure, Row b; after pre-passivation step, Row c after exposure to 70% HF, and Row d; after removal of the scale layer, at 25ºC. 115

Figure 5.23: CT 2 (Duplicate corrosion test): Mild steel coupons (1-7): Row a; before exposure, Row b; after pre-passivation step, Row c; after exposure to 70% HF, and Row d; after removal of the scale layer, at 25ºC. 116

Figure 5.24: CT 7: Mild steel coupons (1-7): Row a; before exposure, Row b; after pre-passivation step, Row c; after exposure to 70% HF, and Row d; after removal of the scale layer at 15ºC. 117

Figure 5.25: CT 12: Mild steel coupons (1-7): Row a; before exposure, Row b; after pre-passivation step, Row c; after exposure to 70% HF, and Row d; after removal of the scale layer, at 0ºC. 118

Figure 5.26: CT 3: Mild steel coupons (1-7): Row a; before exposure, Row b; after pre-passivation step, Row c; after exposure to 70% HF spiked with 0.1% HNO_3, and Row d; after removal of the scale layer, at 25ºC. 121

Figure 5.27: CT 8: Mild steel coupons (1-7): Row a; before exposure, Row b; after pre-passivation step, Row c; after exposure to 70% HF spiked with 0.1% HNO_3, and Row d; after removal of the scale layer, at 15ºC. 122

Figure 5.28: CT 13: Mild steel coupons (1-7): Row a; before exposure, Row b; after pre-passivation step, Row c; after exposure to 70% HF spiked with 0.1% HNO_3, and Row d; after removal of the scale layer, at 0ºC. 123

Figure 5.29: CT 5: Mild steel coupons (1-7): Row a; before exposure, Row b; after pre-passivation step, Row c; after exposure to 70% HF spiked with 0.5% HNO_3, and Row d; after removal of the scale layer, at 25ºC. 126

Figure 5.30: CT 9: Mild steel coupons (1-7): Row a; before exposure, Row b; after pre-passivation step, Row c; after exposure to 70% HF spiked with 0.5% HNO_3, and Row d; after removal of the scale layer at 15ºC. 127

Figure 5.31: CT 14: Mild steel coupons (1-7): Row a; before exposure, Row b; after pre-passivation step, Row c; after exposure to 70% HF spiked with 0.5% HNO_3, and Row d; after removal of the scale layer, at 0ºC. 128

Figure 5.32: CT4 Mild steel coupons (1-7): Row a; before exposure, Row b; after pre-passivation step, Row c; after exposure to 70% HF spiked with 1% HNO_3, and Row d; after removal of the scale layer, at 25ºC. 131

Figure 5.33: CT 6 (Duplicate corrosion test): Mild steel coupons (1-7): Row a; before exposure, Row b; after pre-passivation step, Row c; after exposure to 70% HF spiked with 1% HNO_3, and Row d; after removal of the scale layer, at 25ºC. 132

Figure 5.34: CT 10: Mild steel coupons (1-7): (row a) before exposure, Row b; after pre-passivation step, Row c; after exposure to 70% HF spiked with 1% HNO_3, and Row d; after removal of the scale layer, at 15ºC. 133

Figure 5.35: CT 11 (Duplicate corrosion test): Mild steel coupons (1-7): Row a; before exposure, Row b; after pre-passivation step, Row c; after exposure to 70% HF spiked with 1% HNO_3, and Row d; after removal of the scale layer at 15ºC. 134

Figure 5.36: CT 15: Mild steel coupons (1-7): Row a; before exposure, Row b; after pre-passivation step, Row c; after exposure to 70% HF spiked with 1% HNO_3, and Row d; after removal of the scale layer, at 0ºC. 135

Figure 5.37: CT 16 (Duplicate corrosion test): Mild steel coupons (1-7): (row a) before exposure, Row b; after pre-passivation step, Row c; after exposure to 70% HF spiked with 1% HNO_3, and Row d; after removal of the scale layer, at 0ºC. 136

Figure 5.38: SEM backscattered electron image of a cross-section of mild steel coupon, after exposure to 70% HF for 24 h (pre-passivation step), with corresponding depth profile measurements of the scale layer made using EDS spot analyses and line scans. 139

Figure 5.39: SEM backscattered electron image of a cross-section of mild steel coupon (No. 8), after exposure to 70% HF, with corresponding depth profile measurements of the scale layer made using EDS spot analyses and line scans..... 140

Figure 5.40: SEM backscattered electron image of a cross-section of mild steel coupon (No. 8), after exposure to 70% HF spiked with 0.1% HNO_3, with corresponding depth profile measurements made of the scale layer using EDS spot analyses and line scans. 141

Figure 5.41: SEM backscattered electron image of a cross-section of mild steel coupon (No. 8), after exposure to 70% HF spiked with 0.5% HNO_3, with corresponding depth profile measurements made of the scale layer using EDS spot analyses and line scans. 142

Figure 5.42: SEM backscattered electron image of a cross-section of mild steel coupon (No. 8), after exposure to 70% HF spiked with 1% HNO_3, with corresponding depth profile measurements made of the scale layer using EDS spot analyses and line scans. 143

Figure 5.43: Effect of HNO_3 concentration on fluorite scale thickness of mild steel when corroded in 70% HF, at 25ºC. Error bars obscured by markers in some instances. 144

Figure 5.44: CT 19: Stainless steel (SS 904 L) coupons (1-7): Row a; before exposure, Row b; after pre-passivation step, Row c; after exposure to 70% HF, and Row d; after removal of the scale layer, at 25ºC. 150

Figure 5.45: CT 20: Stainless steel (SS 904 L) coupons (1-7): Row a; before exposure, Row b; after pre-passivation step, Row c; after exposure to 70% HF spiked with 1% HNO_3, and Row d; after removal of the scale layer, at 25ºC..... 151

Figure 5.46: Percentage HF acid consumption after 11 days of mild steel, stainless steel and nickel alloy corrosion, at 25ºC. Error bars obscured by markers in some instances..... 154

Figure 5.47: Effect of percentage HNO_3 acid consumption after 11 days of mild steel, stainless steel and nickel alloy corrosion, at 25ºC. Error bars obscured by markers in some instances. 155

Figure 5.48: CT 17: Nickel alloy (Monel 400) coupons (1-7): Row a; before exposure, Row b; after pre-passivation step, Row c; after exposure to 70% HF, and Row d; after removal of the scale layer, at 25ºC. 157

Figure 5.49: CT 18: Nickel alloy (Monel 400) coupons (1-7): (row a) before exposure, Row b; after pre-passivation step, Row c; after exposure to 70% HF spiked with 1% HNO_3, and Row d; after removal of the scale layer, at 25ºC..... 158

Figure 6.1: Flow chart to demonstrate how a change in HF concentration affects scale formation on mild steel. 160

Figure 6.2: Effect of a pre-passivation step on mass loss with increase in percentage HF in the corrosion solution, at 25ºC. Error bars obscured by markers in some instances: (a) whole range of the mass losses, and (b) lower mass losses. 161

Figure 6.3: Effect of a pre-passivation step on apparent corrosion rate with increase in percentage HF in the corrosion solution, at 25ºC. Error bars obscured by markers in some instances: a) whole range of the mass losses, and b) lower mass losses. 162

Figure 6.4: Effect of a pre-passivation step on mass loss of mild steel, stainless steel and nickel alloy during a PICT, at 25ºC in 70% HF. Error bars obscured by markers in some instances. 165

Figure 6.5: Effect of a pre-passivation step on the apparent corrosion rate of mild steel, stainless steel and nickel alloy during a PICT, at 25ºC in 70% HF. Error bars obscured by markers in some instances. 166

Figure 6.6: Effect of HNO_3 concentration on mass loss of mild steel when corroded in HF at 25ºC in 70% HF. Error bars obscured by markers in some instances. 168

Figure 6.7: Effect of HNO_3 concentration on mass loss of mild steel when corroded in HF (linear trends), at 25ºC in 70% HF. Error bars obscured by markers in some instances. 168

Figure 6.8: Effect of HNO_3 concentration on the apparent corrosion rate of mild steel in HF, at 25ºC in 70% HF. Error bars obscured by markers in some instances. 170

Figure 6.9: Effect of temperature on mass loss of mild steel when corroded in pure HF. Error bars obscured by markers in some instances..... 171

Figure 6.10: Effect of temperature on mass loss of mild steel when corroded in 70% HF spiked with 0.1% HNO_3. Error bars obscured by markers in some instances. 171

Figure 6.11: Effect of temperature on mass loss of mild steel when corroded in 70% HF spiked with 0.5% HNO_3. Error bars obscured by markers in some instances. 172

Figure 6.12: Effect of temperature on mass loss of mild steel when corroded in 70% HF spiked with 1% HNO_3. Error bars obscured by markers in some instances. 172

Figure 6.13: Effect of temperature on apparent corrosion rates of mild steel in pure HF (<50 ppm HNO_3). Error bars obscured by markers in some instances. 173

Figure 6.14: Effect of temperature on apparent corrosion rates of mild steel in 70% HF spiked with 0.1% HNO_3. Error bars obscured by markers in some instances. 174

Figure 6.15: Effect of temperature on apparent corrosion rates of mild steel in 70% HF spiked with 0.5% HNO_3. Error bars obscured by markers in some instances. 174

Figure 6.16: Effect of temperature on apparent corrosion rates of mild steel in 70% HF spiked with 1% HNO_3. Error bars obscured by markers in some instances. 175

Figure 6.17: Effect of HNO_3 concentration on mass loss of stainless steel when corroded in 70% HF at 25ºC. Error bars obscured by markers in some instances..... 177

Figure 6.18: Effect of HNO_3 concentration on the apparent corrosion rate of stainless steel in 70% HF, at 25ºC. Error bars obscured by markers in some instances..... 178

Figure 6.19: Transition from fast initial apparent corrosion rate to slower proceeding rates evident for stainless steel corrosion in 70% HF with 1% HNO_3, at 25ºC. Error bars obscured by markers in some instances. 178

Figure 6.20: Effect of HNO_3 concentration on mass loss of nickel alloy when corroded in 70% HF at 25ºC. Error bars obscured by markers in some instances..... 180

Figure 6.21: Effect of HNO_3 concentration on the apparent corrosion rate of nickel alloy in 70% HF at 25ºC. Error bars obscured by markers in some instances..... 181

Figure 6.22: Effect of HNO_3 concentration on the apparent corrosion rate of nickel alloy in 70% HF at 25ºC. Error bars obscured by markers in some instances..... 182

Figure 6.23: Effect of change in temperature on corrosion rates of mild steel in pure HF. Error bars obscured by markers in some instances..... 185

Figure 6.24: Effect of change in temperature on corrosion rates of mild steel in 70% HF spiked with 0.1% HNO_3. Error bars obscured by markers in some instances. 186

Figure 6.25: Effect of change in temperature on corrosion rates of mild steel in 70% HF spiked with 0.5% HNO_3. Error bars obscured by markers in some instances. 186

Figure 6.26: Effect of change in temperature on corrosion rates of mild steel in 70% HF spiked with 1% HNO_3. Error bars obscured by markers in some instances. 187

Figure 6.27: Effect of temperature and HNO_3 concentration on the corrosion reaction rate of mild steel in 70% HF, displayed on an Arrhenius plot. 189

Figure 6.28: Dissolution rates of mild steel, stainless steel and nickel alloy in pure HF at 25ºC. Error bars obscured by markers in some instances. 191

Figure 6.29: Dissolution rates of mild steel, stainless steel and nickel alloy in 70% HF spiked with 1% HNO_3 at 25ºC. Error bars obscured by markers in some instances. 193

LIST OF TABLES

PAGE

Table 2.1: Alternative steels and metal alloys considered by Pelchem for use in the HF plant (Valkenburgh, 2013). 27

Table 4.1: Steels and metal alloys currently in use at the Pelchem HF plant (Valkenburgh, 2013).. 42

Table 4.2: Conditions and variables and experimental conditions for PICTs conducted. 57

Table 4.3: Criteria for planned interval corrosion tests. 62

Table 4.4: Conditions and variables and experimental conditions for CTs conducted. 63

Table 4.5: Set-up and time intervals for corrosion tests. 65

Table 4.6: Laboratory simulated conditions metals coupons were exposed to during corrosion experiments. 66

Table 5.1: Planned interval corrosion tests for mild steel in 40% HF. 70

Table 5.2: Planned interval corrosion tests for mild steel in 40% HF – pre-passivated. 70

Table 5.3: Planned interval corrosion tests for mild steel in 48% HF. 71

Table 5.4: Planned interval corrosion tests for mild steel in 48% HF – pre-passivated. 71

Table 5.5: Planned interval corrosion tests for mild steel in 70% HF. 72

Table 5.6: Planned interval corrosion tests for mild steel in 70% HF – pre-passivated. 72

Table 5.7: HF acid consumption by mild steel after 8 days when varying HF feed concentration, at 25ºC – pre-passivated. 73

Table 5.8: Observations of corrosion products of PICTs conducted in 40, 48 and 70% HF, after 8 days 76

Table 5.9: Observations of corrosion products of PICTs conducted in 40, 48 and 70% HF, after 8 days – pre-passivated 80

Table 5.10: Verification of Mild steel (SA 516 Grade 70 normalized) composition 90

Table 5.11: Verification of Stainless steel (SS 904 L) composition. 90

Table 5.12: Verification of Alloy 400 (Monel) compositions. 90

Table 5.13: Planned interval corrosion tests for stainless steel in 70% HF. 91

Table 5.14: Planned interval corrosion tests for stainless steel in 70% HF – pre-passivated. 91

Table 5.15: Planned interval corrosion tests for nickel alloy in 70% HF. 92

Table 5.16: Planned interval corrosion tests for nickel alloy in 70% HF – pre-passivated. 92

Table 5.17: HF acid consumption by mild steel, stainless steel and nickel alloy after 8 days when varying the degree of pre-passivation in 70% HF, at 25ºC. 94

Table 5.18: Observations of corrosion products of PICTs conducted on a stainless steel (SS 904 L), after 8 days 96

Table 5.19: Observations of corrosion products of PICTs conducted on a nickel alloy (Monel 400), after 8 days 100

Table 5.20: CT 1: Corrosion test for mild steel in 70% HF, at 25ºC. 104

Table 5.21: CT 3: Corrosion test for mild steel in 70% HF spiked with 0.1% HNO_3, at 25ºC. 104

Table 5.22: CT 5: Corrosion test for mild steel in 70% HF spiked with 0.5% HNO_3, at 25ºC. 104

Table 5.23: CT 4: Corrosion test for mild steel in 70% HF spiked with 1% HNO_3, at 25ºC. 105

Table 5.24: CT 7: Corrosion test for mild steel in 70% HF at 15ºC. 106

Table 5.25: CT 8: Corrosion test for mild steel in 70% HF spiked with 0.1% HNO_3, at 15ºC. 106

Table 5.26: CT 9: Corrosion test for mild steel in 70% HF spiked with 0.5% HNO_3, at 15ºC. 106

Table 5.27: CT 10: Corrosion test for mild steel in 70% HF spiked with 1% HNO_3, at 15ºC. 107

Table 5.28: CT 12: Corrosion test for mild steel in 70% HF, at 0ºC. 107

Table 5.29: CT 13: Corrosion test for mild steel in 70% HF spiked with 0.1% HNO_3, at 0ºC..... 107

Table 5.30: CT 14: Corrosion test for mild steel in 70% HF spiked with 0.5% HNO_3, at 0ºC..... 108

Table 5.31: CT 15: Corrosion test for mild steel in 70% HF spiked with 1% HNO_3, at 0ºC..... 108

Table 5.32: HF acid consumption by mild steel after 11 days when varying the HNO_3 concentration in 70% HF, at 0, 15 and 25ºC. 109

Table 5.33: HNO_3 acid consumption by mild steel after 11 days when varying the HNO_3 concentration in 70% HF, at 0, 15 and 25ºC. 110

Table 5.34: Observations of corrosion products from mild steel in pure HF to see the effect of change in temperature on scale..... 114

Table 5.35: Observations of corrosion products from mild steel in HF spiked with 0.1% HNO_3 to see the effect of change in temperature on scale. (Figures 5.26, 5.27and 5.28: Row c and d). 120

Table 5.36: Observations of corrosion products from mild steel in HF spiked with 0.5% HNO_3 to see the effect of change in temperature on scale. (Figures 5.29, 5.30 and 5.31: Row c and d). 125

Table 5.37: Observations of corrosion products from mild steel in HF spiked with 1% HNO_3 to see the effect of change in temperature on scale. (Figures 5.32, 5.33, 5.34, 5.35, 5.36 and 5.37: Row c and d)..... 130

Table 5.38: CT 19: Corrosion test for stainless steel in 70% HF, at 25ºC..... 145

Table 5.39: CT 20: Corrosion results for stainless steel in 70% HF spiked with 1% HNO_3, at 25ºC. 146

Table 5.40: HF acid consumption by stainless steel after 11 days when varying the HNO_3 concentration in 70% HF, at 25ºC. 146

Table 5.41: HNO_3 acid consumption by stainless steel after 11 days when varying the HNO_3 concentration in 70% HF, at 25ºC. 147

Table 5.42: Observations of corrosion products from a stainless steel (SS 904 L) in HF with lowest to highest HNO_3 contamination, over an 11 day corrosion test (Figures 5.44 and 5.45: Row c and d)..... 149

Table 5.43: CT 17: Corrosion test for nickel alloy (Monel 400) in 70% HF, at 25ºC. 152

Table 5.44: CT 18: Corrosion test for nickel alloy (Monel 400) in 70% HF spiked with 1% HNO_3, at 25ºC. 152

Table 5.45: HF acid consumption by nickel alloy (Monel 400) after 11 days when varying the HNO_3 concentration in 70% HF, at 25ºC. 153

Table 5.46: HNO_3 acid consumption by nickel alloy (Monel 400) after 11 days when varying the HNO_3 concentration in 70% HF, at 25ºC. 153

Table 5.47: Observations of corrosion products from a nickel alloy in HF with lowest to highest HNO_3 contamination, over an 11 day corrosion test (Figures 5.48 and 5.49: Row c and d). 156

Table 6.1: Kinetics data from corrosion tests on mild steel in pure HF. 187

Table 6.2: Kinetics data from corrosion tests on mild steel in HF spiked with 0.1% HNO_3. 188

Table 6.3: Kinetics data from corrosion tests on mild steel in HF spiked with 0.5% HNO_3. 188

Table 6.4: Kinetics data from corrosion tests on mild steel in HF spiked with 1% HNO_3. 188

Table 6.5: Kinetics data from corrosion tests on mild steel, stainless steel and nickel alloy in pure HF at 25ºC. 192

Table 6.6: Kinetics data from corrosion tests on mild steel, stainless steel and nickel alloy in HF spiked with 1% HNO_3, at 25ºC. 193

Table 6.7: Summary of corrosion type, corrosion rate and corrosion resistance data for all metals in service tested in 70% HF contaminated with up to 1% HNO_3 at 25ºC. 198

LIST OF SYMBOLS

SYMBOL	DEFINITION
µm	micro metre
bar	barometer
cm	centimetre
cm^{-3}	cubic centimetre
di	inner diameter
E_a	activation energy
g	grams
g/L	grams per litre
g/L·sec	grams per litre second
h	hour
K	degree Kelvin
k	Rate constant
kg	kilograms
kg/t	kilograms per tonne
kJ/mol	kilojoules per mol
kPa	kilo-Pascal
L	litre
m	meter
M	Molarity
Mg	milligrams
mg/kg	milligram per kilogram
mg/L	milligram per litre
min	minutes
ml	millilitre
mm	millimetre
mol	mole
mol/L·sec	mole per litre second

pH	negative logarithm of the concentration of hydrogen ions.
ppm	parts per million
r	rate of reaction
R^2	correlation coefficient
sec	second
t	time
T	temperature
W	Watt
wt%	weight percent

NOMENCLATURE

Base metals:	More common metals such as copper, tin lead and zinc that are distinct from precious metals.
Corrodibility:	The tendency, or capacity, of a metal to undergo corrosion, i.e. the susceptibility of the metal to corrosion.
Corrosion resistance:	The ability of a metal to withstand corrosion in a given corrosion system.
Corrosivity:	A metal having the property or quality to corrode, erode or be eaten away by a corrosive chemical.
Leaching:	The process of dissolution of valuable elements of a metal by an aqueous solution of the leaching agent.
Lixiviant:	A liquid medium employed to selectively extract the desired metal from an ore mineral.
Mineral:	Natural inorganic substance possessing definite chemical composition and atomic structure. Alternatively, the term is also used to include anything of economic value which is extracted from the earth.
Ore:	An accumulation of minerals in sufficient quantity to be sufficient for economic extraction.
Slurry:	A thick suspension of solids in a liquid where the solid is only slightly soluble (or insoluble).
Spiking:	Increasing the concentration of a species within a sample solution to more than 50 times the concentration found in the unspiked sample, while not increasing the sample volume by more than 5% (so as to avoid unknown effects from dilution of the solution matrix).

CHAPTER 1

INTRODUCTION

1.1. BACKGROUND

Rapid corrosion of steels and nickel alloys due to the presence of low concentrations of an oxidizing acid, such as nitric acid (HNO_3), is an unpredictable phenomenon during the manufacture of hydrofluoric acid (70% HF). Even though the corrosion of construction materials from exposure to hydrofluoric acid in a plant set-up is well documented (Whitaker, 1950; ASM Handbook, 1987; Jones, 1996; Rebak, 2003), no real measures are in place to deal with the unique corrosive conditions resulting from oxidizing impurities in fluorine-containing acids at an HF plant. There is also no knowledge on how to prepare for this type of corrosion in processes that might have to deal with such streams.

The commercial HF production plant in this study was Pelchem SOC Ltd., which is located on the Pelindaba site of Necsa SOC Limited in the Hartbeespoort area, 50 km north-west of Johannesburg. Normalized mild steel, code SA516 Grade 70, has been used in vessels for the storage and distribution of technical grade hydrofluoric acid (70% HF) at this plant since 1993 (Valkenburgh, 2012a). Uniform corrosion of the storage tanks was measured at ~0.5 mm/y and was mitigated in the design. This is because steel in contact with 70% HF leads to the following corrosive reaction:

$$2H^+ + 2F^- + Fe \rightarrow FeF_2 + H_2 \qquad \text{Equation 1.1}$$

initially forming a protective scale inside the tank during its commissioning and then protects the mild steel from further corrosion (Whitaker, 1950; Jennings, 2007).

A leak occurred in March 2012 on the bottom of the V1461 HF storage tank (Figure 3.1), and three months before, the corrosion rate had increased to an average of 3 mm/y and eventually escalated to 30 mm/y measured at, and below, the liquid phase (HF tank level) of the storage vessel when the leak was first detected.

The rapid corrosion was attributed to the presence of an oxidizing acid ($0.1\% \leq HNO_3 \leq 1\%$) which attacked the protective iron fluoride (FeF_2) layer in the liquid phase (Valkenburgh,

2012a). The source of the HNO_3 was traced back to the sulphuric acid (H_2SO_4) used commercially to produce HF from the reaction:

$$CaF_2+H_2SO_4 \rightarrow CaSO_4+2HF \qquad \text{Equation 1.2}$$

Use of an alternative supplier had resulted in a change in the H_2SO_4 feedstock to the HF plant on site and was deemed to be responsible for the increased HNO_3 concentration downstream, which was especially concentrated in the final storage tanks. The combined corrosion effect of the HF and HNO_3 led to the eventual failure and subsequent decommissioning of the first storage tank in May 2012 (Valkenburgh, 2012a).

The incident that occurred at the HF plant thus served as a warning and a motivation for Pelchem, their stakeholders, their immediate suppliers and clients to address the unique corrosive conditions that can occur at the plant. Impurities can come in any form, and can have rapid effects on the corrosion rates of metallic components used in a plant. If alternative sources need to be considered, it must be realised that the feedstock (new mineral reserves or renewable resources) and chemicals may be more corrosive or hold nitrate-containing compounds, which can be released into solution during the aqueous acid manufacturing process. Since impurities and contamination are typically an inevitable occurrence, the extent and rate at which the steels and metal alloys used (and considered for use) in an HF production plant are corroded need to be studied and then accommodated. A reliable way to predict the corrosion rate of the steel in an HF process stream containing increased levels of HNO_3 is currently not in place.

An understanding of the corrosion characteristics and corrosion rates of steels and alloys with higher nitric acid concentrations in a plant that produces technical grade HF will aid in determining economically feasible solutions to increase the service life of HF storage tanks used in industry.

1.2. PROBLEM STATEMENT

Nitrous compounds in the acid feed stream are especially dangerous in the plant set-up (Andersen *et al.* 1980), because unlike uniform surface corrosion by HF, HNO_3 attack can be in the form of pitting, which cannot be effectively observed or easily measured (e.g. by means of thickness measurements) in the plant (Valkenburgh, 2013). Since the reflecting surfaces are not parallel, or due to the pits being larger within the plate than observed on the surface, ultrasonic methods are simply inadequate to detect pitting type corrosion in the steels and alloys used.

Thus, a breakdown or failure from this type of corrosion can occur suddenly, with no warning and can have catastrophic results. Therefore, an understanding and means of addressing and planning for these exceptionally corrosive conditions needed to be established, since no suitable means existed which could predict the corrosion rate of steels or alloys exposed to HNO_3 present in an HF process stream. An economically feasible means to protect the steel and increase its service life time in the presence of HF with increased levels of HNO_3 (>50 ppm) was required.

1.3. AIM AND OBJECTIVES

The aim of the study was to establish the corrosion characteristics of the metals used in the HF plant which could be exposed to >50 ppm HNO_3 impurities in the final HF products (Tanks containing 70% Technical grade HF). The study needed to determine the change in corrosion rates as a function of HNO_3 contamination and identify the associated mechanisms for the types of corrosion. Then from this derive possible prevention or mitigation strategies through the use of alternative metals, chemical additives or a combination of both.

The data collected were then used to develop a suitable way for predicting the corrosion characteristics and rates associated with the unique corrosive environments for the different steels and alloys components currently exposed in an HF plant. These could be used to determine the suitability of application of these materials, while considering cost effectiveness, alternative steels or alloys for the unique corrosive conditions. Data collected for different HNO_3 concentrations in the HF or process streams could then be used to determine the corrosion rates, and also to consider the effect of temperature ranges used for different processes in the plant. The chemical composition of the steels and alloys were also considered when examining the suitability of these materials for use in an HF plant exposed to HNO_3 contamination in the HF product streams.

Objectives

1. To identify the type of corrosion of mild and stainless steels, as well as nickel alloys exposed to nitrous compounds (>50 ppm) present in hydrofluoric acid (70% HF).
2. To determine the corrosion rates and mechanisms of these steels and alloys.
3. To investigate the degree to which the corrosion could feasibly be inhibited by:
    a. Reduction or elimination of nitrous compounds (N_xO_y) species in the acid
    b. Change of construction material
    c. Other corrosion inhibition methods

1.4. HYPOTHESES

1. Corrosion of steel and other alloys used for the construction of HF plants is directly affected by the HNO_3 content, temperature of the acid and the quality (grade and heat treatment of the steel or metallic alloy) used.
2. Nitric acid is an oxidizing acid which attacks the fluoride corrosion layer that protects the substrate from further corrosive attack of HF on the steel shell, and therefore drastically reduces the service lives of mild steel tanks in industry.
3. Acceptable corrosion rates (<0.5 mm/y) in storage tanks manufactured from normalized mild steel is achievable if the HNO_3 content is strictly controlled. This is possible through the alteration of corrosion parameters or controlling the temperature.
4. HNO_3 above 50 ppm in HF significantly increases the corrosion rates of typical steels and alloys used in an HF industry.
5. At excessively higher HNO_3 concentrations (expected at >1100 ppm), steel passivation tends to re-establish, resulting in a reduction of the corrosion rates.
6. Corrosion of steel and alloys used as construction material in HF plants producing AHF (anhydrous hydrogen fluoride) and technical grade HF above 70% can safely be simulated on a laboratory scale and used to make predictions on the change in corrosion rates and characteristics associated with HNO_3 contamination in an HF production plant circuit.
7. The pre-passivation can be replicated in a laboratory set-up by submerging steel coupons in 70% HF for no more than 24 h. This type of pre-passivation is adequate for studying the effect of nitric acid contamination on the corrosion rates of steel vessels used in industry, since it is influenced by the reaction of the fluoride scale formed during the pre-passivation step.
8. Oxidising acids in the feed streams to an HF plant affect the corrosion rates of mild steel and other alloys (such as Alloy 400 and Stainless steel, SS 904 L) by attacking the protective fluoride of mild steel and the oxide layers of nickel alloy and stainless steel.
9. Reproducible and accurate analyses of nitric acid (NO_3^- component) are achievable through ion chromatography (IC) in HF concentrations between 40% and 70% if the HF is effectively precipitated out of solution prior using analytically pure lime (CaO) instead of lithium hydroxide (LiOH).

1.5. RATIONALE

Decreasing quality of feedstock (H_2SO_4 and CaF_2) to HF plants around the world is unavoidable, due to depleting reserves and newer, more cost-effective technologies which focus more on throughput than quality. Therefore, the HF industry needs to adapt and prepare for corrosive contingencies where oxidizing contaminants in process streams are becoming more and more likely. Thus, it should be possible to inhibit corrosion at low temperatures (0 - 25ºC) to significantly extend the service life of mild steel containers used by understanding the corrosion mechanisms associated with higher HNO_3 concentrations.

The corrosive environment experienced in the HF storage tanks needed to be simulated in a laboratory set-up. The purpose of the corrosion experiments was to ascertain the resistance of the selected steel or alloys by placing coupons within concentrated (mother) acid, similar to the environment in the plant. Metal coupons, made from the steels and nickel alloys used in the plant, were exposed to low levels of an oxidizing acid over a given time period. The amounts of HNO_3 introduced to the 70% HF (initially HNO_3 free) were increased to levels found to be detrimental in the HF plant (0.1 - 1% HNO_3). The temperature range selected was also based on typical operation temperatures of the exposed metallic tanks and components in HF manufacturing (0 - 25°C).

The data collected from the mass loss, solution analyses and visual examinations is to produce information to start a database on the corrosivity of the relevant metals currently in use for an HF plant. It is envisaged that the database will contain corrosion behaviour of these steels and nickel alloys in HF streams, as well as tanks when significant concentrations of HNO_3 (between 0.1 and 1%) are present in the process streams. It will serve to summarise the relationships between HNO_3 concentration and corrosion rates of individual metals. No such database existed at the initiation of the project, thus it has great importance to any HF manufacturing plant dealing with varying conditions.

1.6. DISSERTATION LAYOUT

This dissertation consists of the following chapters:

Chapter 1: Introduction
Outline of the corrosion study and the importance of the research conducted.

Chapter 2: Literature survey

Survey of published (and some unpublished) works which pertained to the corrosion investigation with an analysis of that work, as well as the theory base needed for the study.

Chapter 3: Corrosion failure analysis

A short post-mortem study conducted on the decommissioned HF tanks which failed. Findings from this failure investigation prompted the laboratory corrosion test for characterizing corrosion by fluorine containing acids.

Chapter 4: Experimental approach

The methodology employed in attempting to solve the corrosion problems which were posed in the introduction to come to the conclusion.

Chapter 5: Results

A summary of the recorded corrosion data on mass losses, apparent corrosion rates, acid consumptions, pit measurements, scale depth profiles and observations made on the steel and nickel alloy coupons exposed to hydrofluoric acid spiked with nitric acid at various temperatures. The recorded corrosion data were also used to justify the use of a pre-passivation step.

Chapter 6: Discussion

Analyses of the findings made on mass losses, apparent corrosion rates and corrosion kinetics as affected by the change in HNO_3 concentration and temperature in the HF corrosion solutions used. The need for a 24 h pre-passivation step prior to laboratory tests was also discussed.

Chapter 7: Conclusions and recommendations

A summary of discoveries made during the study and their value for solving the problems posed in the introduction. Recommendations made on inhibition strategies for the HF production industries to combat the unique corrosive conditions studied, as well as suggestions for further research.

Appendix A: Error calculations

Appendix B: Considerations for apparent corrosion rate and acid consumption calculations

Appendix C: Publications and conference proceedings from this work.

CHAPTER 2

LITERATURE REVIEW

2.1. HYDROFLUORIC ACID

2.1.1. Hydrofluoric acid production

Hydrofluoric acid is commercially manufactured by the reaction of fluorspar (CaF_2) with sulphuric acid (H_2SO_4) in a rotary tube furnace, which then produces HF as a gas product (Equation 1.2). The HF is then washed, condensed and distilled to produce an anhydrous acid (AHF) to which water is added to produce the final aqueous product (AqHF) for sale (Craig & Anderson, 1994; "HF production-Eurofluor," 2017; Kennedy, 1990). Worldwide this process route is similar to as shown in Figure 2.1. The Pelchem SOC Ltd. is the only commissioned fluorine plant in the southern hemisphere, and exports HF products and other fluorochemicals internationally (Pelchem, 2014).

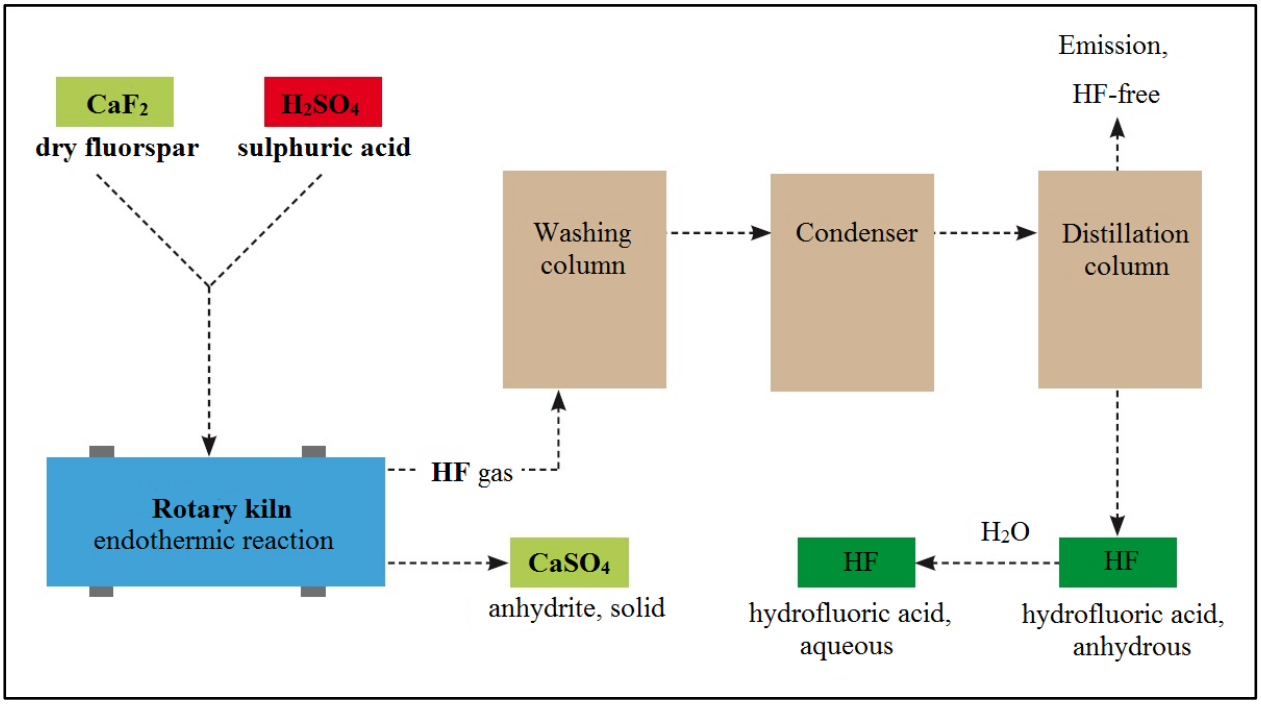

Figure 2.1: General HF production flow sheet (Eurofluor, 2017).

2.1.2. Market for hydrofluoric acid

Hydrofluoric acid is primarily used in the petroleum refining, glass etching and the metallurgical industries (Genuino *et al.*, 2012). It is also used in the production of electronics, pharmaceuticals, agrochemicals and consumer products such as detergents and toothpastes. Since HF dissolves most oxides and silicates it has some specialized applications in scientific research, such as extracting organic fossils and isolating mineral stabilized soil in organic matter (Riding & Kyffin-Hughes, 2010; Sanderman *et al.*, 2017). However, despite the inherent danger of using HF, it is still used in domestic applications such as in the car wash industry (Genuino *et al.*, 2012).

In the nuclear industry, HF, along with fluorine gas, F_2, is used in the uranium enrichment process (Hore-Lacy, 2016). Yellow cake uranium (milled U_3O_8) is dissolved in HNO_3 to produce uranyl nitrate, $UO_2(NO_3)_2$, which is then treated with ammonium diuranate, $(NH_4)_2U_2O_7$, and is subsequently reduced with hydrogen to produce uranium dioxide, UO_2. Reaction of this uranium oxide with HF produces uranium tetrafluoride, UF_4, which is then converted to uranium hexafluoride, UF_6, using F_2. In the nuclear fuel cycle, UF_6 is centrifuged to separate radioactive (fissile) uranium isotopes from non-radioactive (fertile) uranium. This gave the need for the fluorine plant to be commissioned at the South African Nuclear Energy Corporation (Necsa) in 1976 (Pelchem, 2014). Since then, development of the nuclear fuel cycle at Necsa has been placed on hold, and instead the HF production plant built in 1984 produces HF and other fluorochemicals on commercial bases, trading as Pelchem (SOC) Ltd., a subsidiary of Necsa.

Pelchem (SOC) Ltd. produces two HF products:

- high purity AHF, which is diluted to the required grade and typically sold as an export product, and
- 70% industrial grade, which is sold to local stainless steel manufacturers.

In the event of a shortfall in 70% industrial grade HF, AHF is diluted to AqHF and sold as technical Grade (Valkenburgh, 2012a). Since HNO_3 is added to the pickling mixture for the descaling and passivation of stainless steel anyway, the quality of the industrial grade HF sold by Pelchem (SOC) Ltd. is often inconsequential.

2.1.3. Metallurgical importance

In the metallurgical industry specifically, HF finds huge application in metal extraction, metal manufacturing and metal processing, as well as to a lesser extent in fluxing and refining agents (Eurofluor, 2018). Hydrofluoric acid is also used in manufacturing Teflon, which is widely applied as a protective, non-stick coating for metal surfaces. In metal extraction, HF is specifically used in the selective separation of tantalum and niobium from mineral ores (El Hussaini & Rice, 2004). In metal manufacturing, HF is used to produce sodium aluminium fluoride which is an essential part of the electrolyte used to produce pure aluminium from bauxide ($Al_2O_3 \cdot 2H_2O$) by means of electrolysis (Mohanty, 2003; Walter, 1937).

In metal processing, HF is essential to surface treatment of steels and metallic alloys. Here a mixture of HF is used with HNO_3, in a process known as pickling, to remove unwanted oxides and mill scale from the stainless steel surfaces prior to final annealing (Crookes, 2007). The passive layer essential to the corrosion resistance of stainless steel is formed during the passivation step. This passivation of the stainless steel surface is initiated during the pickling process, which is due the oxidizing acid (HNO_3) in solution. Depending on the thickness of the oxide film desired, the final passivation treatment may require additional heating and a supply of oxygen to improve the corrosion resistance. This additional treatment is applicable to specific grades of stainless steels manufactured for construction for application in areas with restricted oxygen supply coupled with unpredictable corrosive conditions (Crookes, 2007).

2.2. CORROSION AND METALLURGY

2.2.1. Corrosion

Corrosion is conventionally defined as the undesirable deterioration of a material through a reaction with its environment (Jones, 1996). This implies that any material can undergo corrosion. Since metals are conductive, their corrosion involves electrochemical reactions and therefore they deteriorate differently from non-conducting materials such as ceramics or plastics. Steels and metallic alloys form stable chemical compounds after corrosive attack by their environment to produce corrosion products which are similar to minerals found in nature (McEwan, 2004; Davis, 2000). In the most common corrosion reaction, iron in steel reacts with moisture, H_2O, and oxygen, O_2, in air to produce an iron hydroxide as per the two half reactions, Equations 2.1 and 2.2:

$$Fe \rightarrow Fe^{2+} + 2e^{-}$$ Equation 2.1

and

$$O_2 + 2H_2O + 4e^{-} \rightarrow 4OH^{-}$$ Equation 2.2

which produces rust in the form of iron hydroxide, $Fe(OH)_2$, as per Equation 2.3.

$$2Fe^{2+} + 4OH^{-} \rightleftharpoons 2Fe(OH)_2$$ Equation 2.3

The mechanism by which the atmospheric corrosion of mild steel in a moist environment takes place follows four distinctive steps as illustrated in Figure 2.2. In the illustration, the corrosion of the steel follows the steps 1 - 4 anticlockwise as follows:

1. Iron is oxidized on the steel surface following an anodic reaction (Equation 2.1) and metal is physically lost by the steel matrix.
2. Electrons (e^-) released during the anodic reaction flow through the conducting steel substrate to the point of oxidation. Electron flow can be measured in terms of current (I) and will exclusively flow through the metal if the water in contact with the steel surface is non-conductive.
3. The free-moving electrons are used by the cathodic reaction (Equation 2.2) to reduce O_2 and produce a hydroxide ion (OH^-) at the point of corrosion.
4. The electrochemical reaction is then completed, since a circuit is formed between the anodic and cathodic sites whereby current can flow through the water on the steel surface. In this instance, the OH^- formed (Equation 2.2) dissolves in the originally non-conducting water and completes the electrical circuit.

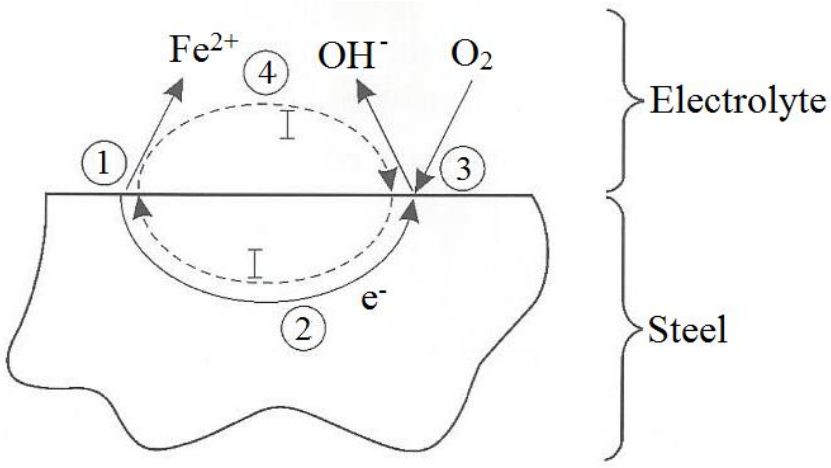

Figure 2.2: Schematic representation of the corrosion mechanism of a steel surface in contact with an electrolyte accompanied by sub-reactions and corresponding steps (1-4) taking place during corrosion (Adapted from McEwan, 2004).

Other steels and metallic alloys also follow the same mechanism when corroding in the presence of an electrolyte. Consequently, for corrosion to occur and then propagate, each of these sub-reactions need to proceed simultaneously (McEwan, 2004). Therefore, by understanding these basic mechanisms involved in the corrosion of steels and metallic alloys, it is possible for metallurgists and corrosion engineers to manipulate any one of the four steps to inhibit, slow down or prevent corrosion of a steel or metallic alloy used as construction materials in an industrial plant (Davis, 2000; Baboian, 2005).

Corrosion is the reverse form of extractive metallurgy, since it essentially is the process of returning a steel or metallic alloy back to its natural state (Jones, 2014). During atmospheric corrosion, the natural state to which mild steel returns is typically hydrated oxides (Equation 2.3), which can lose water when drying to form layers of ferric oxides (ASM Handbook, 1987). These corrosion products form a uniform rust film on the steel substrate which isolates the steel from the corrosive environment and slows down the corrosion rate. However, these hydroxide and oxide corrosion films are not stable or tightly adherent to the underlying steel surface and easily erode (spallation), which causes continual mass loss from the steel surface.

In concentrated HF (≥70% AqHF), mild steel forms an insoluble iron-fluoride film that resists erosion-corrosion at HF flow velocities of up to 0.6 m/s in pipes and containers within an HF plant (Jennings, 2007). The iron-fluoride film improves the erosion-corrosion resistance of mild steel in service better than ferric oxides and hydroxides in atmospheric conditions. Moreover, under non-flow (HF storage) conditions, the fluoride scale builds up and densifies to improve the isolation of the mild steel shell from the HF corrosive environment, effectively extending its service life (Jones & Pujadó, 2008). However, this is assuming only uniform corrosion occurs.

2.2.2. Leaching

In hydrometallurgy, leaching is the process of dissolution of valuable metals minerals from an ore by an aqueous solution of the leaching agent (Jackson, 1986; Young, 2008). Here, the leaching agent is known as the lixiviant, which is the liquid medium employed to selectively extract the desired metal from the ore (Jackson, 1986; Van der Merwe, 2010). During this extractive metallurgical technique, more soluble metals in the ore are converted to soluble salts in the aqueous solution, which can be precipitated out as a result, from dilution or addition of a reagent to the pregnant solution.

During uniform corrosion, metals can be uniformly removed from an alloy surface, while during dealloying (Figure 2.3), it is possible that some metallic constituents are preferentially dissolved

from the alloy matrix in a corrosive solution (Kaesche, 2003; Li *et al.*, 2015). The type of corrosion that applies is also dependent on the lixiviant used. For instance, gold cannot dissolve in any of the strong acids (such as HF, HNO_3 or HCl) at any concentration, but a mixture of HNO_3 and HCl creates an extremely corrosive solution that can easily dissolve gold, and even other noble metals such a platinum, ruthenium and rhodium (Craig & Anderson, 1994; Gökelma *et al.*, 2016). Therefore, adding a second acid to an HF product stream could alter the known corrosive characteristics of the product solution and increase the total amount of metal removed from an alloy, or corroded preferentially to a specific elements from the steel and metallic alloys used as construction materials in a plant.

By studying the metal removal rate of alloys used at the plant, when submerged in HF dosed with varying quantities of HNO_3, it is possible to define the corrosion of the different metals in terms of reaction kinetics. In leaching experiments, dissolution rates are measured by the concentration of a metallic species found in the pregnant solution with increase in residence time (Van Der Merwe & Kasaini, 2011). In the corrosion experiments, the same applies, since metallic coupons are submerged in a corrosive solution and the concentration of the metallic species corroded out over the contact time with the coupon surface, can be determined from ICP (inductively coupled plasma) analyses of the final solution. In a closed system, mass loss by a coupon is directly proportional to the mass of metal gained by a corrosion solution, which makes the use of reaction kinetics applicable to corrosion studies (Jackson, 1986; Bingöl & Canbazoğlu, 2004; Han *et al.*, 2017). After a leaching experiment, if a pregnant solution is found to have a higher concentration of one metallic species in solution relative to others, the removal rate for that metal was automatically higher, which infers that it was preferentially leached.

2.3. OXIDATION OF METALS

2.3.1. Oxygen in acid

Virtually all metals and alloys corrode with an increase in temperature (Khanna, 2002; Young, 2016). This is because oxidation is a chemical reaction in which a metal's oxidation state is increased by the formation of thermodynamically stable compounds such as oxides, fluorides and nitrides by contact with gasses (e.g. Equation 2.1) or in solution (e.g. Equation 1.1). A successful corrosion resistant alloy is one in which the steady state oxidation reaction is prolonged, so that the lifetime of the alloy within a specific corrosive environment is extended (Khanna, 2002; Young, 2016). Thus, all metals corrode, just at different rates (McEwan, 2004;

Jones, 2014) and those alloys that maintain a slow steady state corrosion reaction with its environment last longer (Khanna, 2002; Young, 2016). Increasing the temperature adds heat to a system, which in turn adds energy to the oxidation reaction and results in a reduction in the corrosion resistance of an alloy in service. Similarly, increasing contact of an alloy with an oxidizing agent (e.g. O_2, HNO_3 or HCl) would shift the local equilibrium from a metal system towards an alloy-oxidant system, which signifies the corrosion reaction being driven forward and hence the reaction rate increases.

The way to utilize nickel-based alloys (Monel), which have proven to be inherently resistant to HF (Craig & Anderson, 1994), is to keep dissolved oxygen levels low. Limiting access of the oxidizing agent to the surface of the alloy in HF would ultimately interrupt the corrosion circuit (as discussed in Section 2.21). In this way, nickel-copper alloys (Alloy 400 series) have been successfully used in air-free HF immersion conditions in the AHF production industry at temperatures up to 150ºC (Jennings, 2007). However, at the liquid-air interface, oxygen does dissolve slightly in the acid, which allows for localized attack of these nickel alloys at the liquid level.

In Monel 400 (33 wt% Cu) alloys, stress corrosion cracking in the vapour phase above the liquid level is due to the enrichment of a thin layer of aqueous HF in the vapour with copper fluoride corrosion products, which is oxidized to cupric fluoride due to the higher oxygen concentration there (Craig & Anderson, 1994). Cupric fluoride concentrating in the vapour phase results in a dilution of CuF_2 in the liquid phase, which along with possible segregation of sulphur on grain boundaries in the alloy (Katsamas et al., 2004), makes the alloy more susceptible to corrosion. The reduction of CuF_2 in the liquid phase means less absorption of the fluorides on the alloy surface under the liquid level, which is needed to lower the fracture stress of the alloy operating in HF. The internal stress comes from the operating stress field in the tube walls, which can be attributed to the presence of residual stresses that occur when no stress relief annealing is performed after deformation (Katsamas et al., 2004). The corrosion of Monel in HF is thus accelerated by aeration, O_2, combined with the effect of cupric fluoride depletion at the vapour-liquid interface, which increases corrosion at an already stressed localized environment on the alloy to prompt SCC. Residual stresses in Monel 400 tubes (similar to being used at the Pelchem plant, Figure 2.4) may originate from the in situ bend forming of the tubes during assembly in the production line, which provides a driving force for crack growth from where the SCC (stress corrosion cracking) initiates (Katsamas et al., 2004). To increase resistance of nickel alloy to SCC prior to commissioning, they are passivated at 49ºC exposed to air-free AHF for 24 h (Jennings, 2007).

2.3.2. Passivation

Passivation is a general term used to describe the phenomenon of being resistant and shielded against a corrosive environment. By treating or coating a metal surface, its chemical reactivity is decreased and so the corrosion resistance of an alloy is improved by separating the metal surface from the aggressive environment (Gildenpfennig *et al.*, 2003). Passivation occurs when a thin, stable compound (such as an oxide or fluoride) layer is formed on the surface of an alloy to create a protective barrier (Nazri *et al.*, 1981; Lutton & Scully, 2017). For stainless steel, passivation is specifically attributed to the high chromium enrichment of a steel (>10.5 wt% Cr), which forms an oxide layer through the exposure of the steel surface to oxygen (Crookes, 2007; Zhang *et al.*, 2017). In Monel 400, passivation is accredited to the chemical inertness of the nickel alloys combined with passive film formation (Singh & Gupta, 2001). Thus, the ways in which steels passivate are different from the passivation mechanisms of nickel alloys in corrosive environments.

Passivation of steels

As established in Section 2.2, the passivation of mild steel in concentrated HF (>60% mass per volume) is through the formation of an oxide or fluoride scale layer, which improves the corrosion resistance of the metal in the HF production industry (Whitaker, 1950).

Passivation of stainless steel is dynamic as it involves a constant supply of oxygen for the formation of a passive film for its superior corrosion resistance. The thin oxide film being on the alloy surface is typically between 1-3 nm thick, with the growth of this passive film being dependent on the alloying elements present in the steel and the type of corrosive environment surrounding the steel (Olsson & Landolt, 2003). The passive film growth and formation for stainless steels is mostly dependent on the chromium component in stainless steel, as the passive layer is typically composed of soluble chromium and iron oxides when in acid solutions. The nickel component in austenitic stainless steels does not readily oxidise and stays closer to the metal surface at the metal-oxide interface, where it serves to lower the dissolution of chromium and iron into the passive film (Olsson & Landolt, 2003). The addition of molybdenum to stainless steel improves pitting corrosion resistance, as it not only assists in the diffusion control of hydrogen release from the metal (e.g. Equations 1.1 and 2.3), but also forms molybdenum oxides which contribute to the passive film structure on the steel (Falkenberg *et al.*, 2001; Olsson & Landolt, 2003).

Stainless steel 904 L contains approximately 2 wt% more chromium (~20%) and nearly double the amount of nickel and molybdenum than the more common 316 grade stainless steel (Nage &

Raja, 2006). The 904 L series also contains up to 2 wt% copper, which has proven to assist with the re-establishing and regulation of the passive film of stainless steels exposed to HF solutions (Li *et al.*, 2015). This is because copper segregates to the passive film during corrosion and formation of the passive film. Like stainless steels, the chromium-bearing nickel alloys (Table 2.1) passivate by forming an oxide film on the surface of the alloy and have been used in valves, piping and tubing in AHF production in more oxidizing conditions (Jennings, 2007).

The passive films on stainless steels are not static, and can grow by initially absorbing ions from a changing corrosive environment to form haphazardly on the steel surface. However, passive films have consistently been shown to thicken, with the oxide molecules having a more ordered structure in the film with increased exposure time to oxidizing conditions (Olsson & Landolt, 2003). Thus in a corrosive oxidizing (or oxygen rich) environment, a passive film can grow in an HF solution, but time is necessary for the steel to eventually demonstrate improved corrosion resistance in service.

Passivation of nickel alloys

Noble metals, such as gold, platinum and ruthenium, are characterized as being chemically inert due to their lack of participation in chemical reactions with their environment (Jackson, 1986; Gökelma *et al.*, 2016). This does not mean these metals do not corrode, only that they corrode at a much lower rate in a corrosive environment (McEwan, 2004; Young, 2016). The surfaces of these metals do not passivate in the same way as steels and nickel-based alloys. However, the nickel-rich alloys, such as Monel 400 alloy, has the capacity to both be inherently corrosion resistant and passivate through film formation, depending on the corrosive environment it is in (Singh & Gupta, 2001). Electrochemical corrosion studies of Monel 400 in phosphoric acid, H_3PO_4, acetic acid, CH_3COOH, formic acid, HCOOH, and H_2SO_4 attributed the superior corrosion resistance of the nickel alloy to its chemical inertness (Singh & Gupta, 2001).

Its inherent corrosion resistance has justified the use of Monel 400 in HF alkylation units, distillation columns, heaters, recovery towers, pumps and valves in the HF industry, but only when small amounts of water were present in the air-free HF product streams (Jennings, 2007). In acid mixtures, Monel 400 has shown active, and trans-passive behaviour during which the metal surface would show signs of corrosion pits which were covered with a thin film of hydrated salt and oxides (Singh & Gupta, 2001). Therefore, Monel has an inherent corrosion resistance in the HF industry, but when exposed to mixed acid solutions or oxidizing conditions, it can form an oxide film. However, this hydrated salt and oxide layer does not serve the same

protective purpose as a fluoride scale on mild steel, or oxide film on stainless steel, as it sustains pitting corrosion, intergranular corrosion and SCC under certain conditions.

2.4. HYDROFLUORIC ACID PLANT CORROSION

2.4.1. Hydrofluoric acid corrosion in the international industry

Corrosion typically associated with the materials used in the handling, storage and distribution of commercial grades of HF has been well documented by the NACE international task Group 358 chaired by Jennings (2007). This made it possible to identify the types of corrosion that would take place within a typical HF plant, when specific steels or metal alloys are used within designated sections of an HF production plant (Figure 2.1). In general, the types of corrosion of metallic components, used in most industries or chemical production environments (Jones, 1996), are schematically presented in Figure 2.3. Of these, eight forms of corrosion were found to be applicable to the HF industry, with cases of each type of corrosion experienced at a HF plant, or facility using HF, provided.

Uniform corrosion

Uniform or general corrosion of low carbon steel is the most common form of corrosion in an HF plant and is the most prevalent form of corrosion in stationary HF tanks. Uniform corrosion is the continuous and consistent removal of metal from the whole surface exposed to an atmosphere or corrosive solution (Jones, 1996). This form of corrosion is easily the least undesired form of corrosion, since it is relatively slow, predictable and can be monitored accurately, therefore mitigation can be achieved by design (Jennings, 2007). The use of carbon steel in the HF industry depends on the formation of an insoluble iron-fluoride film, which occurs through the uniform corrosion of the steel surface when exposed to AHF or HF fumes for up to 24 h (Craig & Anderson, 1994; Jennings, 2007; Whitaker, 1950). However, uniform corrosion in HF only occurs by itself if the composition of the carbon steel is homogeneous with very low residual elements such as Cr, Ni, Cu and C (Gysbers *et al.*, 2003), since higher quantities of these elements would lead to galvanic corrosion.

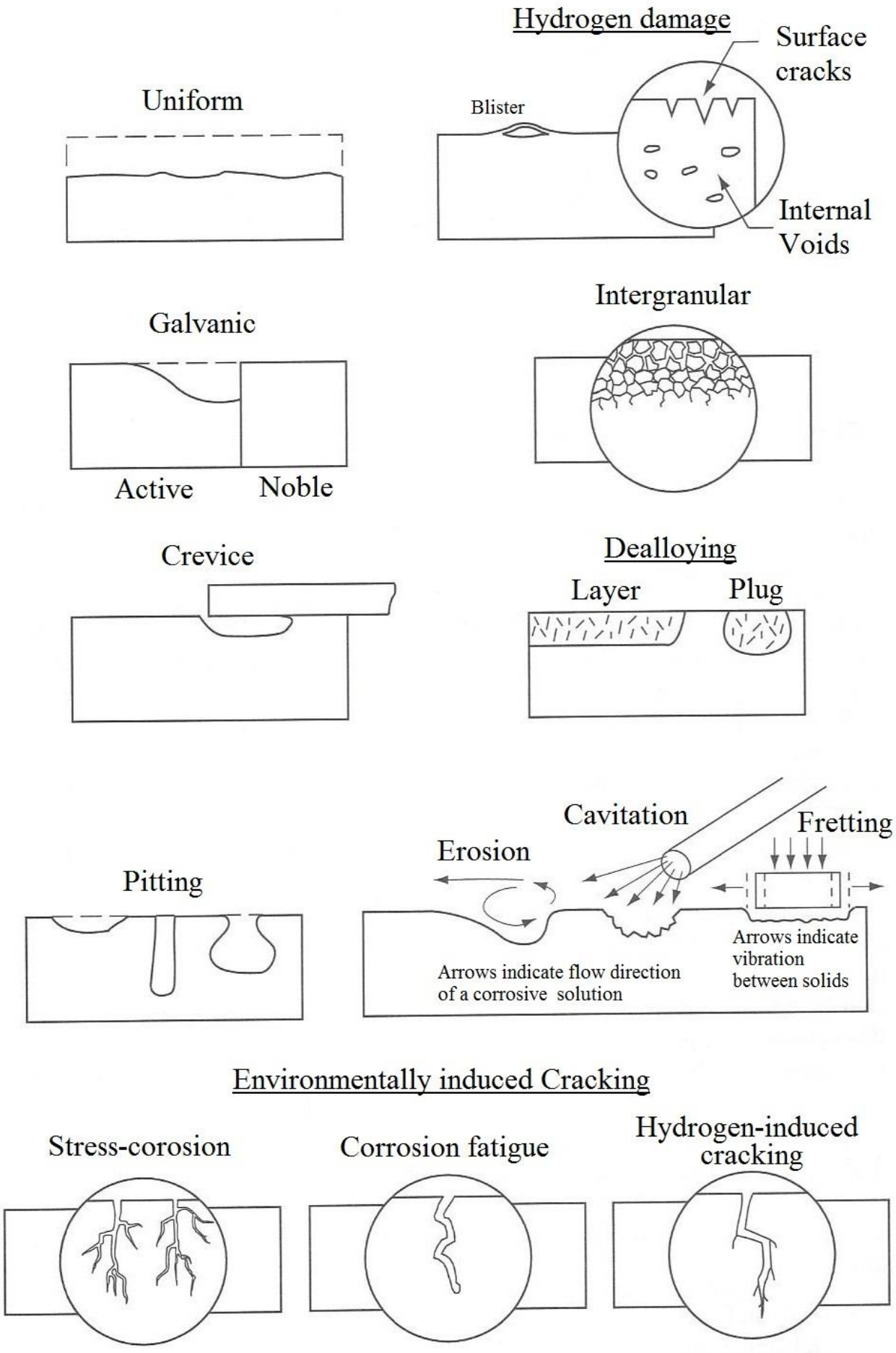

Figure 2.3: Schematic summary of types of metallic corrosion (Adapted from Jones (1996)).

Galvanic corrosion

Galvanic corrosion occurs due to dissimilar alloys being coupled in the presence of an electrolyte (e.g. AqHF), and thus iron will corrode preferentially in a steel matrix to more noble (more positive on the galvanic series) metals present. When elements, such as Cr, Ni and Cu, are in excess of 0.2% in low carbon steel, galvanic corrosion is applicable when operating in AHF at temperatures greater than 66ºC (Annual Book of ASTM standards, 2009). Galvanic dissolution is also certain to occur within the HAZ where steels are directly welded to nickel alloys within a HF plant (Blanchard Jr. & Mack, 1992).

Erosion corrosion

Erosion-corrosion of mild steel in flowing HF can be due to velocity, turbulence or impingement of the corrosive solution or suspended slurries. In these conditions, the formation of the protective fluoride films becomes essential, since the substrate avoids excess corrosion by this type of corrosion (Jennings, 2001). Stagnant or slow-flowing acid will cause uniform corrosion, but rapid movement of the corrosive HF physically erodes away any protective barrier (Jones, 2014). Nickel-rich alloys (>30 wt% Ni) have proven to be resistant to corrosion in flowing AHF and AqHF and are therefore preferred for use in components such as valves, tubing and in pumps to any other alloys in HF production circuits (Craig & Anderson, 1994).

Hydrogen damage

Hydrogen damage, such as blistering, typically occurs when hydrogen accumulates at non-metallic inclusions of steel in contact with a corrosive solution, in which the evolution of H^+ into the process is very high (Li *et al.*, 2017; Rosenberg & Sinaiova, 2017). Hydrogen evolving from the HF occurs through the reaction (Equation 2.4):

$$2H^+ + 2e^- \rightleftharpoons H_2 \qquad \text{Equation 2.4}$$

Hydrogen evolution is associated with corrosion in AHF and 60% AqHF (Whitaker, 1950) which can cause hydrogen stress cracking (HCS), hydrogen induced cracking (HIC) and then stress orientated HIC as shown in Figure 2.2. The use of cleaner (fewer non-metallic inclusions), normalized steels minimizes hydrogen damage (NACE International, 2003; Jennings, 2007), while maintaining the operating temperature at below 150ºC reduces the potential for hydrogen evolution (Equation 2.4).

Dealloying

During the dealloying form of corrosion, the major element in an alloy is likely to be preferentially corroded (Jones, 2014). This makes this corrosion process identical to the

hydrometallurgy extraction process in that selective leaching of one metal to another takes place. De-nickelification of copper nickel alloys in the presence of oxygen in HF is possible (Davis, 2000; Saldanha, 2000).

Crevice corrosion

Crevice corrosion can occur for non-metallic materials, or parts of the same steel or metallic alloy, forming a sheltered volume with a metallic material on the metal surface (Jones, 1996; Lazzari, 2017). At the Harshaw Chemical Company, slight pitting of a nickel pipe was observed, which was used to carry fluorine at 600ºC, and was later attributed to crevice corrosion caused by local organic contamination of the surface of the pipe (Whitaker, 1950). More recently, in other HF production streams, these corrosive crevices can occur between insoluble deposits, non-metallic gaskets or fasteners (Jennings, 2007). Crevice corrosion in HF process streams can be minimized by the use of seamless steel pipes and eliminating flange joints (Jennings, 2007).

Intergranular corrosion

Intergranular corrosion occurs when reactive impurities segregate at grain boundaries of an alloy (Campbell, 2008), or when grain boundaries become depleted of passivating elements such a chromium (Jones, 2014). In an HF plant where nickel-based alloys are used, HF vapours containing oxygen can oxidize cuprous fluoride, CuF, to cupric fluoride, CuF_2, which may lead to intergranular corrosion, as well as stress corrosion cracking (SCC) (Rebak *et al.*, 2001).

Pitting corrosion

Pitting corrosion occurs when the protective film on a metal surface breaks down at isolated sites, and therefore mostly occurs when the corrosion resistance of a steels or metallic alloy is increased by the presence of an oxide film (Richardson *et al.*, 2009; Garverick, 1994). Pitting corrosion is not often observed in an HF plant due to the initial material selection which has been specifically based on a high pitting resistance at high temperatures (Whitaker, 1950; Horn *et al.*, 1992) and because restricted contact with air is maintained in the production process (Valkenburgh, 2013). However, pitting of Monel tubes used in heat exchangers has been observed in processes using HF concentrations in excess of 75% at 130ºC during the production of UF_4 (Hill & Knott, 1960). Pitting corrosion in this process was due to the condensation of HF during the heat-up cycle and the oxygen content in the HF stream being in excess of 1000 ppm (Hill & Knott, 1960; Mannan & Lees, 2005). In baths where HF and H_2SO_4 are used for the pickling of specialized grades of steel, nickel-based alloys containing chromium have also been found to pit (Nickel Development Institute, 2017).

The pitting resistance equivalent (PRE) is an empirical formula determined from salt water, containing dissolved chlorides and oxygen, in contact with various stainless steels (Ahmad, 2006). The higher the PRE for an alloyed austenitic stainless steel, the greater its resistance to localized attack, like pitting and crevice corrosion (Cleland, 1996). When nitrogen is a deliberate alloying element, the pitting resistance equivalent number (PREN) for an alloy can be determined using Equation 2.5:

$$PREN = W_{Cr} + 3.3\,(W_{Mo} + 0.5W_w) + 16_N \qquad \text{Equation 2.5}$$

where W_{Cr} , W_{Mo}, W_W and W_N (wt%) are the percentages of chromium, molybdenum, tungsten and nitrogen respectively - per the total composition of the steel, as it exists in the ISO standard 15156-3 (Lyons *et al.*, 2016). PRENs can be used to compare the pitting resistances of various stainless steels in a corrosive environment. However, the relationship (Equation 2.5) does not serve as a good predictor of relative ranking when nickel alloys are being compared (Lyons *et al.*, 2016). The PREN factor is thus a rough estimate (Ahmad, 2006) and using it as an aid in materials selection in the HF industry carries a high risk (Cleland, 1996).

2.4.2. Hydrofluoric acid corrosion in the South African industry

2.4.2.1. Corrosion failure at Pelchem

The uniform corrosion of tanks and components in any plant producing hydrofluoric acid is well-known (ASM Handbook, 1987; Craig & Anderson, 1994; Jones, 1996) and can be feasibly measured and provisioned by designing for corrosion control (McEwan, 2004). However, since sulphuric acid with sufficiently low levels of HNO_3 (<50 ppm) became less readily available locally, alternative sources of the reactant needed to be considered (Valkenburgh, 2013). Thus, substituting H_2SO_4 introduced into the plant feed stream was without consideration of the potential effect on the corrosion characteristics of the steels and alloys used as construction materials at the plant. A lower quality H_2SO_4 produces an HF product contaminated with corrosive impurities and its effects on the lifecycle of materials used within the production plant and storage tanks becomes unpredictable. For instance, opting for alternative sources of H_2SO_4 for the production of technical grade HF at Pelchem's HF plant was due to the closure of larger manufacturers, or in some instances, these companies choosing to produce smaller volumes of H_2SO_4. This was because the tower plant process (the replacement for the lead chamber process) became preferred, which inherently produces an inferior product with higher HNO_3 levels (Valkenburgh, 2012b).

Low cost sulphuric acid derived from sulphur or sulphur dioxide containing effluent streams, obtained from metal smelters were regularly used in HF production plants in South Africa (Valkenburgh, 2012c). However, after 2010 the use of nitrogen oxide as a more cost effective catalyst became more popular in the production of H_2SO_4, and subsequently, the H_2SO_4 from this process was used as an alternative feed material to the HF production plant (Valkenburgh, 2012b). Depending on the process technology used to produce the sulphuric acid, different impurities can be present. Similarly, with natural resources of fluorspar becoming depleted, alternative sources of fluoride reserves are being considered worldwide, and has the same propensity to be fed into an HF plant, without appreciating the potential impact on the corrosion characteristics of the materials used there (Garverick, 1994). Thus, each new chemical and fluorine source has a relatively unknown history, and although it is still possible to effectively produce hydrofluoric acid, the new corrosion conditions might no longer be predictable in the current plants and could lead to high corrosion rates. With each new chemical introduced to the plant, the probability of more impurities which enhance the corrosiveness of the acid flowing through the plant circuit increases.

One impurity which has been identified in the HF solution is HNO_3. The Pelchem HF plant at Necsa had a dramatic increase in the corrosion of the steels and alloys used in the plant between December 2011 and July 2012 (Valkenburgh, 2012d). The severe increase in the corrosion rate of the mild steel shell, from >1 mm/y to approximately 48 mm/y (20 mm wall thickness loss in 5 months), of the sulphuric acid storage containers was eventually traced back to the nitric acid content of the supposedly pure H_2SO_4, which was measured in the range of 1800 to 2800 ppm. This was 36 – 56 times higher than the accepted 50 ppm limit (Valkenburgh, 2012b). The higher HNO_3 content H_2SO_4 was pumped to the HF plant where it was used to manufacture industrial and technical grade hydrofluoric acid and the HNO_3 collected downstream (after distillation). This caused the mild steel shell to corrode at a rate of 30 mm/y in the liquid phase of the HF storage containers designated for local distribution and sales.

Valkenburgh (2012b) found that the HNO_3 present in the sulphuric acid (98%) feed, had concentrated in the 70% HF products downstream and attacked the protective scale layer of the steel with which it was in contact. This allowed HF to attack the exposed steel and typically form FeF_2, from the reaction with the steel liner (Garverick, 1994) to form a scale layer again (Whitaker, 1950). Subsequently, rapid dissolution of the vulnerable underlying metal surface occurred, which greatly reduced the service lifetime of the equipment. The higher quantity of nitric acid present (>50 ppm) was traced back to the new supplier which manufactured sulphuric acid from liquid steam, instead of flue gas (Valkenburgh, 2012b). This alternative method uses a

liquid oxidation process of nitrosylsulphuric acid, $NOHSO_4$, to convert steam containing SO_2 to H_2SO_4.Thus the use of $NOHSO_4$ essentially increases the nitrogen content of the H_2SO_4 product more than what is producible from smelter flue gas converted only over a vanadium pentoxide catalyst.

Thus, the H_2SO_4 produced using $NOHSO_4$ had a higher HNO_3 content (>50 ppm), which when used to react with CaF at Pelchem, produced a contaminated 70% HF technical grade product (up to 1% HNO_3). This additional HNO_3 changed the corrosion characteristics of the steels and alloys in use at the plant, and how it would affect their service life of the HF storage tanks could not be predicted. The oxidation characteristics of high concentrations of HNO_3 with low concentrations of HF on stainless steel surface treatment are well documented, since HF-HNO_3 mixtures are essentially pickling solution (Davis, 1994; Schillmoller, 1995; Gildenpfennig *et al.*, 2003; Crookes, 2007; Liu *et al.*, 2015). Though, while a study exist on the effects of low levels of nitric acid on the corrosion of steels in sulphuric acid (Andersen *et al.*, 1980), no published data were found on the oxidation characteristics of high HF concentrations with low HNO_3 concentrations.

2.4.2.2. On site HF plant examinations

Since there was no available data, specific to the Pelchem plant, on the corrosion characteristics of mild steel in 70% HF contaminated with HNO_3, some preliminary onsite investigations were conducted. Excessive corrosion of Monel and mild steel equipment in the HF industry circuit of the Pelchem plant was first reported in June 2012 (Valkenburgh, 2012e). The abnormally high corrosion rates were first noticed in the 70% HF carbon steel storage tanks (V1460 and V1461), as well as the Monel and carbon steel dip pipes (Figure 2.4) and not in the tanks used for transporting AqHF (Figure 2.5). This was since the export grade HF products (AqHF) were tapped from the top of the first HF distillations and impurities accumulated into the bottom products of the last distillation (Industrial grade HF).

a  b 

Figure 2.4: (a) Corrosion in the liquid phase, and (b) in the vapour phase above HF liquid level of Monel dip tubes installed on March 2012 into Storage tanks V1460 and removed 2 weeks later due to excessive corrosion (Valkenburgh, 2012e).



Figure 2.5: HF storage tank loading and transportation facility located on site at Necsa.

It was first suspected that an oxidizing substance was introduced to the plant via the H_2SO_4 feedstock when in July 2012 it was reported that "red fumes" were observed in the industrial grade HF circuit (Valkenburgh, 2012d). This initial observation was suggested by the internal plant advisor to be presence of nitrous compounds (HNO_2 and HNO_3). Subsequently, corrosion pits became visible in the HF storage tank walls. The inspection personnel reported this as pitting corrosion (Valkenburgh, 2012d). The corrosion could not be measured or quantified accurately because pitting can occur at any point and is difficult to detect with wall thickness measurements (Valkenburgh, 2012d).

Although nitrous contamination was suspected, the extent of corrosion damage could not be predicted, because no published data on the corrosion rates of carbon steel in low HNO_3 concentrations mixed with 70% HF could be found. However, it was known that dilute nitric acid is severely corrosive to carbon steel, even in the absence of hydrofluoric acid (Craig & Anderson, 1994). To confirm this suspicion, a few elementary visual tests were conducted using pure iron powder to represent the steel used to manufacture the H_2SO_4 and HF storage tanks (Valkenburgh, 2012c). Sulphuric acid received from the supplier (Figure 2.6a) was mixed with the pure iron powder and compared to the same powder that was reacted with analytically pure grade H_2SO_4 (Valkenburgh, 2012c). Similar experiments were also attempted with the HF received from the technical and industrial HF products. The iron powder and acids were left to react for 3 days (Valkenburgh, 2012c) and visual inspection revealed that the H_2SO_4 received from the supplier (Figure 2.6a) reacted vigorously with the iron powder (Figure 2.7b), while the powder in the laboratory pure acid remained visually un-reacted (Figure 2.7a). At the time, together with the settling of large quantities of iron sulphate ($FeSO_4$) in the H_2SO_4 storage tankers on site (Figure 2.6b), this was sufficient to indicate the questionable quality of the H_2SO_4 supplied and the presence of an oxidizing agent in the feedstock. Conversely, the reactions of the HF solutions with the iron powder produced no conclusive visual results (Figure 2.8), because no colour change was apparent. Since it was a metallic powder reaction with the acid, it did not address the corrosive reaction with steel sheets covered with fluoride scale, which demonstrated the need for a detailed examination. With no published or quantitative corrosion data on the corrosivity of an oxidizing agent present, or no reliable methods to effectively analyse for the presence of nitric acid in HF above 70% concentration, it was decided that the carbon steel tanks would be evaluated and inspected for another six months (Valkenburgh, 2012c). This was the only option at that time, since there were no data from laboratory corrosion tests done at Pelchem prior to give comparative results.

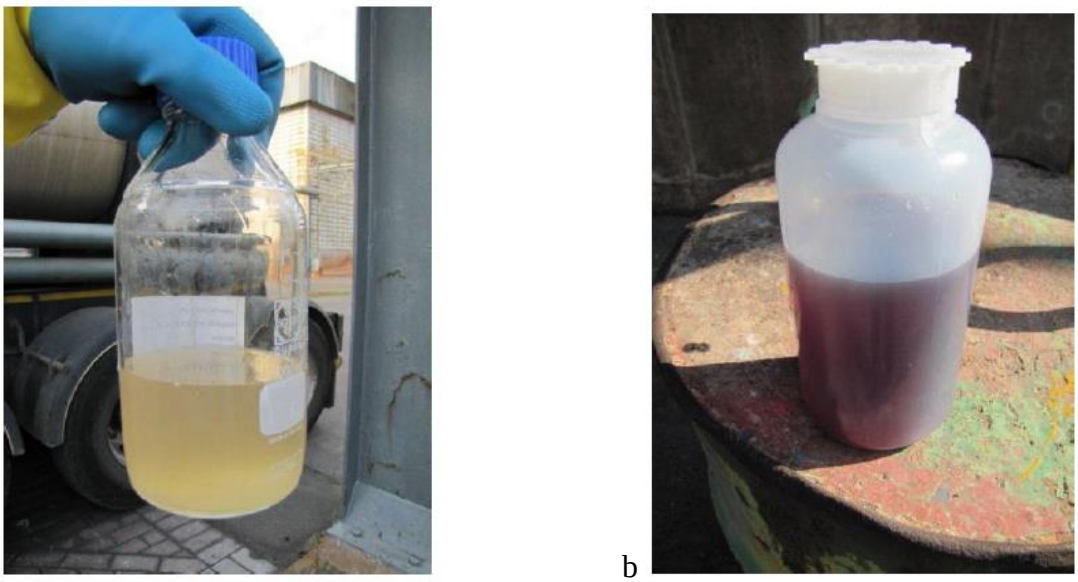

a b

Figure 2.6: (a) H_2SO_4 as-received from the supplier's tanker, and (b) H_2SO_4 from the bottom of the plant storage tanks where the impurity which settled out was predominantly $FeSO_4$ (Valkenburgh, 2012c).

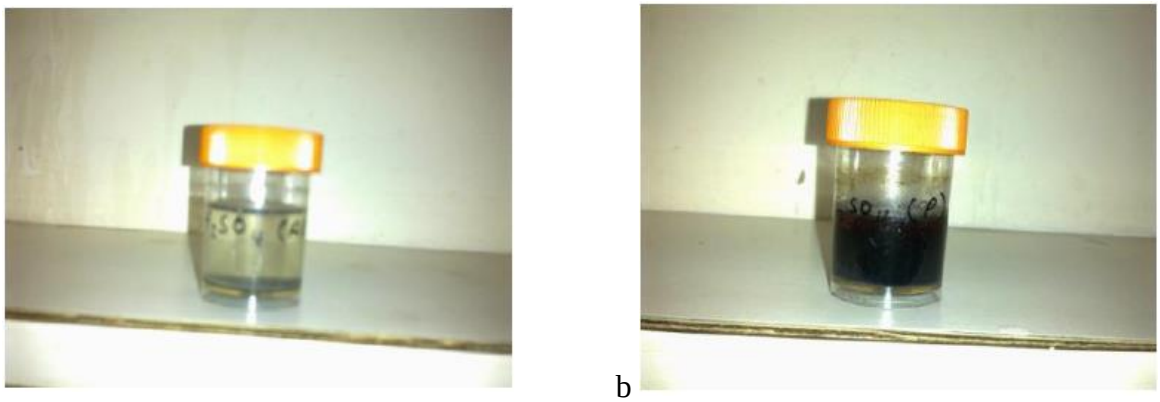

a b

Figure 2.7: (a) 98% Laboratory grade H_2SO_4 indicting no reaction with iron powder, and (b) H_2SO_4 from the supplier which had reacted to form a thick brown residue with the iron powder (Valkenburgh, 2012c).

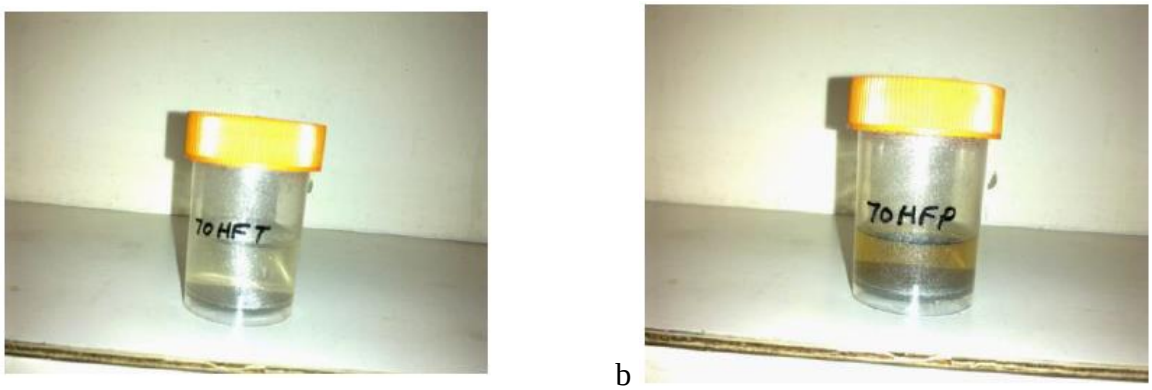

a b

Figure 2.8: (a) 70% technical grade HF indicating no visual reaction with iron powder, and (b) 70% industrial HF showing some visible reaction had occurred with the iron powder (Valkenburgh, 2012c).

From the on-site examinations the need do extensive laboratory corrosion tests to understand the impact HNO_3 contamination on the corrosion of steels and nickel alloys used at the HF plant, became apparent. Using visual characterizations techniques were fast, inexpensive and safe and gave a good indication where the focus needed to be to solve the corrosion problem. However, quantitative data was also needed to predict the corrosion trends and provide definite evidence to the corrosion mechanism. However, conducting laboratory corrosion experiments using 70% HF and successfully analysing the corrosion products had high safety risk implications. Hydrofluoric acid at any concentration is extremely dangerous, and its vapours are extremely hazardous and even fatal to workers. Moreover, HF dissolves silica and silicon in glassware, and typical corrosion set-ups (ASTM, 2009a) are not suitable, because the acid can attack and dissolve the glassware and ceramic probes needed to conduct the corrosion experiments. Furthermore, a high concentration of HF has large quantities of H^+ and F^- ions, which make it extremely difficult to analyse any other ions in solution when using Ion Chromatography (IC). This is due to the high charges associated with the higher concentration acids, which directly influences the accuracy and reproducibility of analyses during nitrate (NO_3^-) quantification in solution.

Considering these safety, experimental and analytical challenges when working with HF, it is often preferable to completely avoid most work related to the direct characterization of HF corrosion. Sulphuric acid is relatively easy to handle, use in experiments and analyse, and is stored in mild steel tanks similar to HF, which also experience corrosion problems associated with impurities in industry (Andersen *et al.*, 1980). Similar to HF, H_2SO_4 is also a reducing acid which produces a passive corrosion layer ($FeSO_4$) on the steel shell which protects the steel, and is also vulnerable to attack from impurities present. These similarities make H_2SO_4 an alternative option to study the effects additional impurities on corrosion in an HF plant (Valkenburgh, 2012c). However, due to the great difference between corrosion rates of the HF and H_2SO_4 storage tanks at the Pelchem plant, the corrosion rates affected by HNO_3 as an impurity in the technical grade HF stream was the priority in the current study.

2.4.2.3. Use of alternative alloys

Alternative steels and metal alloys, suggested by Valkenburgh (2013) to be more resistant to oxidizing acids, were recommended to Pelchem (Table 2.1). These alternative materials were initially considered for the HF plant based on their elemental compositions, microstructure, historic evaluations and economic feasibility (Valkenburgh, 2013). The principle on which the alloys were selected were their nickel and chromium contents, since these two elements play an essential role in the corrosion resistance of the alloys to HF in oxidizing media (Horn *et al.*,

1992). The chromium content in the SS 904 L (20 wt% Cr) contributes significantly to its superior corrosion resistance, by the formation of a protective oxide film, from contact with HNO_3 in a corrosive solution (Noh *et al.*, 2000; Liu *et al.*, 2015). Since the recommended metals all had higher chromium contents than Alloy 400 which was already in service at the plant (>24 wt% Cr), they could have had better corrosion resistances. Their higher chromium contents increased their respective PREN factors, compared to the metals currently used in industry, which theoretically endorses their improved relative pitting resistances (Ahmad, 2006; McGuire, 2008; Lyons *et al.*, 2016).

Table 2.1: Alternative steels and metal alloys considered by Pelchem for use in the HF plant (Valkenburgh, 2013).

Name	**Code / designation**	**Elements (wt%)**						**Supplier**
		Ni	**Cr**	**Mo**	**Fe**	**Cu**	**Mn**	
Alloy 31	X1 NiCrMoCu 32 28 7	31	27	7	32	-	-	VDM Metals (Thyssenkrup VDM, 2013)
Alloy 33	X1 CrNiMoCuN 33 32 1	31	33	2	32	1	-	VDM Metals (Thyssenkrup VDM, 2013)
Nirosta 4565S	X2 CrNiMnMoN 24 17 6 4	17	24	4	-	-	6	Woite edelstahl (M. Woite GmbH, 2017)

2.5. CORROSION OF STEEL AND OTHER METALLIC ALLOYS IN CONTAMINATED ACIDS

2.5.1. Mild steel corrosion in contaminated sulphuric acid

Andersen *et al.* (1980) studied the effect of oxidizing impurities on the corrosion of mild steel in concentrated H_2SO_4. Mild steel is used in the handling and storage of concentrated H_2SO_4 (80-98%). Similar to concentrated HF, pure H_2SO_4 forms a protective sulphate ($FeSO_4$) layer on the metal surface during passivation (Andersen *et al.*, 1980). Pure H_2SO_4 was regularly sourced from sulphur-bearing plants. However, with improvements in emission controls at sulphide smelters, more impurities were expected to be captured in the by-product acid, which would directly influence the quality of the H_2SO_4 produced and in turn the corrosion characteristics of the mild steel tanks holding it. Andersen *et al.* (1980) determined that, if above the sub-ppm range, oxidising impurities would decrease the corrosion resistance of mild steel used as construction materials in systems handling sulphuric acid. The impurities considered to affect the corrosion

resistance of mild steel in concentrated H_2SO_4 the most were nitrogen oxides (HNO_3), sulphur dioxide (SO_2) and ferric ions.

Along with each impurity identified, SO_2, ferric sulphate, $Fe_2(SO_4)_3$, and HNO_3 (up to 1400 ppm), Andersen *et al.* (1980) investigated the effect of temperature (up to 50ºC) on the corrosion of passivated mild steel coupons in concentrated H_2SO_4. Of the impurities tested, only HNO_3 significantly affected the corrosion of mild steel in H_2SO_4. Nitrogen oxides were found to oxidise the ferrous iron to ferric, $Fe(NO)^{2+}$, which changed the colour of the H_2SO_4 solution to a distinct purple colour. Increased iron dissolution from the test coupons caused the ferrous sulphate layer to reform on the mild steel surface, and then in some cases detach from it. The corrosion rate increased to more than 788 mm/y (20 mpy) when adding between 5 and 1000 ppm HNO_3. However, above 1100 ppm HNO_3, the higher nitric acid concentrations assisted in re-establish the passivity of the steel.

When proposed to industry, these results meant that handling nitrate containing H_2SO_4 in mild steel storage tanks would:

- affect customer perception, since changing the light-yellow colour of concentrated H_2SO_4 to pink would imply an inferior product,
- reduce the life cycle of the storage tanks due to increased corrosion, which would have higher cost implications,
- precipitate the less soluble ferrous sulphate and ferrous-nitric-oxides and grow corrosion products until they detached from the steel surfaces, which could build up and cause line or pump clogging, and
- cause enhanced corrosion at unpredictable times and places in the storage tanks, due to the cyclic nature of the ferrous to ferric transformation at the acid-air interfaces.

Ways recommended by Andersen *et al.* (1980) to minimize the corrosive effect of HNO_3 in H_2SO_4 storage tanks would be to lower acid storage temperatures, implement anodic passivation or add sacrificial iron to remove nitrous oxides. However, the last recommendation would imply the implementation of a liquid-solid separation system to remove iron products in solution.

2.5.2. Steel and nickel alloy corrosion in contaminated nitric acid

Just as HNO_3 contamination occurred in the HF industry (Hill & Knott, 1960 and Section 2.3.2), HF contamination (>100 ppm fluorides) of highly concentrated nitric acid (20-65% HNO_3) also occurred, which also affected the corrosion rates of steels and nickel alloys used for handling the

acid in the HNO_3 industry (Horn *et al.*, 1992). These highly concentrated HNO_3 chemicals were typically used for the decontamination of steels and nickel alloys, digestion of apatite ores, $Ca_5(PO_4)_3(F,Cl,OH)$, and processing of nuclear fuel elements (ASM Handbook, 1987). Stainless steel tanks are effectively used for the storage and distribution of concentrated HNO_3 acids and showed limited corrosion. However, when HF levels are above 0.5% in an HNO_3, catastrophic corrosion occurs (Razygraev & Lebedeva, 1982).

Horn *et al.* (1992) studied the effect of mixed HF and HNO_3 on the corrosion of stainless steels and nickel alloys. The effect of various HF and HNO_3 mixtures (0.1 - 2% HF and 3 - 65% HNO_3) were tested on 12 stainless steel and nickel alloy grades, at increasing temperatures (24ºC - 80ºC). The corrosion resistance (or stability) of austenitic and ferritic stainless steels, as well as the nickel alloys, decrease in HNO_3 mixtures as HF concentration increased. However, of all metals tested, nickel-based alloys with a chromium content of between 30 to 35%, showed the lowest corrosion rates (<15 mm/y) in concentrated HNO_3 acids containing up to 1% HF. Ultimately, the alloy with best corrosion resistance was Hastelloy G30 (NiCr30FeMo). This material was selected and used for pickling racks which needed to withstand HNO_3 (10 – 20% concentration) containing up to 3% HF, operating at 65ºC. The racks were installed and had a service life of nearly 10 years (Horn *et al.*, 1992).

2.5.3. Improved passivation in contaminated fluoride solutions

Valkenburgh (2013) recommended the addition of halide salts to the HF storage tanks to consume HNO_3 or to improve the passivity of the steel. However, concerns were raised regarding the addition of other elements such as nickel, copper or cobalt to the HF mix, as it could alter the corrosion resistance of the steel by forming a more corrosive environment, and therefore was never attempted.

Magnesium and magnesium alloys are expected to corrode rapidly in acids because of their positions on the electromotive force (EMF) series and the galvanic series (ASM Handbook, 1987; McCafferty, 2010). HF at concentrations higher than 50% has a pH of <3 (Honeywell International Inc, 2014) and thus based on the on the Potential-pH diagram for the system of magnesium and water at 25ºC, pure magnesium would not be stable in the neutral or the acid range, and favours corrosion at a potentials >-2.8 V and pH>11 in HF (Pourbaix, 1974). However, alloying Magnesium has shown to improve its corrosion resistance (ASM Handbook, 1987). The AZ91D magnesium alloy has been shown to passivate by forming an insoluble MgF_2 deposited film on the alloy surface when activated in 70% HF for 20 min (Li *et al.*, 2009). Like the FeF_2 scale formed in mild steel tanks, this passive film proved to protect the magnesium

alloy against corrosion in fluoride solutions, but not in non-fluoride solutions (Li *et al.*, 2009). For non-fluoride solutions, it was demonstrated by Li *et al.* (2009) that when a magnesium alloy, is exposed a nickel sulphate, $NiSO_4$, solution a replacement reaction takes place whereby the nickel forms part of the alloy and magnesium, as the more active constituent of the alloy, goes into solution. Since iron is also lower than nickel on the galvanic series, the same replacement reaction is applicable to passivated mild steel (covered with FeF_2 scale) in a $NiSO_4$ solution and would therefore also not improve the corrosion resistance of pre-passivated steel in non-fluoride solutions.

Since AZ91D (9.1wt% Al and 90wt% Mg alloy) passivates similarly to mild steel in 70% HF, it is implied that a AZ91D plate suspended into a mild steel HF storage tank would preferentially be attacked by HNO_3 in a 70% HF solution, since it is a more active metal than iron (McCafferty, 2010). Therefore, the use of a passivated magnesium-rich alloy (AZ91D covered with MgF_2 scale) would react with HNO_3 in the contaminated HF product more preferentially to FeF_2 and potentially increase the life cycle of the HF storage tanks. Thus, adding iron-fluoride or iron-oxide salts to the storage tanks should have the same effect. However, since the protective scale on the steel shell is made up of similar fluoride and oxide salts, it cannot be certain which salts would be preferentially consumed by the HNO_3 in the tank.

2.6. CONCLUSION

Hydrofluoric acid is produced in South Africa on an industrial scale at the Pelchem plant and exported internationally. The production of AHF at Necsa was initially reserved for the nuclear industry, but since the 1980s the stainless steel industry became the major consumer of 70% industrial grade HF, due to the pickling requirements of locally produced stainless steels. Due to the metallurgical importance, the demand was growing, which brought some strain on sourcing chemicals (H_2SO_4) and raw materials (CaF) required for the manufacturing of larger quantities of HF. One solution was to use a more abundant, but lower quality, H_2SO_4 as an alternative feed material to the HF plant. The higher HNO_3 content in the feed stream affected the corrosion characteristics of the steels and alloys used as construction materials in the plant. The corrosion associated with this type of HNO_3 contamination was unknown, which made it problematic to predict the life expectancy of the HF storage tanks in use at the plant.

This literature review gave understanding on the basics principles of corrosion reactions with steels and nickel alloys normally used in a HF plant. The forms of corrosion associated with the

production of HF are well known, with much information available on the types and mechanisms of corrosion for the various alloys used at various operating conditions in industry. Eight forms of corrosion were found to be relevant to the HF industry, with cases of each type of corrosion experienced at a plant summarized. Since HNO_3 is an oxidizing acid, the effect of oxygen on the corrosion of steels and nickel alloys were also reviewed.

The current study was unique in that it focussed on the effect of HNO_3 contamination in the HF product on the corrosion of steels and nickel alloys. However, an investigation by Andersen *et al.* (1980) on the effect of nitric acid contamination on mild steel used for storing H_2SO_4 was related to the current study. Other corrosion investigations on stainless steel and nickel alloys conducted by (Horn *et al.*, 1992) concluded that NiCr30FeMo (Hastelloy G30) produced the best corrosion resistance in HNO_3-HF mixtures, used during the pickling of stainless steels. Laboratory investigations on the passivation of magnesium alloys in fluoride solutions conducted by Li *et al.* (2009) demonstrated the possibility of using more active fluoride salts to react with unwanted contaminants in the corrosion solution, to form part of the protective scale on the metal surface.

Thus, the literature survey was essential in providing the necessary background knowledge needed for the corrosion study, and how to interpret the findings in a way that would be useful to the HF industry.

CHAPTER 3

CORROSION FAILURE ANALYSIS

3.1. INTRODUCTION

The corrosion failure analysis was initiated to understand why the HF storage tanks on site at Necsa failed (Figure 3.1a). This corrosion failure analysis was conducted to determine critical factors influencing the corrosion at the plant so that appropriate experimental conditions could be recognized to simulate the corrosion. Thus, the required parameters relevant in duplicating the unique corrosive environment on a laboratory scale were identified. The corrosion study was performed to understand the on-site corrosion problem and to determine the corrosion mechanism. This first-hand look at the corrosion problem has defined the entire study. A practical solution was needed to solve the corrosion problems identified on-site in the form of a corrosion inhibition strategy. This was especially important for the implementation of a solution into a functioning HF production circuit.

The findings from this corrosion analysis were presented on two occasions; at the Microscopy Society of Southern Africa's (MSSA 2015) 53rd Annual Conference, and the 2nd African Corrosion Congress (AfriCORR 16). The abstract summarizing the findings on the corrosion of the mild steel storage tanks in HF is given in Appendix C. Since the study was conducted separately from the laboratory simulated tests, it is reported in a separate chapter, so that these results could later be compared to data from the simulated corrosion tests. This was to assure that the results would be relevant to the HF production industry. Thus, this chapter serves as a brief summary of the corrosion-related failure analyses done on the decommission HF tanks prior to the laboratory simulated corrosion tests.

The ASTM standard for corrosion-related failure analysis (ASTM, 2009b) was used as a reference to conduct the corrosion analysis. The standard covers the procedures for examination of metallic failures, where corrosion is suspected as the root cause. Sampling of the corroded sheets collected was conducted in a similar fashion to forensic investigations specified in ASTM E1459 (ASTM, 2009c).

3.2. BACKGROUND

Uniform corrosion of storage tanks in the Pelchem plant producing hydrofluoric acid (HF) is expected at an average rate of ~0.5 mm/y and considered mitigated in the design of the plant. When steel is exposed to 70% HF, a corrosive reaction takes place (Equation 1.1), whereby scale forms inside the tank during its commissioning and protects the mild steel from further corrosion over its entire lifetime. Three months before the leak, the corrosion rate spiked to 3 mm/y and eventually peaked at 30 mm/y measured in the liquid phase of the storage vessels as determined using ultrasonic methods (Figure 3.1b and Figure 3.2a). The rapid corrosion in the liquid phase resulted in leaks and was attributed to the presence of an oxidizing acid ($0.1\% < HNO_3 < 1\%$) which attacked the protective fluoride scale (FeF_2) (Figure 3.3). Sulphuric acid (H_2SO_4) is used to commercially produce HF (by following the reaction in Equation 1.2). Use of an alternative supplier resulted in a change in H_2SO_4 feedstock on site and was determined to be responsible for the increased HNO_3 concentration downstream. Since it was determined through quantitative analyses, using ion chromatography (IC) at Pelindaba Analytical Labs (PAL) of samples taken from the HF product streams at the plant, that HNO_3 only concentrated in the technical grade HF storage tanks, which unexpectedly failed.

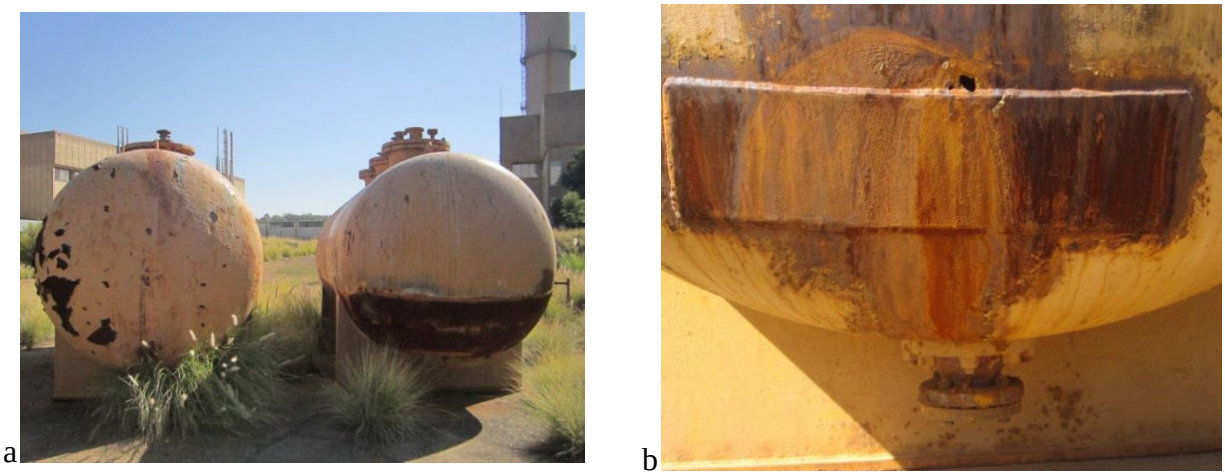

a b

Figure 3.1: Storage tanks V1460 (left) and V1461 (right) which failed on 30 May and 26 March 2012 from excessive corrosion which were removed from the plant (a), and (b) an area where it leaked even after patching.

a 

b 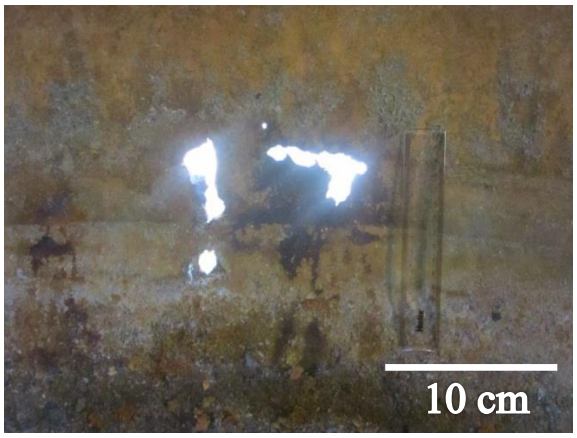

Figure 3.2: Leak in V1460 approximately 300 mm from the vessel bottom due to unusual corrosion, observed (a) from outside, and (b) from inside the storage tank.

3.3. OBJECTIVES OF THE CORROSION FAILURE ANALYSIS

1. Characterisation of the corrosion scale layer which formed on the inside of the storage tanks during its lifetime by:
    a. Scanning electron microscopy (SEM) and energy dispersive X-ray spectroscopy (EDS) on the cross-sections of the microstructure of the steel with the scale, and
    b. X-ray powder diffraction (XRD) of the removable scale to identify the phases that formed during the corrosion process.
2. To determine the type of corrosion on mild steel exposed to nitrous compounds (>50 ppm) present in the technical grade hydrofluoric acid (70% HF) that led to the eventual failure of the tanks.

3.4. MATERIALS AND METHODOLOGY

ASTM Standard Guide G 161 – 00 (ASTM, 2009b) did not address safety aspects related to an on-site examination of tanks, which historically contained hazardous, concentrated HF in a confined space. At the time of the visual examinations, HF fumes were still dissipating from the scale inside the tank and could not effectively vent out. This was because, except for the leak and HF inlet, the decommissioned tanks were still mostly intact and effectively sealed. With assistance from the local fire department (Brits Fire & Emergency service), it was possible to be lowered into the decommissioned HF tanks using a safety harness and rope. An oxygen monitor was used to determine the quality of the air in the tank prior and deemed suitably safe at that time (3 May 2013). Examination of the leaks and liquid levels continued with photographs taken inside, and outside of the tanks using a Canon PowerShot A2200 HD, 14.1 megapixel digital

camera, for later evaluation (Figures 3.1 – 3.5). After examination of the photographs, sections of the tank were selected for sampling. Samples were cut out of the tanks from the outside using an angle grinder and sealed into high density polyethylene (HDPE) bags. Since HF fumes were still escaping from the scale, sampling could only initiate once the collected sheets were dried in a fume cupboard, connected to a KOH scrubber, for approximately 48 hours.

Since failure of the tank was principally as a result of the leak below the liquid line in the tank (Figure 3.3a), the main focus of the corrosion failure analysis was on only one section (Figure 3.4). The section from the welded joint (Figure 3.3b) was not examined further, as the weld and surrounding steel was not damaged, and thus considered as having no immediate influence on the failure of the HF storage tanks, at that stage.

a 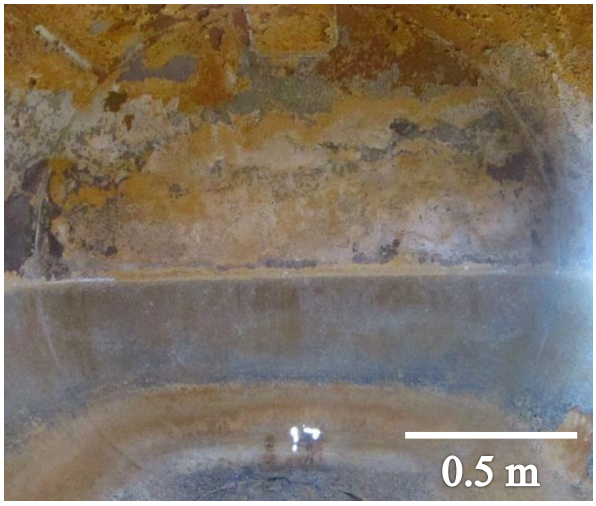

b 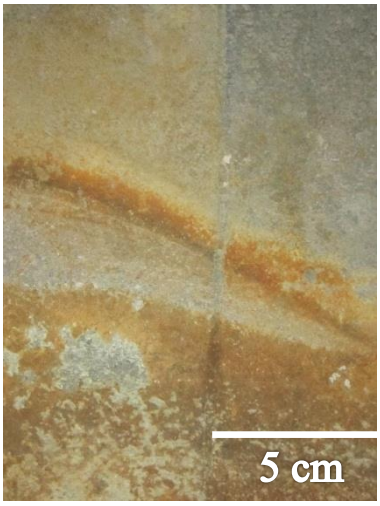

Figure 3.3: Inside V1460, indicating: (a) corrosion at various liquid levels, and (b) weld joint.

To understand why the tank failed, samples were taken from sheets removed from the decommissioned tanks, and were mounted with cross-sections prepared metallographically. Metallographic sample preparation included:

1. cutting out samples from the corroded sections from both the vapour and liquid phases (at points above and below the liquid band shown in Figure 3.4),
2. sectioning the samples into dimensions suitable for the SEM (Figure 3.5),
3. mounting the cross sections in a cold resin,
4. grinding (Paper grits 220, 1200) and polishing the cross-sections, using a Struers Allegro/Largo (15 μm), MD-Dac (3 μm) and MD-Nap (1 μm) polishing discs (and diamond suspensions), to a smooth finish, and
5. carbon coating the surfaces to ensure the non-conductive fluoride scale effectively conducts electrons during SEM and EDS analyses.

The prepared samples were investigated, using the Quanta FEI 200 3D SEM, to 1000× magnification. Elemental analysis of the scale, scale-steel interface and steel substrate were then obtained using EDS spot analyses.

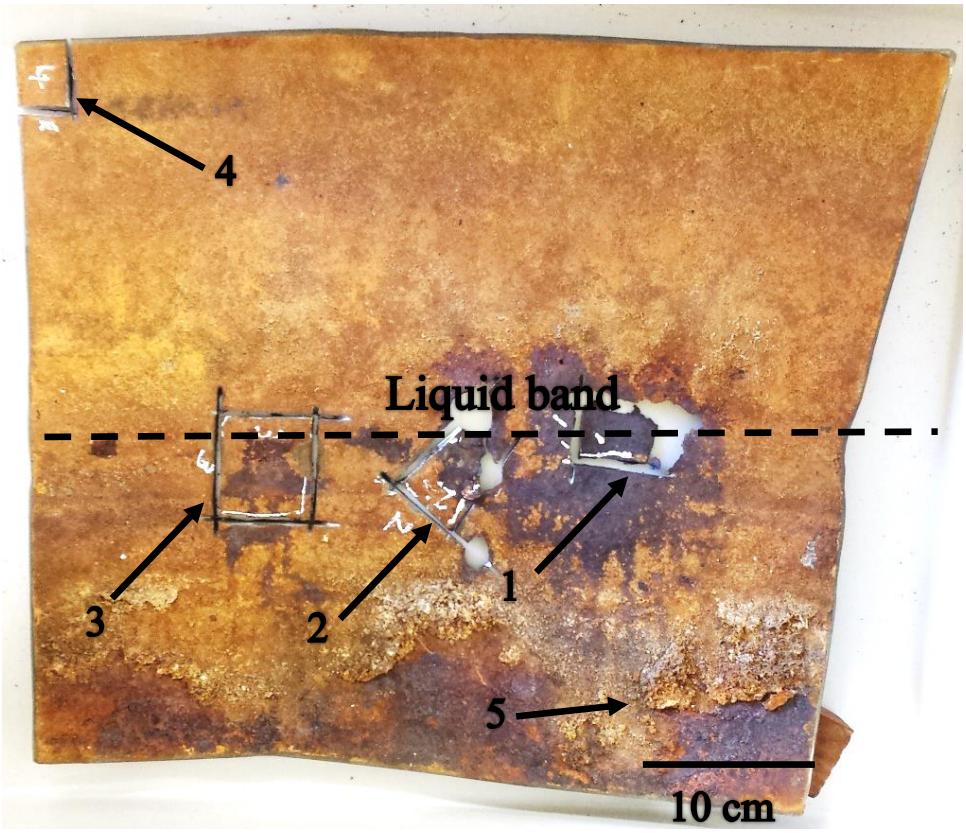

Figure 3.4: Samples cut from storage tank V1460 (Figure 3.1a) at the area where the HF leak initiated (Figure 3.2), the level of the liquid phase of the HF, is shown (also visible in Figure 3.3a).

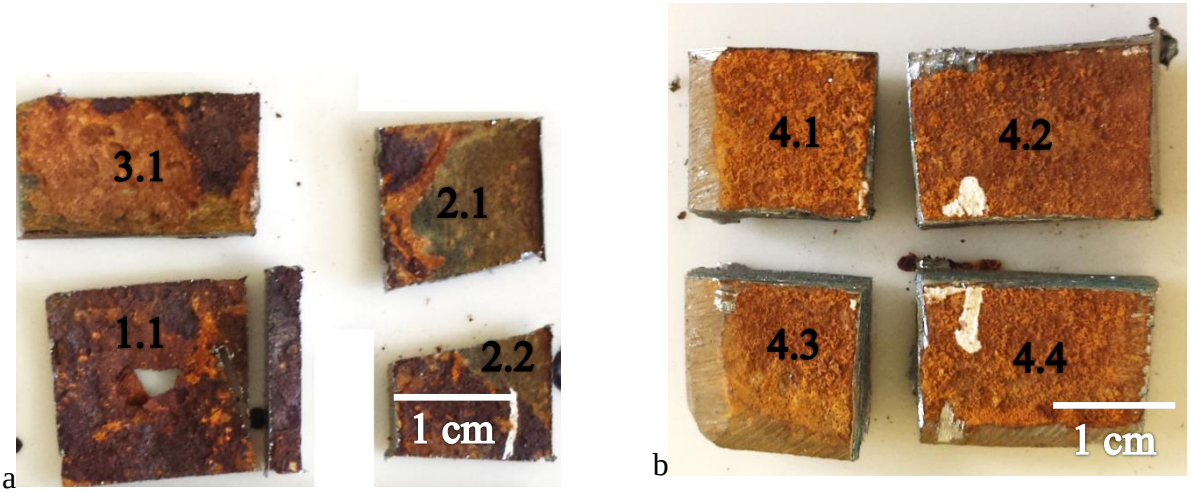

Figure 3.5: Samples sectioned from the sheet cut from storage tank V1460 (Figure 3.4) at: (a) the point where the HF leak initiated, and (b) the area well above the liquid band.

Large agglomerates of scale (>4 cm in length) were removed from the inside of the storage tank (Figure 3.2b) in an area where corrosion occurred (e.g. point 5 in Figure 3.4), at points below the leaks (e.g. point 1 and 2 in Figure 3.4). This was slightly below the liquid band. Based on its colour and texture, this removable scale visually resembled iron fluorides which typically form when HF reacts with the exposed steel during corrosion. The scale was loose and relatively large compared to the protective scale that should have formed on the inside of the mild steel tanks. It was collected and examined, as the corrosion products were relevant to the catastrophic failure of the V1460 technical grade HF storage tank. Analysis of the composition of this scale was conducted by X-ray diffraction (XRD), after pulverising the scale to powder. Phase identification of the XRD pattern was done using the 2007 PDF-2database.

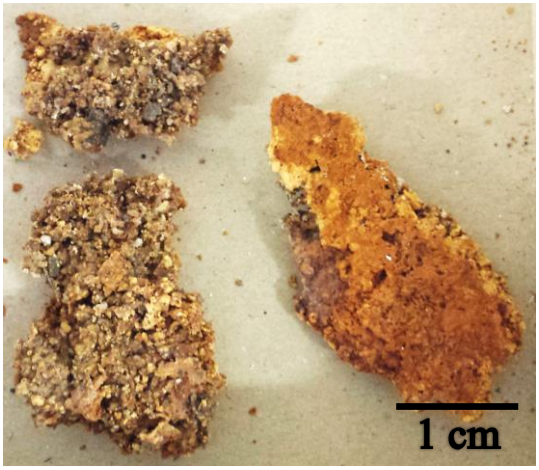

Figure 3.6: Removable scale, collected from below the liquid band (point 5 in Figure 3.4) on the inside of the HF storage vessel (Figure 3.2b), for XRD analysis.

3.5. RESULTS

The cross-sections of the corrosion layers, at above and below the liquid phase, on the inside of the tank are given in Figures 3.7 and 3.9. The cross sectional depth profile through EDS spot analyses are shown in Figures 3.8 and 3.10. A larger (~230 μm) more porous corrosion layer was formed in the liquid phase (Figure 3.9), while the deposit was three times smaller and noticeably more dense in the vapour phase (Figure 3.7). Therefore, corrosion was significantly higher in the liquid phase, which was attributed to the higher HNO_3 concentrations in the technical grade HF product during the 3 months in which corrosion rates of the storage tanks also peaked.

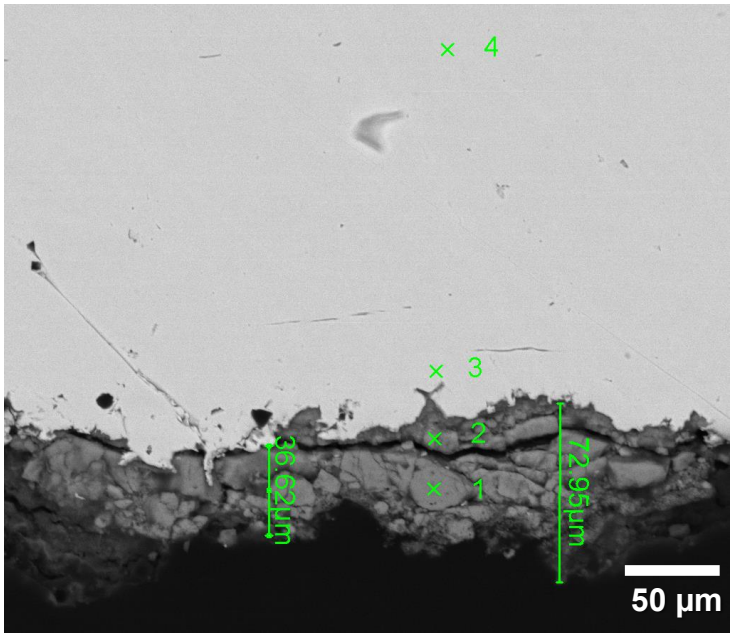

Figure 3.7: SEM-BSE image of a cross-section of the mild steel with corrosion, showing scale formation above the liquid band (sampled from point 4 in Figure 3.4).

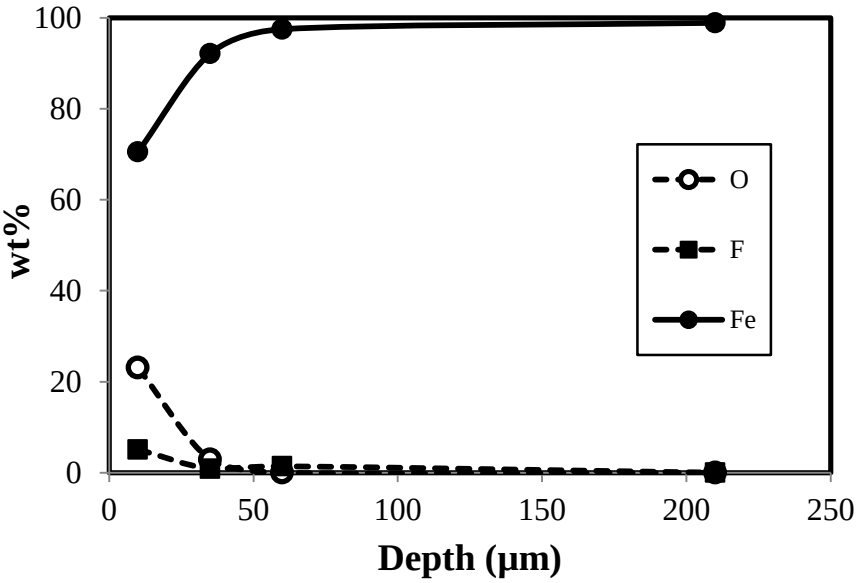

Figure 3.8: Depth profile of the corrosion layer above the liquid band (EDS of Figure 3.7).

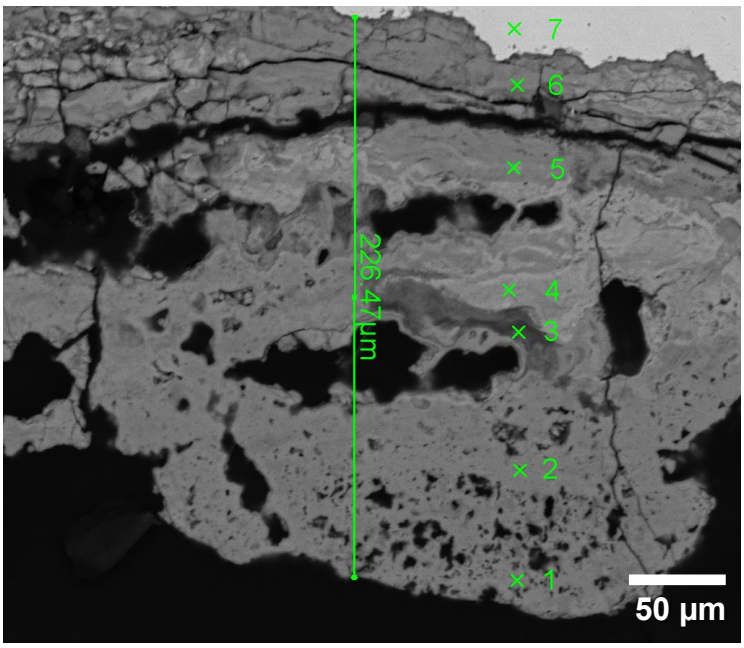

Figure 3.9: SEM-BSE image of the cross-section of mild steel with corrosion, showing scale formation in the liquid phase (sampled from point 1 in Figure 3.4).

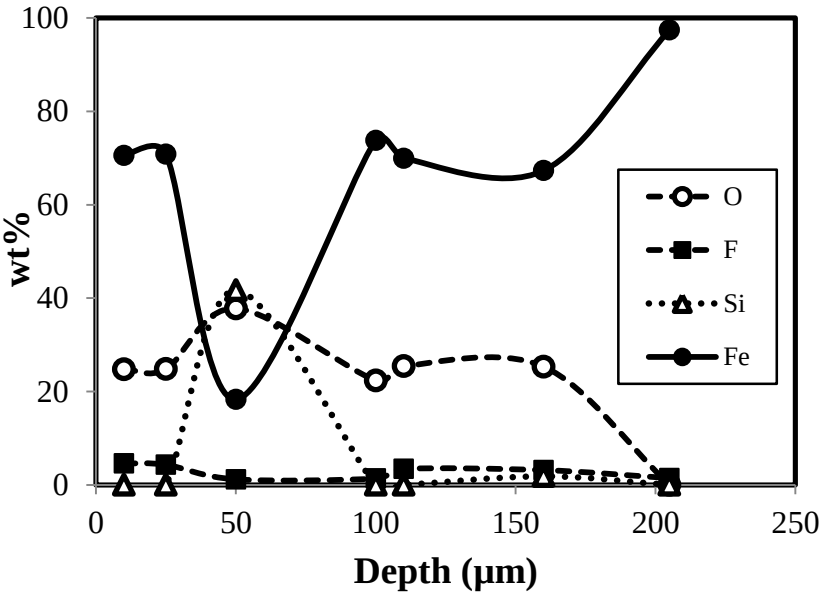

Figure 3.10: Depth profile of the corrosion layer in the liquid phase (EDS of Figure 3.9).

Figure 3.11 shows the XRD results of scale (collected from point 5 in Figure 3.4) to be a mixture of hydrated iron fluoride, $FeF_3(H_2O)_3$; iron oxide hydroxide, FeO(OH); iron oxides, Fe_2O_3, and Fe_3O_4; iron fluoride, FeF_2; silicon and silicon oxide, SiO_2; manganese oxide, Mn_3O_4; and manganese oxide-silicate, $Mn_7O_8(SiO_4)$. Peaks that were not identified (marked as UI in

Figure 3.11) were due to the limitations of the PDF-2database used for XRD phase analyses at Necsa's Radiation Science (RS) department, which has not been updated since 2007.

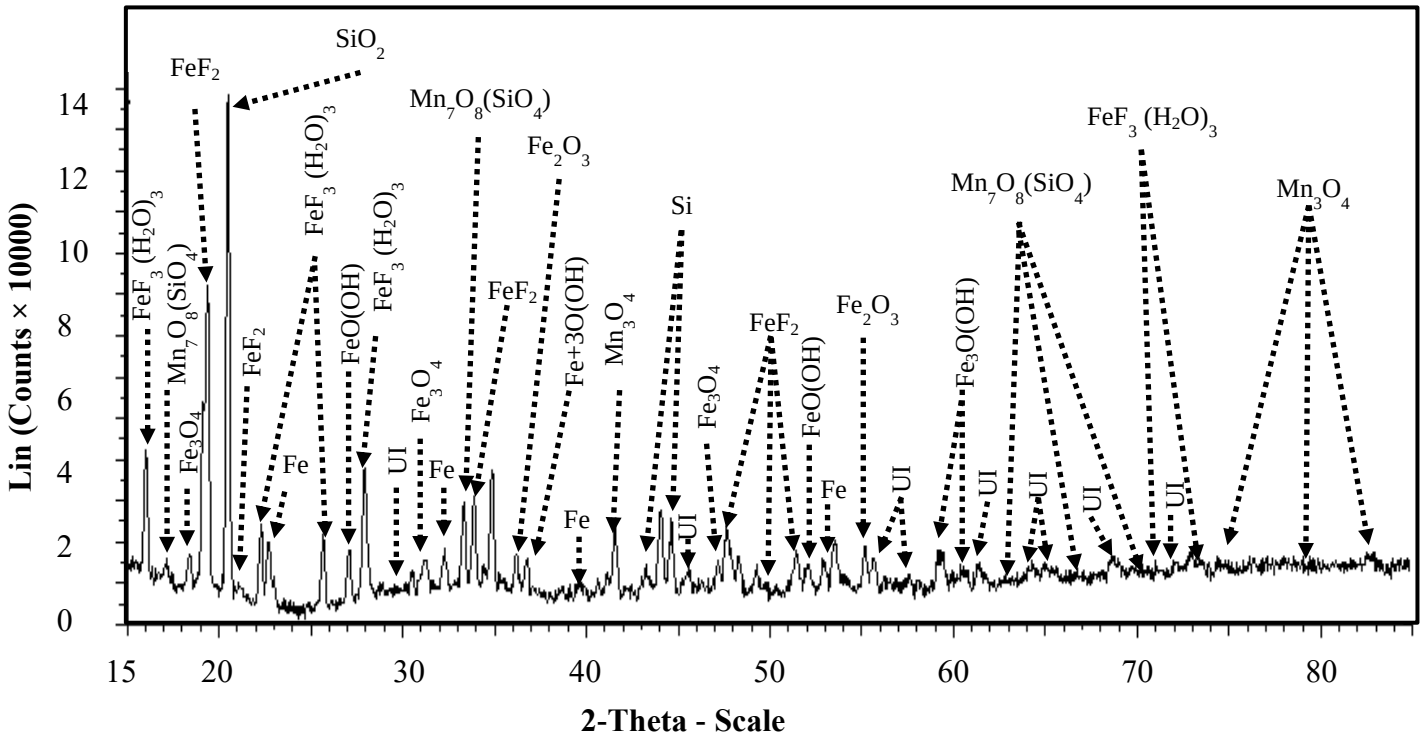

Figure 3.11: XRD pattern of the corrosion products (removable scale). Unidentified peaks were marked by UI.

3.6. DISCUSSION

Figure 3.8 shows a depth profile of the corrosion found in the vapour phase which was representative of the scale forming during the normal operation (e.g point 4 in Figure 3.4). This scale was a dense compact iron (II/III) oxide and fluoride mixture (~5 wt% F and ~23 wt% O, detected 10 μm into the scale) that was protective of the steel by increasing its corrosion resistance when it was in contact with HF (Figures 3.7 and 3.8). Figure 3.9 shows a thicker porous layer contaminated with silicon, indicating that the steel was being corroded by HF gaining access to the steel shell through the porous scale, implicating the early failure. A small silicon-rich phase (>41 wt%) detected 50 μm into the scale, was found in the scale below the liquid band (Figure 3.10). One explanation for this is that dissolved silicon is always present in the HF manufacturing process and is typically found in the technical grade acid stream, and can easily precipitate in the fluoride scale that forms on the steel during corrosion. A second explanation is that silica (SiO_2) sand was used to sand blast the mild steel sheets before construction of the storage vessels (Valkenburgh, 2012a). This SiO_2 residue on the steel surface was susceptible to attack by the HF that corroded the mild steel and then formed part of the

passive layer. Thus, the presence of a silicon-rich phase in the fluoride scale (at 50µm in Figure 3.10) is not an unusual occurrence in an HF plant.

The $FeF_3(H_2O)_3$ identified by XRD indicated the FeF_2 was oxidized by the HNO_3 and became sufficiently porous to allow HF access to the steel substrate. The steel then reacted repeatedly with fresh HF and formed a succession of scale layers, similar to when a pre-passivation step was used in the commissioning of the storage vessels. This combined attack from HNO_3 and HF continued and the porous scale layers increased to more than 220 µm (Figure 3.9), allowing corrosion of the steel underneath the scale. This continued until the scale formed large, unstable pieces (visible in Figure 3.6), which eventually peeled off exposing the steel to high corrosion rates.

3.7. CONCLUSIONS

SEM and XRD results showed that the scale formed, after the HF had higher HNO_3 content in the liquid phase, were mostly a mixture of iron fluorides, oxides and hydroxides. The scale kept growing, forming large unstable pieces, which fell off and weakened the steel. The process continued until the failure occurred. The corrosion scale was successfully characterized and the failure analysis of HF storage tank V1460 and V1461 completed.

3.8. RECOMMENDATONS

The same analytical methods used in the failure investigation were recommended for the corrosion products from the laboratory corrosion simulations. Sand blasting of the coupons designated for laboratory corrosion tests was suggested, as the surface containing SiO_2 sand residue, would be similar to the surface finish of the SA 516 Grade 70 normalized steel used as construction material for the V1460 and V1461 HF storage vessels.

Scale formation was demonstrated to be essential to the corrosion resistance of mild steel. Therefore, it was recommended that the thickness and composition of the fluoride scale, as affected by nitric acid contamination, be examined, in addition to other objectives set out in the remainder of the study.

CHAPTER 4

EXPERIMENTAL PROCEDURE

4.1. MATERIALS

4.1.1. Steels and metallic alloys

All experiments were performed to establish the corrosion resistance of the current steels and alloys used in the Pelchem HF plant (Table 4.1). This was done by studying the effect of by low concentrations of nitric acid contamination in the process streams.

Table 4.1: Steels and metal alloys currently in use at the Pelchem HF plant (Valkenburgh, 2013).

Name	**Code / designation**	**Apparent density (g/cm^3)**	**Elements (wt%)**						**Component / Area used within plant**	**Temp. range (°C)**
			Ni	**Cr**	**Mo**	**Fe**	**Cu**	**Mn**		
Mild steel	SA516 Grade 70 normalized	7.85	-	-	-	99	-	-	HF transportation tanks	0 – 40
SS 904 L	X1NiCrMoCu N 25 205	7.90	25	20	5	46	2	2	Kiln lining and the Y-piece extraction pipe	50 – 350
Alloy 400	NiCu30Fe	8.80	65	-	-	2	30	1	Dip pipes in 70% HF tanks and Crude HF pumps	25 – 40

4.1.2. Chemicals and reagents

The HF used for the corrosion tests was aqueous hydrogen fluoride (70% Industrial grade) collected from the Pelchem SOC Ltd. flourochemical plant situated on the site at Necsa. The 70% HF was a high quality product (fluorosilicic acid ≤100 ppm, sulphuric acid ≤200 ppm and nitric acid <5 ppm) received in sealed 25 L bottles, which were intended for export and sale by Protea Chemicals (Inland). A 70% HF acid with a HNO_3 concentration below 50 ppm was essential for the corrosion tests. Since the technical grade (70% HF stream to the V1460 and V1461 storage tanks) was the product stream most susceptible to contamination with HNO_3 in the plant, the high purity export grade 70% HF product also produced by Pelchem SOC Ltd. was adequate for use in the current study. Thus, the contaminated technical grade HF was simulated

in the laboratory set-up by spiking known concentrations of analytical grade HNO_3 into the relatively pure industrial grade acid, produced at the same plant.

Planned Interval Corrosion Tests (PICTs) were conducted prior to the corrosion tests to determine typically how long a corrosion tests should last when allowing mild steel to corrode in an HF solution. The PICT experiments were initially conducted using lower concentrations HF (40% and 48%) which were analytical grade solutions purchased from Merck (Pty) Ltd. The findings from the PICT experiments, initially used for the required safety risk assessment, led to the methodology used throughout this study.

The oxidizing acid, used to simulate the nitrous contamination deemed to be responsible for the increased corrosion and premature failure of the HF storage tanks, was analytical grade HNO_3 (65% purity) purchased from Merck (Pty) Ltd. The HF acid used in all the corrosion tests was never diluted to below 69%. Thus, maintaining a concentration within ±1% of the 70% HF used meant that when introducing the HNO_3 (25% H_2O content) to the HF corrosion tests, no more than 13.6 mL (spiking to a maximum HNO_3 concentration of 1.2%) could be introduced into the corrosion medium. Consequently, it was assumed that the small volume of HNO_3 introduced to the HF corrosion tests did not significantly affect the HF concentration that needed to be maintained. Examples of the concentration calculations of corrosion media are provided in Appendix B.

Chemically pure acetone, purchased from Merck (Pty) Ltd., was used for the cleaning of coupons, Teflon bottles and CRRRs (Cylindrical Reinforced Resistant Racks) before and after each corrosion experiment. Coupons were submerged in acetone and ultrasonically cleaned for 30 minutes to remove oil, grease, organic compounds, as well as inorganic salts that were present on the surfaces. These substances (including free mill scale) were typically left behind during the heat treatment and sand-blasting of the metal coupons. Moreover, acetone served to remove excess water from the coupon surfaces and dry the coupons faster. This was especially relevant when doing corrosion tests on mild steel, which starts showing signs of atmospheric corrosion within hours after sand-blasting. To combat this, mild steel coupons were routinely washed with acetone, dried and subsequently stored in a desiccator for the remainder of the corrosion studies.

Absolute ethanol (99.9% pure), also purchased from Merck (Pty) Ltd., was used for cleaning the polished cross sections of the original and corroded coupons (coupon No. 8) selected from each corrosion test. This was in accordance with the metallographic method used in the sample preparation of coupons prepared for microscopic evaluations.

Tap water was used for all other unspecified cleaning purposes, especially during the rinsing off of the HF solution, from corroded coupons after removal from the corrosion reactor, or during the cleaning steps when removing the corrosion layers from coupons surfaces. Compressed air was used for the drying of the washed coupons and served to remove excess water from the corroded surface prior to storage in the vacuum desiccator.

Hydrated lime (CaO) and calcium gluconate ($C_{12}H_{22}CaO_{14}$) were available on hand as a safety precaution. The CaO powder was purchased from Idwala Industrial Holdings and served to neutralize acid spillages. Calcium gluconate is essential in treatment of HF burns on the skin in the event that there was exposure to the acid during corrosion experiments.

4.1.3. Handling of metals

4.1.3.1. Material selection

The materials of interest to the study were the three metals currently being used during the storage and distribution of HF at the Pelchem fluorochemical production plant (Table 4.1). These metals included mild steel (SA 516 normalized) stainless steel (SS 904 L) and a nickel alloy (Alloy 400).

The steels and metal alloys were sourced from Special Alloys & Metallurgical Services (SAMS) located on the R104, Pelindaba. SAMS was also employed to hot roll the metals to 3 mm thickness (Figure 4.3). Normalization was required to produce the same microstructure as the original steels used in the manufacture of the HF storage tanks. The stages in the sample preparation for the corrosion tests are shown in Figure 4.1.

4.1.3.2. Cutting of the coupons

Coupons were cut to 25 x 25 x 3 mm sizes, as recommended by standard guide for conducting corrosion coupon tests in field applications (ASTM standard guide G 4 – 95). Water-jet cutting was preferred over hydraulic shear cutting, grinding and laser cutting, as it produced the least amount of cold working on the cut-edges of the coupons. This finding was supported by comparing the microstructures of cut-edges made by the different cutting techniques available. It was established that waterjet cut-edges were least susceptible to corrosion. The results on the microscopic study on the effect of cutting on the microstructure of mild steel used for corrosion tests are summarized in an abstract published in the MSSA 2015 conference proceedings in Appendix C. Waterjet cutting was done at Afriqcut waterjet profiling in Pretoria, and was

effective in consistently cutting the coupons to size, as well as cutting the inner hole (8 mm diameter) required to hang the coupons freely in the HF solution (Figure 4.3), from the corrosion rack (Figure 4.8b).

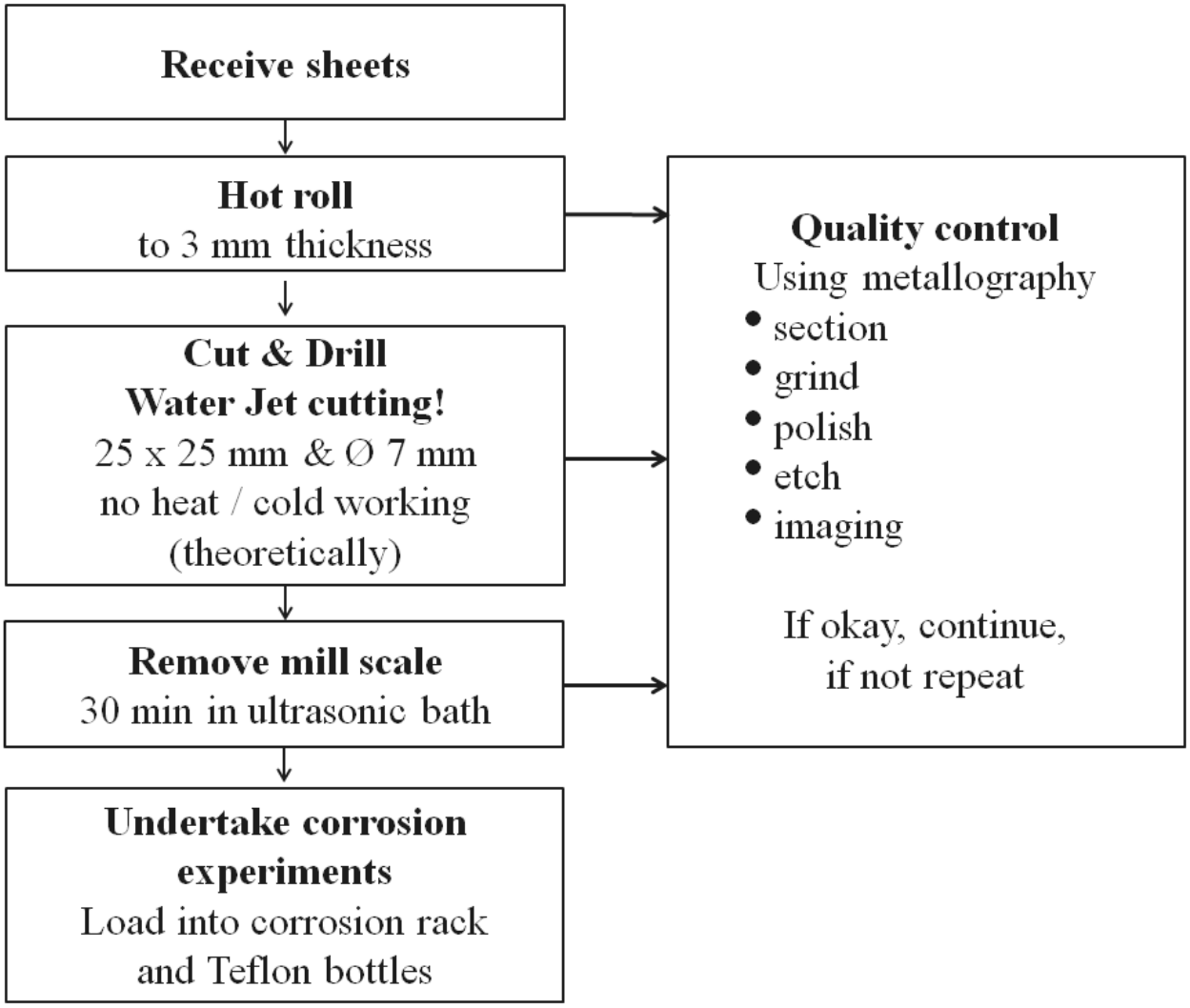

Figure 4.1: Steps for sample preparation prior to corrosion experiments and analyses.



Figure 4.2: Example of the original steel received from hot rolling received after sand-blasting.

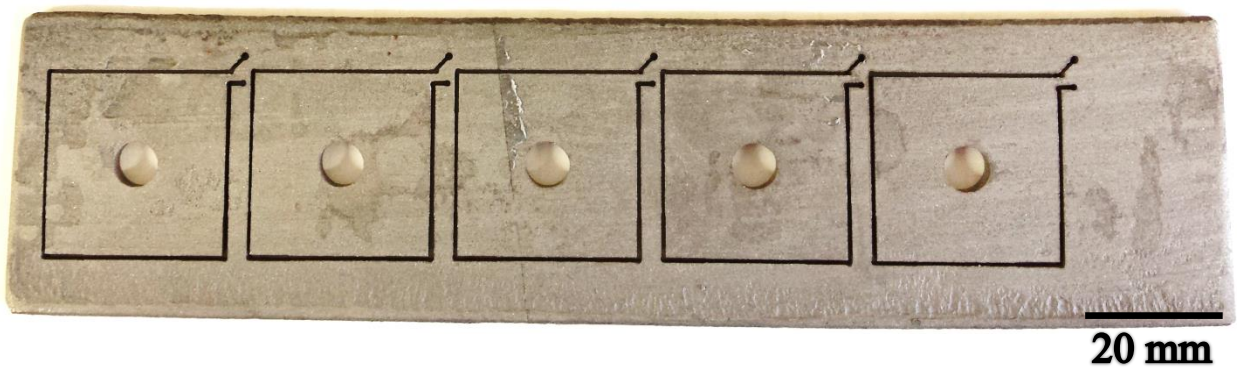

Figure 4.3: Example of a sandblasted template made by water-jet cutting.



Figure 4.4: Examples of final coupons, after washing with acetone, prepared for corrosion immersion tests, with sequencing marks on the bottom edges.

A 1 mm part kept each coupon attached to the profile cut from the bulk metal sample and could easily sheared of and collected for each corrosion experiment. However, this method did leave behind a slightly work-hardened 1 mm burr which needed to be cut and filed down before each experiment. The slightly deformed burr served as a reference mark during the orientation of the coupons into the corrosion reactor and was a valuable reference point during the macroscopic and microscopic examinations of the coupons before and after each test.

Coupons were cut from the centre of each rolled bulk sample (Figure 4.2) as the edges of the steels oxidized during hot rolling. This is visible from the white area in the etched microstructure of the mild steel (Figure 4.5). This practice ensured that representative and homogeneous samples were used during all corrosion tests and analyses.

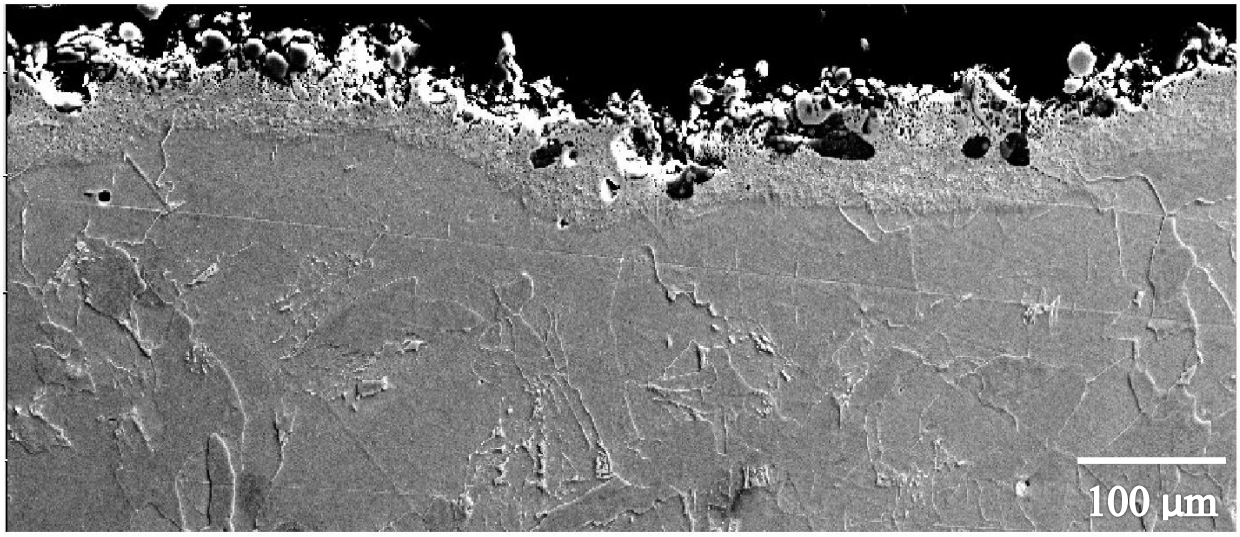

Figure 4.5: SEM-BSE micrographs showing the original hot rolled edges of the mild steel after etching with 3% Nital.

After water-jet cutting, the cut profiles were taken for sand-blasting and then immediately stored in a desiccator. This was done to minimize the atmospheric corrosion of the mild steel in air prior to the HF corrosion tests.

Prior to corrosion tests, coupons were individually marked using a sequence of lines that started from the filed burr - earlier deemed as the reference point. These marks were made by lightly clamping the edge of the coupon with using a side-cutter (diagonal pliers). The number of marks made on a coupon depended on the sequence in which it was to be removed from a corrosion test. A coupon with one mark would be removed first, while a coupon with eight marks would be removed last (Figure 4.5). In situations where more than one corrosion test was running parallel, a coupon was also marked on the vertical side (e.g. Figure 5.27 in Section 5.2.2.2) that related to the test number. This was done to avoid mixing up samples during the concurrent removal of the coupons from the different HF corrosion tests, which needed to be safely sampled at the same time.

4.1.3.3. Cleaning

Before each corrosion test, coupons were removed from the water-jet cut template (Figure 4.3) marked (Figure 4.4) and ultrasonically cleaned with acetone for 30 minutes. The coupons were allowed to air dry and then weighed, after which “before” photos were taken under fluorescent light. Subsequently, the coupons were loaded into the corrosion rack and placed into a desiccator. Once the corrosion set-up was ready, the assembled corrosion rack was retrieved

from the desiccator and placed into the Teflon bottle to which the HF was introduced to start the 24 hour pre-passivation step.

After pre-passivation, the corrosion rack containing the pre-passivated coupons was removed from the Teflon bottle and immediately rinsed with water. The coupons were then carefully separated from the rack and individually rinsed with tap water until the free HF was removed from the corroded coupon surface. The scale that formed during the pre-passivation step was resilient and adhered well to the coupon surfaces, and could not be removed by cleaning using the mild rinsing action employed. The washed pre-passivated coupons (e.g. of the pre-passivated condition is shown in Row b in Figure 5.24, Section 5.2.2.1) were then dried with compressed air and subsequently rinsed with acetone to remove any excess remaining moisture. The coupons were then weighed, photographed and assembled back into the corrosion rack as described above. The pre-passivated coupons were the initial state of the metals prior to corrosion tests. The protective scale formed during pre-passivation was expected to be the same as in commercial HF tanks, as they are normally treated before usage.

After the corrosion tests, coupons were removed and cleaned in the same way as employed after the pre-passivation step. However, in the instances where nitric acid was introduced during the corrosion experiments, the protective scale was either completely removed or was very loosely adhering to the coupon. Therefore, the rinsing and cleaning procedure was carefully conducted to effectively keep the remaining scale. After drying, the coupons were weighed and photographs taken to record the condition of the coupon prior to cleaning. For the final cleaning, each individual coupon was then placed in 50 mL warm water and ultrasonically cleaned for 30 minutes (which mostly meant removing the remaining scale).

Ultrasonic cleaning succeeded in effectively removing the fluorite scale from the coupon surface and was deemed to produce comparable cleaning results to mechanical cleaning. Surfaces of corroded coupons cleaned using ultrasonic cleaning and mechanical cleaning methods were compared using a scanning electron microscope (SEM) and energy dispersive spectroscopy (EDS), optical microscopy and glow discharge - optical emission spectroscopy (GD-OES). The results from the analyses showed that even though mechanical cleaning removed slightly more scale (an average scale thickness averaging of 0.017 μm) than ultrasonic cleaning (an average scale thickness of 0.057 μm), it scratched and deformed the surface too much to allow meaningful visual observations. Therefore, it was decided that ultrasonic cleaning produced comparable results to mechanical cleaning, with the benefit of keeping the necessary surface structures of post corrosion (especially pitting and uniform corrosion). All wash water containing

the dissolved scale from ultrasonic cleaning was captured. The water was heated in a drying oven at 80ºC for 48 hours and the dried cake was collected and weighed.

The ultrasonically washed coupons were then dried, weighed and photographs were captured in the same way described for pre-passivated coupons. These final coupons were then individually sealed in plastic bags and stored.

4.2. ANALYSES

4.2.1. Solution samples

All aqueous samples of the corrosion solutions were analysed for hydrofluoric acid concentration (% HF) and nitrate concentration (NO_3^- in mg/kg) using volumetric titrations at Pelindaba Analytical Labs (PAL) at Necsa. The aqueous corrosion solutions collected after the pre-passivation step (Pre-Pass) and at the end of a corrosion test (Final Prod) were analysed for all possible metals in solution, using inductively coupled plasma optical emission spectrometry (ICP-OES).

The excessively high HF concentrations (>40%) made the analyses for nitric acid (NO_3^- ions) in the corrosion solutions with ion chromatography (IC) very difficult. It was later established that precipitating the HF using calcium instead of lithium produced more stable precipitates and subsequently more accurate results. To establish the reliability of the analytical results obtained, three HF solutions with known HNO_3 concentrations were selected and analysed separately at PAL. The three HF solutions had varying HF concentrations (40%, 48% and 70%), with two of the solutions from external suppliers (Merck) and their nitrate concentrations were known from the certificate of analyses (COA). Consequently, the analytical results for HF analyses from PAL were compared with those acquired from the COA and the percentage error on HF analyses established. To verify nitric acid analyses in concentrated HF solutions, known quantities of nitric acid (1% HNO_3) were spiked into three 70% HF solutions and sent for analyses. It was established that the solution analysis conducted at PAL, carried a ±18.3% error for nitrate (NO_3^-) and ±0.44% for HF (Appendix A).

Acid consumption

The amount of acid consumed per mass of solids leached is a critical parameter in controlling operational costs associated with hydrometallurgical plants (Van der Merwe, 2010). The concept

of gangue acid consumption (GAC) is just as applicable in monitoring the corrosion behaviour of metals used to resist attack by aqueous acids. When HF corrodes the vessel used to store it, a significant quantity of the steel or nickel alloy used to construct the storage vessel will dissolve into the acid. Determining the quantity of nitric acid and hydrofluoric acid consumed during the corrosion tests produced significant information used to support corrosion reaction kinetics when establishing the rate controlling conditions in each test.

Acid consumption is typically calculated as the difference between the total acid introduced (HF or HNO_3) to the corrosion reactor and the free (unreacted) acid still present in the Teflon bottle at the end of the corrosion test. Typically, GAC is measured in kilogram of acid consumed per kilogram of iron removed (kg/kg Fe) (Mular, 2002). This was especially applicable when corroding mild steel, as approximately 99% of the SA 516 Grade normalized steel used was iron (Fe). However, because of the size of the corrosion tests (>500 mL) and the small quantities of iron removed from a coupon per test for this project, gram acid per gram Fe (g HF/g Fe) was preferred.

The total acid used was directly determined from the total volume of HF and/or HNO_3 introduced per corrosion test, for the combined mass of the four coupons present in the bottle at the start of each experiment (Appendix B). The remaining acid concentration (free acid) in the final corrosion solution was measured from the 40 mL sample sent for analyses at PAL. Mass of acid consumed per mass of iron introduced to the system was then determined by subtracting the free acid from the total acid used and expressing as a percentage:

$$\frac{(\text{Acid in Feed})-(\text{Acid in Product})}{\text{Acid in Feed}} \times 100 \qquad \text{Equation 4.1}$$

or gram of acid per gram of iron removed from the coupons (g Acid)/(g Fe) :

$$\frac{\text{Total acid consumed}}{\text{Mass of coupons}} - \frac{\text{Free Acid}}{\text{Mass of coupons}} \qquad \text{Equation 4.2}$$

4.2.2. Solid samples

The solids analysed in the corrosion tests were:

- Metal coupons - before and after cleaning,
- Scale (fluoride) removed from the corroded coupon surfaces - after cleaning,

- Corrosion products collected at the bottom of the Teflon bottles at the end of the corrosion tests, and
- Other oxide films that formed on the corroded coupon surfaces (for stainless steel and nickel alloy corrosion tests).

4.2.2.1. Mass loss

Mass loss measurements and visual examination of specimen surfaces using the procedures stipulated in ASTM Standard G 4-95 (ASTM, 2009a) were the crux of the study, and the samples were cleaned and weighed using Practice G1-03 (ASTM, 2009d). The instrument used was a Precisa XR 405 analytical balance from Air and Vacuum Technologies Pty. which could measure to an accuracy of ±0.001 g. The mass losses over the entire time interval were used to evaluate the changes in the corrosion rate with exposure time and were compared to the results from the corrosive solutions (HF corrosion products after each test).

Since scale formation was such a significant factor in the corrosion resistance of mild steel used in this study, the effect of the HNO_3 concentration and corrosion solution temperature on the mass of the scale formed during a corrosion test was also recorded. This was achieved by considering the mass of the scale washed off during cleaning, after a corrosion test, and comparing it to the mass of the original (orig.) and the pre-passivated (pre-pass) coupon. Therefore, coupons for the corrosion experiments were pre-passivated to represent the starting condition of the steel when calculating the percentage mass loss (% Mass loss), using the following equation:

$$\%\ \text{Mass loss} = \frac{(\text{Mass of orig. coupon}) - (\text{Mass of corroded coupon})}{\text{Mass of orig coupon}} \times 100 \qquad \text{Equation 4.3}$$

4.2.2.2. Apparent corrosion rate

Since the apparent density for each steel and metal alloy (Table 4.1) and the mass loss of each coupon was known, the apparent corrosion rate of each coupon during a corrosion experiment was determinable. To determine the apparent corrosion rate (CR) in mm/y, the following equation was used:

$$CR = 87.6 \times (W/\rho At) \qquad \text{Equation 4.4}$$

where W = weight loss (mg), r = density (g/cm^3), A =area (cm^2) of the coupons exposed to the corrosion solution over time (h) as per the ASTM Standard G31-72 (ASTM, 2009a). Here, the constant 87.6 is a dimensionless constant used to convert the units of mg, cm and h to the required units (mm/y). These constants are useful to corrosion engineers to convert easily between the different units (e.g. "mils per year" or micron/y) used when expressing corrosion rate (Davis, 2000; Jones, 1996).

4.2.2.3. Corrosion examination and observations

Scanning electron microscopy

The effects of the corrosion conditions tested in this study on scale formation on selected coupons were also more extensively examined by using a FEI Quanta 200 3D Scanning Electron Microscope (SEM) coupled with an Energy Dispersive X-ray Spectroscope (EDS). SEM and EDS analyses on cross-sections of the coupons were used to measure the effect a change in corrosion parameters had on the scale formation on the steel substrates. Depth profiles were drawn from EDS spot, and line scans were used to measure the depth of the scale and the change in composition when moving from the substrate to the surface scale (e.g. Figure 5.39).

The last coupon collected at the end of each corrosion test was directly mounted in a cold resin (not cleaned) and carefully sectioned using a Mintom precision cut-off machine (low speed diamond blade). The cold resin assisted in keeping the scale layer intact during cutting. A water-free cutting fluid was used during sectioning, as the fluoride scale was soluble in water. Subsequently, the cross-section was metallographically prepared using the automated grinding and polishing Tegra system from Struers. Samples were polished to a surface finish of 1 µm and then carbon-coated to produce a conductive layer over the cross-sectioned corroded coupon.

Since the metal substrate was much easier to prepare than the brittle fluoride scale, a great deal of the scale was pulled out during sample preparation. Therefore, during imaging, only the largest portions of the scale kept intact between the resin and the metal coupon were considered for spot analyses and line scans of the corrosion layers.

EDS analyses are not typically suited for quantification of light elements (low atomic mass), such as carbon, oxygen and fluorine (EDAX, 2013). However, using the latest TEAM software packages from EDAX allowed for considerably more accurate elemental quantification of all relevant elements in the study (Ni, Cr, Mo, Fe, Cu, Mn, F, O & C) which were comparable to glow discharge spectroscopy (GDS) and ICP-OES (Tables 5.10, 5.11 and 5.12) when quantitative results were normalized. SEM imaging with EDS quantification were also used in

distinguishing between the types of corrosion, particularly when distinguishing between pitting corrosion and uniform corrosion in instances when the pits were very small (<1 μm).

Digital photography

High resolution digital photography (13 megapixels) was used to establish the type and uniformity of surface corrosion (e.g. Figure 5.2 in Section 5.12). Photographs were taken of the coupons at different stages throughout the corrosion process on both sides of the coupon, including:

- Before a corrosion tests (sand-blasted coupon surfaces),
- After pre-passivation step, and
- At the end of a corrosion test.

These photographs were used to record the corrosion on the coupon surface and were compared with those collected at different times from the corrosion solution. The colours of the scales and oxide layers formed on the coupons over the period of a corrosion tests were also used to characterize the scales formed on the surface. After cleaning, or in instances when no scale formed during corrosion tests, the coupons were examined for other corrosion features. This could include pitting, uniform and erosion type corrosion.

Optical Microscopy

Optical microscopy was recommended for the examination of the coupon surfaces in ASTM Standard G4-95. General examinations of etching, pitting, dealloying, tarnishing, filming and scaling visible after corrosion were conducted at low magnifications (50× – 500×) using an Olympus BXiS microscope.

Pitting was evaluated using Practice G 46 - 94 (ASTM, 2009e). Direct pit measurements were conducted using a DSX510 high-resolution upright motorized microscope. Using the Olympus stream software packages available, it was possible to acquire 3D images of the original and corroded coupon surfaces (2 x 2 mm area) and then compare the pit depths. The motorized stages enabled a Z-stacking feature which made it possible to focus at the lowest point of a sample surface (in this case, the pit), acquire an optical image, step to a slightly higher focus point (a micron step), refocus and acquire another image. This process was repeated until optical images of the entire sample surface had been acquired (pit bottom to highest peak) and then combined to produce one, focussed, 3D image of the sample surface. This image was then converted into a 3D height map, 2D height image or 2D contour map in which colours were used to indicate height differences between the peaks and the valleys measured on the sample surface. Typically,

the darkest colours were used to indicate pits and lighter colours were used for the peaks (e.g. Figure 5.8). Using this technique, the formation of individual pits on the coupon surface associated with changes in the corrosion conditions (HF and HNO_3 concentration and corrosion solution temperature) could be examined. Subsequently, it was possible to compare pit measurements in terms of the number of pits identified on a coupon area selected (2 x 2 mm area) to the pit mouth diameters for each of those pits identified and individually measured (e.g. Figures 5.12 and 5.13) This gave a relatively good indication of susceptibility of a steel or alloy to pitting corrosion under the conditions tested and the degree to which this pitting occurred.

Glow discharge spectroscopy

Glow discharge optical emission spectroscopy (GD-OES) is an analytical technique specific to surface and depth profiling of thick (>100 μm), and more recently, extremely thin (10 nm) films (Philippe, 2001). The method works by using Argon ions (Ar^+) produced at low pressures (5 to 10 torr) during high negative potential (-800 to -1200 V) which is applied to the sample surface to cause plasma formation when the collision of Ar^+ with argon gas takes place. This plasma is called a glow discharge. The high velocity Ar^+ present is applied to uniformly sputter (or mill out) the material from the sample. The sputtered material then diffuses into the plasma, where it dissociates in atomic particles and proceeds in an excited state. Light emission from these excited atoms (as they collapse back to lower energy levels) is unique to each element present in the sample. Finally, the spectrum produced is used to determine the composition of the sample layer-by-layer. This technique allows for rapid and accurate description of the surface and bulk composition of both conducting and non-conducting materials. Depth profiles of an element in a solid sample can be acquired over several microns, by detecting emissions from atoms accommodated in plasma by sputtering.

Due to the porous nature of the corrosion scale and oxide layers formed on the coupons after corrosion tests, the application of GD analyses were limited because the samples needed to have a flat, preferably, polished surface which would produce a vacuum seal between the sample (cathode) and the GD lamp (anode). Due to this inherent limit of the instrument, depth profiles of the fluoride scale and oxide layers were primarily conducted using SEM and EDS analyses of cross-sections of the samples prepared. Therefore, the Leco GDS 850 at Necsa was mainly used for:

- Verification of steel and nickel alloy compositions prior to corrosion tests (Tables 5.10 to 5.12),
- Establishing the degree of scale removal from corrosion coupons after cleaning, and

- Verifying the accuracy of depth profiles produced from SEM-EDS type analyses.

Since GDS analyses, through optical immersion spectroscopy, was also a surface analytical technique and more sensitive (±0.1 wt%), it was useful in supporting results from EDS analyses.

X-ray diffraction

X-ray diffraction (XRD) was also needed to determine the phases on the specimen surfaces after corrosion. This technique was especially applicable in determining the difference in fluoride species formed in the post-mortem corrosion study, when comparing corrosion scale before and after exposure to HNO_3 in the storage vessels.

Electrochemical analyses

Corrosion experiments and examinations were conducted in accordance with the relevant ASTM (2009) standards practices (G31 – 72) and guides (G161 – 00) for corrosion tests and examinations (ASTM, 2009a; ASTM, 2009d). However, these procedures assume that all experiments can be conducted in glass reactors and using probes and measuring instruments that are completely resistant to chemical attack by the corrosive solutions prepared. Glass and materials reinforced with glass fibres (such as fibreglass or fibre-reinforced plastics), as well as materials rich in silica and silicon are not resistant to HF (ASM Handbook, 1987). For lower concentrations of HF (>4% HF), antimony probes can be used for potentiostatic and potentiodynamic polarization measurements used for corrosion testing. However, for higher concentrations, custom-made and extremely specialized potentiostatic experimental set-ups had to be employed. Therefore, all experiments needed to be conducted in highly HF resistant reactors (Teflon) with examination and handling of corrosion products only conducted in glassware when all the un-reacted HF had been completely washed off the corrosion products. Regrettably, corrosion could not be characterized and examined by electrochemical means at Necsa since the components (electrodes, glass ware and membranes) of Autolab 302 dynamic potentiostae available was not compatible with to 70% HF and the existing set-up could not be modified.

4.2.2.4. Verification of the alloy compositions

The compositions of the alloys were verified using three analytical techniques: glow discharge spectroscopy (GDS), SEM-EDS (scanning electron imaging in combination with elemental dispersive spectroscopy) and ICP-OES (inductively coupled plasma - optical emission spectrometry). SEM-EDS analyses relied on X-rays generated from a spot on the surface of the alloy (di = ~5 µm and 5 µm deep, at 30 kV) while ICP-OES were bulk analyses where 3.5 g of

the alloy was completely digested and then analysed. GDS was a combination of both techniques in which bulk analysis is conducted on a 10 mm wide surface (5 - 20 µm deep) of the alloy with the plasma generated during the burn being analysed using optical emission spectroscopy.

4.3. SAFETY CONSIDERATIONS

Aqueous HF and AHF (anhydrous hydrogen fluoride) are extremely hazardous chemicals. Even the fluoride salts that form as corrosion products are toxic in high concentrations (ASM Handbook, 1987). Painful, persistent burns result from contact with aqueous HF or AHF, and inhalation of high concentrations of the vapours causes lung damage which may be fatal. Therefore, safety was the top priority in this corrosion study, and the experiments could not be undertaken until all regulations related to working with HF had been implemented and obeyed.

A safety risk assessment had to be conducted before any experiments were done in any laboratories at Necsa. Category "A" signifies negligibly low risk and those experiments could be conducted as normal. However, any concentration more than 40% HF in a volume more than 2.5 mL fell within in a Category "C" on the internal Necsa Safety Risk Evaluation system (Louw, 2014). Therefore, in addition to the regular safety risk assessment, a process description, a "what if" analysis, as well as an external Hazard and operability study (HAZOP) needed to be conducted before the facility manager on-site could allow the experiments to be conducted at the Applied Chemistry (AC) Laboratories at Necsa. Then, only after the case for the use of HF had been considered and approved by all significant stakeholders (Safety Officer, Radiation Protection Officer, Facility Manager, Laboratory Manager and Line Manager) present in a project safety committee (PSC), were the corrosion experiments allowed to commence. Findings made during the PSC meeting were that the set-up and ventilation in the laboratories were adequate for handling up to 2.5 L 70% HF per experiment, and that during the handling (loading and removal of coupons) a second trained chemical worker needed to be present to assist during the experiment. This person was especially tasked with venting off HF fumes to the KOH scrubber during set-up or cleaning.

Assessment of the safety risks and construction of an experimental set-up to safely address all safety concerns associated with the corrosion experiments became a significant part of the study. The greatest resistance in furthering corrosion related research in an HF media is due to the great health risks and numerous precautions associated with working with the acid in any concentration. Since much effort went into the safety risk assessment and addressing all concerns

before the corrosion tests could commence, a paper was written to summarize the findings from the safety risk assessment (Appendix C).

4.4. PLANNED INTERVAL CORROSION TESTS

4.4.1. Planned interval corrosion test methods

Planned interval corrosion tests (PICTs) were preferred in the initial stages of the study as they required smaller volumes of acid, smaller quantities of coupons and were quicker and much safer to conduct. Therefore, several PICTs could be conducted to discover the conditions best suited for the longer, more comprehensive corrosion tests (CTs). The conditions and variables which were relevant and altered during the PICT are given in Table 4.2 (with considerations for coupon sizes addressed in Appendix B).

Table 4.2: Conditions and variables and experimental conditions for PICTs conducted.

No.	**Conditions**	**Values**
1.	Agitation	None
2.	Pre-passivation step	24 hours
3.	Effective reactor volume	463 ml (initial 500 ml minus displacement of corrosion rack and coupon volumes)
4.	Total contact time	8 days (192 hours)
5.	Coupon surface area	15.39 cm^2
No.	**Variables**	**Values**
1.	Material	1) Mild steel, Code: SA516 Grade 70 2) Stainless steel: SS 904 L 3) Nickel alloy: Monel (Alloy) 400
2.	Metals analysed in solution	Fe, Mn, Cr, Ni, Cu and Si
3.	Percentage HF	40, 48 and 70%
4.	Percentage HNO_3	0% (>50 ppm)
5.	Pressure	100 kPa (STP)
6.	Temperature	25°C (STP)

Apparatus

Planned interval corrosion tests (PICTs) were used to determine the necessary duration of a typical corrosion test when safely conducting immersion type corrosion tests in HF (ASTM, 2009a). Only when the most suitable conditions were determined in this phase, would the effect

of nitric acid and temperature be tested in the next phase, where more comprehensive corrosion tests (CTs) were conducted.

PICTs were carried out in a 500 mL Teflon bottle (Figure 4.7a) placed in a 10 L 1800 Watt Memmet water bath which maintained the corrosion solution at a constant temperature. A photograph of the working immersion type corrosion set-up, as prescribed by ASTM standard practice G3 – 72 (ASTM, 2009a), is given in Figure 4.6. Since ambient temperature in the fume cupboard frequently was above 25ºC, a Julabo FT402 immersion cooler was used to cool the water in the bath. The water bath could only regulate water by heating, hence external cooling needed to be implemented to maintain an opposing reduced temperature. The water bath was supplied standard with a steel lid, which was replaced with a polypropylene lid that was custom-made to cover the bath and allowed the immersion cooler to hang freely in the water (Figure 4.6). A Pt100 sensor was connected to the immersion cooler and was suspended from the water bath lid to measure temperature at the same point as the water bath's own thermometer. In this way, the sensors would match readings to facilitate the water bath heating and immersion cooling to reach a steady state at 25ºC, after an hour.

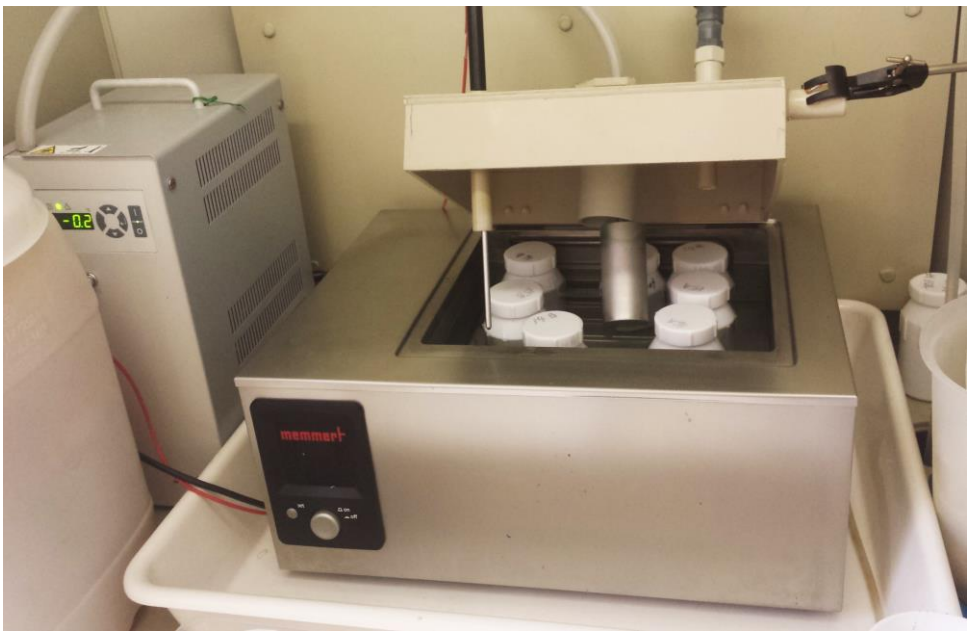

Figure 4.6: Water bath with immersion cooler set-up for corrosion tests.

Maintaining the temperature below 25ºC meant HF fuming was reduced (a reduction in vapour pressure), effectively lowering the safety risk of working with 70% HF in the Teflon bottles. Additionally, a 2 mm hole was drilled into the centre of the Teflon bottle's lid to allow for the release of HF fumes in order to avoid any pressure build-up over the duration of the PICT. The HF-resistant lid was made to shield the immersion cooler from fumes that may have escaped

during the corrosion reaction and it had a release valve in the open position, which channelled any fumes away from the apparatus and water to the extraction line of the fume cupboard, which led out to the KOH scrubber.

For each test, coupons were assembled into a cylindrical rack which was machined out of a Teflon pipe (45 mm diameter x 130 mm height). A significant portion of the pipe was machined away to produce elongated gaps along the entire circumference of the rack (Figure 4.7b), to serve three purposes:

1) effectively reduce the volume of corrosion solution displaced by the rack in the Teflon bottles,
2) permit interaction between the HF and the coupons (i.e. not create a circulation barrier), and
3) hold the 46 mm Teflon rod (7 mm diameter) in place, from which the coupons were hung during the test (Figure 4.8).

a  b 

Figure 4.7: Corrosion reactor components: (a) Teflon bottle, and (b) cylindrical corrosion rack with Teflon rod to the suspend coupon.



Figure 4.8: Top view of a complete assembly for a planned interval corrosion test.

Procedures of planned interval corrosion tests

For each PICT, the three coupons were assembled into the cylindrical rack (Figure 4.7b) and placed upright into the Teflon bottle (Figure 4.8). The HF corrosion solution was then poured into the bottle until the cylindrical rack was completely covered. The bottle lid was then screwed on to seal the corrosion reactor, and the bottle placed in the water bath (Figure 4.6). The lid of the water bath was closed, the immersion cooler submersed into the water in the bath, and the Pt100 sensor aligned with the water bath thermometer. The corrosion reaction was then allowed to take place, unhindered, for the allotted time.

To pre-passivate the coupons, the same procedure was used as for conducting a corrosion test, except that the coupons were exposed to fresh HF for 24 hours. Typically, a uniform scale formed covering the whole surface of the coupon. These coupons were then removed from the acid, rinsed with water, and dried for use in the actual PICTs. Corrosion of the coupons then took place by exposing the coupons to the prepared corrosion solution for periods of time experimentally determined by the planned interval tests of Wachter and Treseder (1947) in ASTM Standard G 31-72 (ASTM, 2009a). The procedures of a typical PICT are described in the paper already published on this part of the corrosion study (Appendix C).

To measure the mass loss, corrosion rate and estimate the susceptibility of the steel and metal alloys to corrosion, coupons were successively removed from the bottle after 1, 4 and 8 days. To estimate the effect of the corrosion reaction on the liquid corrosiveness of the HF over time, a new coupon was introduced to the system on the 4th day and then removed with the last remaining coupon on the last day.

When removing a coupon during the corrosion tests, the water bath lid was opened; the Teflon bottle containing the corroding coupon was removed from the bath and then placed in a spill tray inside the fume cupboard. The elephant trunk used to vent off HF fumes was then positioned over the bottle and the lid was removed. Fumes were allowed to vent off before the corrosion rack was removed from the bottle and placed in a separate Teflon cylinder. The coupon was then removed from the rack with minimal disturbance to the remaining coupons. The removed coupon was then placed in its own Teflon holder and sealed. The rack with the remaining coupons was then reintroduced to the Teflon bottle still holding the corrosion solution. The lid of the Teflon bottle (with the 2 mm hole in) was then screwed on, and the bottle was reintroduced to the water bath to continue the test. Care was taken to remove coupons swiftly to minimize the impact of the disruption to the test.

To verify the quality of the HF used for each test, 40 mL of fresh HF was taken from the purchased HF solutions (40%, 48% 70% HF) and was sent for analyses. For each PICT, a 40 mL sample of the corrosion solution collected after 8 days (Final product) was also sent for analyses at Pelindaba Analytical Labs (PAL) at Necsa. This sample was collected by sucking up the solution from the top of the corrosion reactor, using a polyethylene pipette connected to a pro-pipette, prior to removing the rack with corroded coupons from the Teflon bottle.

On completion of a PICT, the water bath and immersion cooler were switched off. The Teflon bottle was removed from the bath and the coupons and corrosion rack taken out and rinsed in a Teflon holder inside the fume cupboard. The remaining corrosion solution was poured into a 25 L high density polyethylene (HDPE) waste bottle for disposal. The Teflon bottle, corrosion rack and coupons were rinsed with tap water until all traces of HF was removed. The bottle and rack were cleaned, dried and reassembled with new coupons for the next test.

4.4.2. Effect of pre-passivation on mild steel

Following ASTM Standard Practice G 31 – 72 (ASTM, 2009a), the procedures for planned interval type corrosion tests, as described by Watcher and Treseder (1947) in the ASTM practice, were followed to evaluate the HF corrosiveness and the susceptibility of the metals that were selected for testing (Jones, 1996). In adhering to the prescribed method, four coupons were exposed to the same corrosion solution at different time intervals (Table 4.3). The test started with three coupons in the HF solution (A_1, A_t and A_{t+1}) with the first coupon (A_1) being removed after only 1 day in solution (ASTM, 2009a). The second coupon (A_t) was removed from the corrosion solution after four days and replaced by the final coupon (B), which was then allowed to corrode with coupon 3 (A_{t+1}) until the end of the test. Thus, specific to the PICTs conducted in this study, the subscripts "1" (from A_1) signifies 1 day, subscript "t" (in A_t) selected as 3 days, and therefore subscript t+1 (from A_{t+1}) indicating a total of 4 days in the corrosion solution (ASTM, 2009a). Subsequently, by comparing the apparent corrosion rates determined for coupons 3 and 4, the liquid corrosiveness was evaluated using the criteria set out in the ASTM practice (Table 4.3). In the same way, the susceptibility of the metal coupon (corrosion resistance) to the HF corrosion solution was evaluated by comparing the corrosion rate determined for coupon B to that of coupon A_2. The mass loss value required to determine the apparent corrosion rate for coupon A_2 was calculated by subtracting the mass losses of coupons A_t and A_{t-1} (e.g. Table 4.3).

Table 4.3: Criteria for planned interval corrosion tests.
(Adapted from ASTM standard practice G31 – 72)

Occurrence During Corrosion Test		**Criteria**
Liquid corrosiveness	unchanged	$A_1 = B$
	decreased	$B < A_1$
	increased	$A_1 < B$
Susceptibility to corrosion (Metal corrodibility)	unchanged	$A_2 = B$
	decreased	$A_2 < B$
	increased	$B < A_2$
Combinations of Situations		
Liquid corrosiveness	**Susceptibility to corrosion**	**Criteria**
1. unchanged	unchanged	$A_1 = A_2 = B$
2. unchanged	decreased	$A_2 < A_1 = B$
3. unchanged	increased	$A_1 = B < A_2$
4. decreased	unchanged	$A_2 = B < A_1$
5. decreased	decreased	$A_2 < B < A_1$
6. decreased	increased	$A_1 > B < A_2$
7. increased	unchanged	$A_1 < A_2 = B$
8. increased	decreased	$A_1 < B > A_2$
9. increased	increased	$A_1 < B < A_2$

To determine the corrosiveness of the HF solution with time, and the susceptibility of mild steel to corrosion by HF in varying concentrations, the temperature was kept constant at 25ºC. In addition, the effects of pre-passivating the mild steel for the recommended 24 hours prior to the PICTs were compared to the experiment with the raw, untreated (non pre-passivated) coupons. However, in the instances where stainless steel and nickel alloys were tested, the pre-passivation step (submerging coupons for 24 h in 70% HF) served to be a cleaning step, prior to a corrosion test.

4.4.3. Effect of HF concentration on mild steel

A series of PICTs was conducted to determine the effect of an increase in concentration of hydrofluoric acid in the corrosion solution on the corrosion resistance of mild steel. HF solutions with concentrations lower than 60% HF would produces marginally less fumes under the experimental conditions considered, than HF concentrations which were higher than 70%. For this reason, corrosion experiments conducted in 40% and 48% HF carried a significantly lower safety risk when conducted at atmospheric pressures. Thus, initially it was considered that corrosion tests be conducted at lower HF concentrations (>60%) to reduce the safety risk associated with the study. In establishing the conditions and HF concentrations for the corrosion experiments an added benefit was that the effect of HF concentrations on the SA 516 Grade 70 normalized steel could be established (as described in the article for African Journal of Corrosion, in Appendix C)

4.4.4. Effect of steel and alloy composition

Planned interval corrosion tests on each of the stainless steels and nickel alloys used in the plant (Table 4.1) were also conducted. This was to determine whether the corrosion test parameters established for mild steel corrosion could be used for the steels and nickel alloys chosen. The necessity for a pre-passivation step prior to corrosion tests was also determined through these PICTs.

4.5. CORROSION TESTS

4.5.1. Corrosion test methods

Corrosion tests (CTs) were the more extensive corrosion tests where the effect of temperature and nitric acid concentration in the corrosion solution were the main focus. The experimental conditions specific to this phase of the study was established during the PICTs conducted in the previous Section and are given in Table 4.4.

Table 4.4: Conditions and variables and experimental conditions for CTs conducted.

No.	**Conditions**	**Values**
1.	Agitation	None
2.	Pre-passivation step	24 hours
3.	Effective reactor volume	Reactor A + B = 926 mL
4.	Total contact time	11 days (192 hours)
5.	Coupon surface area	15.39 cm^2
No.	**Variables**	**Values**
1.	Material	1) Mild steel, Code: SA516 Grade 70 2) Stainless steel: SS 904 L 3) Nickel alloy: Monel (Alloy) 400
2.	Metals analysed in solution	Fe, Mn, Cr, Ni, Cu and Si
3.	Percentage HF	70, 69.92, 69.6 and 69.21 vol.% (Dependent on vol. of 65% HNO_3 spiked)
4.	Percentage HNO_3	0, 0.1, 0.5 and 1 vol.%
5.	Pressure	100 kPa (Atmospheric pressure)
6.	Temperature	0, 15 and 25°C

Apparatus

Corrosion tests were carried out in the same Teflon bottles and corrosion rack set-up as described for PICT (Section 4.4.1), except that two corrosion reactors (with a combined volume of nearly

1 L) were used per test. This was because the CTs differed from the PICTs in that double the amounts of coupons (eight) were corroded over an 11 day period. Since twice the amount of coupons needed to be tested, the volume of HF which was used in the PICTs needed to be adjusted to maintain the same acid volume per coupon area ratio in the CT (Appendix B). Having more samples to take out over more regular time intervals meant that more comprehensive corrosion data were generated. This was especially important in determining corrosion kinetics and monitoring the consistency (sensitivity) of corrosion results when altering a parameter.

Procedures

The procedures for conducting corrosion tests were predominantly the same as described for the PICT, with the only exception being the sequence in which the coupons were removed at each allocated time interval (Table 4.5). The two Teflon bottles used per CT were labelled as corrosion reactors A and B. Since all the coupons were equally spread over two bottles, one coupon would be removed from bottle A on the first day, and one from bottle B on the next day. This sequence (A, B, A, B…) was maintained until the end of the experiment where both coupons 7 and 8 were removed from bottles A and B respectively on the last day. Maintaining this sequence over the period of a corrosion tests maintained a relatively constant acid volume to coupon area ratio over the entire corrosion test run time. The acid volume per coupon area ratio was identified as a significant factor in the PICTs. Therefore, this alternating sequence of removing coupons from the bottles mitigated the effect of the change in coupon surface area (reduction in available coupons to corrode per bottle) on the acid corrosivity and the susceptibility of the remaining coupons to corrosion. This proved to be an effective experimental technique as subsequent corrosion data produced did not deviate much from linearity (e.g. Figure 6.11 for CT to Figure 6.7 for PICT), where all corrosion data generated were from one bottle.

Procedures for the collection of samples after pre-passivation (Pre-pass) and at the completion of a CT (Final Prod.) were identical to PICT. However, to save on analytical costs, solution samples were only collected from Teflon Bottle A. Thus, corrosion data from corroded coupons numbered 1, 3, 5 & 7 (collected from Bottle A) were used in determining the effect of temperature and HNO_3 concentration on acid consumption.

Table 4.5: Set-up and time intervals for corrosion tests.

Coupon No.	Hours in solution	Days in solution	Day	Days between sampling	Remove from Teflon bottle
Pre-pass	0		Thursday		
1-8	24	1	Friday		A + B
			Saturday		
			Sunday		
	0	0	Monday		
1	24	1	Tuesday	1	A
2	48	2	Wednesday	1	B
3	72	3	Thursday	1	A
4	96	4	Friday	1	B
	120	5	Saturday		
	144	6	Sunday		
5	168	7	Monday	3	A
	192	8	Tuesday		
6	216	9	Wednesday	2	B
	240	10	Thursday		
7 + 8	264	11	Friday	2	A + B

The procedures followed after the completion of CTs were similar to those of PICTs with HF and corrosion products disposed of in the same 25 L HDPE bottles. The Teflon bottles A and B, their respective corrosion racks and coupons were rinsed with tap water until all traces of HF were removed. The bottles and racks were cleaned, dried and reassembled with new coupons, for the next test.

4.5.2. Mild steel corrosion

4.5.2.1. Effect of nitric acid concentration

A series of corrosion tests were conducted to determine the effect of increasing nitric acid concentration (% HNO_3), present in the mother acid (70% HF), on the corrosion rate of the SA 516 Grade 70 normalized mild steel. Pre-passivated coupons were immersed in 70% HF which was spiked with different volumes of HNO_3 to make up the required concentrations for each corrosion test in stage 1 (Table 4.6). The amount of mild steel coupons made from the specific grade of mild steel used to manufacture the HF storage tanks commissioned in 1993 was limited. For this reason, corrosion experiments were only duplicated for selected tests. Repeats of

corrosion tests at a given set of conditions (HNO_3 concentration and temperature) were conducted to validate the reproducibility of the experiments.

Table 4.6: Laboratory simulated conditions metals coupons were exposed to during corrosion experiments.

Stage	**Coupon (metal)**	**HNO_3 (wt%)**	**Temperature (ºC)**
1	Mild steel	0*, 0.2, 0.5 and 1*	25
2	Mild steel	0, 0.2, 0.5 and 1*	15
3	Mild steel	0, 0.2, 0.5and 1*	0
4	Alloy 400 - Monel	0 and 1	25
5	Stainless steel- 904 L	0 and 1	25

*Duplicate corrosion test conducted

4.5.2.2. Effect of temperature

In the second and third corrosion test stage, the corrosion tests were conducted at lower temperatures (15ºC and 0ºC) varying the HNO_3 concentration (Table 4.2). The lower temperatures were achieved by replacing the water in the bath with antifreeze (Shell Thermia D Heat transfer fluid). As a precaution, it was specified that the Thermia D be heated to above 55ºC for 3 hours to allow for all the residual water to evaporate from the bath. Subsequently, uniform cooling could be achieved by means of the immersion cooler which was linked to a thermocouple (Pt100 sensor) submerged into the anti-freeze. 70% HF freezes as below -36ºC (Honeywell International Inc, 2014), therefore, liquid interaction between the coupons and acid was ensured throughout the colder tests. Corrosion tests above 25ºC were abandoned due to 70% HF's fuming capacity at higher temperatures (vapour pressure is 20 to 40 kPa at 20ºC), which produces hydrogen fluoride fumes on spilling (Hathaway & Proctor, 2014; Pelchem, 2015). To avoid pressure build-up, from escaping HF fumes in the 500 mL Teflon corrosion reactors, a 2 mm hole was drilled into the reactor lids. Preliminary tests proved that no more than 2.5 mL of HF per day escaped from the reactor at 25ºC, and did not affect the acid volume per coupon area requirement set per test (>0.3 mL/mm^2) over the two weeks of testing (Appendix B).

4.5.2.3. Effect on scale thickness

An attempt was made to determine the effect of HNO_3 in a 70% HF corrosion solution on the scale, which typically formed on the mild steel coupons during the pre-passivation step. This investigation was limited due of the probability of removing significant portions of the water

soluble fluoride scale during the metallographic sample preparation of the cross-sections. Moreover, in most instances, the scale was porous enough to allow the cold resin to diffuse into the scale during mounting. Removal of these carbon artefacts from the EDS spectra was problematic due to the carbon introduced during carbon-coating of the cross-sections, which was essential for SEM imaging. Therefore, for the purpose of this investigation, the mostly intact and largest portions of the scale visible on the surface of each cross-section were selected for examination, with carbon recorded as it was. Scanning electron microscopy (SEM) and energy dispersive spectroscopy (EDS) were done on the cross-sections of the samples.

4.5.3. Nickel alloy and stainless steel corrosion

Monel 400 was used as construction material for the dip tubes used in sampling HF in the storage tanks (Table 4.1). Stainless steel (SS 904 L) was used as construction material of the Y-piece of the pipes which connects the kiln (where HF is first formed) to the rest of the plant. The 904 L steel is also used throughout the plant, especially in high temperature applications where HF is involved (>50ºC) for instance, the lining of the rotary kiln.

The alloys were hot-rolled and water-jet cut to the same specifications as the mild steel coupons tested. Pre-passivation was not a prerequisite, as nickel alloys and stainless steels are resistant to corrosion by oxidizing and reducing acids (ASM Handbook, 1987) and are typically used as-received in commercial HF plants. However, pre-passivation was still applied to make the results comparable to mild steel corrosion data. PICTs revealed that exposing the Alloy 400 to 70% for 24 h had a minimal effect on the corrosion (<0.1% mass loss) and served more as a chemical cleaning step as no passive layer formed (Figure 5.18, Section 5.13). Conversely, the steel corroded significantly over the 24 h time period (~1% mass loss) with an unstable, black, oxide, scale (Figure 5.16, Section 5.13) forming on the surface after the passivation step.

Corrosion test parameters

The worst-case scenario corrosion tests were carried out at conditions found to produce the highest corrosion rates in the mild steel corrosion tests (stages 1-3 in Table 4.6). Conducting corrosion tests at the harshest possible corrosion conditions provided a benchmark for other alloys tested (Table 4.6). Moreover, the corrosion tests served as a relatively quick evaluation method to determine the suitability of the steels and alloys used and considered for use in an HF plant exposed to significant HNO_3 contamination in the stream.

The harshest corrosion parameters achievable in the current set-up were identified as (Section 4.5.2):

- HNO_3 concentration = 1%
- HF concentration = 69.21%
- Temperature = 25ºC

when using a constant coupon size 25 x 25 x 3 mm and maintaining an acid volume / coupon area of more than 0.3 mL/mm^2 (Appendix B).

CHAPTER 5

RESULTS

5.1. PLANNED INTERVAL COROSION TESTS

5.1.1. Introduction

The planned interval corrosion tests (PICTs) were carried out to determine the necessary duration of an immersion type corrosion test when conducted in a HF corrosion solution (40 - 70% HF). The formation of a fluoride scale on the mild steel is an essential pre-passivation step that contributes greatly to the corrosion resistance of mild steel in an HF environment (Jennings, 2007). To validate this type of scale formation for this study, PICTs were carried out on steels and nickel alloys both with and without pre-passivation.

Corrosion data collected during the PICT were relevant and showed the unique corrosion characteristics pertinent to these conditions early on. It was later found that these shorter tests compared well to the more comprehensive eleven day Corrosion Tests (CTs) and could be used to verify the corrosion data up to eight days, for when no nitric acid was present.

5.1.2. Effect of pre-passivation on mild steel

Susceptibility to HF corrosion

The criterion used to distinguish whether the corrosion resistance of the steel was affected, and how much, by the corrosivity of HF during a PICT, was adapted from ASTM standard practice G31 – 72 (ASTM, 2009a) and summarized in Table 4.3 in the previous section. The benchmark for corrosion resistance of pre-passivated mild steel set for this study was 1 mm/y, from perceived acceptable corrosion rates in an HF plant (Valkenburgh, 2012a). Thus, the criterion for decreased corrosion resistance was a corrosion rate below 1 mm/y, while an increased susceptibility of the mild steel to corrosion by HF were corrosion rates above 1 mm/y.

The resulting corrosion behaviour of mild steel in 40% HF indicated that the corrosion rate calculated for the A_2 value was smaller than the rate measured for B, and therefore the steel's susceptibility to corrosion (corrodibility) decreased at these conditions (Tables 4.3 and 5.1). Conversely, pre-passivation of the steel slightly reduced the corrosion resistance of the coupons in this test, which showed a decrease in the susceptibility of the steel to 40% HF corrosion

(Table 5.2), when correlated to the employed criteria (Tables 4.3). This was because the apparent corrosion rate for the pre-passivated coupon, A_2, was only 1.3 times slower than the B coupon. However, when compared to the corrosion rate of the untreated coupons, it was at least 20 times slower. This indicated that pre-passivation of the coupon effectively increased the susceptibility of the mild steel to corrosive attack in more diluted HF corrosion solutions (≤48% HF).

With or without pre-passivation, corrosion rates of coupon B were smaller than coupon A_1 and therefore the liquid corrosivity of the acid decreased over time. The situation ($A_2 < B < A_1$) indicated that the 40% HF significantly decreased in corrosiveness during the test. According to ASTM Standard Practice G 31 – 72, adherence to this criterion likely indicates the formation of a protective scale on the steel. However, this scale covering the coupon surface did not serve to mitigate corrosion of the steel under these conditions, since the mass losses and apparent corrosion rates were higher (Table 5.2).

Table 5.1: Planned interval corrosion tests for mild steel in 40% HF.

Coupon No.	**Interval (days)**	**Mass loss (g)**	**Apparent corrosion rate (mm/y)**
1) A_1	0 – 1	5.01	151.5
2) A_t	0 – 4	5.65	42.6
3) A_{t+1}	0 – 8	5.71	21.6
4) B	4 – 8	1.32	10.0
Calc. A_2	4 – 8	0.07	0.5
0.5 mm/y < 10.0 mm/y < 151.5	**Liquid corrosiveness:**		Decreased
Therefore : $A_2 < B < A_1$	**Susceptibility to corrosion:**		Decreased

Table 5.2: Planned interval corrosion tests for mild steel in 40% HF – pre-passivated.

Coupon No.	**Interval (days)**	**Mass loss (g)**	**Apparent corrosion rate (mm/y)**
1) A_1	0 – 1	5.03	152.2
2) A_t	0 – 4	5.63	42.6
3) A_{t+1}	0 – 8	6.04	22.8
4) B	4 – 8	0.524	4.0
Calc. A_2	4 – 8	0.407	3.1
3.1 mm/y < 4.0 mm/y < 152.2 mm/y	**Liquid corrosiveness:**		Decreased
Therefore : $A_2 < B < A_1$	**Susceptibility to corrosion:**		Decreased

The highest concentration analytical grade HF (≥5ppm nitrate) available at the time was 48% HF (Table 5.3). The PICT tests conducted with 40% HF produced excessively high corrosion rates

for mild steel because in the lower HF concentration it did not form a stable scale layer on the surface, which was essential to protect mild steel in such an aggressive HF environment.

Unexpectedly, the higher HF concentration did not show an increase in either the corrosivity of the 48% HF used or the susceptibility of the steel (Table 5.4).

Table 5.3: Planned interval corrosion tests for mild steel in 48% HF.

Coupon No.	**Interval (days)**	**Mass loss (g)**	**Apparent corrosion rate (mm/y)**
1) A_1	0 – 1	5.65	170.7
2) A_t	0 – 4	5.50	41.5
3) A_{t+1}	0 – 8	5.50	20.8
4) B	4 – 8	5.69	43.0
Calc.) A_2	4 – 8	0.90	6.8
6.8 mm/y < 43 mm/y < 170.7 mm/y	**Liquid corrosiveness:**		Decreased
Therefore : $A_2 < B < A_1$	**Susceptibility to corrosion:**		Decreased

Table 5.4: Planned interval corrosion tests for mild steel in 48% HF – pre-passivated.

Coupon No.	**Interval (days)**	**Mass loss (g)**	**Apparent corrosion rate (mm/y)**
1) A_1	0 – 1	6.06	183.1
2) A_t	0 – 4	5.54	41.8
3) A_{t+1}	0 – 8	6.12	23.1
4) B	4 – 8	1.01	7.6
Calc.) A_2	4 – 8	0.58	4.4
4.4 mm/y < 7.6 mm/y < 183.1 mm/y	**Liquid corrosiveness:**		Decreased
Therefore : $A_2 < B < A_1$	**Susceptibility to corrosion:**		Decreased

The 70% HF PICTs were conducted under the same conditions as the 40 and 48% HF tests. However, the corrosion rates determined for A_2, B and A_1 decreased significantly (more than 4.8, 5 and 87 times smaller). As with all previous HF corrosion experiments conducted (Tables 5.1 – 5.4), the liquid corrosiveness and the susceptibility of the mild steel to corrosion decreased in all instances (Tables 5.5 and 5.6).

Regarding the necessity of a pre-passivation step, conversely to the findings made when conducting the experiments with 40 and 48% HF (Tables 5.2 and 5.4), the corrosiveness of the 70% HF effectively reduced when the steel was pre-passivated. The untreated mild steel corroded 1.6 times faster than the pre-passivated steel (A_1 value in Table 5.5 compared to its

counterpart in Table 5.6), thus indicating that 70% HF reacted less readily with the pre-passivated steel.

Table 5.5: Planned interval corrosion tests for mild steel in 70% HF.

Coupon No.	**Interval (days)**	**Mass loss (g)**	**Apparent corrosion rate (mm/y)**
1) A_1	0 – 1	0.11	3.4
2) A_t	0 – 4	0.16	1.2
3) A_{t+1}	0 – 8	0.28	1.1
4) B	4 – 8	0.20	1.5
Calc. A_2	4 – 8	0.13	0.9
0.9 mm/y < 1.5 mm/y < 3.4 mm/y	**Liquid corrosiveness:**		Decreased
Therefore : $A_2 < B < A_1$	**Susceptibility to corrosion:**		Decreased

Table 5.6: Planned interval corrosion tests for mild steel in 70% HF – pre-passivated.

Coupon No.	**Interval (days)**	**Mass loss (g)**	**Apparent corrosion rate (mm/y)**
1) A_1	0 – 1	0.07	2.1
2) A_t	0 – 4	0.20	1.5
3) A_{t+1}	0 – 8	0.32	1.2
4) B	4 – 8	0.20	1.5
Calc. A_2	4 – 8	0.12	0.9
0.9 mm/y < 1.5 mm/y < 2.1 mm/y	**Liquid corrosiveness:**		Decreased
Therefore : $A_2 < B < A_1$	**Susceptibility to corrosion:**		Decreased

Acid consumption

A change in HF acid consumed, owing to the percentage HF available to react with the coupons, had an opposing impact. A higher concentration of HF available should have resulted in more acid being available to attack the surface of the mild steel coupons. However, in the case of HF corrosion, the lower the concentration of the HF used, the higher the mass of acid consumed during the reaction (Table 5.7). Pre-passivated coupons exposed to the 40% HF had consumed two times more acid than coupons exposed to 48% and nearly four times more than the equivalent mass of coupons exposed to 70% HF (Figure 5.1).

The typical mechanism involved in HF corrosion of mild steel is the formation of a fluoride scale on the mild steel surface which mitigates further attack. Throughout this study, this scale was not very stable and observed to be soluble in water, during cleaning procedures (Section 4.1.3.3). Irrespective of the high initial attack of HF on a clean mild steel coupon surface, the corrosion rate quickly dropped after 24 hours due to the formation of a passive oxide fluoride layer (Tables

5.8 and 5.9). Thus, when a pre-passivated coupon is exposed to fresh 70% HF solution, acid consumption is reduced because of the stable protective scale preventing access to the steel substrate. When using lower concentration HF corrosion solutions (40% and 48%) the scale layer did not form as consistently because fluorine (F^-) needed from the HF to form the fluoride layer in solution, and the fluorine was significantly less (30% and 22% less) than 70% HF. Additionally, the higher water content of the more dilute acids (>50% H_2O) tended to dissolve the fluoride scale that did form under these challenging conditions. This led to continual corrosive attack of the exposed mild steel surface and therefore higher acid consumption of the less concentrated acids (Figure 5.1).

Table 5.7: HF acid consumption by mild steel after 8 days when varying HF feed concentration, at 25ºC – pre-passivated.

Feed HF concn. (%)	**Product HF concn. (% HF)**	**Mass of acid in feed (g)**	**Mass of acid in product (g)**	**Mass of Coupons (g)**	**Acid Consumed**	
					$\left(\text{g HF}/\text{g Fe}\right)$	**(%)**
40.95*	38.09	189.77	176.52	39.14	0.34	7.0
48.65*	46.86	230.07	217.16	48.84	0.17	3.7
70.02*	68.81	324.49	318.88	61.23	0.09	1.7

*Average value from triplicate solution analyses conducted with errors captured in the graphs discussed.

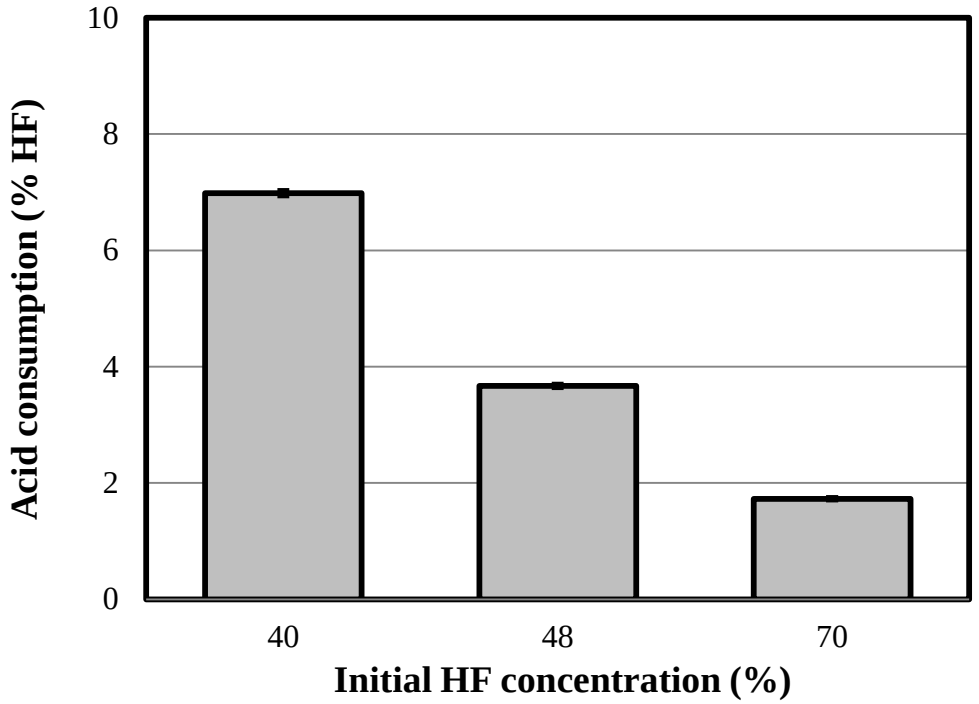

Figure 5.1: Effect of an increase in percentage HF in the corrosion solution on percentage acid consumption after 8 days of mild steel corrosion, at 25ºC. Error bars obscured by markers in some instances.

Observations of photographs of corroded coupons

The photographs taken of the mild steel coupons before and after exposure to HF, as well as after removal of the scale layer, are shown in Figures 5.2 - 5.7. From Haynes (2016) the physical form of compounds are provided (for solids at room temperature), through which colour and other descriptive features tabulated were used to distinguish between different crystal systems. Using XRD data (Section 3.5) and information from EDS analyses (Figures 5.38 – 5.42 in Section 5.2.2.2) made it possible to tie compounds found on corroded coupon surfaces to crystal systems (and their colours) identified in Haynes (2016). Scale formed on the surfaces of coupons exposed to HF was identified to be either oxides or fluorides, depending on the degree of oxidation that took place. Thus, scale was either composed of black or red iron oxides, grey fluorides or yellow-brown ferric-fluoride-hydrates. Since only ultrasonic cleaning was employed when cleaning the coupons, a thin fluoride layer was still visibly present on the surface of most coupons and found to have a negligible impact on the mass loss determinations (Tables 5.8 and 5.9). This was confirmed by mechanically cleaning coupons (steel brush washed), which have already been ultrasonically cleaned, consistently losing less than 0.001 g.

Corrosion products in the form of scale or discolouration on the coupon surfaces were examined together with visible holes and other corrosion damage on the surfaces exposed after cleaning. To support the observations made, the corrosion solution collected at the end of a PICT was analysed for dissolved metal content to determine the quantity of an element removed from the coupon surfaces during the test. Regrettably, in the PICTs where coupons were exposed to 40% and 48% HF for the first time, solutions samples from the corrosion products were not collected for ICP-OES analyses and were prematurely disposed (Table 5.8). This was because these PICTs were only needed in the initial stages of the study when establishing the conditions for the detailed corrosion tests (CTs) and therefore not originally considered for solution analysed. The relevance of the corrosion results generated from these two tests was only appreciated afterwards, after visual examinations of the surfaces were done.

Sand-blasted mild steel coupons had a silver grey colour and a matt-like surface (Figures 5.2 – 5.7: Row a). The observations made on the individual coupons collected after each PICT conducted on mild steel are summarized in Tables 5.8 and 5.9. For the PICTs conducted on mild steel, all coupons showed a heavily oxidized surface after pre-passivation (Figures 5.4 – 5.6). The corrosive attack on the mild steel coupons, as affected by the change in HF concentration and pre-passivation, was best observed after cleaning the coupons and could be individually compared.

Pitting corrosion was visible over the entire surface of coupons exposed to 40% HF (Figures 5.2 and 5.5), and was also confirmed by high magnification optical microscopy on the cleaned surfaces (Figure 5.9). Scale did form on the coupons during the 40% HF PICT, but could not prevent corrosive attack by pitting, which penetrated through the visibly porous passivation scale and aggressively kept corroding underneath the scale. In corrosion tests where only HF corrosion was involved, attack by 40% HF was more detrimental to the coupons than any other test conducted to date (Figures 5.2 and 5.5).

The 48% HF produced a visibly more aggressive attack over the entire surface of the coupons and was a more uniform corrosion (Figures 5.3 and 5.6). Compared to the 40% HF test (Figure 5.9), optical microscopy did not reveal more pits on the surfaces attacked by 48% HF (Figure 5.10). The iron concentrations of the varying HF concentrations solutions were determined and are given in Figure 5.9. The corrosion product solutions from the 48% PICT had nearly three times less iron in than for the 40% HF test. This supported observations made on the quality of the scale, since more iron was present in the solid scale in the 48% HF test, than for the 40% PICT. The 40% and 48% HF PICTs were the only corrosion tests in which solid residues (scale) were collected at the bottom of the bottles. Therefore, after growing to a reasonable size, the scale easily broke off during the test and fell to the bottom of the bottle (Table 5.9). A freshly exposed mild steel coupon surface could corrode again, which repeated the cycle of continual scale formation. Thus, even though more scale formed in lower HF concentrations (≥48% HF), this scale was more unstable and thus less effective at protecting the steel surfaces compared to scale formed in higher concentration HF solutions (≥70% HF).

Table 5.8: Observations of corrosion products of PICTs conducted in 40, 48 and 70% HF, after 8 days (Figures 5.2, 5.3 and 5.4: Column 3).

	40% HF	**48%HF**	**70%HF**
Appearance of coupons before cleaning	Thick black scale (heavily oxidized), uniform.	Thick black scale (heavily oxidized), uniform.	Thin black, loose scale remnant on the edges with light brown (FeF_2) scale and silver grey regions expose beneath where scale flaked off.
Appearance of coupons after cleaning	Silver grey surface comparable to the original sandblasted coupon with edges slightly corroded away.	Severe attack of 1/3 of the sample surface with pitting corrosion visible. Light brown tint over 2/3 of surface indicative of remaining fluoride scale.	No visible corrosion. Clean surface.
Composition of final corrosion solution	*Not analysed*	*Not analysed*	69.1% HF 0.054% Fe 6 ppm Cr 1 ppm Mn 7.7 ppm Si
Total metals in solution			554.7 ppm

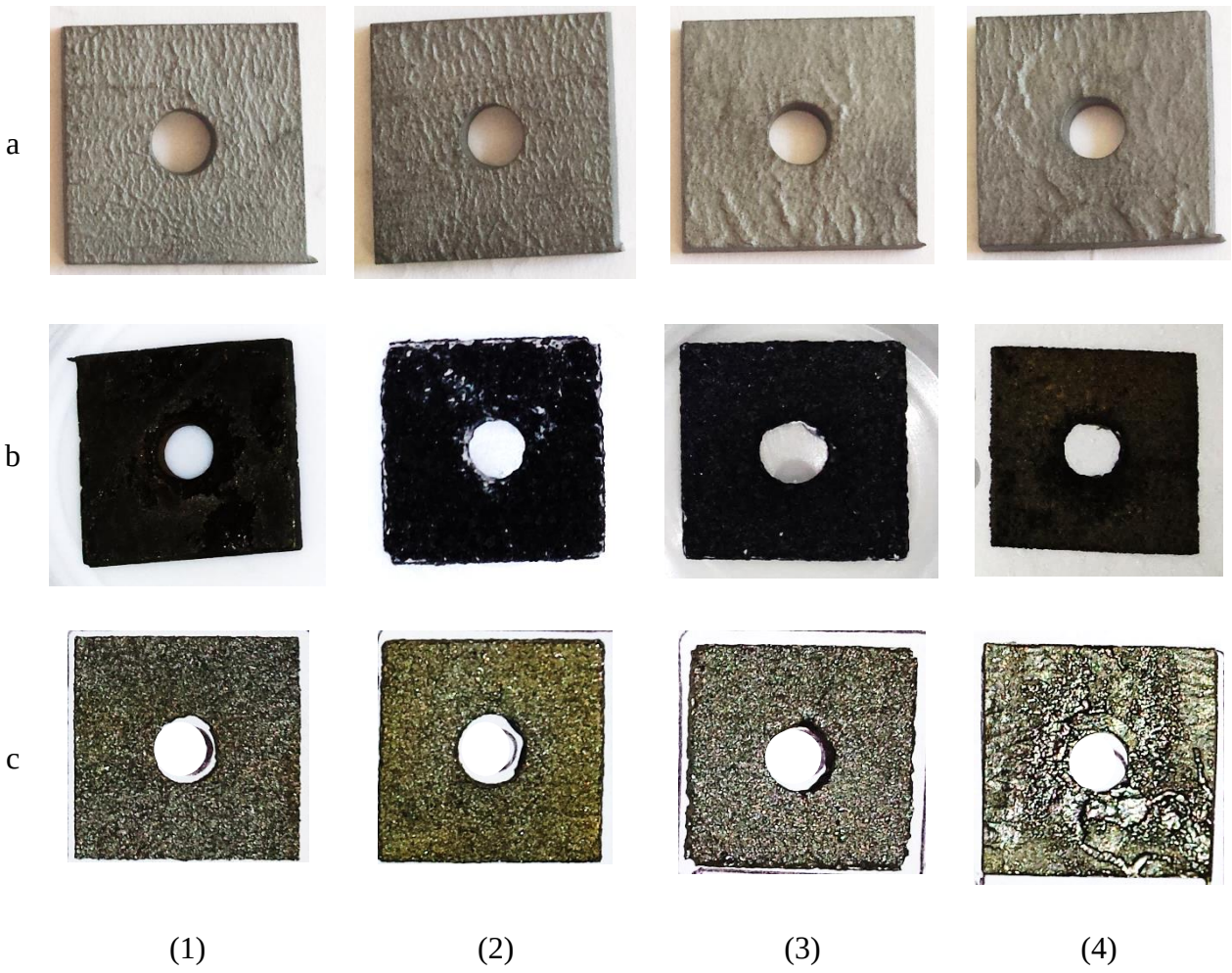

Figure 5.2: PCT 1: Mild steel coupons: (1) A_1 (2) A_t (3) A_{t+1} and (4) B: Row a; before, and Row b; after exposure to 40% HF, with Row c; after removal of the scale layer.

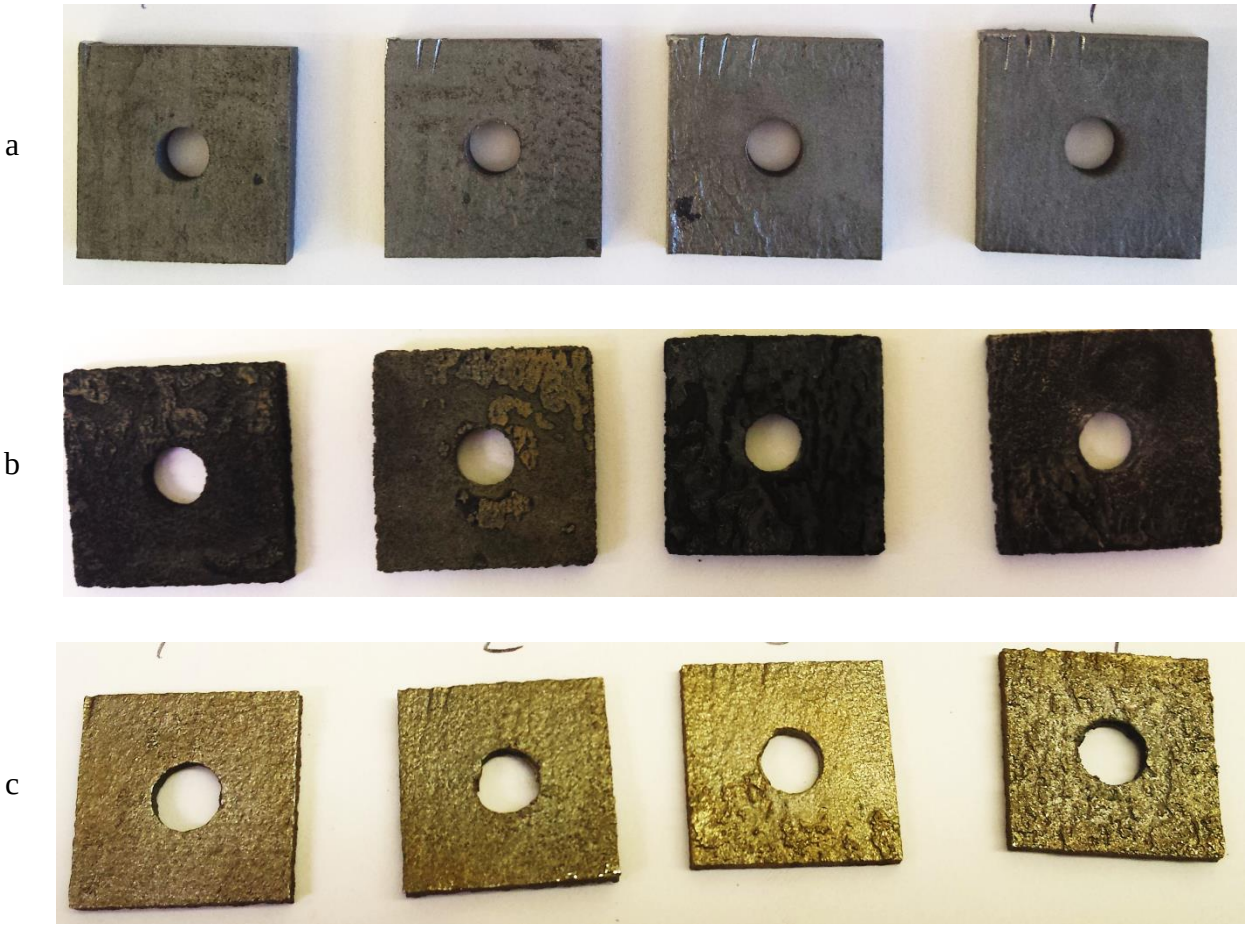

Figure 5.3: PICT 3: Mild steel coupons: (1) A_1 (2) A_t (3) A_{t+1} and (4) B: Row a; before, and Row b; after exposure to 48% HF, with Row c; after removal of the scale layer.

a



b



c



(1) (2) (3) (4)

Figure 5.4: PICT 6: Mild steel coupons: (1) A_1 (2) A_t (3) A_{t+1} and (4) B: Row a; before, and Row b; after exposure to 70% HF, with Row c; after removal of the scale layer.

Table 5.9: Observations of corrosion products of PICTs conducted in 40, 48 and 70% HF, after 8 days – pre-passivated (Figures 5.5, 5.6 and 5.7: Column 3).

	40% HF		**48%HF**		**70%HF**	
Appearance of coupons before cleaning	Thick black scale with silver grey pits. Edges heavily corroded away (evident size reduction).		Black, mottled with dark brown scale. Exposed silver grey portions also visible.		Thin grey with mottled light brown scale. Silver grey regions expose beneath where scale flaked off.	
Appearance of coupons after cleaning	Pitting corrosion visible on sliver grey surface. Excessive corrosion.		Severe attack of entire sample surface over entire period of test.		No visible corrosion. Clean surface. Metallic lustre not comparable to silver grey of original sandblasted coupons	
Composition of final corrosion solution	<u>Pre-pass step</u>	<u>Pre-passivated</u>	<u>Pre-pass step</u>	<u>Pre-passivated</u>	<u>Pre-pass step</u>	<u>Pre-passivated</u>
	39.1% HF	38.1% HF	46.0% HF	46.7% HF	68.6% HF	68.8% HF
	1.65% Fe	1.98% Fe	0.815% Fe	0.71% Fe	0.016% Fe	0.069% Fe
	17 ppm Cr	11 ppm Cr	36 ppm Cr	45 ppm Cr	5 ppm Cr	3 ppm Cr
	434 ppm Mn	410 ppm Mn	10 ppm Mn	5 ppm Mn	3 ppm Mn	5 ppm Mn
	<1 ppm Si	<1 ppm Si	144 ppm Si	130 ppm Si	18 ppm Si	16 ppm Si
Total metals in solution	1.69%	2.02%	0.836%	0.728%	0.019%	0.071%

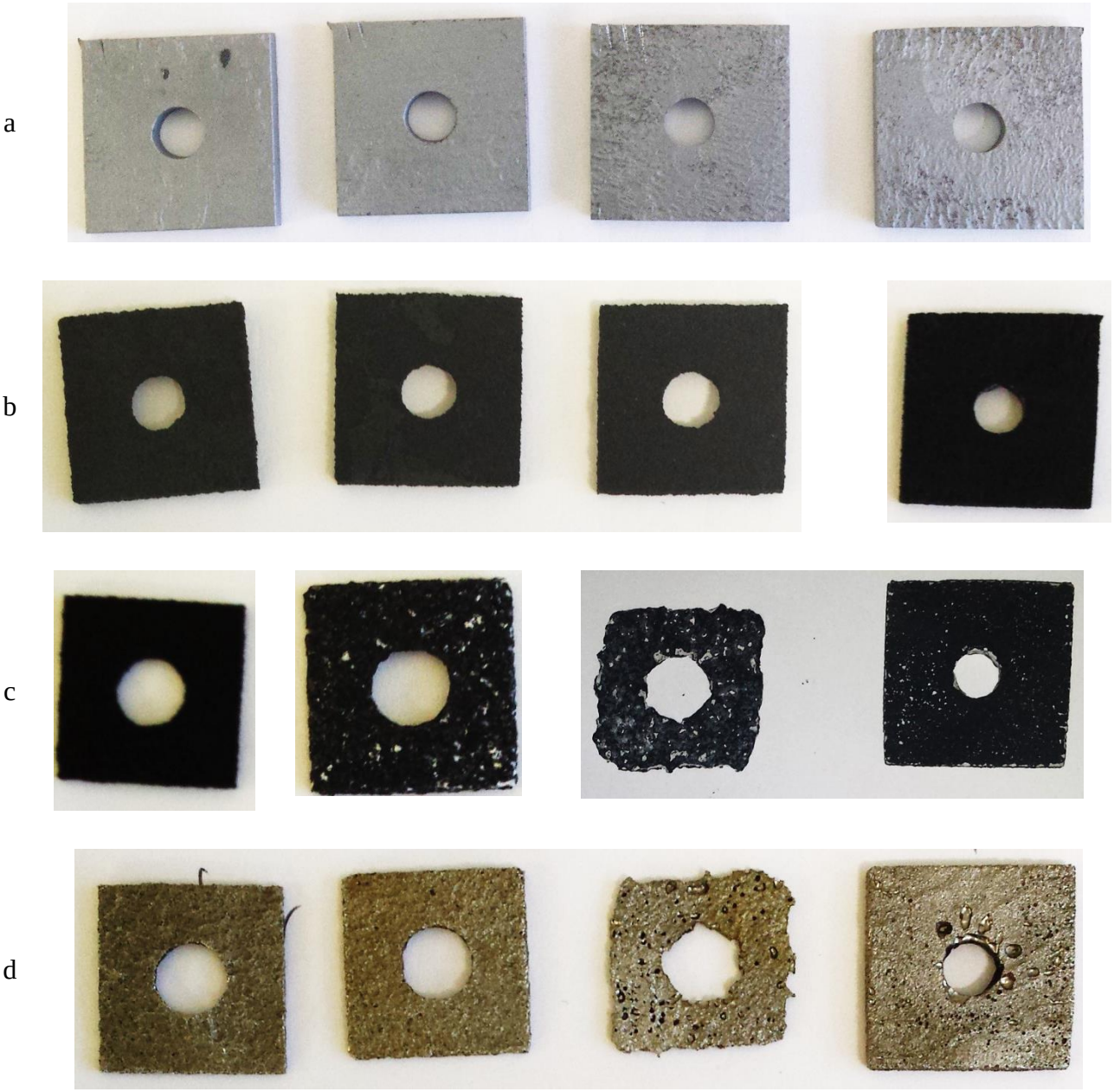

Figure 5.5: PICT 2: Mild steel coupons: (1) A_1 (2) A_t (3) A_{t+1} and (4) B: Row a; before exposure, Row b; after pre-passivation step, Row c; after exposure to 40% HF, and Row d; after removal of the scale layer.

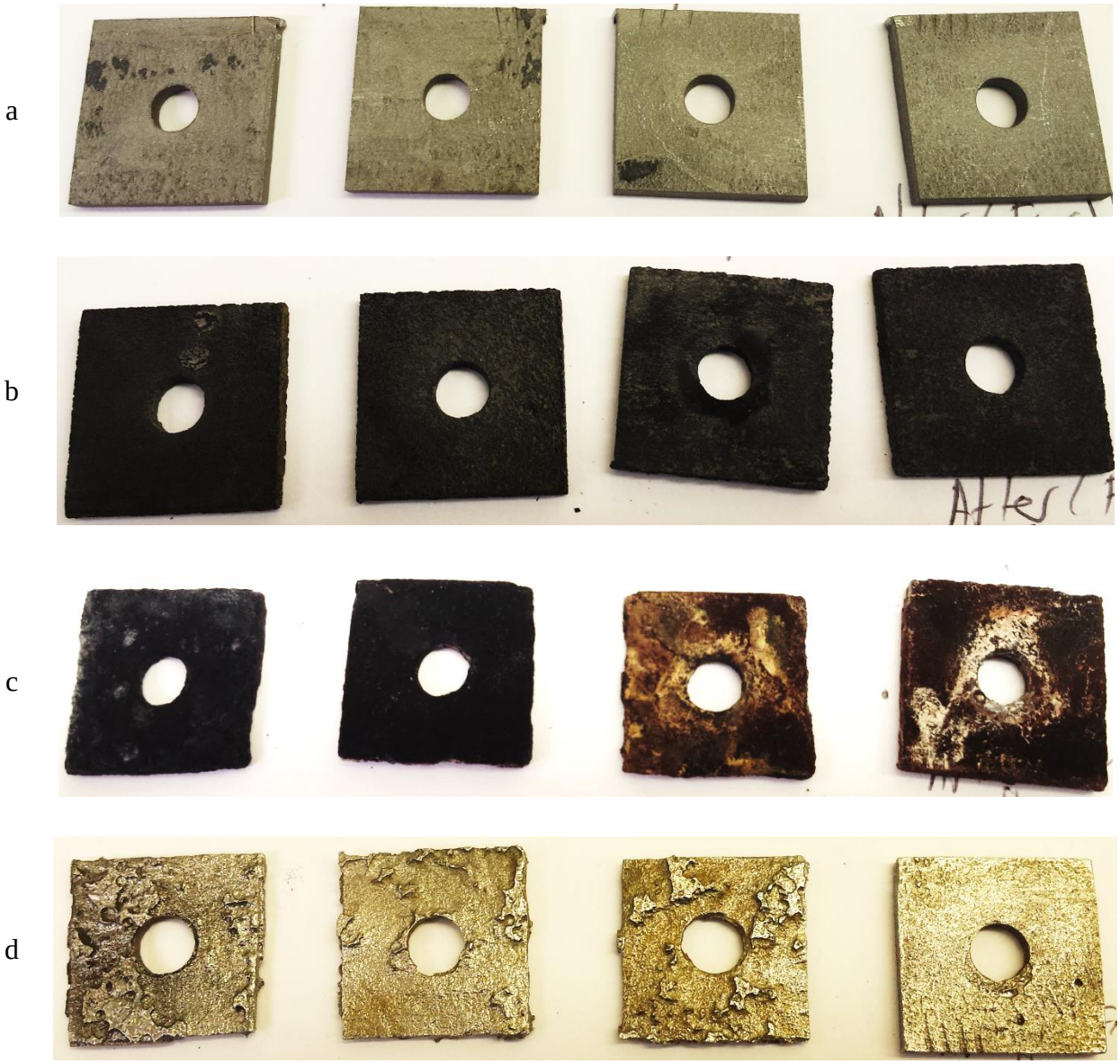

Figure 5.6: PICT 5: Mild steel coupons: (1) A_1 (2) A_t (3) A_{t+1} and (4) B: Row a; before exposure, Row b; after pre-passivation step, Row c; after exposure to 48% HF, and Row d; after removal of the scale layer.

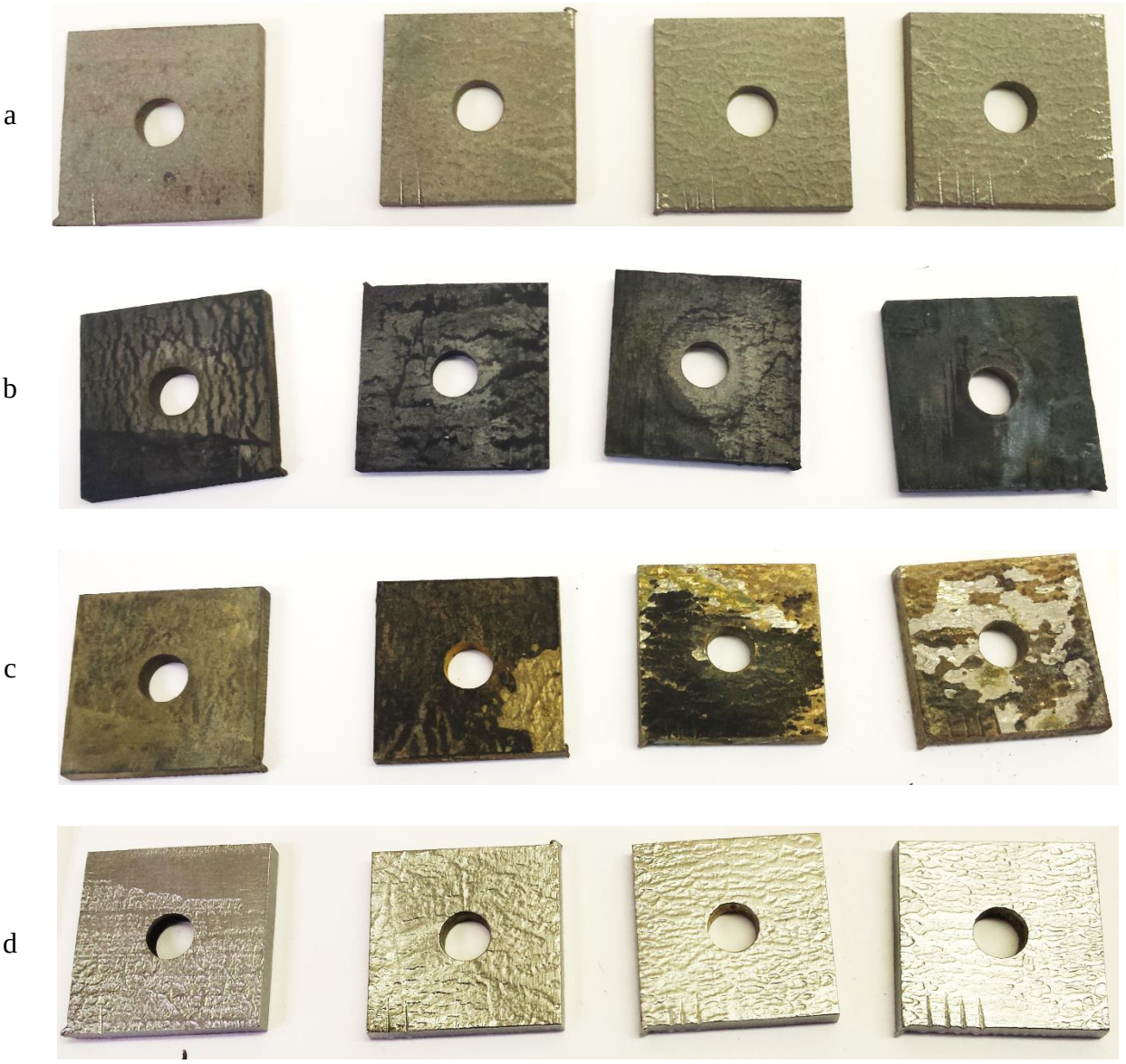

Figure 5.7: PICT 7: Mild steel coupons: (1) A_1 (2) A_t (3) A_{t+1} and (4) B: Row a; before exposure, Row b; after pre-passivation step, Row c; after exposure to 70% HF, and Row d; after removal of the scale layer.

Pit measurements using optical microscopy

Areas of 2 x 2 mm on cleaned coupons' surfaces, before (Figure 5.5: Row a, Column 3) and after exposure to 40% HF (Figure 5.5: Row d, Column 3), 48% HF (Figure 5.6: Row d, Column 3) and 70% HF (Figure 5.7: Row d, Column 3), were examined for pitting corrosion using optical microscopy. Using the Olympus stream software available 3D images of each of the selected areas were created and converted to 2D height and contour maps, shown in Figures 5.8 - 5.11. Peaks and pits were distinguished in each image by colour coding the height range for each contour. However,

for the contour map option (Figures 5.8e, 5.9e, 5.10e and 5.11e), only 4 colours were available (yellow, green, blue and black) with each contour spacing made in intervals calculated from the highest peak divided by four (e.g. in Figure 5.8, the highest peak is ~57.1 µm and therefore each contour spacing is equal to 57.1 µm / 4 = ~14.3 µm, with 0 – 14.3 µm = black, 14 – 28.6 µm = blue, 28.6 – 42.8 µm = green and 42.8 – 57.1 µm = yellow).

Up to eleven individual measurements were made on each coupon to determine each pit's height and width with each of these measurements numbered as indicated on (Figures 5.9a, 5.10a and 5.11a). The resulting pit mouth diameters (pit widths) and depths were categorized according to number of pits that fell within a selected size range (Figures 5.12 and 5.13). This made it possible to compare the effect of HF concentration on the size of pits created over eight days of corrosive attack.

Valleys present on the sand-blasted coupons that were not exposed to HF were not considered as pits and therefore not represented in the figures. However, the selected area examined did have one valley that was in excess of 57 µm (Figure 5.8).

The coupons exposed to 40% HF were most aggressively corroded with pits, which were even visible without an optical microscope (Figure 5.5: Row 4, Column 3 and 4). Of the pits formed on the surface, more than half had pit mouth diameters in excess of 500 µm (Figure 5.12) and more than 100 µm deep (Figure 5.13).

The 48% HF produced smaller pits (>500 µm) and mostly between 10 and 50 µm deep. Pitting by 48% HF was less visible (Figure 5.6: Row 4 Column 3) compared to 40% HF. Therefore, since pits were much smaller (Figure 5.12) and shallower (Figure 5.13), surface attack (uniform corrosion) was considered the predominant means of corrosion in 48% HF.

Exposure of the coupons to 70% HF produced the least amount of pitting corrosion with pit mouth diameters not exceeding 200 µm at depths between10 to 20 µm. Most of the pits visible, after the scale was washed off, were smaller than 100 µm (Figure 5.12) and less than 10 µm deep (Figure 5.13). Therefore, when compared to the sizes of pits measured on the raw, sand-blasted coupons, the 70% HF did not pit the mild steel, but rather corroded the surface uniformly.

Individual pit measurements was a laborious procedure, as mentioned in Practice G 46 - 94 (2005) (ASTM, 2009e). Therefore, due to limited time allowed on the Olympus DSX510 microscope at Mintek, only one 2 x 2 mm area on each of the four coupons selected was examined.

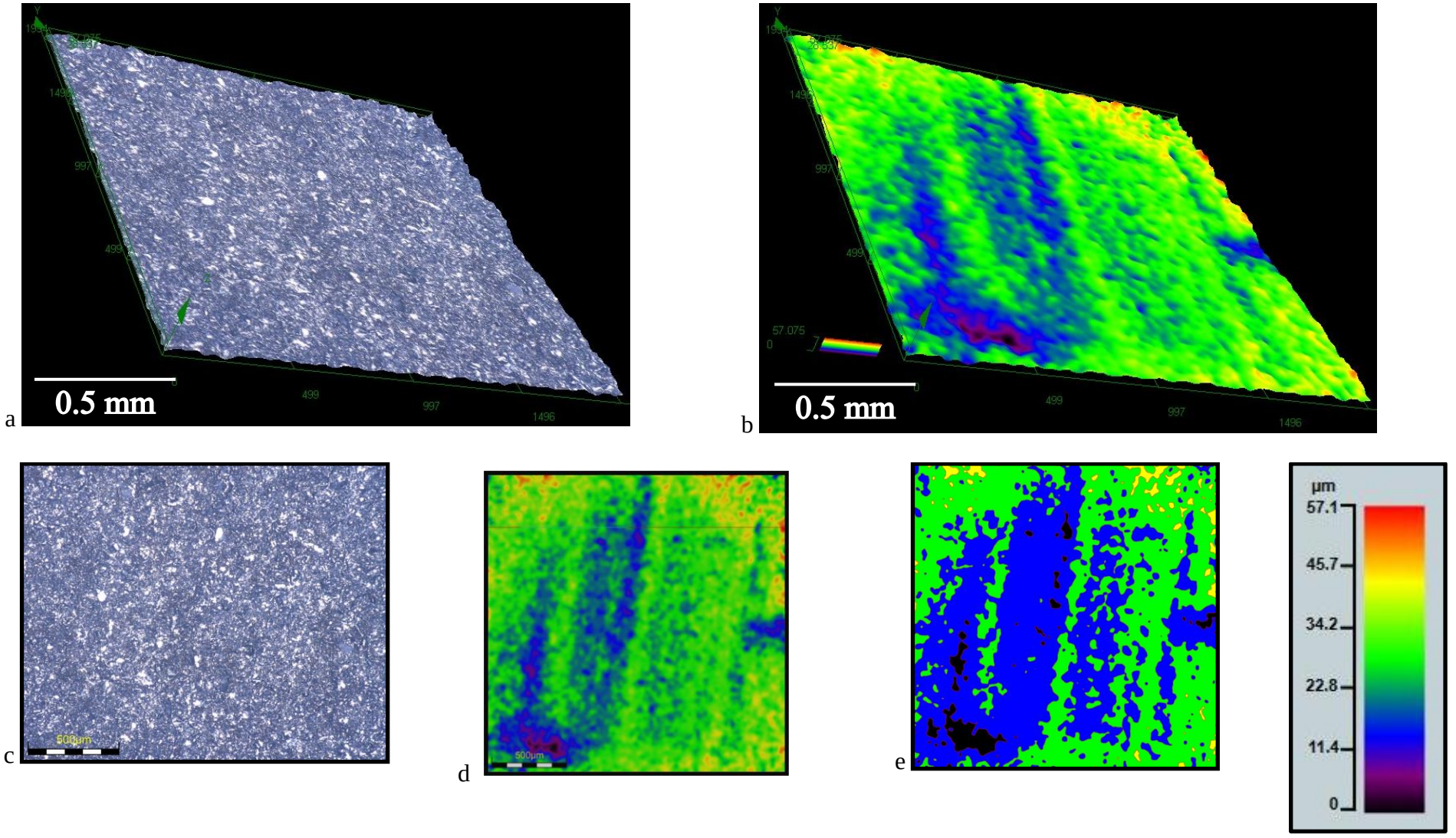

Figure 5.8: Pit depth and distribution measurements of 2 x 2 mm of a sand-blasted mild steel surface before corrosion tests, using optical microscopy to construct: (a and b) 3D height images, (c and d) 2D height profiles and (e) contours.

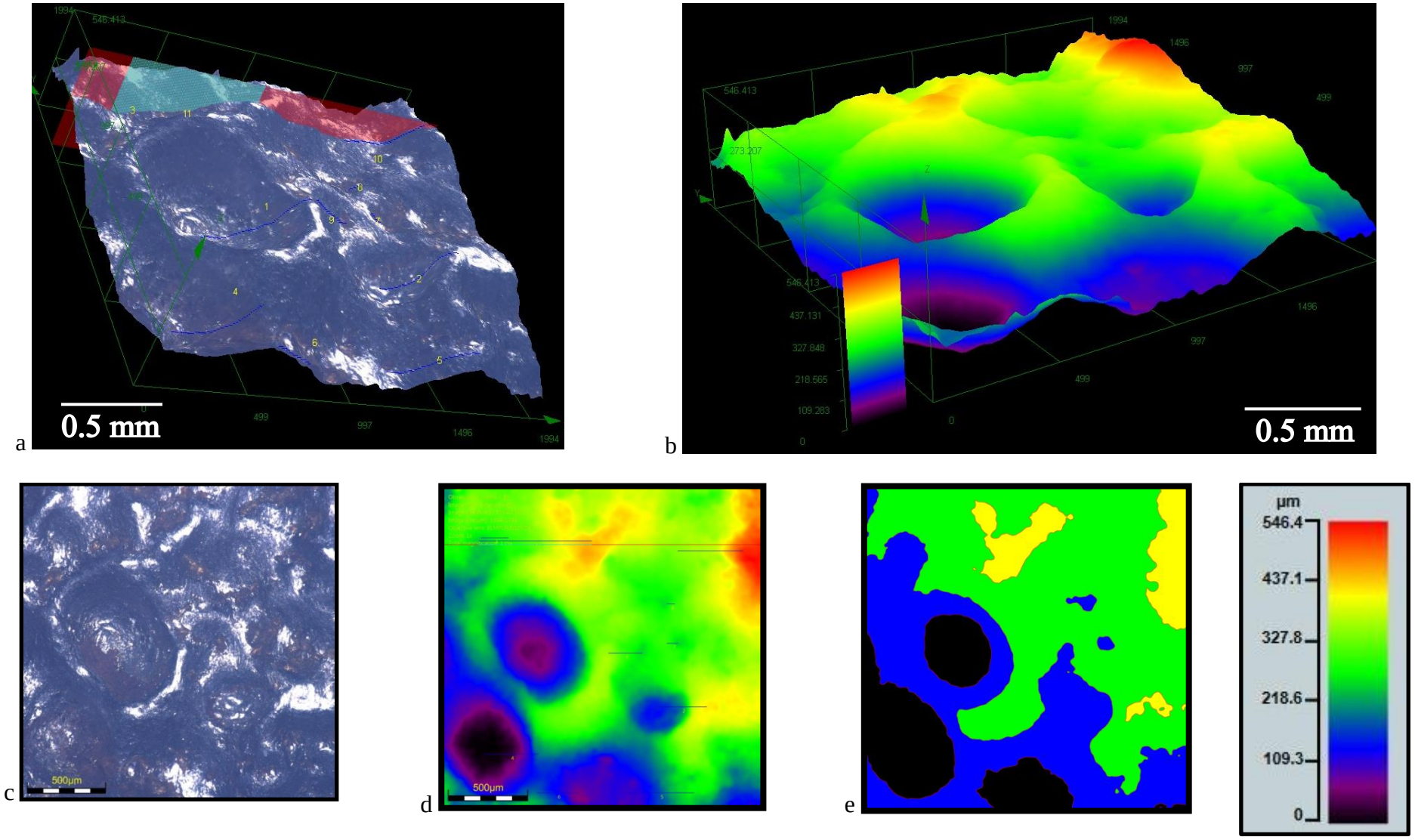

Figure 5.9: Pit depth and distribution measurements of 2 x 2 mm of a mild steel surface corroded in 40% HF for 8 days at 25ºC, using optical microscopy to construct: (a and b) 3D height images, (c and d) 2D height profiles and (e) contours.

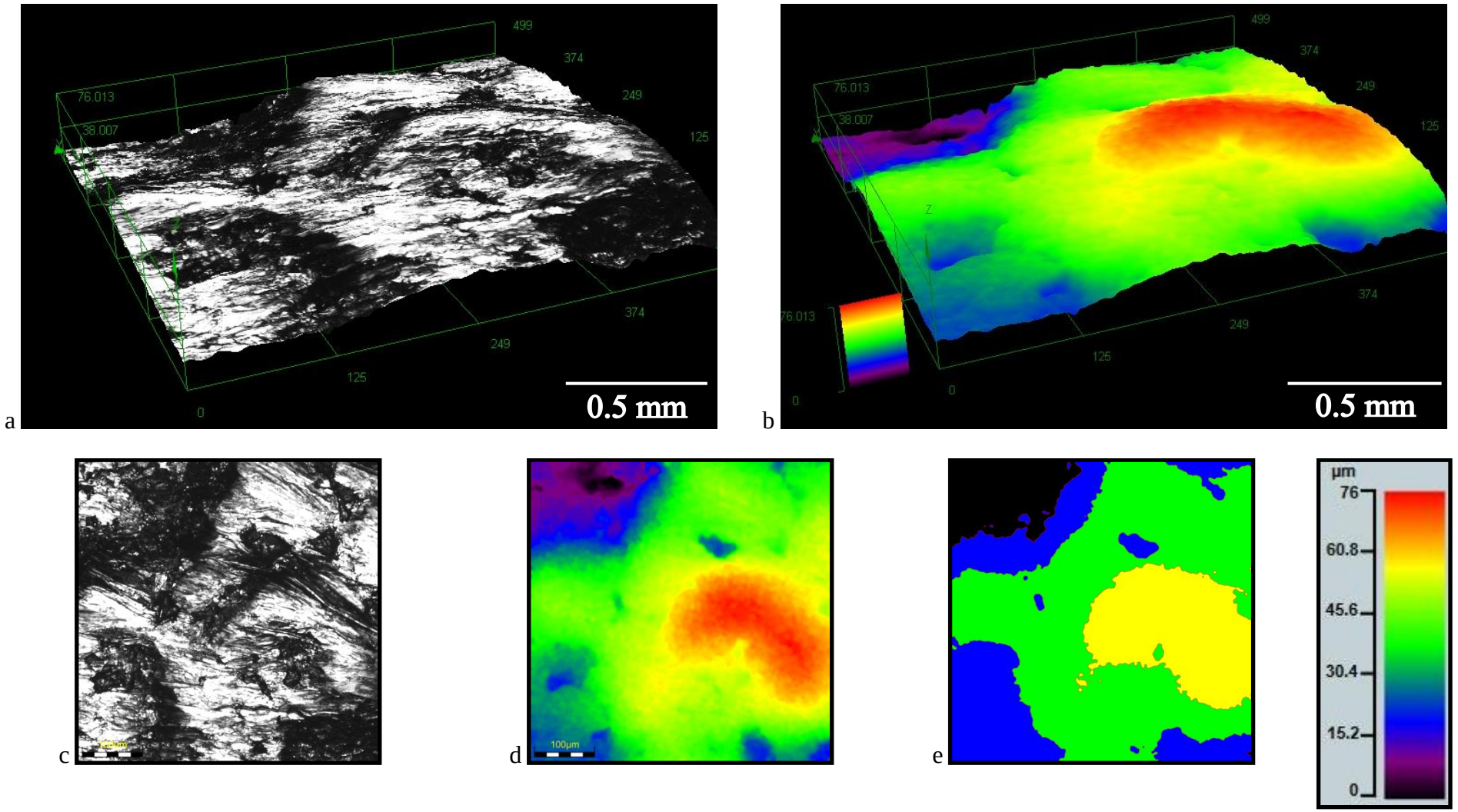

Figure 5.10: Pit depth and distribution measurements of 2 x 2 mm of a mild steel surface corroded in 48% HF for 8 days at 25ºC, using optical microscopy to construct: (a and b) 3D height images, (c and d) 2D height profiles and (e) contours.

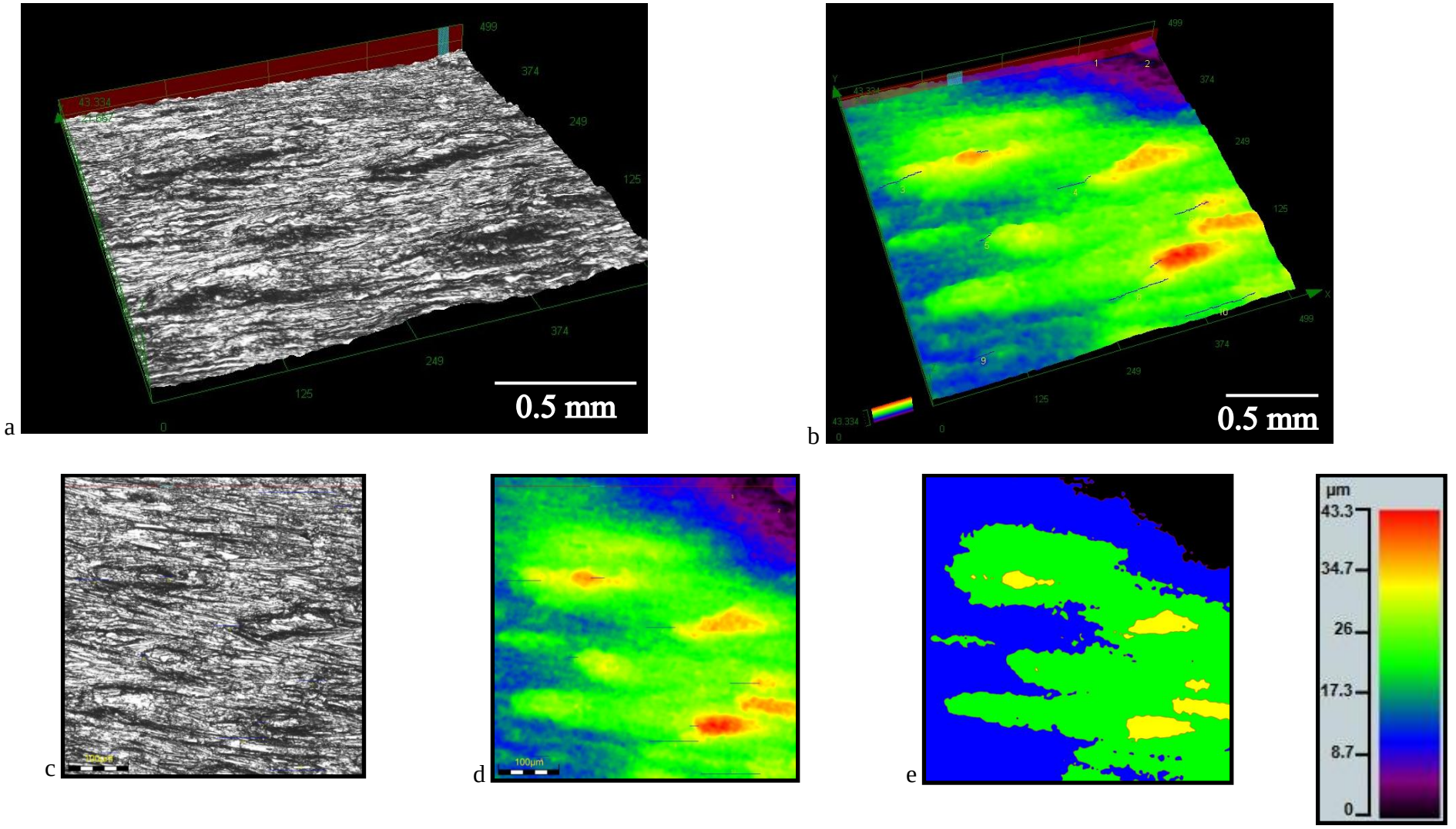

Figure 5.11: Pit depth and distribution measurements of 2 x 2 mm of a mild steel surface corroded in 70% HF for 8 days at 25ºC, using optical microscopy to construct: (a and b) 3D height images, (c and d) 2D height profiles and (e) contours.

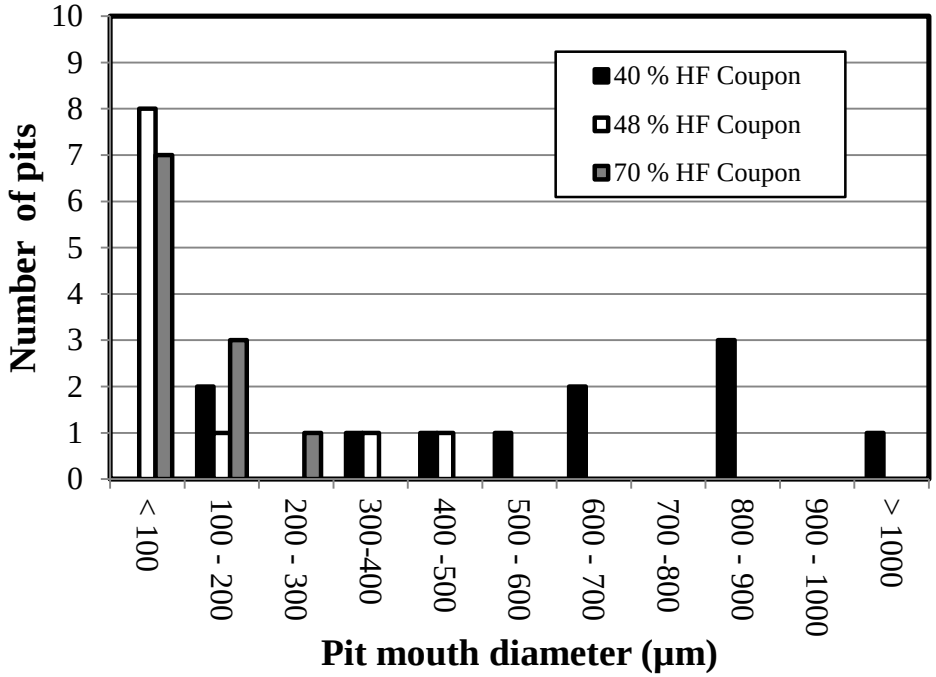

Figure 5.12: Effect of HF concentration in the corrosion solution on pit mouth diameters and distribution after 8 days of mild steel corrosion, at 25ºC.

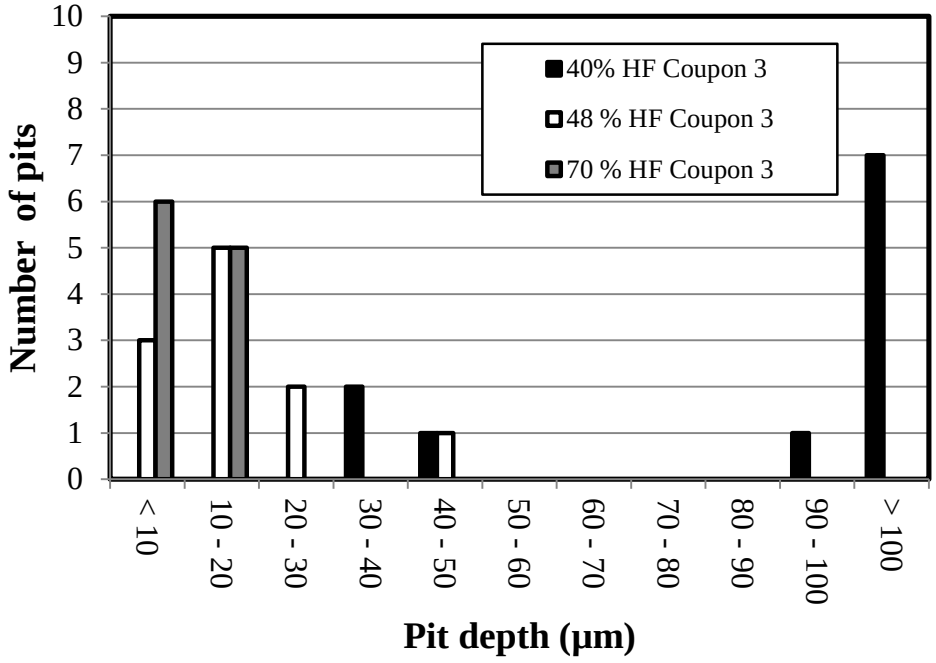

Figure 5.13: Effect of HF concentration in the corrosion solution on pit depth and distribution after 8 days of mild steel corrosion, at 25ºC.

5.1.3. Effect of steel and alloy composition

Verification of the Alloy compositions

The mild steel, stainless steel and nickel alloy sheets sourced through SAMS did not come with certificates of analyses (COA), therefore a variety of analyses were conducted to verify the compositions of the alloys delivered (and hence their suitability for using the metals to relate to the corrosion behaviour of the alloys used in the HF plant). Irrespective of the three analytical techniques varying greatly in their method and detection limits, the analytical results compared well (Tables 5.10 – 5.11). Thus, composition of the mild steel (Table 5.10), the stainless steel (Table 5.11) and the nickel alloy (Table 5.12) were verified and found to meet the original compositional specifications.

Table 5.10: Verification of Mild steel (SA 516 Grade 70 normalized) composition.

Analytical Technique	**Elements (wt%)**						**Total**
	Fe	**Si**	**Mn**	**Cr**	**C**	**O**	
Specification	99	-	-	-	-	-	100.0
GDS (±0.1%)	96.8	0.5	1.0	0.2	0.03	0.9	99.4
SEM-EDS (±1%)	98.1	0.3	1.3	0.3	-	-	100.0
ICP-OES (±5%)	100	-	-	-	-	-	100.0

Table 5.11: Verification of Stainless steel (SS 904 L) composition.

Analytical Technique	**Elements (wt%)**						**Total**
	Ni	**Cr**	**Mo**	**Fe**	**Cu**	**Mn**	
Specification	25	20	5	46	2	2	100.0
GDS (±0.1%)	24.8	21.4	3.9	46.4	1.6	1.6	99.7
SEM-EDS (±1%)	22.5	20.8	2.8	50.3	1.6	2.1	100.0
ICP-OES (±5%)	26.0	21.0	4.0	46.0	2.0	2.0	100.0

Table 5.12: Verification of Alloy 400 (Monel) compositions.

Analytical Technique	**Elements (wt%)**						**Total**
	Ni	**Cr**	**Mo**	**Fe**	**Cu**	**Mn**	
Specification	65	-	-	2.0	30	1	100.0
GDS (±0.1%)	65.1	-	-	1.9	31.8	1.0	99.8
SEM-EDS (±1%)	64.4	-	-	1.9	32.4	1.3	100.0
ICP-OES (±5%)	65.0	-	-	2.0	32.0	1.0	100.0

Susceptibility to HF corrosion

The apparent rate of stainless steel corrosion was nearly constant throughout the PICT tests (~4.8 mm/y), and did not allow for much difference between the A_2, B and A_1 (Tables 5.13 and 5.14). However, applying the criteria summarized in Table 4.3 revealed that HF corrosiveness increased slightly when reacted with the sand-blasted steel surface. Conversely, the susceptibility of the metal to the acid remained unaffected (Table 5.13). The corrosion rate dropped slightly when comparing the values determined for B and A_1 (Table 5.14). This drop of approximately 0.25 mm/y was indicative of pre-passivation decreasing the HF corrosiveness. Conversely, the susceptibility of the coupons to corrosion by 70% HF showed a slight increase (A_2 determined at 0.23 mm/y faster than B value) when stringently applying the criteria for PICTs (Table 5.14). Thus, because the mass loss from the stainless steel coupons with time in HF was so consistent, determining the susceptibility of the metal to corrosion by HF was nearly insignificant. Irrespective of stainless steel's unchanged susceptibility to HF corrosion, putting the stainless steel through the same 24 h pre-passivation step as mild steel slightly mitigated the corrosion of the metal when compared after 8 days. When weighed, the pre-passivated stainless steel corroded 0.3 mm/y slower than the untreated coupons.

Table 5.13: Planned interval corrosion tests for stainless steel in 70% HF.

Coupon No.	**Interval (days)**	**Mass loss (g)**	**Apparent corrosion rate (mm/y)**
1) A_1	0 – 1	0.15	4.6
2) A_t	0 – 4	0.56	4.3
3) A_{t+1}	0 – 8	1.22	4.6
4) B	4 – 8	0.66	5.0
Calc.) A_2	4 – 8	0.66	5.0

5.00 mm/y = 4.99 mm/y < 4.60	**Liquid corrosiveness:**	Increase
Therefore : $A_2 = B > A_1$	**Susceptibility to corrosion:**	Unchanged

Table 5.14: Planned interval corrosion tests for stainless steel in 70% HF – pre-passivated.

Coupon No.	**Interval (days)**	**Mass loss (g)**	**Apparent corrosion rate (mm/y)**
1) A_1	0 – 1	0.16	4.9
2) A_t	0 – 4	0.63	4.7
3) A_{t+1}	0 – 8	1.28	4.8
4) B	4 – 8	0.62	4.7
Calc.) A_2	4 – 8	0.65	4.9

4.92 mm/y > 4.69 mm/y < 4.94	**Liquid corrosiveness:**	Decreased
Therefore : $A_2 > B < A_1$	**Susceptibility to corrosion:**	Increase

The average apparent corrosion rate determined for nickel alloy was approximately 0.3 mm/y, which was nearly 16 times lower than the average rate calculated for the stainless steel. Therefore, the differences needed to distinguish between an increase and a decrease in susceptibility of the nickel alloy to corrosion by 70% HF was even more subtle (Tables 5.15 and 5.16). However, applying the criteria for PICTs as specified by ASTM standard practice G31-72 (Table 4.3) indicated a very slight increase in the HF corrosiveness (A_1 determined at 0.03 mm/y slower than B) when the nickel alloy underwent pre-passivation (Table 5.16). This increase is virtually negligible and leans more towards HF corrosiveness being unchanged throughout the PICT, as was the case with the untreated nickel coupons (Table 5.15). The susceptibility of the nickel alloy to be attacked by 70% HF consistently decreased. The corrosion rate determined for A_2, in both the treated and untreated coupons, was marginally less (0.03 – 0.19 mm/y) than the B values in both tests conducted in 70% HF. Therefore, the nickel alloy effectively resisted any attack by 70% HF so that after 4 days in solution, the corrosion rate effectively began to decrease. This was indicative of passivation of the metal occurring in the HF solution. The implementation of a pre-passivation step merely supports this further passivation occurring naturally in the corrosion solution. This was also supported by the mass loss of the untreated nickel coupons standing at 0.01 g more than the pre-passivated coupons, after 8 days in solution.

Table 5.15: Planned interval corrosion tests for nickel alloy in 70% HF.

Coupon No.	**Interval (days)**	**Mass loss (g)**	**Apparent corrosion rate (mm/y)**
1) A_1	0 – 1	0.15	0.4
2) A_t	0 – 4	0.06	0.4
3) A_{t+1}	0 – 8	0.09	0.3
4) B	4 – 8	0.06	0.4
Calc. A_2	4 – 8	0.03	0.2
0.21 mm/y < 0.40 mm/y = 0.39	**Liquid Corrosiveness:**		Unchanged
Therefore : $A_2 < B = A_1$	**Susceptibility to corrosion:**		Decreased

Table 5.16: Planned interval corrosion tests for nickel alloy in 70% HF – pre-passivated.

Coupon No.	**Interval (days)**	**Mass loss (g)**	**Apparent corrosion rate (mm/y)**
1) A_1	0 – 1	0.01	0.3
2) A_t	0 – 4	0.04	0.2
3) A_{t+1}	0 – 8	0.08	0.3
4) B	4 – 8	0.05	0.3
Calc. A_2	4 – 8	0.04	0.3
0.29 mm/y < 0.32 mm/y > 0.29	**Liquid Corrosiveness:**		Increased
Therefore : $A_2 < B > A_1$	**Susceptibility to corrosion:**		Decreased

Acid consumption

To determine the amount of acid consumed during the pre-passivation step, the remaining solution from each bottle, in which the pre-passivation step was conducted, was sampled and analysed for its HF content. Except for the nickel alloy, the highest acid consumption measured for each metal occurred during the 24 hour pre-passivation step and was determined to be nearly 1.5 times higher than the consumption of the corresponding 8 day PICT where no pre-passivation was involved (Table 5.14). Acid consumption during pre-treatment of the nickel alloy was nearly equal to the 8 hour test and agreed with Table 5.16 in that the HF corrosiveness remained unchanged. The nearly 1% lower acid consumption determined for the pre-passivated nickel alloy maintained that the acid consumed during the pre-passivation step did not further increase the susceptibility of the metal to HF corrosion. Thus, HF consumed during the 24 hour pre-passivation step succeeded in passivating the surface of the nickel coupons to such an extent that even less acid was consumed in the following 8 hour test, when compared to the untreated coupons.

Stainless steel produced the highest acid consumption overall. The mass of stainless steel introduced to 463 ml of HF consumed nearly four times more acid than the equivalent mass of mild steel exposed to the same volume of acid over the same time period. Even the equivalent mass of nickel alloy exposed to the same conditions delivered acid consumptions half than measured for the stainless steel (Table 5.14). This was supported by mass losses measured and corrosion rates determined for mild steel being nearly 4 times less than stainless steel (Tables 5.5 and 5.7 compared with Tables 5.16 and 5.14). Thus, the stainless steel consumed more acid than mild steel as it was being corroded more.

Conversely, nickel alloy hardly underwent any corrosion (Tables 5.15 and 5.16) but consumed the second most acid (>5% HF) out of the three metals tested (Table 5.14). The only difference being in the pre-passivation of the nickel alloys when compared to the steels. The nickel alloy did not passivate through the formation of a scale layer as in the instances of the mild steel and the stainless. Instead, the nickel alloy visibly kept its clean metallic finish (Figures 5.17 and 5.18) throughout the PICT. Thus, consuming more HF than mild steel, but still less than stainless, to create the passive barrier that more effectively prevented it’s corrosion over the 8 days of exposure.

Table 5.17: HF acid consumption by mild steel, stainless steel and nickel alloy after 8 days when varying the degree of pre-passivation in 70% HF, at 25ºC.

Metal	Degree of Pre-passivation	Product HF concn. (% HF)	Mass of acid in product (g)	Mass of Coupons (g)	Acid Consumption	
					$\left(\frac{\text{g HF}}{\text{g Alloy}}\right)$	(%)
Mild Steel	Pre-pass step	68.60	317.91	61.35	0.11	2.0
	Pre-passivated	68.81	318.88	61.23	0.09	1.7
	Not Pre-passivated	69.11	320.27	61.76	0.07	1.3
SS 904 L	Pre-pass step	64.93	300.90	53.59	0.44	7.3
	Pre-passivated	65.74	304.65	53.02	0.37	6.1
	Not Pre-passivated	65.64	304.19	53.95	0.38	6.3
Monel 400	Pre-pass step	66.47	308.04	71.67	0.23	5.1
	Pre-passivated	66.98	310.40	71.62	0.20	4.3
	Not Pre-passivated	66.32	307.34	72.23	0.24	5.3

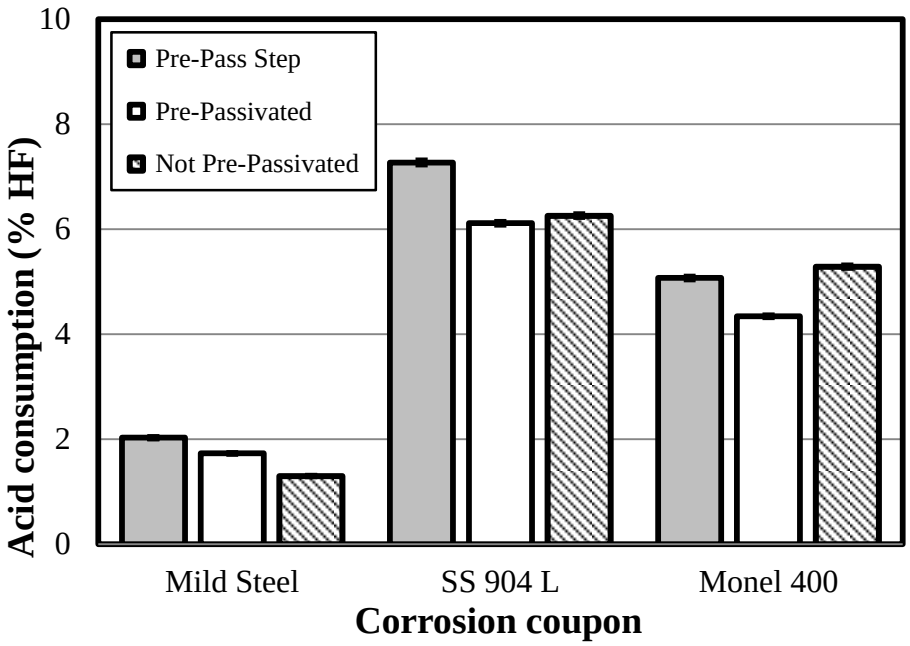

Figure 5.14: Effect of pre-passivation on percentage acid consumption during PICTs - comparing mild steel, stainless steel and nickel alloy corrosion in 70% HF at 25ºC. Error bars obscured by markers in some instances.

Observations from photographs of the samples

Stainless steel reacted fairly similarly to mild steel when exposed to 70% HF in that scale formed over the surface of the entire coupons after the pre-passivation step (Table 5.18), although it was more of a dark grey colour (Figure 5.16; Row b). Therefore, the scale was deduced to be closer to iron fluoride than the black iron oxide formed on the mild steel during its pre-passivation.

However, at the completion of the corrosion test, the remnants of a thick black scale were visible on the coupon edges, which indicated that the scale oxidized further over the duration of the PICT (Figures 5.15; Row b, and 5.16; Row c). This scale was not as resilient as that formed on mild steel and flaked off easily during handling of the coupons. SEM-EDS spot analyses conducted on flakes collected before cleaning confirmed that they were oxides since they had the same ratios of Fe, Ni, Cr and Mo as the clean stainless steel surface analysed (Table 5.11), except for ~2 wt% fluorine and ~12 wt% more oxygen. Cleaning of the coupons exposed a metallic sheen under the scale with hardly any signs of corrosion damage visible on the surface (Figures 5.15; Row c, and 5.16; Row d).

The corrosion product solutions collected were only analysed for metals that were in the stainless steel (Table 5.11) and summarized in Table 5.18. Where applicable, this included corrosion products collected after the 24 hour pre-passivation step and the following 8 day PICTs. Considering the combined mass of all metals analysed (Fe, Cr, Mn, Ni and Si), approximately 2.95% was removed from the four coupons that did not undergo pre-passivation. Conversely, only 2.65% was removed from the pre-treated coupons. However, since approximately 1.22% of steel was already removed from the stainless steel coupons during the 24 hour pre-passivation step, this implied that cumulatively about 1% more of the alloy was already corroded when pre-passivation was employed.

The metals that made up the bulk of the stainless steel were ~46 wt% Fe, ~20 wt% Cr and ~25 wt% Ni (Table 5.11). This was related to how much of each metal present in the coupons reported to the final corrosion solutions analysed (Table 5.18). During the pre-passivation step, these three metals corroded from the coupon surfaces were proportional to their mass percentage in the steel (1.2 – 1.3% Fe, Cr and Ni). However, during both the 8 hour PICTs, the Cr and Ni preferentially corroded (>3.9% from the mass of the Cr and Ni originally present in coupons). These were twice the amount for iron (~1.9% Fe) which conversely had the largest component with in the steel. Therefore, irrespective of low metal concentrations (>3.5 g/L total), a selective corrosion of 70% HF towards Cr and Ni was observed, with the iron component in the alloy having higher resistance to corrosive attack. This was regardless of whether or not the coupons were pre-passivated.

The reduction in Si concentration (111 ppm to 19 ppm) was indicative of surface cleaning as HF dissolved the residue left behind during the sand-blasting of the coupons.

Table 5.18: Observations of corrosion products of PICTs conducted on a stainless steel (SS 904 L), after 8 days (Figures 5.15 and 5.16: Column 3).

	No pre-passivation Step	**Pre-passivated**	
Appearance of coupons before after 24 hours pre-passivation	N/A	Dark grey matt colour.	
Appearance of coupons before cleaning	Remnants of thin black scale that evidently flaked off during handling that exposed the coupon surface having a clean metallic lustre.	Remnants of thin black scale that evidently flaked off during handling that exposed the coupon surface having a clean metallic lustre.	
Appearance of coupons after cleaning	No visible corrosion. Clean surface except for black tarnish (scale smearing) on the area where the coupons were marked.	No visible corrosion. Clean surface except for black tarnish (scale smearing) on the area where the coupons were marked.	
Composition of final corrosion solution	65.74% HF 1008 ppm Fe 1114 ppm Cr 14 ppm Mn <1 ppm Cu 1186 ppm Ni 111 ppm Si	<u>Pre-pass step</u> 64.93% HF 709 ppm Fe 285 ppm Cr 19 ppm Mn <1 ppm Cu 369 ppm Ni 32 ppm Si	<u>Pre-passivated</u> 65.64% HF 975 ppm Fe 925 ppm Cr 16 ppm Mn <1 ppm Cu 1108 ppm Ni 19 ppm Si
Total metals in final solution	3433 ppm	1414 ppm	3043 ppm

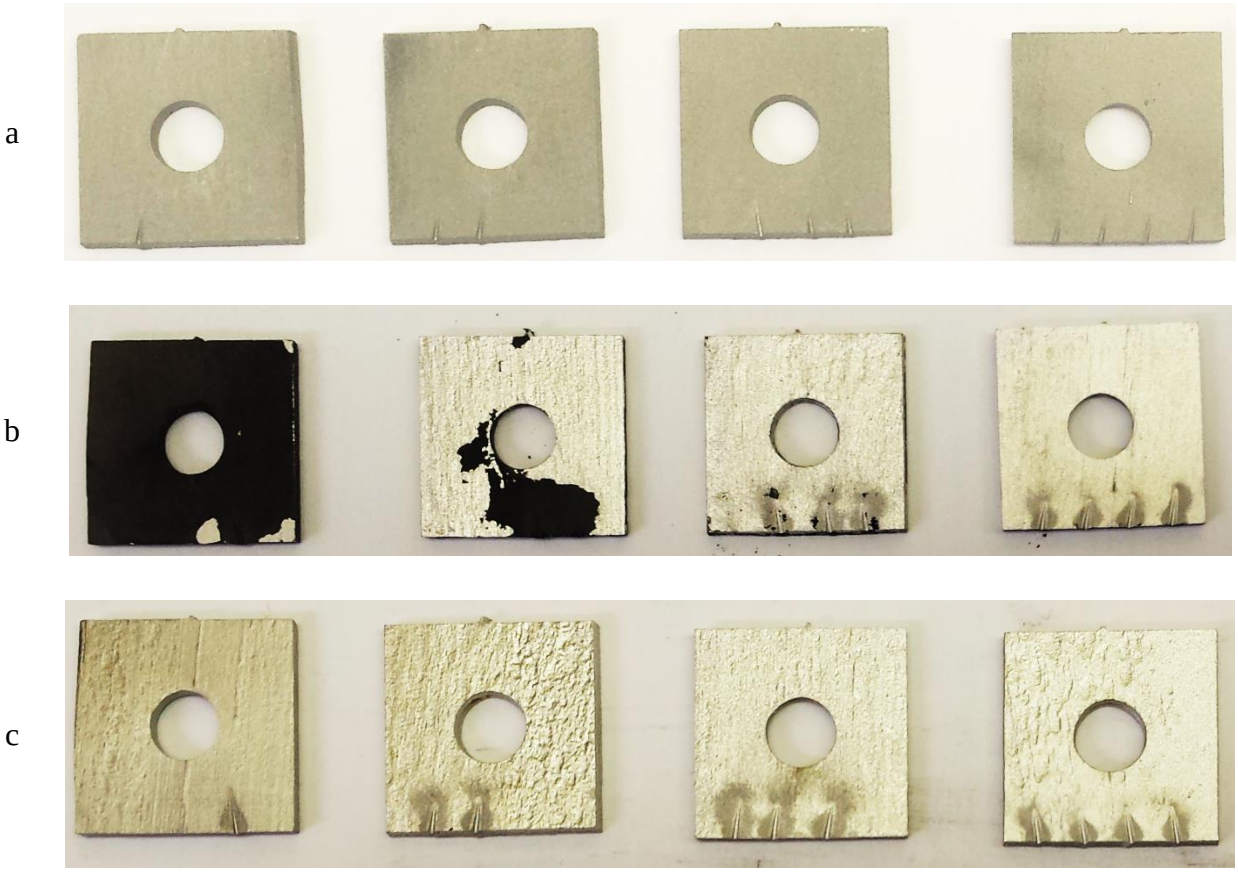

Figure 5.15: PICT 10: Stainless steel coupons (SS 904 L): (1) A_1 (2) A_t (3) A_{t+1} and (4) B: Row a; before, and Row b; after exposure to 70% HF, with Row c; after removal of the scale layer.

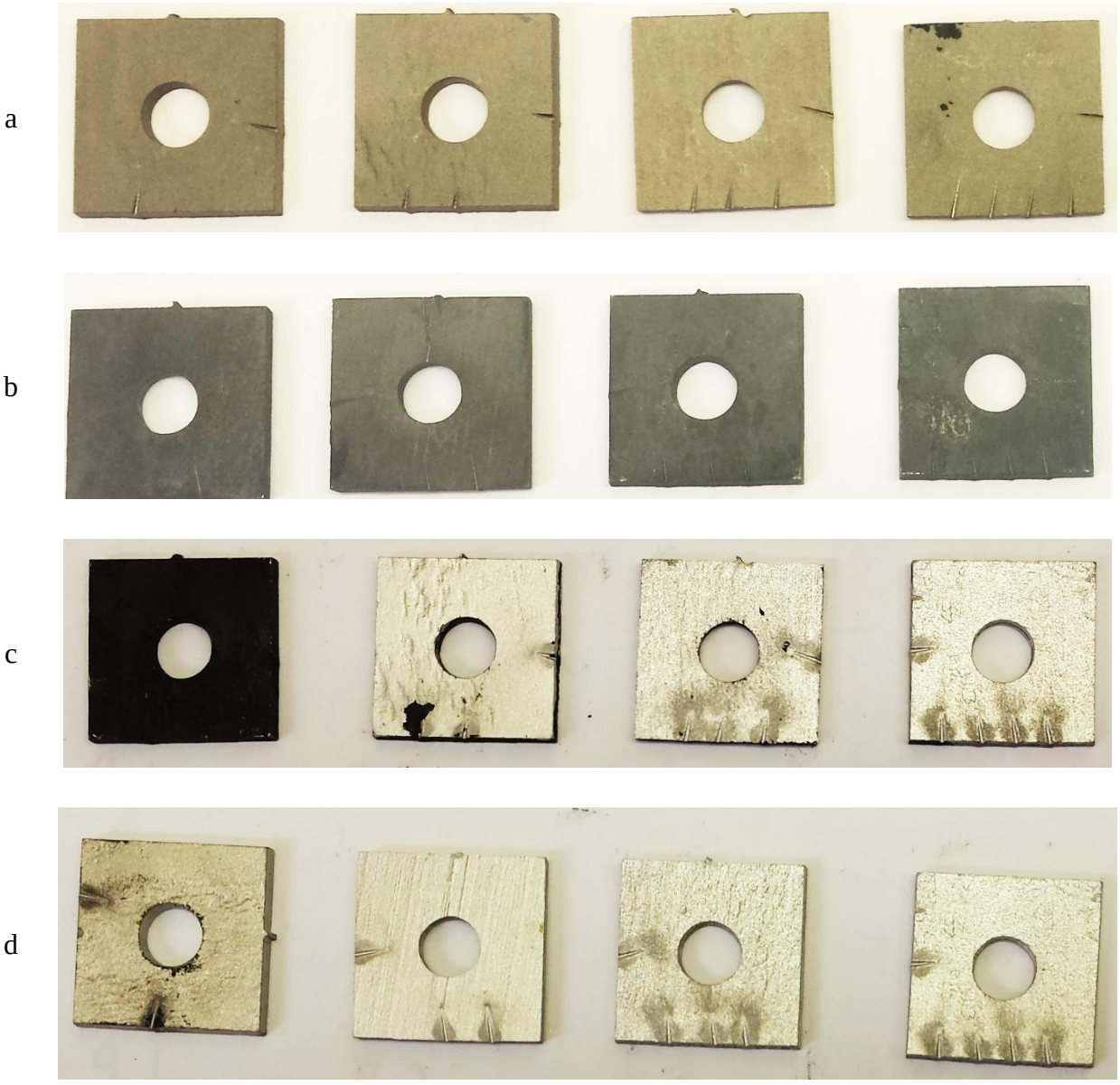

Figure 5.16: PICT 8: Stainless steel coupons (SS 904 L): (1) A_1 (2) A_t (3) A_{t+1} and (4) B: Row a; before exposure, Row b; after pre-passivation step, Row c; after exposure to 70% HF, and Row d; after removal of the scale layer.

When compared to observations made on mild steel and stainless steel surfaces exposed to 70% HF, the nickel alloy showed no signs of corrosion or scale formation during any of its PICTs (Table 5.19). Exposure of the nickel alloy coupons to 70% HF changed the coupons from a grey matt colour (produced by sand-blasting) to a clean metallic sheen. Washing the coupons did not improve on the metallic lustre the coupons already exhibited and did not reveal any underlying corrosion (Figures 5.17 and 5.18).

A slight pink tint was observed on a single coupon that was exposed to 70% HF for 4 days, without prior pre-passivation. The composition of this pink residue could not be determined through SEM-EDS analyses because the fluorine and oxygen levels were well below the detection limits of the instrument (<1 wt%). However, GDS-OES analyses of the same surface revealed the presence of a 3 nm thick carbon layer over the clean metallic surface. Thus, the unique colour was possibly due to thin-film interference by the thin carbon layer. Nevertheless, this residue washed off easily during cleaning and had a negligible impact on the corrosive behaviour of the alloy.

Of all PICTs conducted in 70% HF, the total mass of metal removed from the nickel alloys was by far the least. No more than 373 ppm of metal was analysed in the corrosion solutions collected (Table 5.19). This was nearly a tenth of that analysed for stainless steel itself and nearly half of the total metal content of the mild steel corrosion solution products.

The metals that made up the bulk of the nickel alloy were ~2 wt% Fe, ~ 30 wt% Cu and ~65 wt% Ni (Table 5.12). Only 0.2% of the mass of Ni and Cu present in the coupons was found in to the final solutions analysed. However, despite the low Fe, Cu and Ni concentrations analysed in the final solutions, iron showed a definite trend of being more selectively removed from the alloy during the pre-passivation step, as well as from the untreated coupons. Iron was the lowest component in the alloy by mass and during the pre-passivation step five times more iron was removed compared to any of the other metal components. In the PICT where no pre-passivation was conducted, the mass of iron removed from the iron component in the coupons was at 2 wt% after 8 days. Conversely, iron removed from the pre-passivated nickel alloy was only at 0.23%. Since iron only corroded in significant quantities from the untreated coupons, it is likely that the relatively higher iron extraction from the coupons were from mill scale or residue that was present on the coupon surfaces prior to testing. Therefore, just as the increase in Si concentration (up to 111 ppm) in the corrosion products indicate cleaning of the nickel alloy surface, the same cleaning action of HF was applicable in iron removal from visible surface residues (light grey matt colour of coupons in Row a of Figures 5.17 and 5.18).

Table 5.19: Observations of corrosion products of PICTs conducted on a nickel alloy (Monel 400), after 8 days (Figures 5.17 and 5.18: Column 3).

	No pre-passivation Step		**Pre-passivated**			
Appearance of coupons before after 24 hours pre-passivation	N/A		Light grey matt colour similar to original sandblasted surface.			
Appearance of coupons before cleaning	Metallic lustre with a slight pink tint on cut edges.		Metallic lustre not comparable to grey matt colour of original sandblasted coupons.			
Appearance of coupons after cleaning	No visible corrosion. Clean surface.		No visible corrosion. Clean surface.			
Composition of final corrosion solution	66.32% HF 65 ppm Fe 14 ppm Cr <1 ppm Mn 70 ppm Cu 215 ppm Ni 9 ppm Si		<u>Pre-pass step</u> 66.47% HF 9 ppm Fe <1 ppm Cr <1 ppm Mn 28 ppm Cu 54 ppm Ni 9 ppm Si		<u>Pre-passivated</u> 66.98% HF 7 ppm Fe <1 ppm Cr 3 ppm Mn 112 ppm Cu 238 ppm Ni <1 ppm Si	
Total metals in final solution	373 ppm		100 ppm		360 ppm	

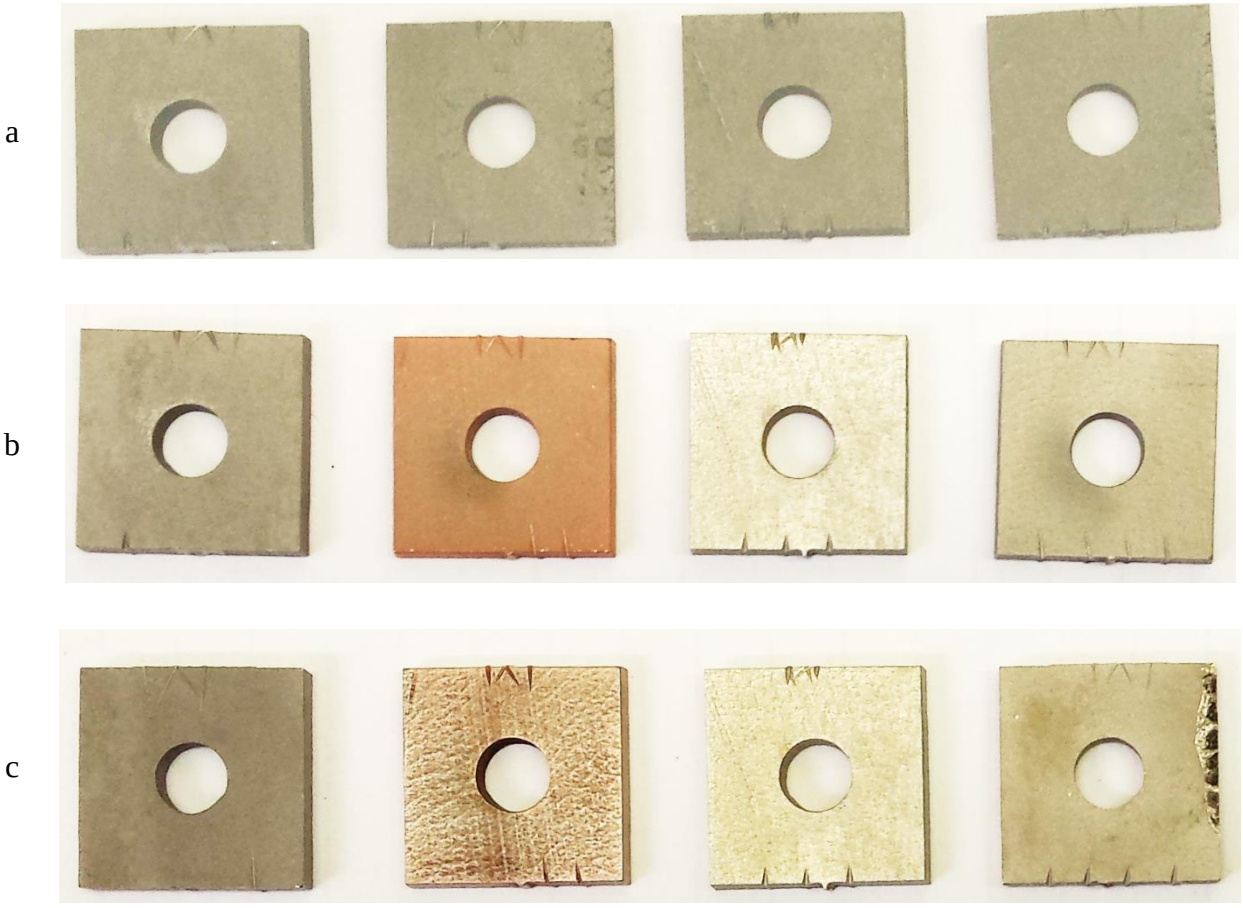

Figure 5.17: PICT 11: Nickel alloy (Monel 400): (1) A_1 (2) A_t (3) A_{t+1} and (4) B: Row a; before, and Row b; after exposure to 70% HF, with Row c; after removal of the scale layer.

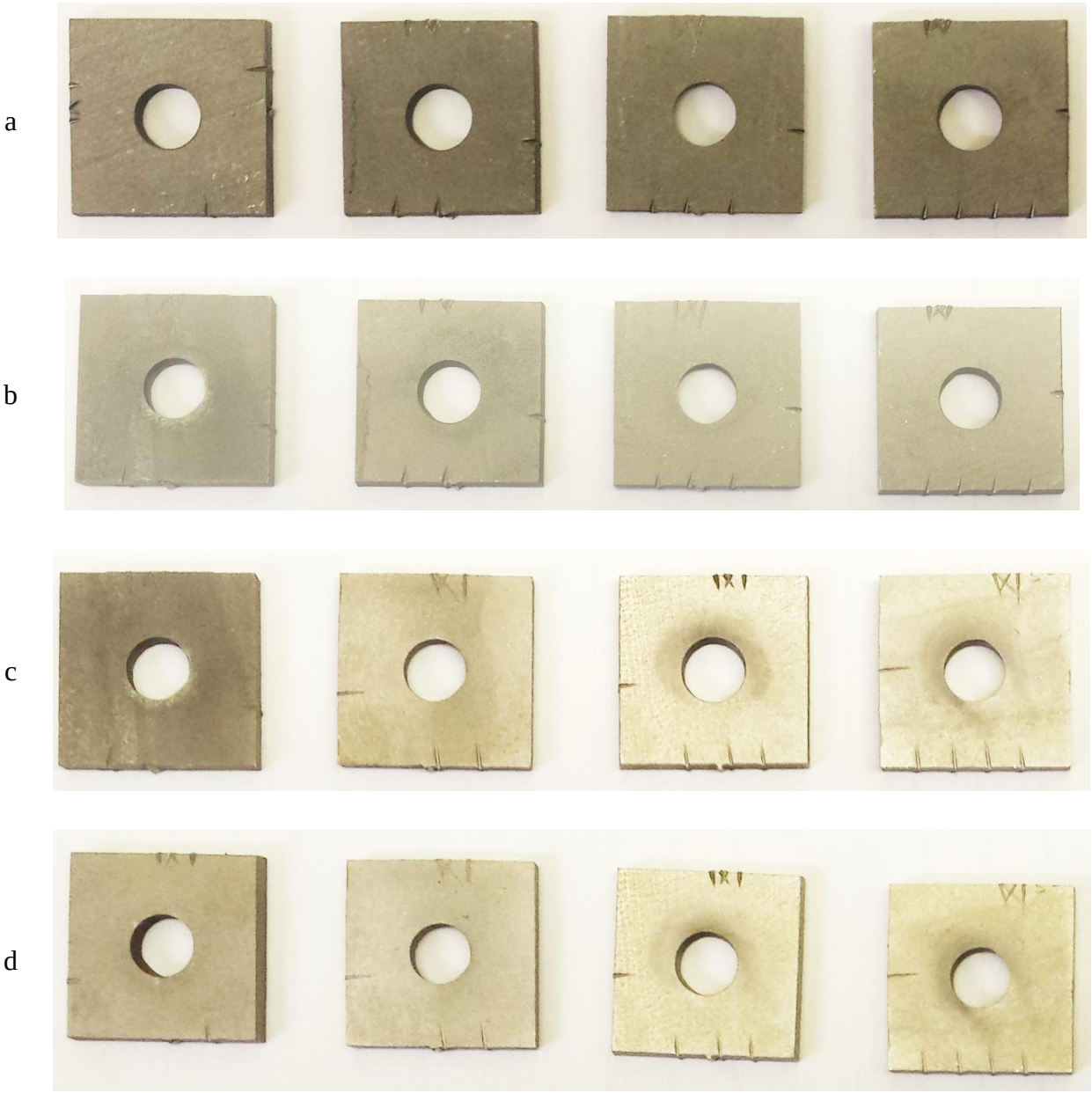

Figure 5.18: PICT 9: Nickel alloy (Monel 400): (1) A_1 (2) A_t (3) A_{t+1} and (4) B): Row a; before exposure, Row b; after pre-passivation step, Row c; after exposure to 70% HF, and Row d; after removal of the scale layer.

5.2. CORROSION TESTS

5.2.1. Introduction

Results from corrosion tests (CTs) in this section are the longer (11 day) corrosion tests in which the same corrosion conditions used in the PICT were used to establish the effect of HNO_3 concentration and temperature on mild steel corrosion in 70% HF. More coupons were used in the CTs to obtain more data points for the effect of time spent in the HF corrosion solutions tested (summary of conditions tested is given in Table 4.5). The harshest corrosive conditions established for mild steel in HF was when 1% HNO_3 was spiked into the corrosion solution and the temperature kept at 25ºC. Based on this result, corrosion was conducted on the other two alloys used in the HF production process at these conditions, to determine their suitability for use as construction materials in the plant. The presence of HNO_3 was found to influence the susceptibility to attack by HF of all the metals tested, and the suitability of these materials under such unique (yet probable) corrosive conditions was established.

5.2.2. Mild steel corrosion

5.2.2.1. Effect of HNO_3 concentration in HF

Mass loss and apparent corrosion rates

The data collected from the corrosion tests conducted on mild steel in 70% HF kept at 25ºC, spiked with different quantities of HNO_3 are shown in Tables 5.20 to 5.23. When the temperature was kept constant, the mass loss was directly proportional to the time spent in the corrosion solution. An increase in HNO_3 concentration increased the iron lost to the corrosion solution. However, the increase in HNO_3 to the corrosion solution did not affect the relationship between mass loss and time spent in the acid, as it remained directly proportional throughout the tests conducted (Tables 5.20 – 5.23).

Apparent corrosion rates were fastest during the first 24 hours in each of the corrosion tests and then slowed down later. Increasing the HNO_3 concentration to 0.1% effectively doubled the corrosion rate within the first 24 h when compared to corrosion rates determined for HF with no HNO_3 contamination (Tables 5.20). Correspondingly, when the HNO_3 was increased to a maximum of 1% in the HF corrosion solution, mild steel corroded nearly 10 times faster. Conversely, at 11 days in solution the corrosion rate did not exceed 5 mm/y (Table 5.23), but was still four times faster than the apparent corrosion rate determined for HF not spiked HNO_3 (Table 5.20).

Table 5.20: CT 1: Corrosion test for mild steel in 70% HF, at 25ºC.

Coupon No.	Interval (days)	Mass loss (g)	Fe in solution (g/L)	Apparent corrosion (mm/y)	Photograph, column
1	1	0.093±0.008	0.19±0.02	2.8±0.2	Figure 5.22 & 5.23 , 1
2	2	0.114±0.002	0.25±0.01	1.8±0.0	Figure 5.22 & 5.23, 2
3	3	0.136±0.005	0.30±0.01	1.4±0.1	Figure 5.22 & 5.23, 3
4	4	0.172±0.004	0.37±0.01	1.3±0.0	Figure 5.22 & 5.23, 4
5	7	0.249±0.026	0.50±0.06	1.1±0.1	Figure 5.22 & 5.23, 5
6	9	0.292±0.029	0.59±0.06	1.0±0.1	Figure 5.22 & 5.23, 6
7	11	0.338±0.047	0.66±0.10	0.9±0.1	Figure 5.22 & 5.23, 7
Total in reactor A		0.816±0.077	1.64±1.76	0.17±0.17	
Total		1.394±0.107	2.85±3.01	0.23±0.23	

Table 5.21: CT 3: Corrosion test for mild steel in 70% HF spiked with 0.1% HNO_3, at 25ºC.

Coupon No.	Interval (days)	Mass loss (g)	Fe in solution (g/L)	Apparent corrosion rate (mm/y)	Photograph, column
1	1	0.1923	0.41	5.8	Figure 5.26, 1
2	2	0.2149	0.46	3.2	Figure 5.26, 2
3	3	0.2444	0.53	2.5	Figure 5.26, 3
4	4	0.2714	0.59	2.0	Figure 5.26, 4
5	7	0.3621	0.78	1.6	Figure 5.26, 5
6	9	0.3749	0.81	1.3	Figure 5.26, 6
7	11	0.4540	0.98	1.2	Figure 5.26, 7
Total in reactor A only		1.2528	2.70		
Total		2.114	4.56		

Table 5.22: CT 5: Corrosion test for mild steel in 70% HF spiked with 0.5% HNO_3, at 25ºC.

Coupon No.	Interval (days)	Mass loss (g)	Fe in solution (g/L)	Apparent corrosion rate (mm/y)	Photograph, column
1	1	0.6601	1.42	19.9	Figure 5.29, 1
2	2	0.7219	1.56	10.9	Figure 5.29, 2
3	3	0.7906	1.71	8.0	Figure 5.29, 3
4	4	0.8141	1.76	6.1	Figure 5.29, 4
5	7	0.9693	2.09	4.2	Figure 5.29, 5
6	9	1.037	2.24	3.5	Figure 5.29, 6
7	11	1.0969	2.37	3.0	Figure 5.29, 7
Total in reactor A only		3.5169	7.59		
Total		6.0899	13.14		

Table 5.23: CT 4: Corrosion test for mild steel in 70% HF spiked with 1% HNO_3, at 25ºC.

Coupon No.	Interval (days)	Mass loss (g)	Fe in solution (g/L)	Apparent corrosion (mm/y)	Photograph, column
1	1	1.187±0.125	2.56±0.271	35.9±3.8	Figure 5.32 & 5.33 , 1
2	2	1.267±0.050	2.73±0.107	19.1±0.8	Figure 5.32 & 5.33, 2
3	3	1.197±0.037	2.58±0.080	12.1±0.4	Figure 5.32 & 5.33, 3
4	4	1.391±0.048	3.00±0.103	10.5±0.4	Figure 5.32 & 5.33, 4
5	7	1.374±0.046	2.96±0.099	5.9±0.2	Figure 5.32 & 5.33, 5
6	9	1.469±0.038	3.17±0.083	4.9±0.1	Figure 5.32 & 5.33, 6
7	11	1.632±0.078	3.52±0.168	4.5±0.2	Figure 5.32 & 5.33, 7
Total in reactor A		5.389±0.212	11.63±0.458		
Total		9.516±0.253	20.53±0.545		

5.2.2.2. Effect of temperature

Mass loss and apparent corrosion rates

To ascertain whether corrosive attack by HNO_3 could be mitigated by a reduction in temperature, the same HNO_3 concentrations in HF corrosion solutions as in the previous section were repeated at lower temperatures, and the data collected (Tables 5.24 – 5.31). The relationship between mass loss by the coupons and time spent in the corrosive solutions still remained directly proportional, irrespective of HNO_3 concentration (0 – 1%) present or temperature (0 – 25ºC).

In the absence of HNO_3 in the corrosion solution, the corrosion rate nearly halved when the temperature was reduced from 25 to 15ºC (2.8 to 1.5 mm/y) within the first 24 h (Tables 5.20 and 5.24). Over the same time interval (up to 1 day), the corrosion rate dropped to nearly 1 mm/y when the temperature was kept at a minimum of 0ºC. Over the rest of the HNO_3 free corrosion tests, corrosion steadily reduced to just less than 1 mm/y (>0.6 mm/y) with the higher temperatures still producing the fastest corrosion rates up until the end of the experiment (11 days in Tables 5.20, 5.24 and 5.28). Conversely, when HNO_3 concentration was increased at the lower temperatures (15 and 0ºC), the differences between the corrosion rates were much smaller (~0.4 mm/y) compared to rates determined for the HNO_3 free solutions (Tables 5.21, 5.25 and 5.29). When the HNO_3 concentration was increased, the impact of temperature was even less (~0.1 mm/y difference). Therefore, the higher the HNO_3 concentration in the solution, the less the corrosion rate was affected by a change in temperature (when comparing apparent corrosion rates in Tables 5.23 to 5.27 and 5.31).

Table 5.24: CT 7: Corrosion test for mild steel in 70% HF at 15ºC.

Coupon No.	Interval (days)	Mass loss (g)	Fe in solution (g/L)	Apparent corrosion rate (mm/y)	Photograph, column
1	1	0.0510	0.11	1.5	Figure 5.24, 1
2	2	0.0723	0.16	1.1	Figure 5.24, 2
3	3	0.0871	0.19	0.9	Figure 5.24, 3
4	4	0.0965	0.21	0.7	Figure 5.24, 4
5	7	0.1893	0.41	0.8	Figure 5.24, 5
6	9	0.2206	0.48	0.7	Figure 5.24, 6
7	11	0.2749	0.59	0.8	Figure 5.24, 7
Total in reactor A only		0.6023	1.30		
Total		0.9917	2.14		

Table 5.25: CT 8: Corrosion test for mild steel in 70% HF spiked with 0.1% HNO_3, at 15ºC.

Coupon No.	Interval (days)	Mass loss (g)	Fe in solution (g/L)	Apparent corrosion rate (mm/y)	Photograph, column
1	1	0.2014	0.43	6.1	Figure 5.27, 1
2	2	0.2093	0.45	3.2	Figure 5.27, 2
3	3	0.2392	0.52	2.4	Figure 5.27, 3
4	4	0.2095	0.45	1.6	Figure 5.27, 4
5	7	0.3211	0.69	1.4	Figure 5.27, 5
6	9	0.3289	0.71	1.1	Figure 5.27, 6
7	11	0.4139	0.89	1.1	Figure 5.27, 7
Total in reactor A only		1.1756	2.54		
Total		1.9233	4.15		

Table 5.26: CT 9: Corrosion test for mild steel in 70% HF spiked with 0.5% HNO_3, at 15ºC.

Coupon No.	Interval (days)	Mass loss (g)	Fe in solution (g/L)	Apparent corrosion rate (mm/y)	Photograph, column
1	1	0.6549	1.41	19.8	Figure 5.30, 1
2	2	0.6869	1.48	10.4	Figure 5.30, 2
3	3	0.6619	1.43	6.7	Figure 5.30, 3
4	4	0.6965	1.50	5.3	Figure 5.30, 4
5	7	0.8365	1.81	3.6	Figure 5.30, 5
6	9	0.9121	1.97	3.1	Figure 5.30, 6
7	11	1.0816	2.33	3.0	Figure 5.30, 7
Total in reactor A only		3.2349	6.98		
Total		5.5304	11.93		

Table 5.27: CT 10: Corrosion test for mild steel in 70% HF spiked with 1% HNO_3, at 15ºC.

Coupon No.	Interval (days)	Mass loss (g)	Fe in solution (g/L)	Apparent corrosion (mm/y)	Photograph, column
1	1	1.074±0.010	2.32±0.021	32.5±0.3	Figure 5.34 & 5.35 , 1
2	2	1.191±0.038	2.57±0.081	18.0±0.6	Figure 5.34 & 5.35, 2
3	3	1.239±0.123	2.67±0.266	12.5±1.2	Figure 5.34 & 5.35, 3
4	4	1.267±0.028	2.73±0.061	9.6±0.2	Figure 5.34 & 5.35, 4
5	7	1.371±0.118	2.96±0.254	5.9±0.5	Figure 5.34 & 5.35, 5
6	9	1.403±0.014	3.03±0.030	4.7±0.0	Figure 5.34 & 5.35, 6
7	11	1.580±0.154	3.41±0.331	4.3±0.4	Figure 5.34 & 5.35, 7
Total in reactor A		5.265±0.385	11.36±0.830		
Total		9.126±0.436	19.69±0.942		

Table 5.28: CT 12: Corrosion test for mild steel in 70% HF, at 0ºC.

Coupon No.	Interval (days)	Mass loss (g)	Fe in solution (g/L)	Apparent corrosion rate (mm/y)	Photograph, column
1	1	0.0350	0.08	1.1	Figure 5.25, 1
2	2	0.0426	0.09	0.6	Figure 5.25, 2
3	3	0.0629	0.14	0.6	Figure 5.25, 3
4	4	0.0641	0.14	0.5	Figure 5.25, 4
5	7	0.1372	0.30	0.6	Figure 5.25, 5
6	9	0.1868	0.40	0.6	Figure 5.25, 6
7	11	0.2247	0.48	0.6	Figure 5.25, 7
Total in reactor A only		0.4598	0.99		
Total		0.7533	1.63		

Table 5.29: CT 13: Corrosion test for mild steel in 70% HF spiked with 0.1% HNO_3, at 0ºC.

Coupon No.	Interval (days)	Mass loss (g)	Fe in solution (g/L)	Apparent corrosion rate (mm/y)	Photograph, column
1	1	0.1538	0.33	4.6	Figure 5.28, 1
2	2	0.1867	0.40	2.8	Figure 5.28, 2
3	3	0.2116	0.46	2.1	Figure 5.28, 3
4	4	0.1961	0.42	1.5	Figure 5.28, 4
5	7	0.2598	0.56	1.1	Figure 5.28, 5
6	9	0.2614	0.56	0.9	Figure 5.28, 6
7	11	0.3756	0.81	1.0	Figure 5.28, 7
Total in reactor A only		1.0008	2.16		
Total		1.645	3.55		

Table 5.30: CT 14: Corrosion test for mild steel in 70% HF spiked with 0.5% HNO_3, at 0ºC.

Coupon No.	Interval (days)	Mass loss (g)	Fe in solution (g/L)	Apparent corrosion rate (mm/y)	Photograph, column
1	1	0.5732	1.24	17.3	Figure 5.31, 1
2	2	0.6505	1.40	9.8	Figure 5.31, 2
3	3	0.6864	1.48	6.9	Figure 5.31, 3
4	4	0.7207	1.56	5.4	Figure 5.31, 4
5	7	0.8198	1.77	3.5	Figure 5.31, 5
6	9	0.8935	1.93	3.0	Figure 5.31, 6
7	11	1.0001	2.16	2.7	Figure 5.31, 7
Total in reactor A only		3.0795	6.65		
Total		5.3442	11.53		

Table 5.31: CT 15: Corrosion test for mild steel in 70% HF spiked with 1% HNO_3, at 0ºC.

Coupon No.	Interval (days)	Mass loss (g)	Fe in solution (g/L)	Apparent corrosion rate (mm/y)	Photograph, column
1	1	0.988±0.029	2.13±0.063	29.8±0.9	Figure 5.36 & 5.37 , 1
2	2	1.139±0.027	2.46±0.059	17.2±0.4	Figure 5.36 & 5.37, 2
3	3	1.138±0.058	2.46±0.124	11.5±0.6	Figure 5.36 & 5.37, 3
4	4	1.192±0.098	2.57±0.212	9.0±0.7	Figure 5.36 & 5.37, 4
5	7	1.322±0.125	2.85±0.269	5.7±0.5	Figure 5.36 & 5.37, 5
6	9	1.376±0.089	2.97±0.192	4.6±0.3	Figure 5.36 & 5.37, 6
7	11	1.679±0.021	3.62±0.046	4.6±0.1	Figure 5.36 & 5.37, 7
Total in reactor A		5.127±0.174	11.06±0.376		
Total		11.458±4.046	19.06±0.721		

Acid consumption

For the two acids in the corrosion solutions for the CTs, the HF acid component was kept relatively constant (69.2 – 70% HF), while the HNO_3 component was varied (0 - 1%) with temperature (Tables 5.32 and 5.33). Mild steel coupons exposed to the corrosion solution reacted with the two acids present to form iron salts (fluorides and nitrates) and gasses (hydrogen, nitrogen dioxide and nitrogen monoxide) which reduced the concentration of the acids present in the solution, as corrosion continued. One way to relate mild steel corrosion to acid consumption is by dividing the mass of acid consumed by the mass of the coupons introduced to the corrosion solution. Another way is to track the mass of acid consumed in the system and expressing it as a percentage. Since the mass of coupons introduced to each CT varied little (±2.4 g), the acid consumption expressed using both means produced very similar findings (Tables 5.32 and 5.33).

At low temperatures (0 and 15ºC) and nitric acid concentrations (<0.5% HNO_3), HF acid consumption was minimal (<0.15 g_{HF}/g_{Fe}). Conversely, when HNO_3 in the corrosion solution was increased to 1%, the HF consumption also increased (>0.15 g_{HF}/g_{Fe}). Additionally, increasing the temperature increased the acid consumption from 2.6% at 0ºC to nearly 6% at 25ºC. Therefore, increasing temperatures and HNO_3 content effectively increased HF consumption, which increased corrosion of the mild steel coupons in the solution (Table 5.32).

Nitric acid quantities spiked into the corrosion solutions (1-11 mL of HNO_3) were minor compared to the concentration of the hydrofluoric acid (463 mL of 70% HF) present. This resulted in HNO_3 acid consumption measurements, in terms of $g_{Acid}/g_{Coupons}$ being nearly negligible (>0.08 g_{HNO_3}/g_{Fe}). Conversely, measuring acid consumption in terms of mass of acid in against mass of acid out produced better results for determining HNO_3 consumption. Irrespective of changes in temperature and HNO_3 concentration, acid consumption for HNO_3 was consistently in excess of 98% (Table 5.33). Nearly all the HNO_3 introduced to a corrosion test containing pre-passivated mild steel was consumed, as it reacted with the scale on coupon surfaces. A break down, or complete dissolution, of the protective scale then permitted corrosion of mild steel in the predominantly HF solution remaining.

Table 5.32: HF acid consumption by mild steel after 11 days when varying the HNO_3 concentration in 70% HF, at 0, 15 and 25ºC.

Temp.	Feed HNO_3 concn. (%)	Feed HF concn. (%)	Product HF concn. (%)	Mass of HF in feed (g)	Mass of HF in product (g)	Mass of Coupons ** (g)	Acid consumption	
							$\left(\frac{g\ HF}{g\ Fe}\right)$	(%)
0ºC	0.0	70.00	69.14	324.40	320.41	59.46	0.07	1.2
	0.1	69.92	68.01	324.03	315.17	58.93	0.15	2.7
	0.5	69.60	68.30	322.54	316.52	62.74	0.10	1.9
	1.0	69.21	67.44	320.74	312.51	55.95	0.15	2.6
15ºC	0.0	70.00	69.21	324.40	320.74	60.00	0.06	1.1
	0.1	69.92	68.44	324.03	317.17	63.09	0.11	2.1
	0.5	69.60	68.12	322.54	315.68	59.78	0.11	2.1
	1.0	69.21	66.74*	320.74	309.27	60.21*	0.19	3.6
25ºC	0.0	70.00	69.04*	324.40	319.95	57.22*	0.06	1.0
	0.1	69.92	66.24	324.03	306.97	54.89	0.30	5.2
	0.5	69.60	67.55	322.54	313.04	58.62	0.12	2.3
	1.0	69.21	64.96*	320.74	301.04	58.12*	0.66	5.8

*Average value from duplicate corrosion tests or solution analyses conducted with errors captured in the graphs discussed.

**Only the contents of reactor A was analysed for each corrosion test, therefore total coupon mass considered were from the combined weight of coupon 1, 3 5 & 7 in each instance.

Table 5.33: HNO_3 acid consumption by mild steel after 11 days when varying the HNO_3 concentration in 70% HF, at 0, 15 and 25ºC.

Temp.	Feed HNO_3 concn. (%)	Product HNO_3 concn. (mg/kg)	Mass of HNO_3 in feed (mg)	Mass of HNO_3 in product (mg)	Mass of Coupons ** (g)	Acid consumption	
						$\left(\frac{\text{g HF}}{\text{g Fe}}\right)$	(%)
0ºC	0.0	0.00	0.00	0	59.46	0.00	0.0
	0.1	2.61	463.42	1	58.93	0.01	99.7
	0.5	35.40	2317.12	20	62.74	0.04	99.1
	1.0	64.06	4634.24	36*	55.95*	0.08	99.2
15ºC	0.0	0.00	0.00	0	60.00	0.00	0.0
	0.1	12.00	463.42	7	63.09	0.01	98.5
	0.5	31.00	2317.12	18	59.78	0.04	99.2
	1.0	23.00	4634.24	13*	60.21*	0.08	99.7
25ºC	0.0	0.00*	0.00	0	57.22*	0.00	0.0
	0.1	13.00	463.42	7	54.89	0.01	98.4
	0.5	10.00	2317.12	6	58.62	0.04	99.8
	1.0	4.50*	4634.24	3	54.71*	0.08	99.9

* Average value from duplicate corrosion tests or solution analyses conducted with errors captured in the graphs discussed.

** Only the contents of reactor A was analysed for each corrosion test, therefore total coupon mass considered were from the combined weight of coupon 1, 3 5 & 7 in each instance.

HF acid consumption was related to HNO_3 consumption in Figure 5.19 to demonstrate how differently the two acids were consumed within the same corrosion solution, when kept at 25ºC and allowed to react with the same coupons for up to 11 days. Irrespective of any change in HNO_3 concentration, HF continued to uniformly corrode mild steel as shown by its low acid consumption (<10%) maintained throughout. Conversely, HNO_3 consumption was nearly 10 times higher than HF acid consumption. This was indicative of all the HNO_3 spiked into the corrosion solution reacting to dissolve the scale formed during pre-passivation and then reacting with the exposed steel substrate. Higher HF consumptions (>2%) were prevalent in corrosion tests where HNO_3 were present, since they were more readily consumed to react with the freshly exposed steel which resulted from HNO_3 corrosion.

Conducting corrosion tests at lower temperatures (0ºC and 15ºC) effectively lowered HF acid consumption in the presence of HNO_3 acid (Figure 5.20). However, when only HF was present in the corrosion solution, the HF acid consumption remained unchanged at ~1% over 11 days at all temperatures tested.

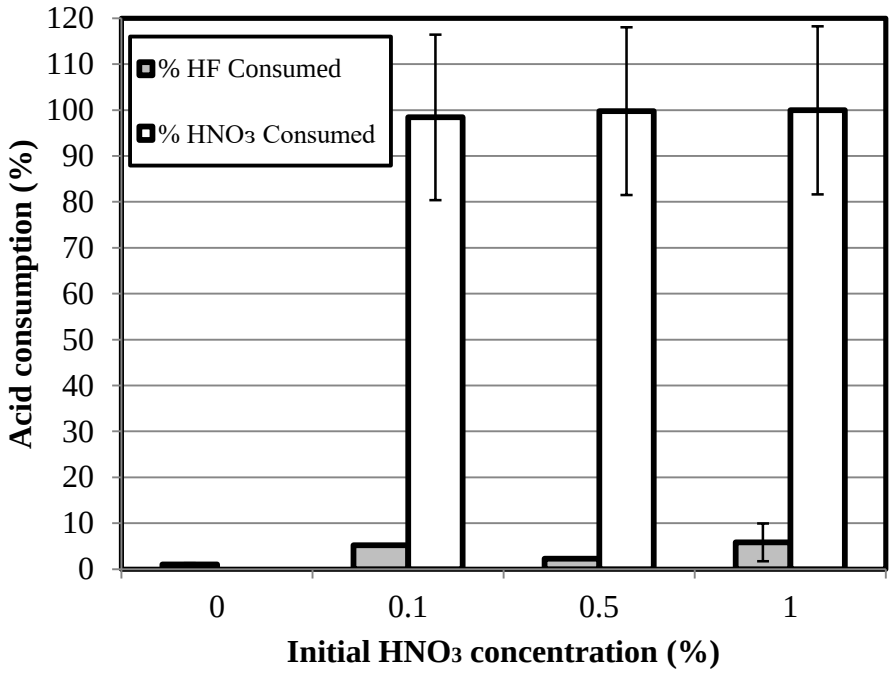

Figure 5.19: HF and HNO_3 acid consumption after 11 days of mild steel corrosion, at 25ºC. Error bars obscured by markers in some instances.

Nitric acid consumption showed no variation with change in temperature, since more than 98% of all HNO_3 spiked into each corrosion solution was consumed during each of the 11 day corrosion tests conducted (Figure 5.21). Thus, any HNO_3 (≥1% concentration) introduced to a 70% HF corrosion solution rapidly reacted with oxide and fluoride scale present as well as the any exposed mild steel substrate, until it was completely consumed.

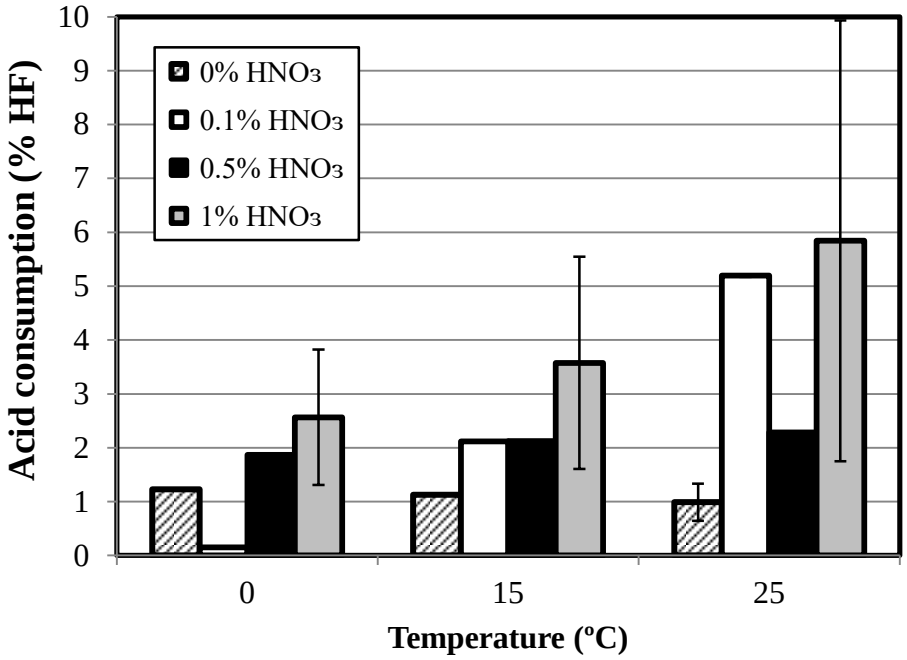

Figure 5.20: Effect of temperature on percentage HF acid consumption after 11 days of mild steel corrosion. Error bars obscured by markers in some instances.

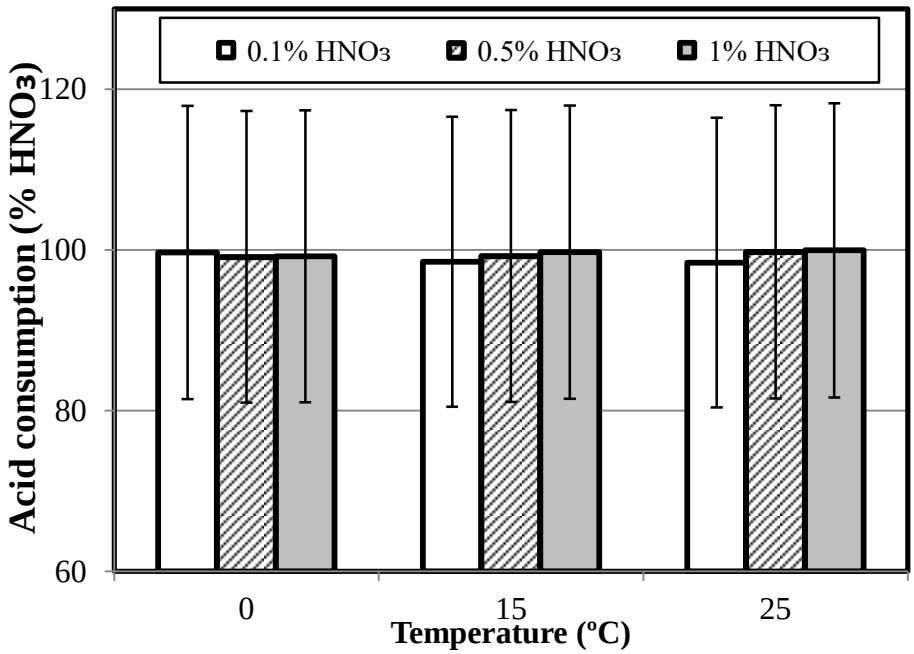

Figure 5.21: Effect of temperature on percentage HNO_3 acid consumption after 11 days of mild steel corrosion. Error bars obscured by markers in some instances.

Observations of photographs of corroded coupons

The digital photographs taken of the mild steel coupons before and after the pre-passivation step, and then again after exposure to the corrosion solutions in which temperatures and HNO_3 concentrations were varied are given in Figures 5.22 – 5.37. The condition of the fluoride scale observed after exposure to the various corrosion solutions was described, as well as the conditions of the corroded coupon surfaces visible after cleaning off their scale, and these are summarized in Tables 5.34 to 5.37.

The dark grey with mottled light brown scale became a recognizable feature on the surfaces of pre-passivated mild steel coupons (Figures 5.22 – 5.37: Row b), which were first identified in the PICTs (Section 5.1.2). This scale was identified as a mixture of iron (II/III) oxides (black), iron fluoride (grey) and ferric hydroxide (light yellow-brown)(Haynes, 2016) by visual examinations, Section 3.5. Hence, exposure of the pre-passivated coupons to the corrosion solution either visibly thickened the scale formed during the pre-passivation step, or resulted in it thinning due to its partial dissolution and removal of the scale.

In corrosion tests where no HNO_3 was spiked, the change in temperature had little impact on the visual quality of the coupons (Table 5.34). Compared to the colour of the scale on the original pre-passivated coupons introduced to 70% HF, the scaled turned darker. The black scale was a sign of the scale oxidizing, or predominantly consisting of iron (II/III) oxides (Haynes, 2016).

However, prolonged exposure of this oxidized scale to concentrated HF eventually converted it to a fluoride (light brown colour in Figures 5.23, 5.25 and 5.24: Row c), Equation 5.1:

$$Fe_2O_3 + 6HF \rightarrow 2FeF_3.3H_2O \qquad \text{Equation 5.1}$$

Increasing the temperature facilitated this conversion, since more coupons had the light brown scale on the surface at higher temperatures (3/4 coupons at 15ºC and 4/7 coupons at 25ºC) than compared to 0ºC (0/7 coupons in Figure 5.25: Row c). During ultrasonic cleaning, the black scale which had formed on the coupons at 0ºC was more resilient, and was not completely removed during washing (Figure 5.25: Row d). Washing of the coupons exposed an underlying brown tint on the sample, indicative of fluoride forming on the mild steel surface during corrosion (Table 5.34). When no HNO_3 was present, HF improved the quality of the scale formed on the steel surface, which mitigated any further corrosive attack by HF (>69% HF), effectively protecting the scale with exposure time. Iron concentration in the product solution collected from the 0ºC corrosion tests was nearly 1.5 times lower (>425 ppm) than the other two tests. This indicated that less iron was removed from the coupon surfaces at a lower temperature and therefore HF corrosion was hindered by reducing the temperature of the corrosion solution.

Table 5.34: Observations of corrosion products from mild steel in pure HF to see the effect of change in temperature on scale. (Figures 5.22, 5.23, 5.24 and 5.25: Row c and d).

	0ºC	**15ºC**	**25ºC**
Appearance of coupons before cleaning	Black scale remnant of pre-passivation maintained over entire corrosion test (11 days)	Black scale remnant of pre-passivation maintained for the first 3 days, turning grey with mottled light brown scale after 4 days.	Black scale remnant of pre-passivation maintained for the first 2 days, turning grey with mottled light brown scale after 3 days.
Appearance of coupons after cleaning	Black scale was resilient and could not adequately be cleaned from any of the coupons. Cleaning exposed black with mottled light brown scale on coupons that were in longer than 7 days.	Black scale was resilient and could not adequately be cleaned from coupons removed between 1 and 4 days. Coupons removed after 4 days has no visible corrosion with some underlying brown scale exposed on the cleaned surface.	Black scale was resilient and could not adequately be cleaned from coupons removed between 1 and 3 days. Coupons removed after 4 days has no visible corrosion with some underlying brown scale exposed on the cleaned surface.
Composition of final corrosion solution	69.14% HF 2.9 mg/kg HNO_3 425 ppm Fe <2 ppm Cr 4 ppm Mn 114 ppm Si	69.2% HF <2 mg/kg HNO_3 703 ppm Fe <2 ppm Cr 5 ppm Mn 115 ppm Si	* 69.73% HF <2 mg/kg HNO_3 * 647 ppm Fe * 5 ppm Cr * 5 ppm Mn * 87 ppm Si

* Average value determined from duplicate tests and analyses

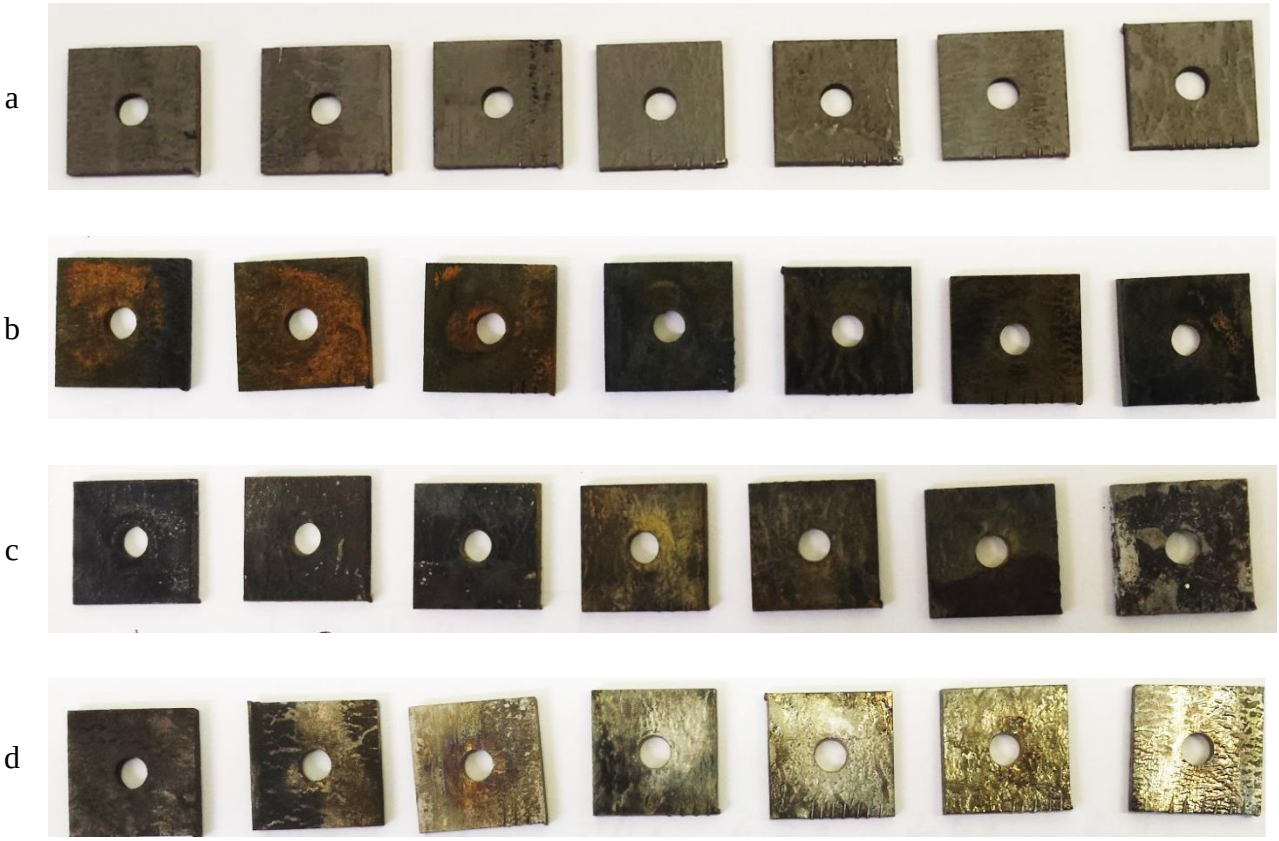

Figure 5.22: CT 1: Mild steel coupons (1-7): Row a; before exposure, Row b; after pre-passivation step, Row c after exposure to 70% HF, and Row d; after removal of the scale layer, at 25ºC.

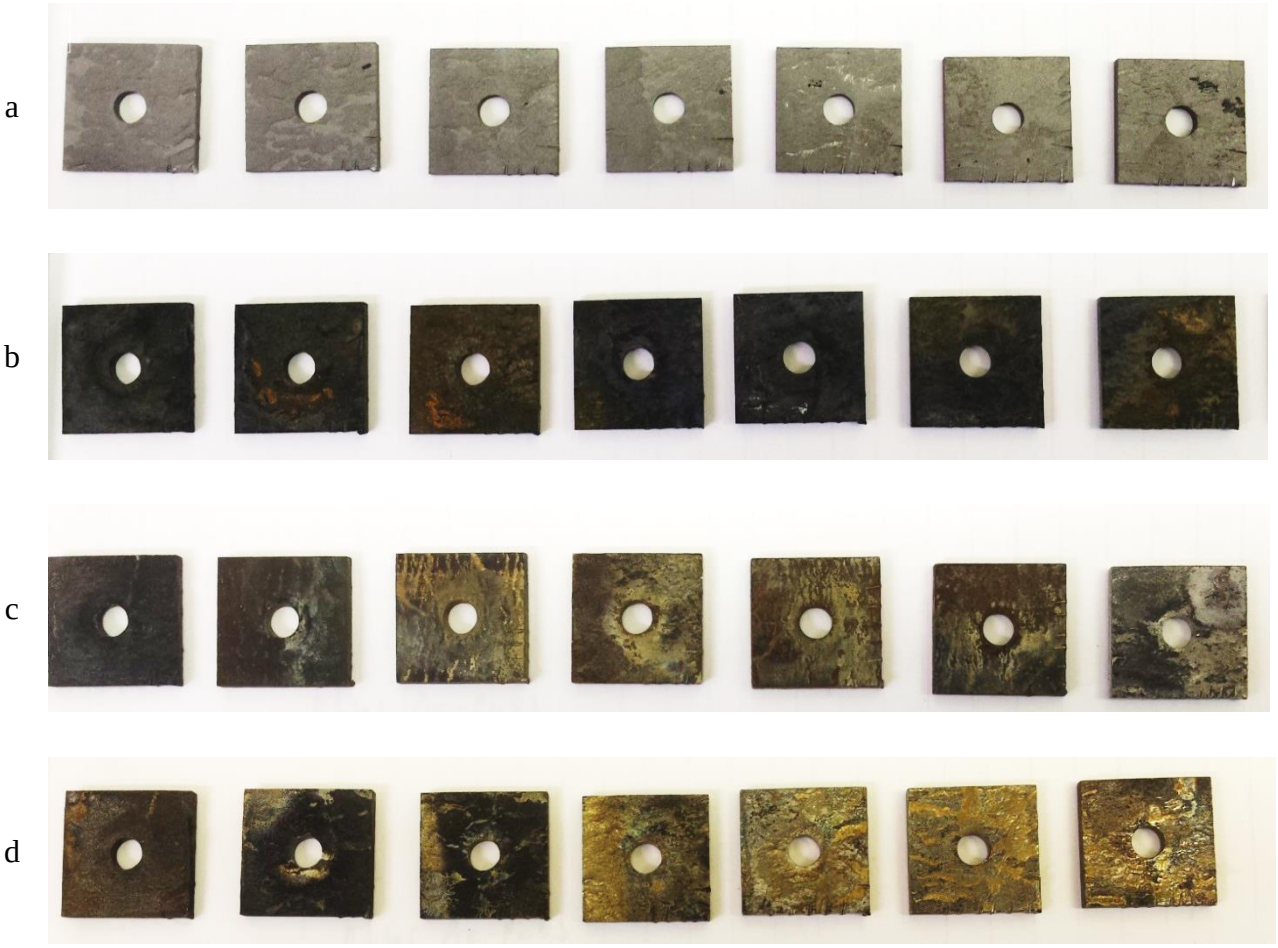

Figure 5.23: CT 2 (Duplicate corrosion test): Mild steel coupons (1-7): Row a; before exposure, Row b; after pre-passivation step, Row c; after exposure to 70% HF, and Row d; after removal of the scale layer, at 25ºC.

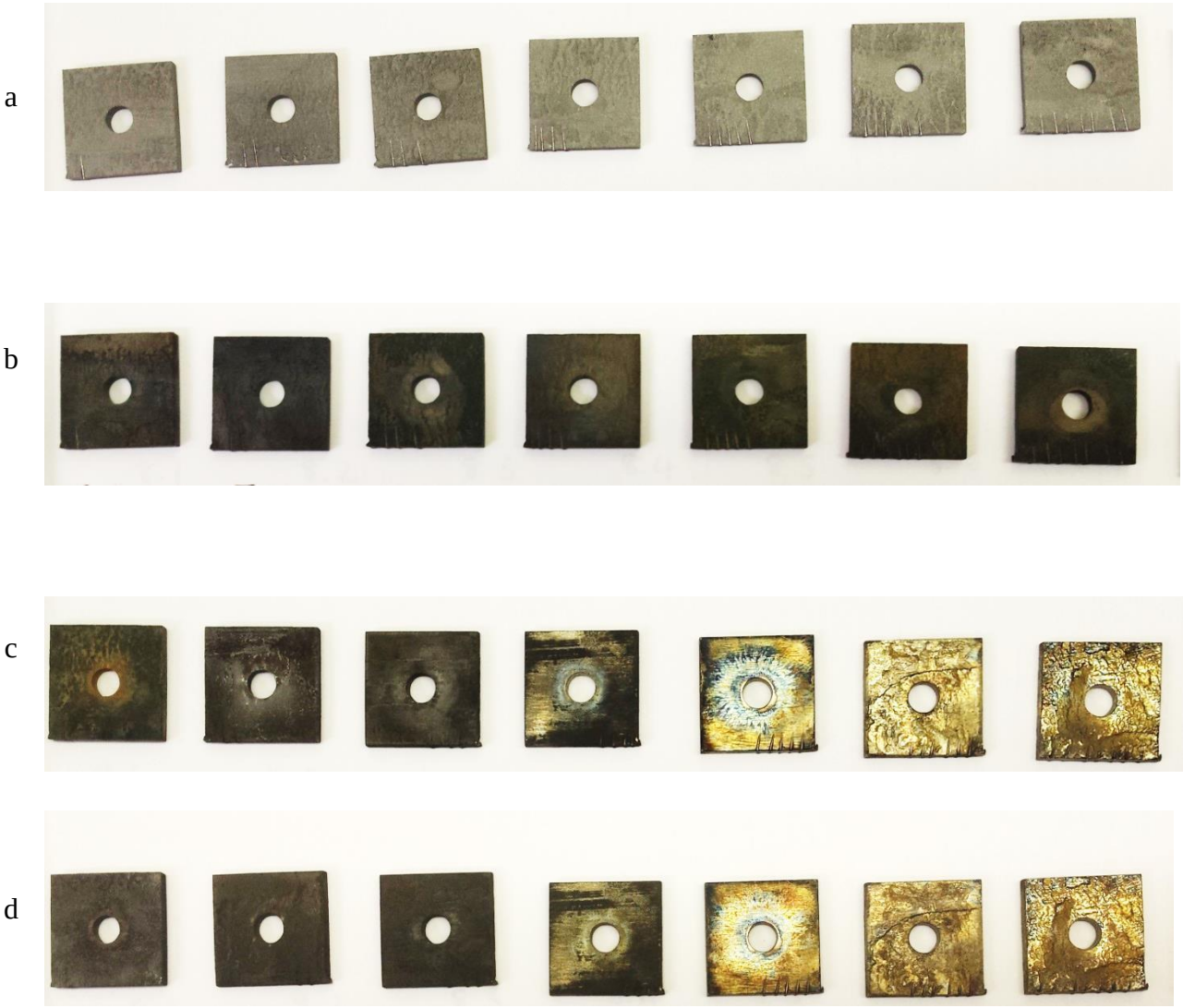

Figure 5.24: CT 7: Mild steel coupons (1-7): Row a; before exposure, Row b; after pre-passivation step, Row c; after exposure to 70% HF, and Row d; after removal of the scale layer at 15ºC.

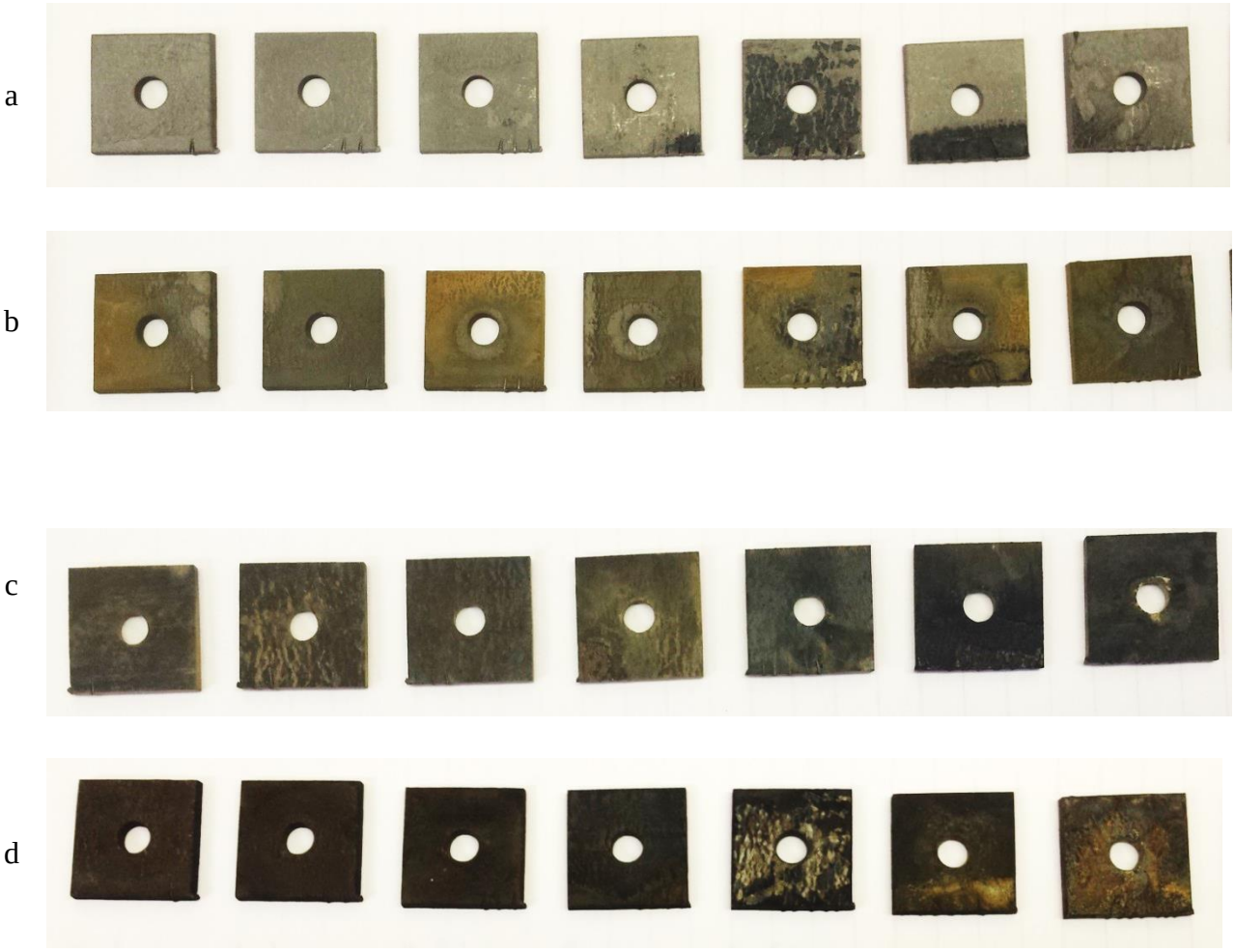

Figure 5.25: CT 12: Mild steel coupons (1-7): Row a; before exposure, Row b; after pre-passivation step, Row c; after exposure to 70% HF, and Row d; after removal of the scale layer, at 0ºC.

When the nitric acid concentration was slightly increased (to 0.1%), the effect on mild steel and its protective scale was recorded with changes in temperature (Table 5.35). The black oxide scale was present over the coupon surface for a longer time (>9 days) compared to coupons where no HNO_3 was spiked (Table 5.34). Hence, HNO_3 preferentially attacked the fluoride (yellow-brown scale), leaving behind the black iron oxide scale on the coupon surfaces (Figures 5.26 - 5.28: Row c). Increased temperature assisted the HNO_3 to dissolve the scale on the surfaces, as evident by the exposed metal substrate starting to be visible after nine days, when the corrosion solution was kept at 25ºC (Figure 5.26: Row c). During ultrasonic washing of the corroded coupons, it was observed that the scale was more readily removed (unstable) on coupons tested at higher temperatures (≥15ºC, Figures 5.26 and 5.27: Row d), indicating enhanced corrosion at higher temperatures, in the presence of 0.1% HNO_3.

The iron concentration found in the product corrosion solution was nearly three times that of the corrosion tests where no nitric acid was present. An increase in temperature also led to an increase in iron in concentration (>2200 ppm at 25ºC), supporting that increasing temperature assisted HF and HNO_3 corrosion of mild steel.

Table 5.35: Observations of corrosion products from mild steel in HF spiked with 0.1% HNO_3 to see the effect of change in temperature on scale. (Figures 5.26, 5.27and 5.28: Row c and d).

	0ºC	**15ºC**	**25ºC**
Appearance of coupons before cleaning	Black scale remnant of pre-passivation maintained for the first 2 days. Turned grey with mottled light brown scale after 3 days with the silver grey metal exposed at the edges.	Black scale remnant of pre-passivation maintained for 9 days. Turned grey on the last day, exposing the silver grey steel substrate at the edge of the coupon.	Black scale remnant of pre-passivation maintained for 7 days. Turned grey with mottled light brown scale after 9 days, also exposing the silver grey steel substrate at the edge of the coupon.
Appearance of coupons after cleaning	Black scale was resilient and not adequately cleaned from coupon removed after 2 days. Cleaning exposed light brown scale on coupon surfaces that were in for longer than 3 days with the silver grey steel substrate also exposed at the edges.	Black scale was more easily removed from the all the coupons exposing a grey with mottled light brown scale with grey steel substrate exposed at the edges.	Black scale was more easily removed from the all the coupons exposing a grey with mottled light brown scale. Corrosion of the steel visible on the surface of the coupons where the steel was exposed.
Composition of final corrosion solution	68.01% HF 2.6 mg/kg HNO_3 1375 ppm Fe 3 ppm Cr 10 ppm Mn 57 ppm Si	68.44% HF 12 mg/kg HNO_3 1527 ppm Fe 3 ppm Cr 9 ppm Mn 120 ppm Si	66.24% HF 13 mg/kg HNO_3 2204 ppm Fe 22 ppm Cr 4 ppm Mn 131 ppm Si

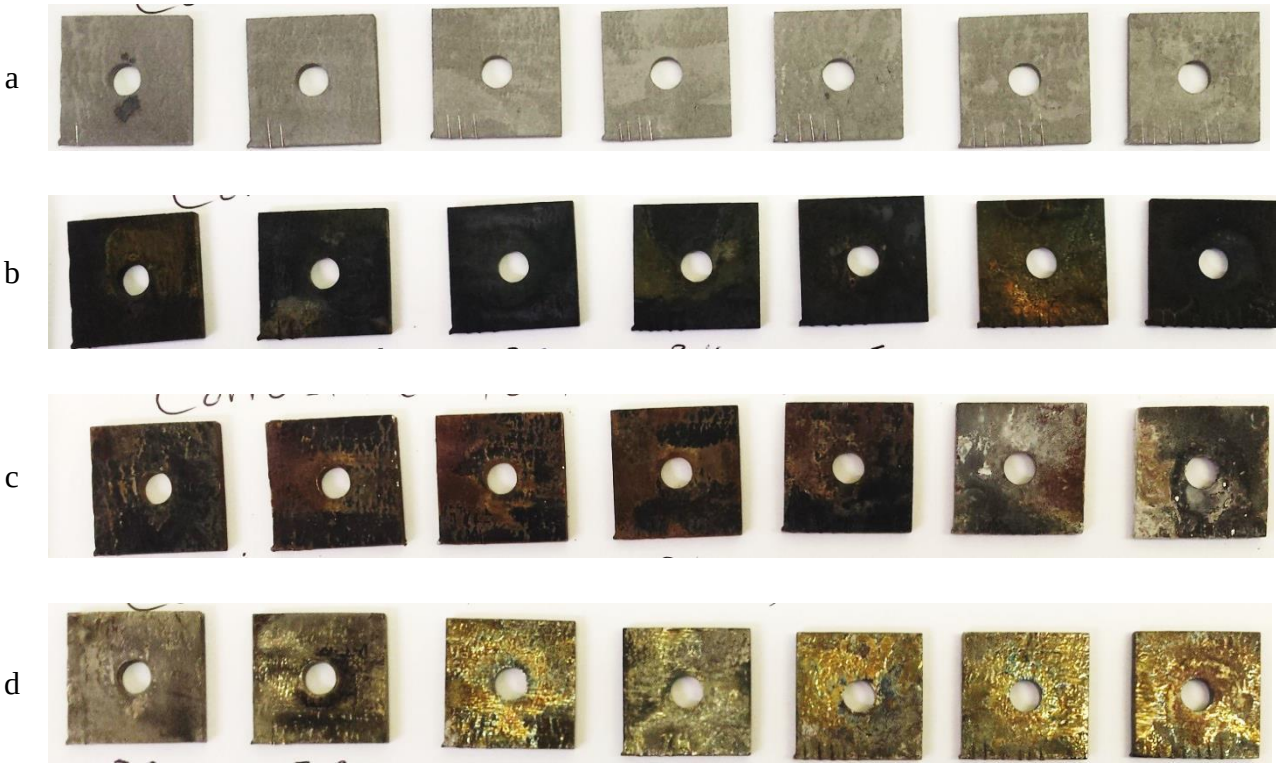

Figure 5.26: CT 3: Mild steel coupons (1-7): Row a; before exposure, Row b; after pre-passivation step, Row c; after exposure to 70% HF spiked with 0.1% HNO_3, and Row d; after removal of the scale layer, at 25ºC.

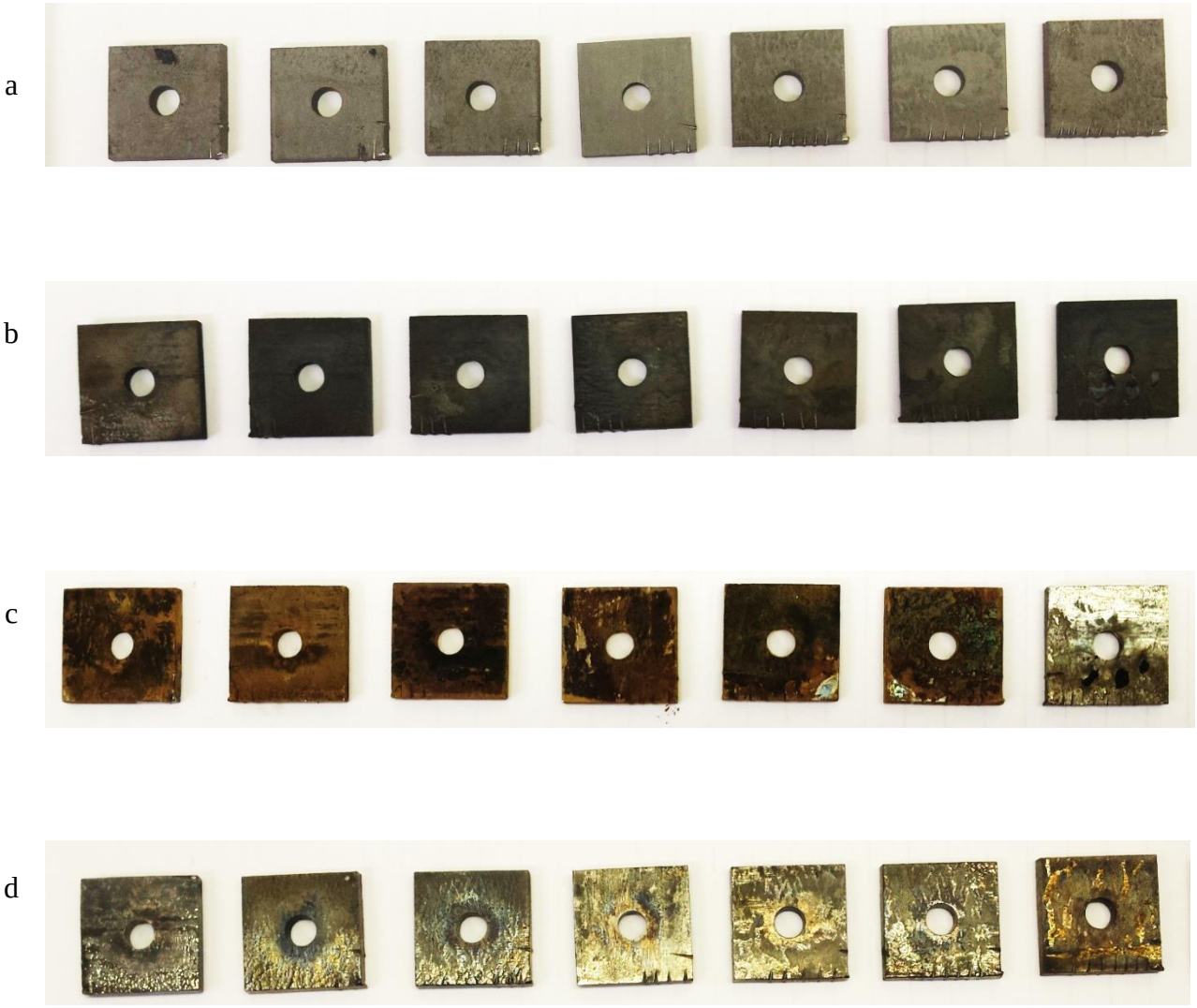

Figure 5.27: CT 8: Mild steel coupons (1-7): Row a; before exposure, Row b; after pre-passivation step, Row c; after exposure to 70% HF spiked with 0.1% HNO_3, and Row d; after removal of the scale layer, at 15ºC.

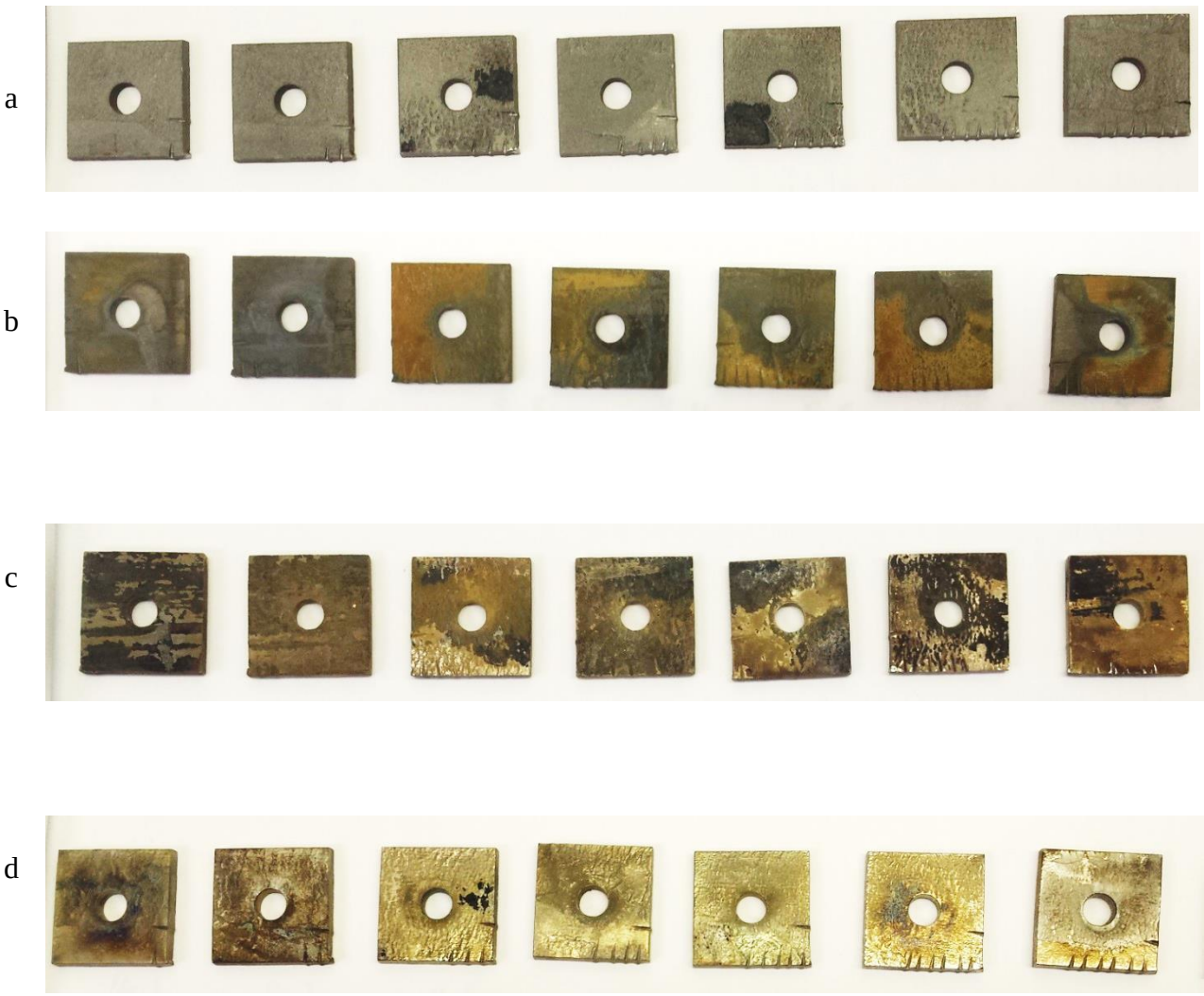

Figure 5.28: CT 13: Mild steel coupons (1-7): Row a; before exposure, Row b; after pre-passivation step, Row c; after exposure to 70% HF spiked with 0.1% HNO_3, and Row d; after removal of the scale layer, at 0ºC.

Slightly increasing the HNO_3 concentration to 0.5% in the 70% HF corrosion solution had a significant effect on the colour of the scale formed and the steel substrate revealed after cleaning (Table 5.36). At 0ºC, none of the black oxide scale was visible on the coupon surfaces (Figure 5.31: Row c). Conversely, at 15ºC and 25ºC, black scales with mottled red-brown portions were visible over the surfaces of all the coupons (Figures 5.29 and 5.30: Row c). Dilute nitric acid can react with iron to produce iron nitrate:

$$Fe+2HNO_3 \rightarrow Fe(NO_3)_2+H_2 \qquad \text{Equation 5.2}$$

However, iron nitrate has a violet colour (Haynes, 2016) and is readily soluble in water. Therefore, the red colour observed on the surface was more likely to be iron (III) oxides (red-

brown crystals of Fe_2O_3) in the scale which formed when the black iron (II) oxides were oxidized in the presence of HNO_3 (an oxidizing acid). The silver grey steel substrate was visible on the surface of the coupons, even before cleaning and consequentially after cleaned, virtually scale free surfaces were revealed. Unlike with the corrosion test conducted at 15ºC, at 0ºC the light brown fluoride scale was still visible after cleaning, thus indicating the HNO_3 did not dissolve the scale as effectively at lower temperatures. Iron concentration in the product solutions from corrosion more than tripled compared to solutions analysed for the same temperatures at 0.1% HNO_3 (>5000 ppm in final corrosion solution). In contradiction with corrosion tests with lower HNO_3 concentrations ($\leq$ 0.1%), the iron concentration did not show an increasing trend with increase in temperature when 0.5% HNO_3 was used (Table 5.36). Therefore, at higher HNO_3 concentrations ($\geq$0.5%), corrosion is more dependent on oxidizing acid concentration than temperature change.

Table 5.36: Observations of corrosion products from mild steel in HF spiked with 0.5% HNO_3 to see the effect of change in temperature on scale. (Figures 5.29, 5.30 and 5.31: Row c and d).

	0ºC	**15ºC**	**25ºC**
Appearance of coupons before cleaning	Light brown and red scale over the surface of all coupons (11 days) with the silver grey metal exposed at the edges.	Predominantly black and red scale over the surface of all coupons (11 days) with mottled light brown scale exposed where the scale was weakest.	Black and red scale maintained for the first 4 days. Exposed silver grey portions after 7 days where the scale was weakest.
Appearance of coupons after cleaning	Cleaning readily exposed the light brown scale on coupon surfaces with the silver grey metal substrate also visible on the edges.	Cleaning readily exposed the metal substrate, with light brown scale also visible in some parts. Metallic lustre of the corroded metal was not comparable to the grey matt colour of original sand-blasted coupons.	Black and red scale was easily removed from coupons removed after 2 days, leaving behind some light brown scale on all coupons. Coupons removed after 7 days had visible corrosion with pitting and a clean metallic lustre.
Composition of final corrosion solution	68.3% HF 35.4 mg/kg HNO_3 6171 ppm Fe 12 ppm Cr 38 ppm Mn 742 ppm Si	68.1% HF 31 mg/kg HNO_3 5085 ppm Fe 11 ppm Cr 25 ppm Mn 128 ppm Si	67.55% HF 10 mg/kg HNO_3 6791 ppm Fe 17 ppm Cr 15 ppm Mn 148 ppm Si

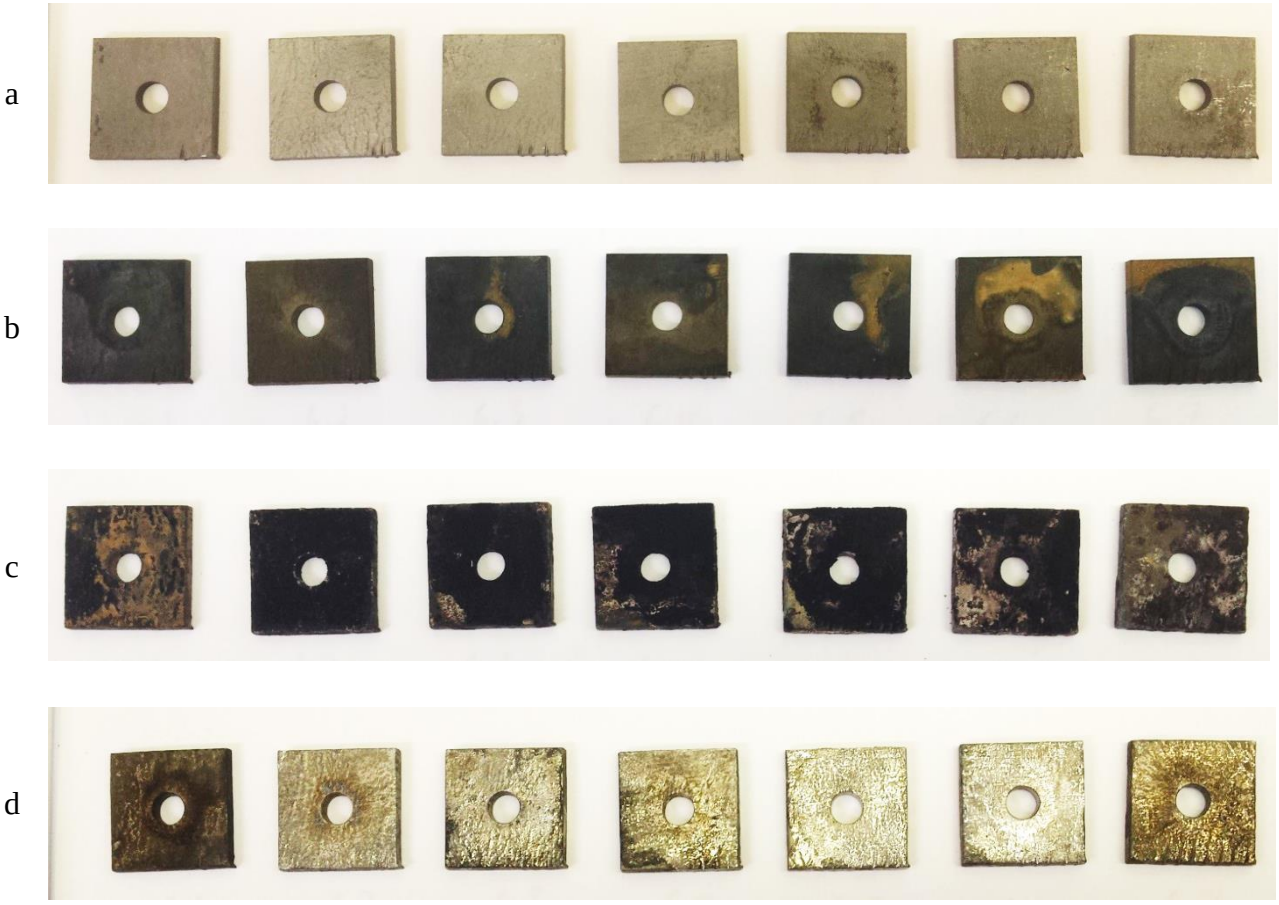

Figure 5.29: CT 5: Mild steel coupons (1-7): Row a; before exposure, Row b; after pre-passivation step, Row c; after exposure to 70% HF spiked with 0.5% HNO_3, and Row d; after removal of the scale layer, at 25ºC.

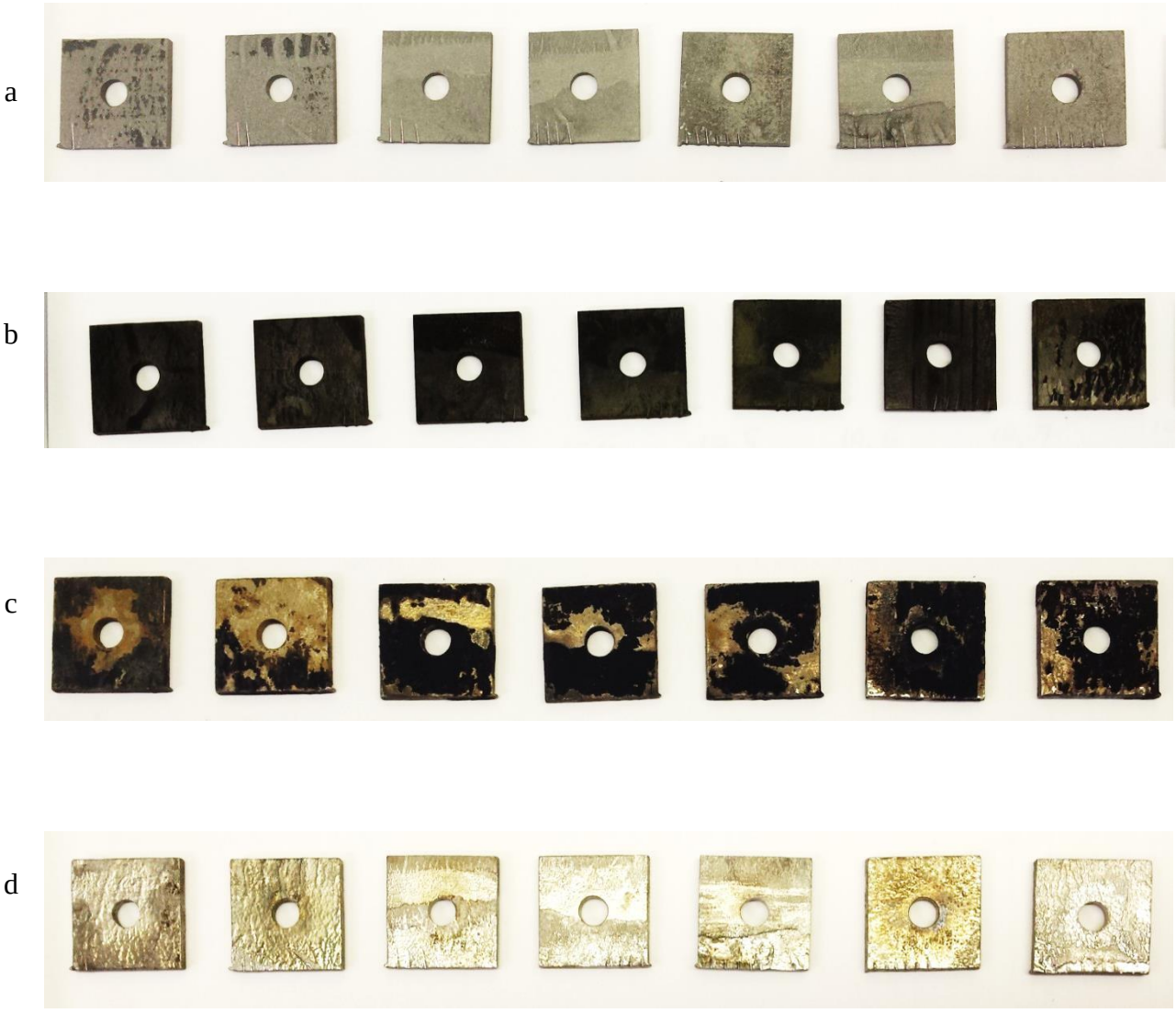

Figure 5.30: CT 9: Mild steel coupons (1-7): Row a; before exposure, Row b; after pre-passivation step, Row c; after exposure to 70% HF spiked with 0.5% HNO_3, and Row d; after removal of the scale layer at 15ºC.

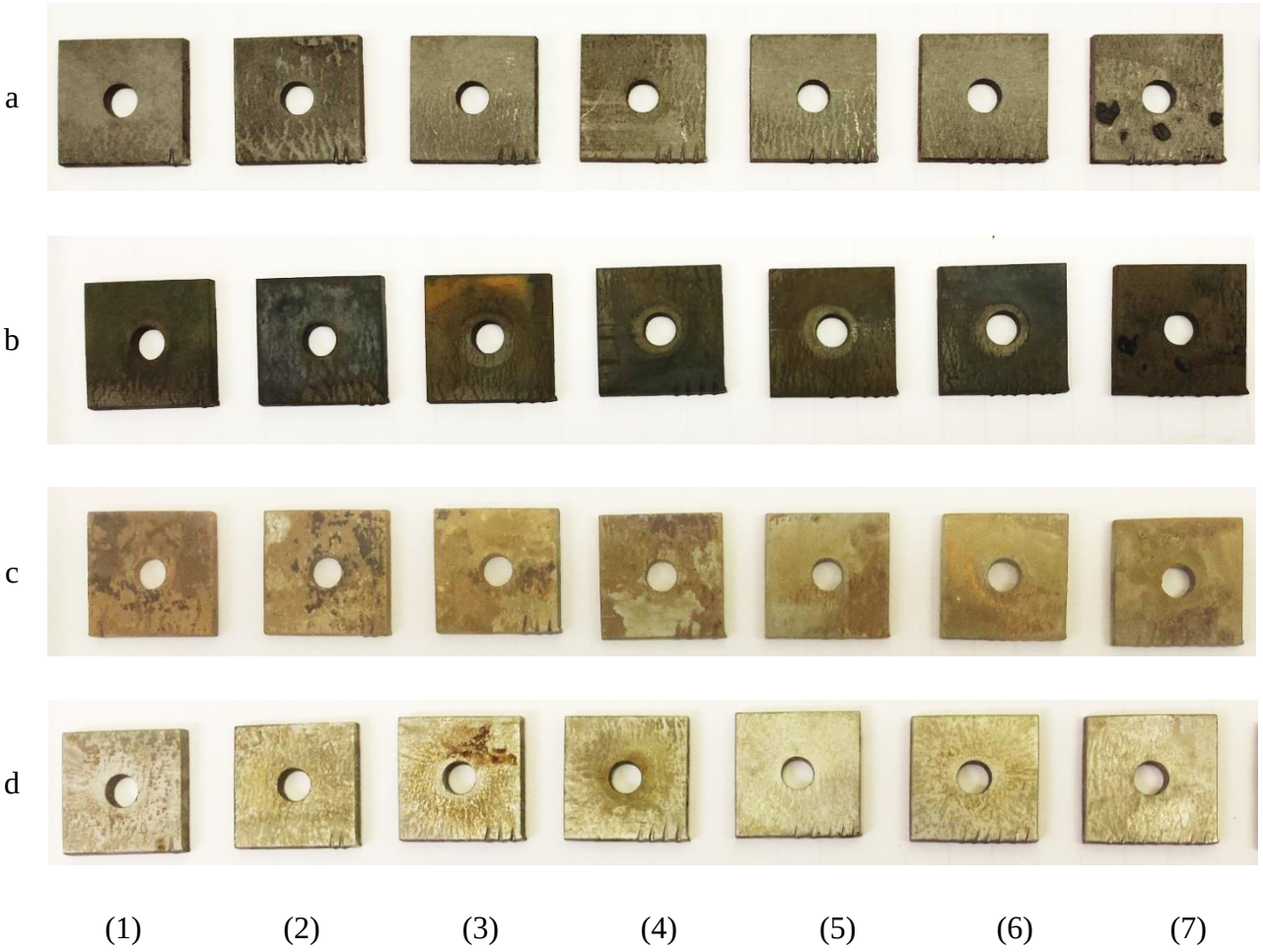

Figure 5.31: CT 14: Mild steel coupons (1-7): Row a; before exposure, Row b; after pre-passivation step, Row c; after exposure to 70% HF spiked with 0.5% HNO_3, and Row d; after removal of the scale layer, at 0ºC.

The highest concentration of HNO_3 spiked into the HF corrosion solution was 1% and had a similar effect on the scale and mild steel substrate as half the HNO_3 concentration (0.5%) (Table 5.37). However, red in the scale was more noticeable at 0ºC and 25ºC (Figures 5.32 and 5.33: Row c). Nearly all visible scale washed off the coupons tested at 15ºC, with visible corrosion of the mild steel surfaces (Figure 5.34: Row c). The coupons tested at 0ºC and 25ºC (Figures 5.35 and 5.36: Row d) showed remnants of the light brown fluoride scale with mottled red scale which could not be completely washed off. The effect of temperature on the corrosion of the coupons at these high HNO_3 concentrations was not as distinct as for the 0.5% HNO_3 tests, and the corrosive attack did not appear to be regulated by the change in temperature. After cleaning, pitting corrosion was visible around the drill holes and isolated areas on the coupon surfaces.

In contradiction to the clear effect of an increase in temperature with HNO_3 (up to 0.1%), the concentration of iron in the final corrosion solution analysed at 25ºC was nearly 1.5 times less than measured for 15ºC and 1.6 times less for 0ºC. The amount of iron extracted from the steel coupons and scale by the corrosion solution decreased with increased temperature. Thus, when the corrosion solution was tested at lower temperature, the effect of temperature was insignificant when compared to the corrosive attack by increased HNO_3 in the solution (Table 5.37).

Table 5.37: Observations of corrosion products from mild steel in HF spiked with 1% HNO_3 to see the effect of change in temperature on scale. (Figures 5.32, 5.33, 5.34, 5.35, 5.36 and 5.37: Row c and d).

	0ºC	**15ºC**	**25ºC**
Appearance of coupons before cleaning	Light brown and red scale over the surface of all coupons (11 days) with the silver grey metal exposed at the edges.	Predominantly black and red scale over the surface of all coupons (11 days) with silver grey portions exposed at the edges. More silver grey portions were exposed over the entire surface of the last coupon removed.	Black, mottled with dark red and brown scale. Exposed silver grey portions also visible on coupons removed after 7 days.
Appearance of coupons after cleaning	Cleaning readily exposed the light brown scale on coupon surfaces with the silver grey metal substrate also visible on the edges. Pitting corrosion visible over the areas where the metal substrate was exposed.	After cleaning, the light brown scale on the coupon was hardly visible. All coupons had clean metallic lustre with pitting type corrosion on all coupon surfaces.	The black and red scale was easily removed from all coupons, leaving behind a light brown scale. Severe attack of entire coupon surface over entire period of test. Pitting corrosion around drill holes and edges of coupons.
Composition of final corrosion solution	* 67.4% HF * 64.1 mg/kg HNO_3 * 8261 ppm Fe * 20 ppm Cr * 7 ppm Mn * 369 ppm Si	* 66.7% HF * 23 mg/kg HNO_3 * 7728 ppm Fe * 22 ppm Cr * 11 ppm Mn * 144 ppm Si	* 66.9% HF * 6 mg/kg HNO_3 * 5069 ppm Fe * 18 ppm Cr * 9 ppm Mn * 152 ppm Si

* Average value determined from duplicate tests and analyses

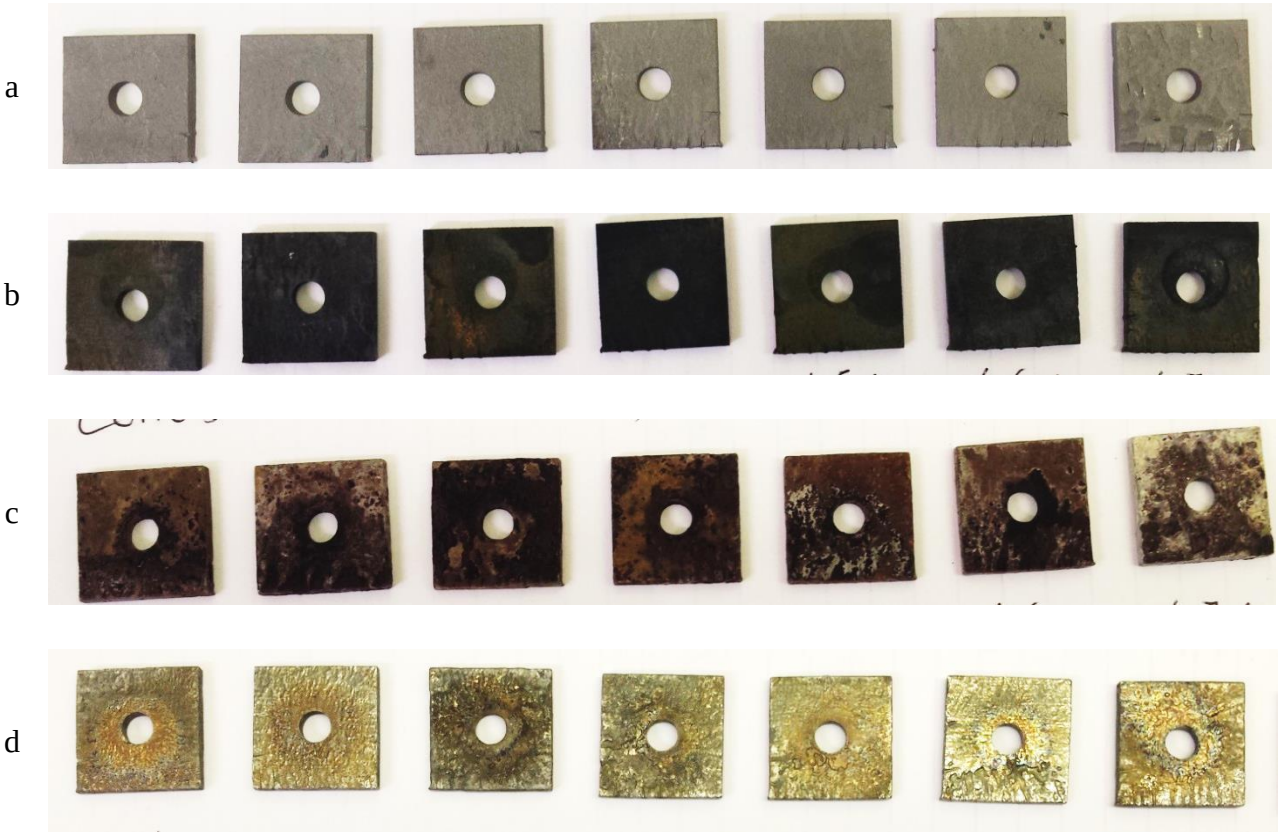

Figure 5.32: CT4 Mild steel coupons (1-7): Row a; before exposure, Row b; after pre-passivation step, Row c; after exposure to 70% HF spiked with 1% HNO_3, and Row d; after removal of the scale layer, at 25ºC.

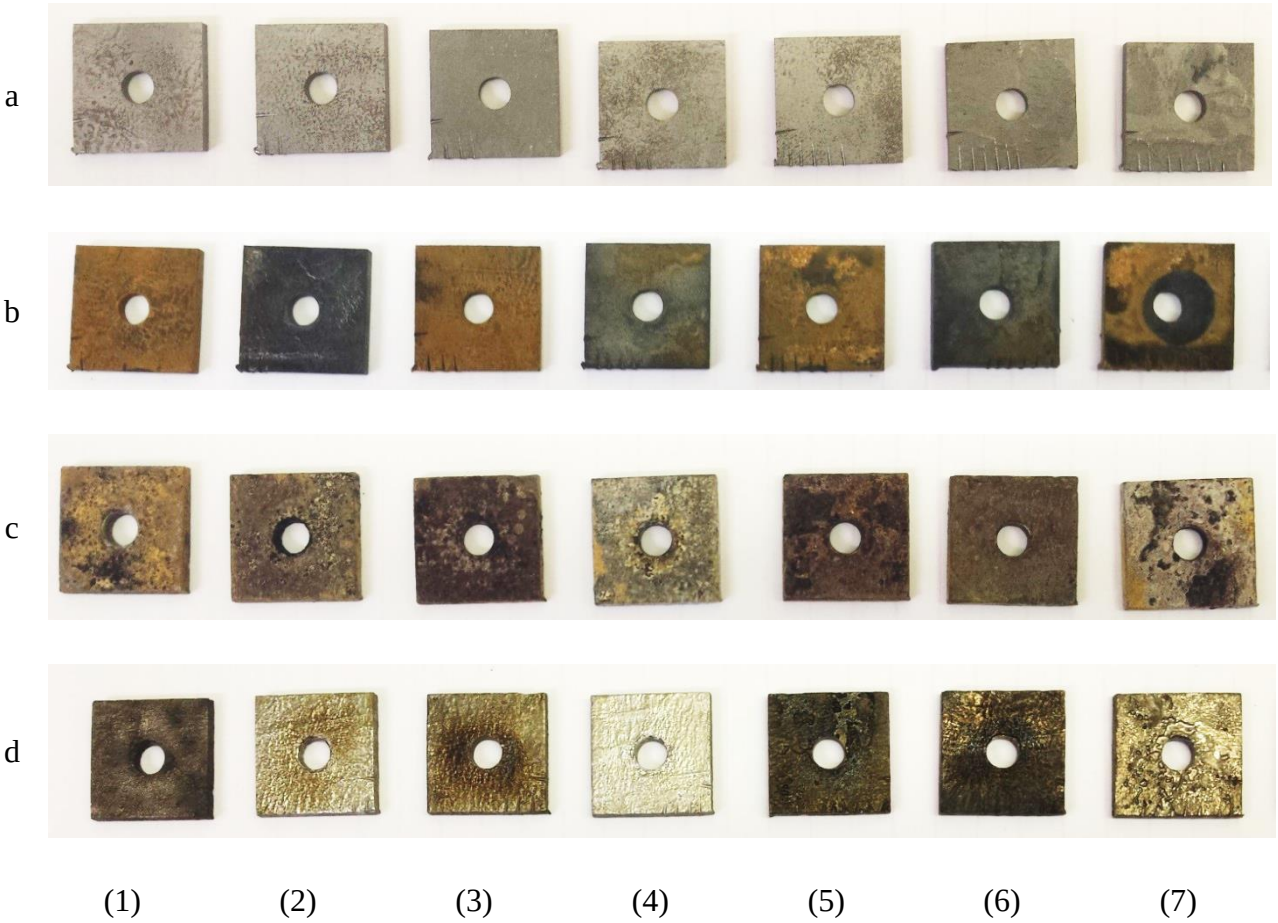

Figure 5.33: CT 6 (Duplicate corrosion test): Mild steel coupons (1-7): Row a; before exposure, Row b; after pre-passivation step, Row c; after exposure to 70% HF spiked with 1% HNO_3, and Row d; after removal of the scale layer, at 25ºC.

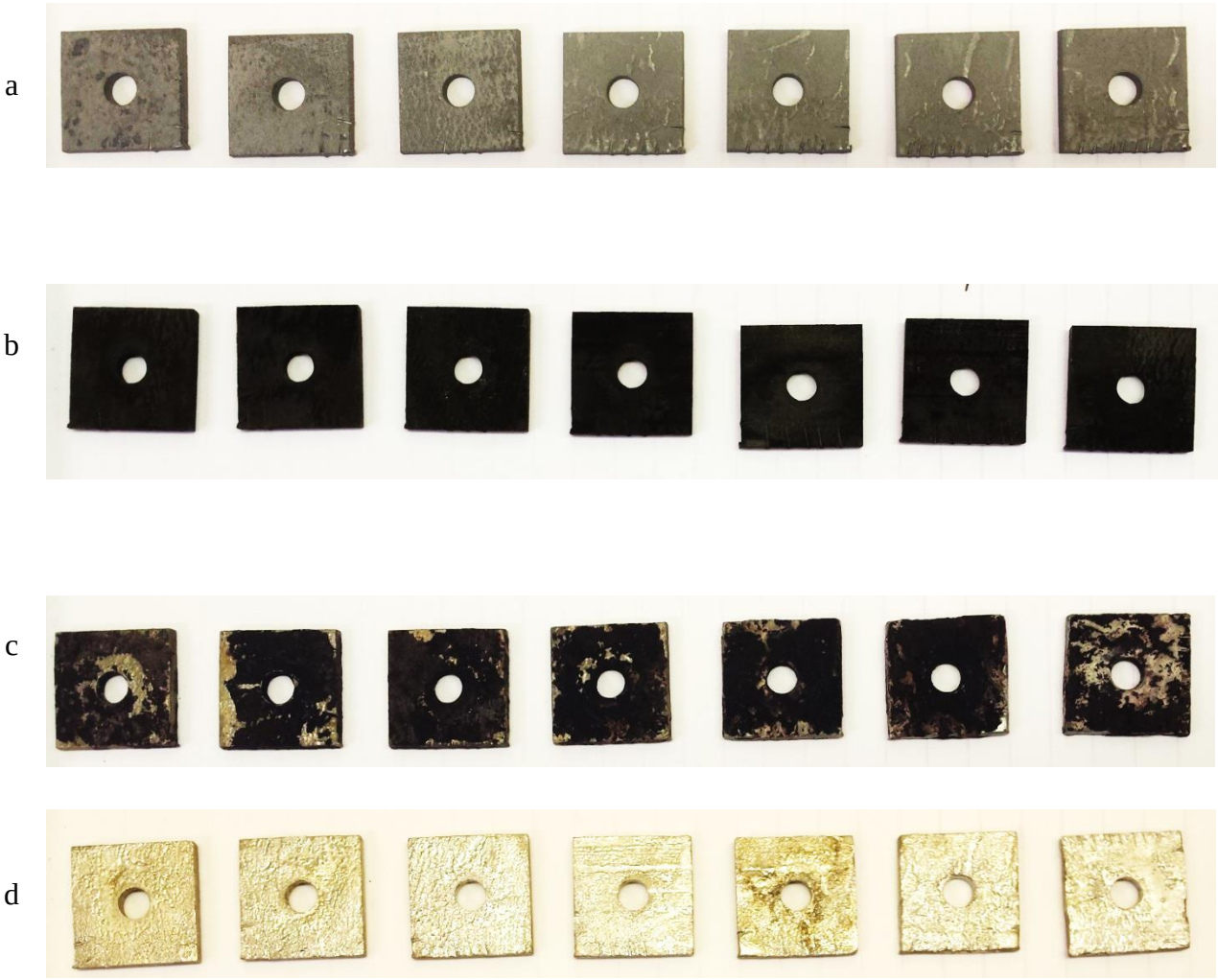

Figure 5.34: CT 10: Mild steel coupons (1-7): (row a) before exposure, Row b; after pre-passivation step, Row c; after exposure to 70% HF spiked with 1% HNO_3, and Row d; after removal of the scale layer, at 15ºC.

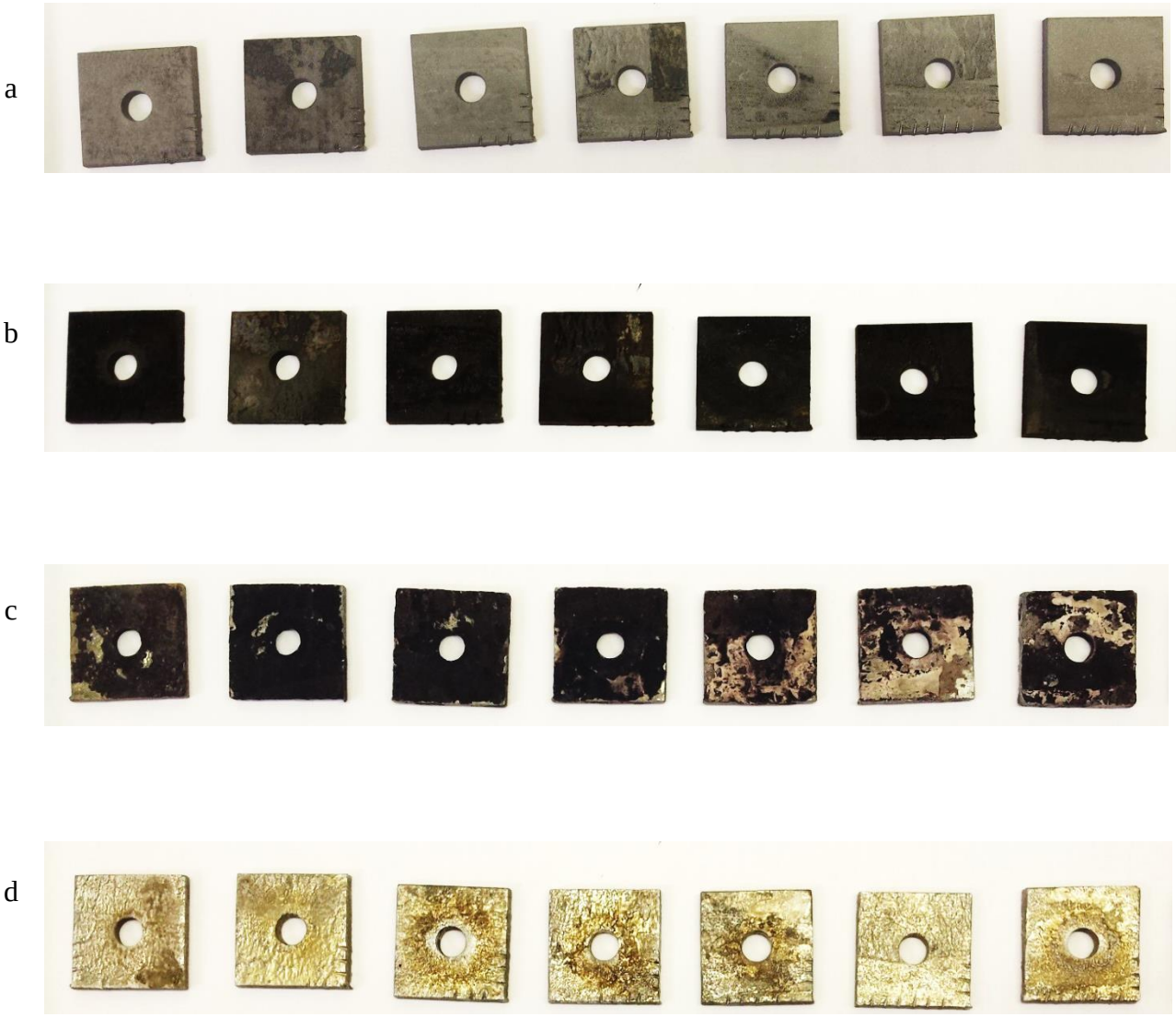

Figure 5.35: CT 11 (Duplicate corrosion test): Mild steel coupons (1-7): Row a; before exposure, Row b; after pre-passivation step, Row c; after exposure to 70% HF spiked with 1% HNO_3, and Row d; after removal of the scale layer at 15ºC.

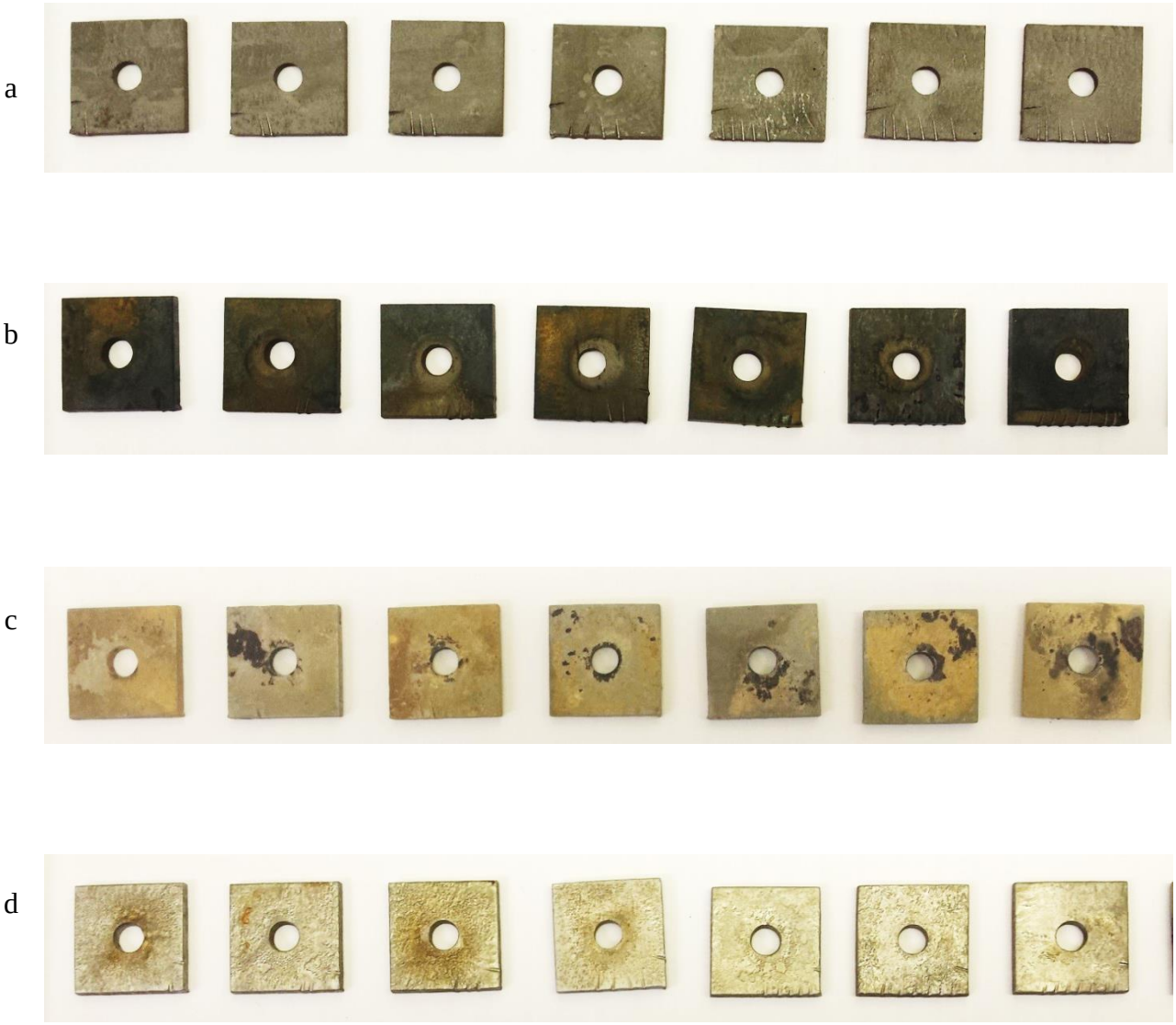

Figure 5.36: CT 15: Mild steel coupons (1-7): Row a; before exposure, Row b; after pre-passivation step, Row c; after exposure to 70% HF spiked with 1% HNO_3, and Row d; after removal of the scale layer, at 0ºC.

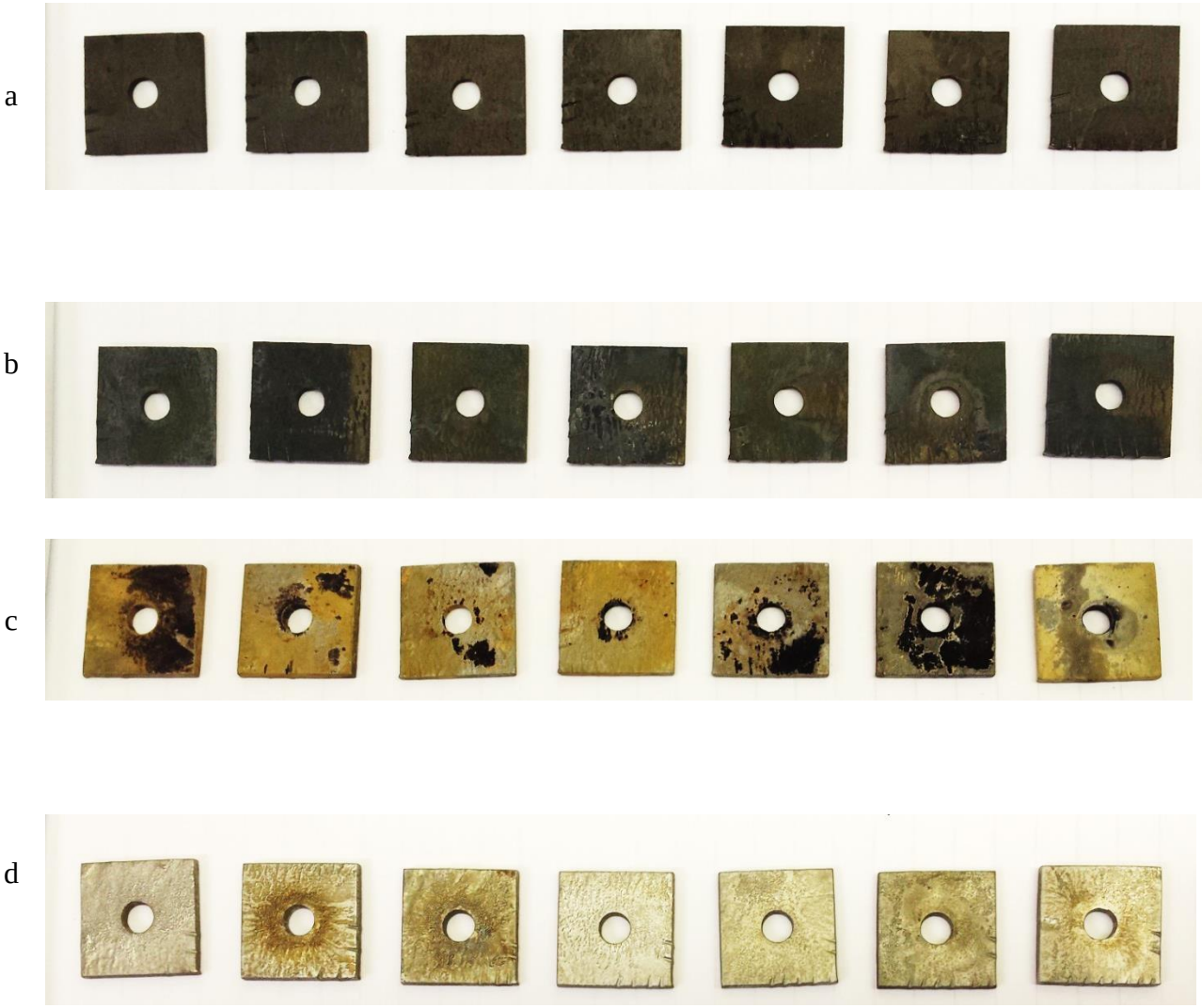

Figure 5.37: CT 16 (Duplicate corrosion test): Mild steel coupons (1-7): (row a) before exposure, Row b; after pre-passivation step, Row c; after exposure to 70% HF spiked with 1% HNO_3, and Row d; after removal of the scale layer, at 0ºC.

Depth profiles of scale cross-sections

The limitations associated with measuring scale thicknesses on the corroded coupons while tracking the change in composition with scale depth were described in Section 4.5.2.3. Sufficient data were collected to draw depth profiles from EDS analyses and related well to similar analyses done on the cross-sections of the samples taken from the HF storage tanks (described in Section 3.5). Figures 5.38 to 5.42 contains the source data from SEM and EDS analyses done on the scale which formed over mild steel coupons during each of the corrosion tests conducted at 25ºC.

During the 24 h pre-passivation step, scale with an average thickness of 9.2 ±2 µm formed on the surface of the coupons when the corrosion solution was kept at 25ºC (Figure 5.38). The scale was considered porous since carbon from the mounting resin penetrated up to 10 µm into the scale, and also because carbon reduced from ~22 wt% at the scale surface to ~1 wt% at the steel substrate. Iron content was at ~60 wt% at the scale surface and dropped to nearly 40 wt% when measured 2 µm deeper. Fluorine showed the opposite trend, increasing from 6 wt% to 38 wt% over the same 2 µm depth, which indicated that corrosion took place beneath the surface of the mild steel to form the fluoride scale there. The oxygen, ~13 wt% at surface decreasing to 2 wt% at the steel surface, was either from the cold resin used or from oxide scale forming together with the fluoride, during the pre-passivation.

The introduction of the pre-passivated coupons to a fresh 70% HF (<50 ppm HNO_3) solution for a further 11 days allowed the scale to grow nearly six times larger (an average thickness of 61.7 ± 12 µm). A visible change in the microstructure of the scale indicated the location between the scale which formed during the pre-passivated step and the scale which formed during the corrosion test (Figure 5.39). Compared to the scale formed during the pre-passivation (Figure 5.38), the scale formed during the corrosion tests was not only thicker, but more impermeable to cold resin. This finding was based on depth profiles correlated at 10µm into the scale, which indicated the scale on the pre-passivated coupon had nearly double the carbon content and half the fluorine content (~20 wt%, Spot 2 in Figure 5.38) compared to the coupon that was pre-passivated and then left for the duration of the corrosion test (carbon <10 wt% and fluorine ~40 wt%, Spot 2 in Figure 5.39). The scale formed on the mild steel coupons (Figures 5.38 and 5.39) was similar to the scale formed inside the HF storage tanks, which were not exposed to HNO_3 contamination (Figure 3.7), when examined using the same analytical techniques as used for the corrosion failure analysis (depth profile in Figure 3.8). The concentration of HNO_3 pumped to the HF storage tanks was between 0.1 and 1% HNO_3, based on mass balances conducted at the plant the time of the failure of the first storage tanks (Valkenburgh, 2013).

Exposure of the pre-passivated coupons to 70% HF spiked with 0.1% HNO_3 drastically increased the thickness of the scale to an average of 173 ± 13 µm. This was the thickest scale measured for a coupon in the entire study (Figure 5.40) and could be correlated to the ~230 µm scale measured for the HF storage tank exposed to HF contaminated with HNO_3 (Figure 5.39). Similar to that corrosion layer (Figure 3.10), the depth profile drawn for Figure 5.40 showed the scale to be porous and inhomogeneous, since the carbon, iron, fluorine and oxygen content fluctuated considerably between the scale surface and the steel substrate. The microstructures

showed large pores (~50 µm wide) filled with resin (>40 wt% carbon) where the HNO_3 concentration was low enough to allow the HF to react and grow the scale as it corroded the steel, while still being high enough to dissolve parts of the scale as corrosion continued (Figure 5.40).

In an HF corrosion solution spiked with 0.5% HNO_3, the thickness of the scale was reduced to 135.4 ± 26 µm after 11 days (Figure 5.41) compared to corrosion tests done with 0.1% HNO_3 (Figure 5.40). Iron concentration was highest at the scale surface and substrate-scale interface (>97 wt% Fe). Therefore, corrosion took place below the mild steel surface while the higher concentration of the oxidizing acid (0.5% HNO_3) dissolved part of the scale and made it porous (25 – 26 wt% C at 60 – 80 µm into the scale). Fluorine was at its highest concentration closest to the steel substrate (56 wt% F at 100 µm into the scale) while oxygen was higher than fluorine (~9 wt% O) closest to the scale surface. This related well to observations made of the coupons (Table 5.40), where the black oxide scale was observed before washing, and the light brown fluoride scale was observed after washing of the black scale (Figure 5.29: Row c and d).

In Figure 5.42, the highest nitric acid concentration (1% HNO_3) spiked into 70% HF showed the thinnest scale formation (18.3 ± 0.2 µm). Nearly all the scale dissolved with less than 20 wt% F detected at 10 µm above the substrate. Once again, iron was highest at the scale surface (>70 wt%) indicating that corrosion took place below the mild steel surface. The carbon content was the second highest (>20 wt%), which indicated that mostly cold resin was present there and that the scale either completely dissolved during the experiment, or was so fragile that sample preparation (grinding and polishing) removed most of it. Either way, the scale was non-existent, which demonstrated the detrimental effect of HNO_3 contamination in HF (1% HNO_3 concentration in solution) to mild steel pre-passivation and corrosion.

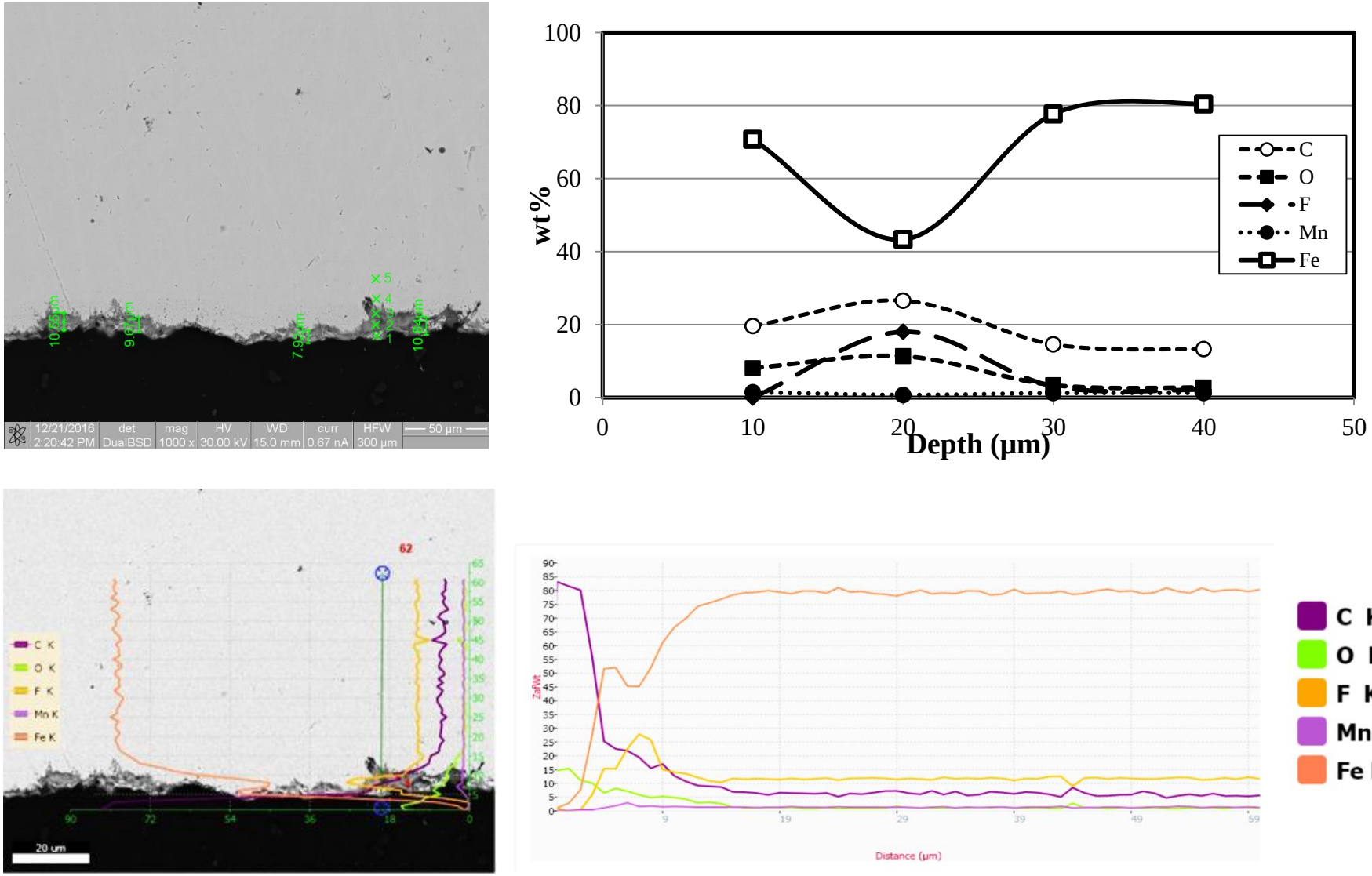

Figure 5.38: SEM backscattered electron image of a cross-section of mild steel coupon, after exposure to 70% HF for 24 h (pre-passivation step), with corresponding depth profile measurements of the scale layer made using EDS spot analyses and line scans.

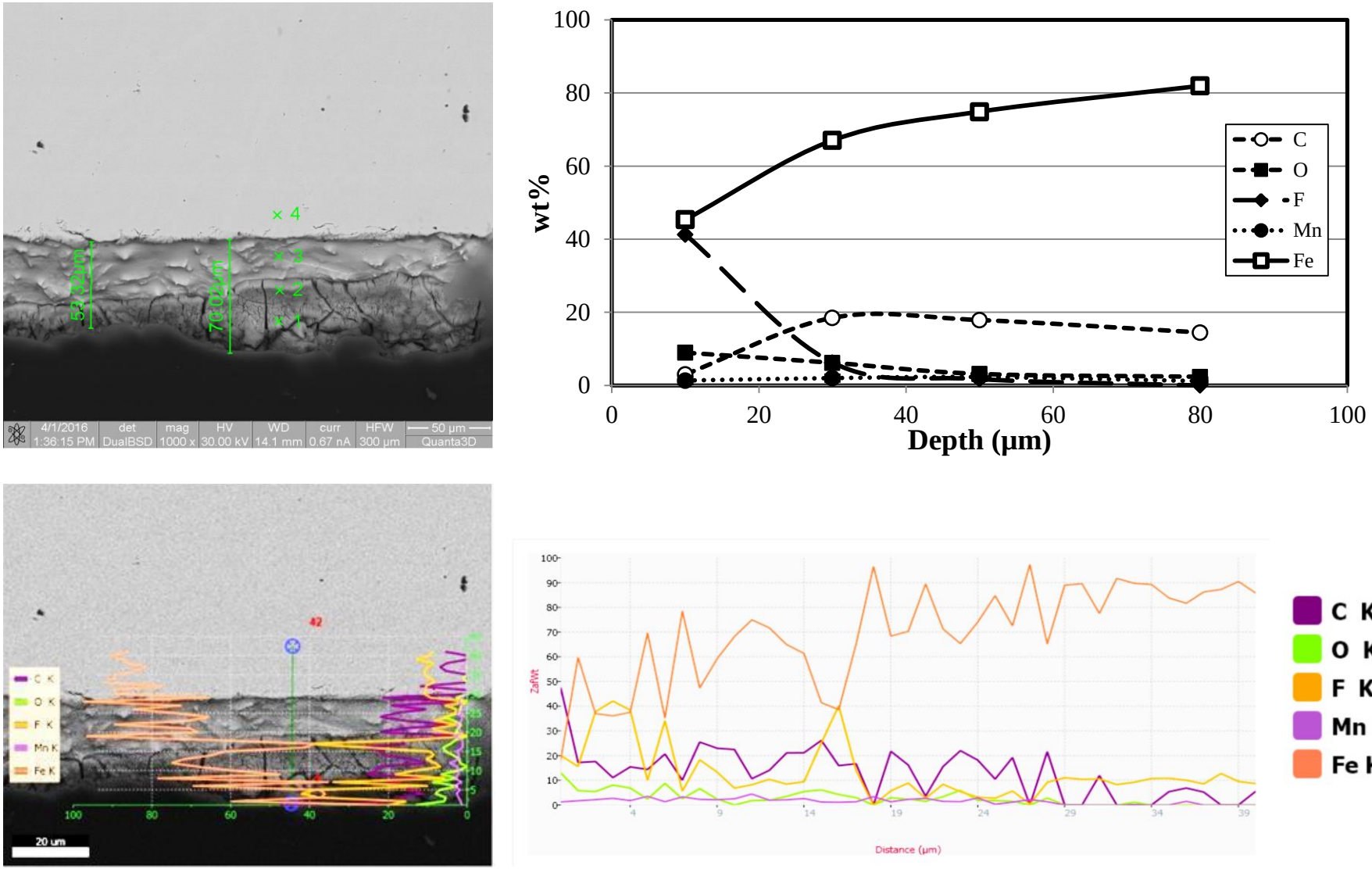

Figure 5.39: SEM backscattered electron image of a cross-section of mild steel coupon (No. 8), after exposure to 70% HF, with corresponding depth profile measurements of the scale layer made using EDS spot analyses and line scans.

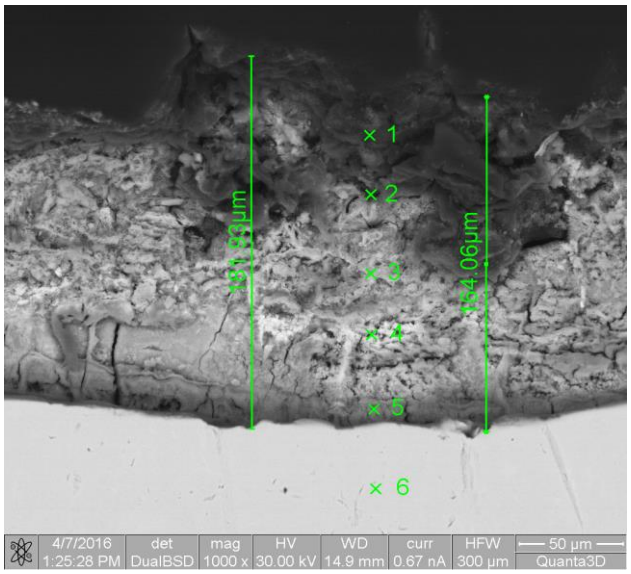

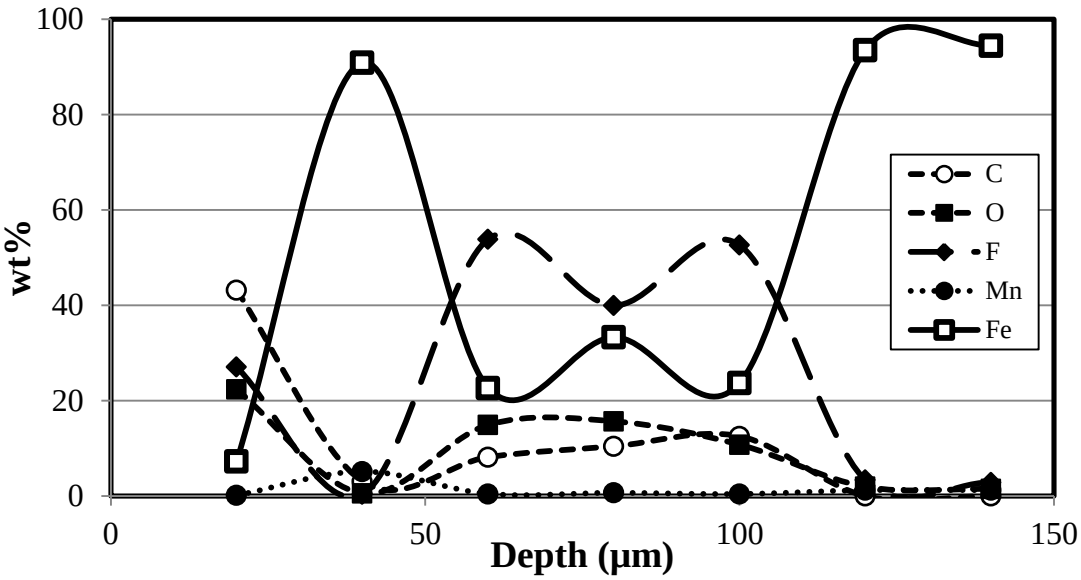

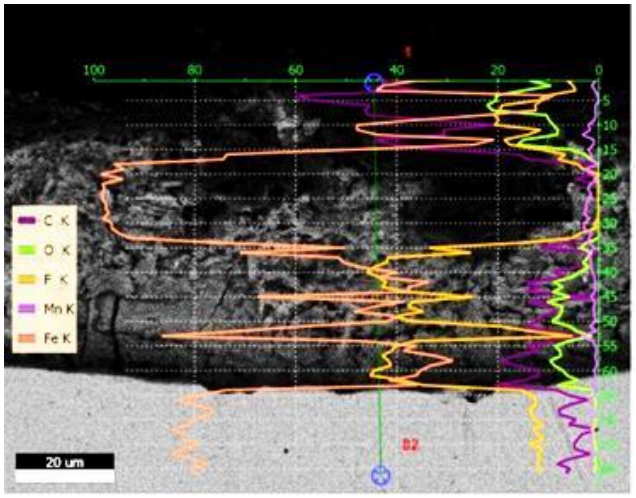

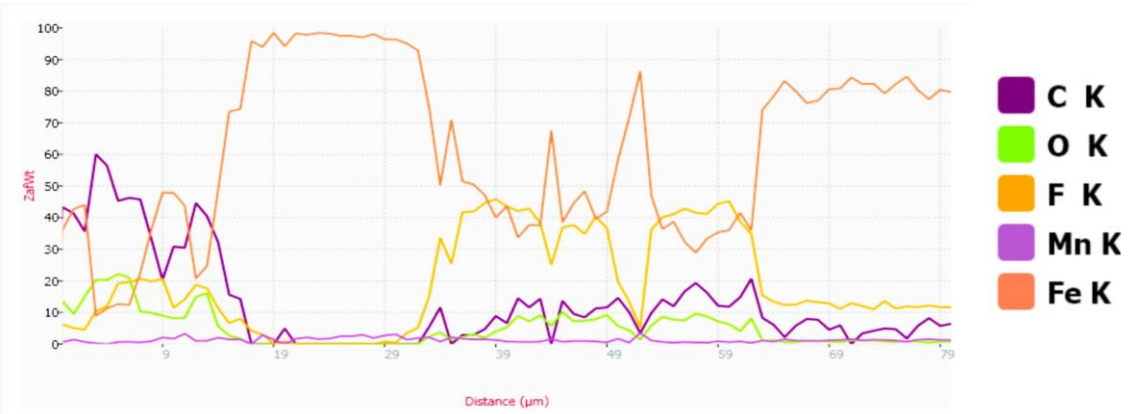

Figure 5.40: SEM backscattered electron image of a cross-section of mild steel coupon (No. 8), after exposure to 70% HF spiked with 0.1% HNO_3, with corresponding depth profile measurements made of the scale layer using EDS spot analyses and line scans.

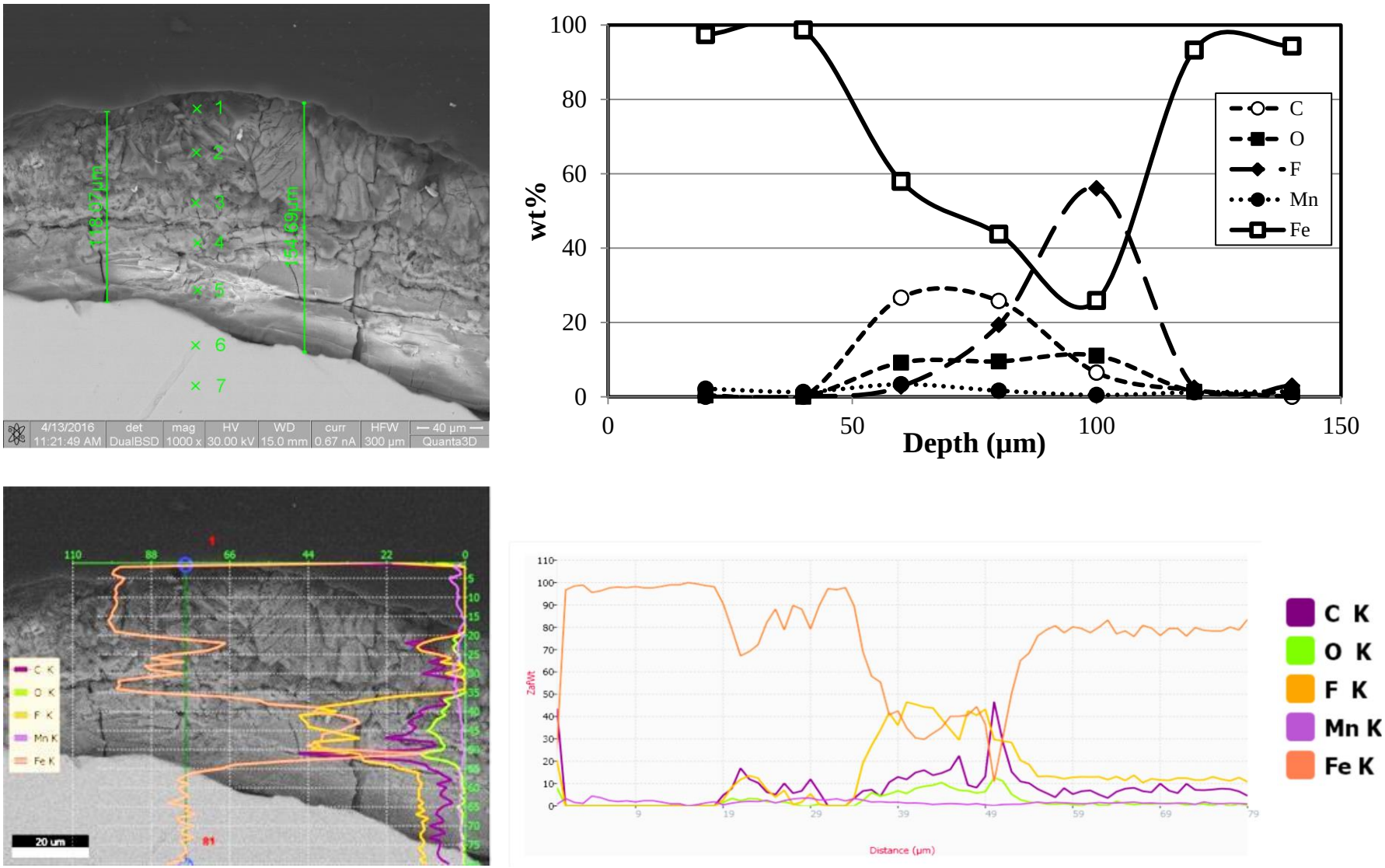

Figure 5.41: SEM backscattered electron image of a cross-section of mild steel coupon (No. 8), after exposure to 70% HF spiked with 0.5% HNO_3, with corresponding depth profile measurements made of the scale layer using EDS spot analyses and line scans.

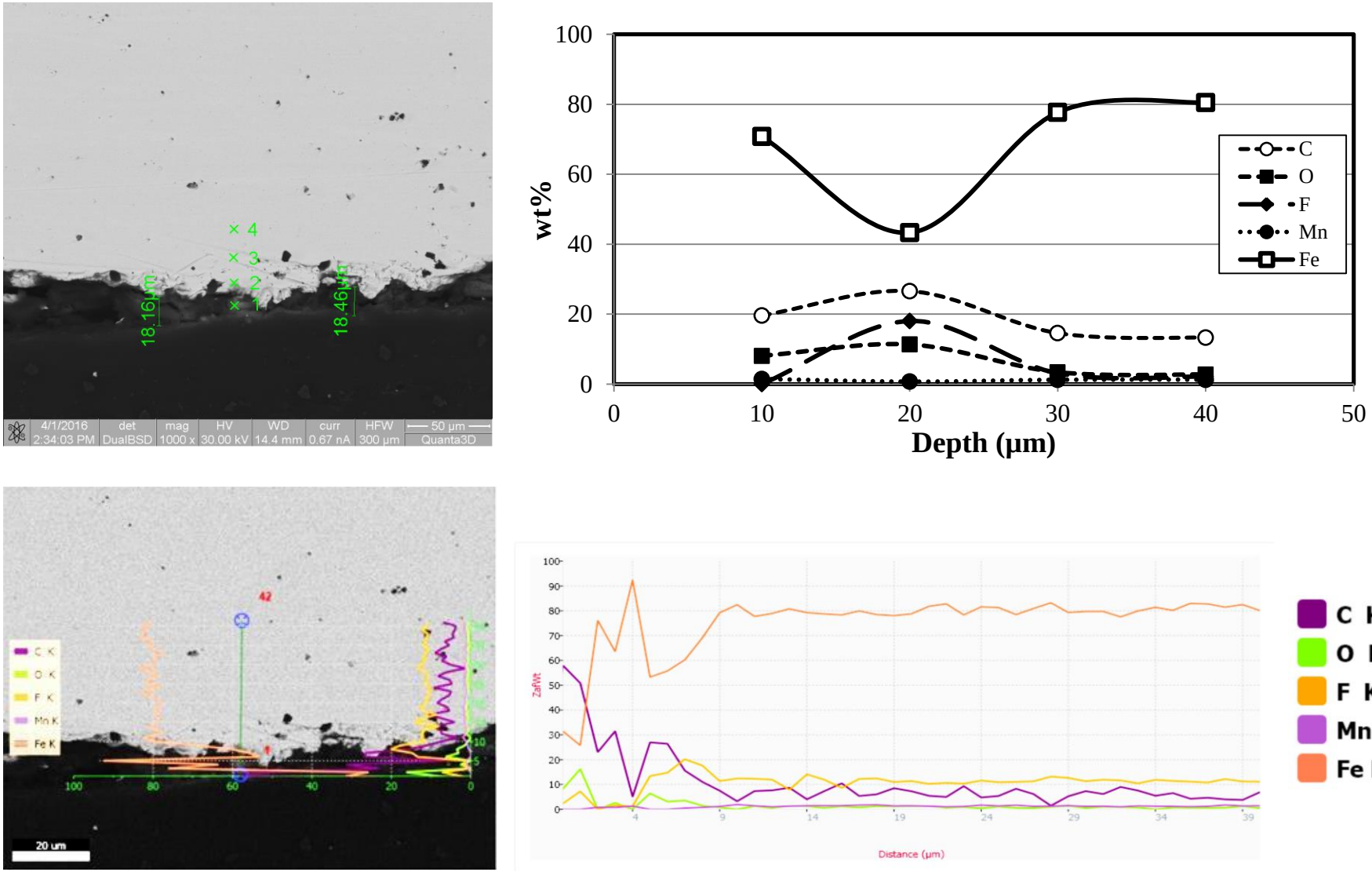

Figure 5.42: SEM backscattered electron image of a cross-section of mild steel coupon (No. 8), after exposure to 70% HF spiked with 1% HNO_3, with corresponding depth profile measurements made of the scale layer using EDS spot analyses and line scans.

A summary of change in the average scale thickness, as measured after 11 days on each SEM image (Figures 5.38 – 5.42), with increase in HNO_3 concentration in the corrosion solution, is presented in Figure 5.43. It was apparent that at low nitric acid concentrations (<50 ppm HNO_3 considered to be relatively pure HF), HF reacted with the mild steel to form a scale layer on the steel substrate that steadily grew to about 60 µm thick within 11 days. When a low concentration of nitric acid (≤0.1% HNO_3) was introduced, the scale was attacked and dissolved by the oxidizing acid which in turn exposed the steel substrate to repeated HF corrosion so that scale continually formed. This in turn led to added scale formation, to nearly 180 µm thick. The combined attack by the HNO_3 and HF eventually produced a thicker, but porous scale (Figure 5.40). Increasing the HNO_3 in solution (to ≥0.5% HNO_3) had a similar effect on thickening the scale formed on the steel, except that since HNO_3 was at a higher concentration, it dissolved the scale more readily than the products from HF corrosion (Equation 1.1) formed it on the steel. Hence, the thickness of the scale decreased by nearly 40 µm when the HNO_3 concentration increased five-fold. Subsequently, doubling the HNO_3 concentration in the HF solution (to 1% HNO_3) destroyed the scale layer completely, as the HNO_3 mostly dissolved the scale (<20 µm scale layer left).

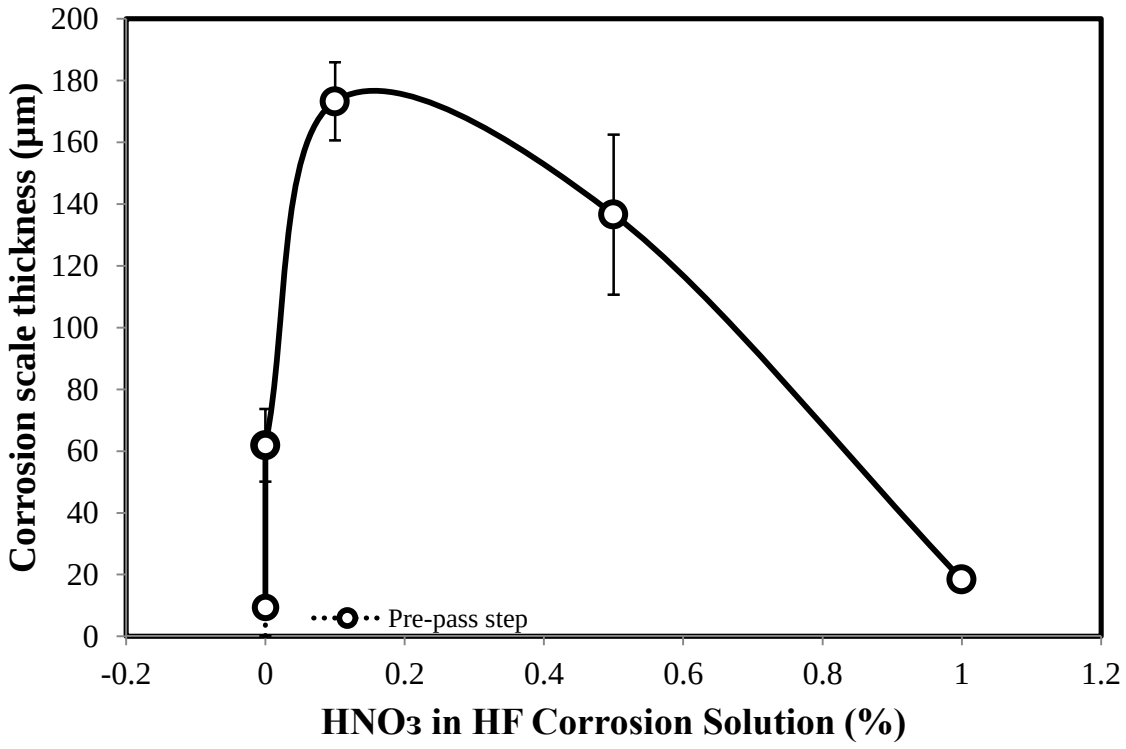

Figure 5.43: Effect of HNO_3 concentration on fluorite scale thickness of mild steel when corroded in 70% HF, at 25ºC. Error bars obscured by markers in some instances.

5.2.3. Stainless steel corrosion

5.2.3.1. Effect of nitic acid concentration

Mass loss and apparent corrosion rates

Stainless steel 904 L is significantly more costly than mild steel and was only used in areas within the plant where higher temperature HF vapour corrosion was a problem. In the HF plant, this steel was also exposed to corrosive attack by industrial grade HF products (70% AqHF), which were contaminated with HNO_3. Therefore, this steel was also tested to establish its suitability for use in the unique corrosive environment created by the high levels of HNO_3 (up to 1%) present in the HF process streams.

When exposed to a 70% HF corrosion solution, with no HNO_3 contamination at 25ºC, stainless steel coupons corroded at a constant rate of between 4.7 and 5.1 mm/y (Table 5.38). Mass loss by the steel over the 11 days was directly proportional to time spent in the pure HF solution. Unlike other metals tested (Tables 5.31 and 5.43), the corrosion rate of stainless steel slowed down significantly when exposed to HNO_3 in solution (Table 5.39). Except for the first 24 hours, corrosion rates measured for SS 904 L in 70% HF containing 1% HNO_3, did not exceed 1 mm/y.

Table 5.38: CT 19: Corrosion test for stainless steel in 70% HF, at 25ºC.

Coupon No.	Interval (days)	Mass loss (g)	Metal in solution* (g/L)	Apparent corrosion rate (mm/y)	Photograph, column
1	1	0.1628	0.35	4.89	Figure 5.44, 1
2	2	0.3116	0.67	4.68	Figure 5.44, 2
3	3	0.4699	1.01	4.70	Figure 5.44, 3
4	4	0.6406	1.38	4.81	Figure 5.44, 4
5	7	1.1097	2.39	4.76	Figure 5.44, 5
6	9	1.4731	3.18	4.91	Figure 5.44, 6
7	11	1.8644	4.02	5.09	Figure 5.44, 7
Total in reactor A only		3.6068	7.78		
Total		6.0321	13.02		

* Metal in solution is the combined mass of Cr, Cu, Fe, Mn, Mo, Mn and Ni removed from each coupon that transported to the corrosion solution over the duration of the corrosion test.

Table 5.39: CT 20: Corrosion results for stainless steel in 70% HF spiked with 1% HNO_3, at 25ºC.

Coupon No.	Interval (days)	Mass loss (g)	Metal in solution* (g/L)	Apparent corrosion rate (mm/y)	Photograph, column
1	1	0.0751	0.16	1.29	Figure 5.45, 1
2	2	0.1303	0.28	1.08	Figure 5.45, 2
3	3	0.1582	0.34	0.87	Figure 5.45, 3
4	4	0.2147	0.46	0.88	Figure 5.45, 4
5	7	0.3157	0.68	0.74	Figure 5.45, 5
6	9	0.4016	0.87	0.73	Figure 5.45, 6
7	11	0.4575	0.99	0.68	Figure 5.45, 7
Total in reactor A only		1.0065	2.17		
Total		1.7531	3.78		

* Metal in solution is the combined mass of Cr, Cu, Fe, Mn, Mo, Mn and Ni removed from each coupon that transported to the corrosion solution over the duration of the corrosion test.

Acid consumption

Hydrofluoric acid consumption by stainless steel (Table 5.32) was nearly double that of mild steel (Table 5.40) under the same conditions. However, when 1% HNO_3 was introduced to the corrosion solution, HF consumption was at the lowest levels detected for any corrosion test (<0.0.22 g_{HF}/g_{Alloy}) which agreed with the lower corrosion rates observed for the steel in the presence of HNO_3 (Table 5.39). Similarly, nitric acid consumption was lowest (<64%), indicating minimal reaction of HNO_3 in the corrosion solution with the stainless steel. Therefore, HNO_3 in the corrosion solution initially reacted with the stainless steel surface to passivate it, which in turn prevented further corrosive attack by HF.

Table 5.40: HF acid consumption by stainless steel after 11 days when varying the HNO_3 concentration in 70% HF, at 25ºC.

Feed HNO_3 concn. (%)	Feed HF concn. (%)	Product HF concn. (%)	Mass of HF in feed (g)	Mass of HF in product (g)	Mass of Coupons* (g)	Acid consumption $\left(\frac{g\ HF}{g\ Alloy}\right)$	Acid consumption (%)
0.0	70.00	68.62	324.40	318.00	55.82	0.115	2.0
1.0	69.21	68.94	320.74	319.48	57.27	0.022	0.4

*Average value from duplicate corrosion tests or solution analyses conducted with errors captured in the graphs discussed.

Table 5.41: HNO_3 acid consumption by stainless steel after 11 days when varying the HNO_3 concentration in 70% HF, at 25ºC.

Feed HNO_3 concn. (%)	**Product HNO_3 concn. (mg/kg)**	**Mass of HNO_3 in feed (mg)**	**Mass of HNO_3 in product (mg)**	**Mass of Coupons** * **(g)**	**Acid consumption**	
					$\left(\frac{\text{g HNO3}}{\text{g Alloy}}\right)$	**(%)**
0.0	0	463.42	0.00	55.83	0.000	0.00
1.0	4634	463.42	1681	57.27	0.052	63.70

*Average value from duplicate corrosion tests or solution analyses conducted with errors captured in the graphs discussed.

Observations of photographs of corroded coupons

Similar to mild steel (Table 5.34), stainless steel also produced a black oxide scale when in exposed to 70% HF during the pre-passivation step. Conversely for mild steel, the scale had an ash-like texture and was easily broken free from the coupons during handling (Figure 5.44: Row c). This type scale did not protect the stainless steel during the corrosion tests, since it did not adhere well to the coupon surfaces and readily allowed HF to access the steel substrate. Washing the coupons produced a lustrous surface finish, which signified all surface modifications (matt finish) from sandblasting were corroded away in the 70% HF test (Table 5.42).

In the corrosion test where 70% HF was spiked with 1% HNO_3, the scale formed during the pre-passivation step completely dissolved and left behind a sheen surface finish, even before washing the coupons (Figure 5.45: Row c). Relating the clean condition of the coupons observed at the end of the test (Table 5.42) to corrosion data collected during the corrosion tests (Tables 5.40 and 5.41) indicated that the HNO_3 consumed during the test dissolved all the oxide scale present on the surface. Subsequently, the HNO_3 passivated the clean stainless steel surface, as it typically does (Dillon, 1995; Crookes, 2007; Jones & Pujadó, 2008), and mitigated further corrosion by the HF still present in solution.

In pure HF (70% HF), chromium and nickel were significantly removed (>5%) from the stainless steel coupons. Copper in the coupons were not attacked by HF, with less than 0.5 ppm being found in the corrosion product solution (Table 5.42). Iron in the steel represented nearly half of the coupon weight, but was significantly more resistant to attack, as less than 2.4% of iron was removed from the coupons and ended up the final solution.

In 70% HF spiked with 1% HNO_3, the stainless steel showed superior resistance, because no more than 2% of each metal analysed (Fe, Cu, Cr and Ni) was removed from the coupons over the 11 day test (Table 5.42). Therefore, the HNO_3 in the HF reacted with the steel surface and passivated it on contact (supplied oxygen to the surface). This prevented any further corrosive attack by HF on the coupons that lead to the low metal concentrations recorded in the final corrosion solution analysed.

Table 5.42: Observations of corrosion products from a stainless steel (SS 904 L) in HF with lowest to highest HNO_3 contamination, over an 11 day corrosion test (Figures 5.44 and 5.45: Row c and d).

	0% HNO_3	**1% HNO_3**
Appearance of coupons before cleaning	Thin black, loose scale remnant on the edges with light brown (FeF_2) scale and a metallic lustre in regions expose beneath where scale flaked off.	No visible corrosion. Clean surface except for black tarnish (scale smearing) on the area where the coupons were marked.
Appearance of coupons after cleaning	No visible corrosion. Clean surface. The metallic lustre of the corroded metal was not comparable to grey matt surface of original sand-blasted coupons.	No visible corrosion. Ultrasonic cleaning did not improve the cleanliness the coupons after removal from the HF corrosion solution.
Composition of final corrosion solution	68.62% HF >50 mg/kg HNO_3 1336 ppm Fe 1300.5 ppm Cr 18.9 ppm Mn 0.5 ppm Cu 1566 ppm Ni 19.2 ppm Si	68.94% HF 2973 mg/kg HNO_3 1035 ppm Fe 444.8 ppm Cr 31.1 ppm Mn 48.8 ppm Cu 564 ppm Ni 4.4 ppm Si

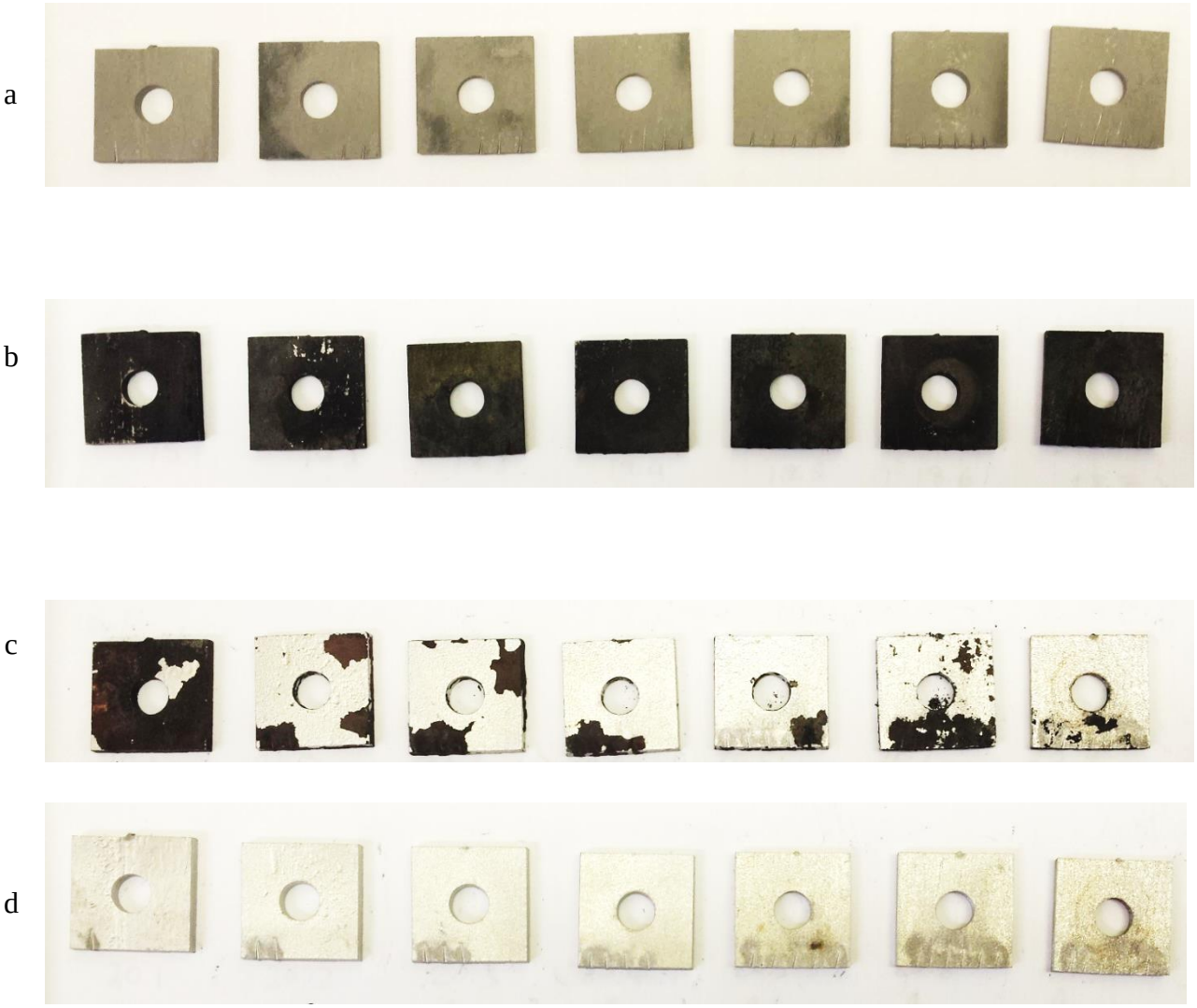

Figure 5.44: CT 19: Stainless steel (SS 904 L) coupons (1-7): Row a; before exposure, Row b; after pre-passivation step, Row c; after exposure to 70% HF, and Row d; after removal of the scale layer, at 25ºC.

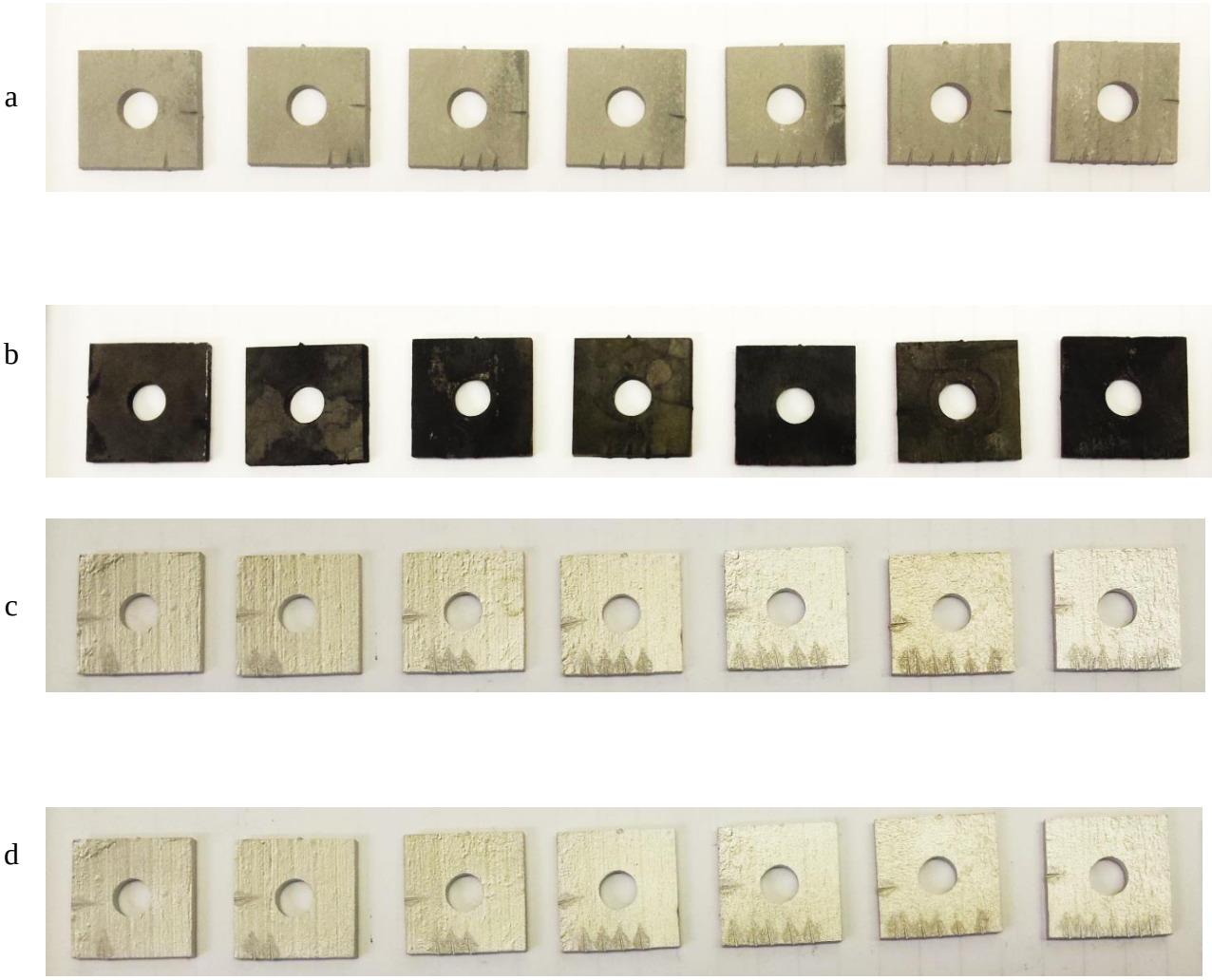

Figure 5.45: CT 20: Stainless steel (SS 904 L) coupons (1-7): Row a; before exposure, Row b; after pre-passivation step, Row c; after exposure to 70% HF spiked with 1% HNO_3, and Row d; after removal of the scale layer, at 25ºC.

5.2.4. Nickel alloy corrosion

5.2.4.1. Effect of nitic acid concentration

Mass loss and apparent corrosion rates

Apparent corrosion rates for the Monel 400 nickel alloy in 70% HF were found to be the slowest measured of any of the three metals used by the HF plant (<0.33 mm/y), and thus its selection for used for dip tubes in the HF storage tanks well warranted (Table 5.43). However, the failure of these dip tubes, as seen in Figure 2.1, in the presence of higher levels (1% HNO_3) in the tanks, also occurred in the laboratory corrosion tests by the excessively high corrosion rates reported in Table 5.44.

Table 5.43: CT 17: Corrosion test for nickel alloy (Monel 400) in 70% HF, at 25ºC.

Coupon No.	Interval (days)	Mass loss (g)	Metal in solution* (g/L)	Apparent corrosion rate (mm/y)	Photograph, column
1	1	0.0124	0.03	0.33	Figure 5.48, 1
2	2	0.0150	0.03	0.20	Figure 5.48, 2
3	3	0.0243	0.05	0.22	Figure 5.48, 3
4	4	0.0320	0.07	0.22	Figure 5.48, 4
5	7	0.0628	0.14	0.24	Figure 5.48, 5
6	9	0.0917	0.20	0.27	Figure 5.48, 6
7	11	0.1270	0.27	0.31	Figure 5.48, 7
Total in reactor A only		0.2265	0.49		
Total		0.3652	0.79		

* Metal in solution is the combined mass of Cu, Fe, Mn and Ni removed from each coupon that transported to the corrosion solution over the duration of the corrosion test.

Table 5.44: CT 18: Corrosion test for nickel alloy (Monel 400) in 70% HF spiked with 1% HNO_3, at 25ºC.

Coupon No.	Interval (days)	Mass loss (g)	Metal in solution* (g/L)	Apparent corrosion rate (mm/y)	Photograph, column
1	1	1.5054	3.25	40.57	Figure 5.49, 1
2	2	2.0921	4.51	28.19	Figure 5.49, 2
3	3	2.4108	5.20	21.66	Figure 5.49, 3
4	4	2.8327	6.11	19.09	Figure 5.49, 4
5	7	3.3079	7.14	12.74	Figure 5.49, 5
6	9	3.2437	7.00	9.71	Figure 5.49, 6
7	11	3.3129	7.15	8.12	Figure 5.49, 7
Total in reactor A only		10.5370	22.73		
Total		18.7055	40.36		

* Metal in solution is the combined mass of Cu, Fe, Mn and Ni removed from each coupon that transported to the corrosion solution over the duration of the corrosion test.

Acid consumption

Hydrofluoric acid consumption by Monel 400 (Table 5.45) coupons were between that of mild steel (Table 5.32) and stainless steel (Table 5.40), and at approximately 1.5% of total HF introduced to the corrosion reactor. However, when the corrosion of the nickel alloy was tested in an HF corrosion solution containing 1% HNO_3, the acid consumption effectively doubled. This was 2% less acid consumed compared to mild steel under the same conditions. Similar to mild steel, ultimately all the HNO_3 was consumed (>99.9%). Compared to stainless steel, the Monel 400 coupons consumed approximately 1.4 times more g_{HNO_3}/g_{Alloy} than the SS 904 L (Table 5.46).

Table 5.45: HF acid consumption by nickel alloy (Monel 400) after 11 days when varying the HNO_3 concentration in 70% HF, at 25ºC.

Feed HNO_3 concn. (%)	**Feed HF concn. (%)**	**Product HF concn. (%)**	**Mass of HF in feed (g)**	**Mass of HF in product (g)**	**Mass of Coupons*** **(g)**	**Acid consumption**	
						$\left(\frac{\text{g HF}}{\text{g Alloy}}\right)$	**(%)**
0.0	70.00	68.92	324.40	319.39	69.50	0.072	1.5
1.0	69.21	95.71	320.74	304.52	64.84	0.232	5.1

*Average value from duplicate corrosion tests or solution analyses conducted with errors captured in the graphs discussed.

Table 5.46: HNO_3 acid consumption by nickel alloy (Monel 400) after 11 days when varying the HNO_3 concentration in 70% HF, at 25ºC.

Feed HNO_3 concn. (%)	**Product HNO_3 concn. (mg/kg)**	**Mass of HNO_3 in feed (mg)**	**Mass of HNO_3 in product (mg)**	**Mass of Coupons** * **(g)**	**Acid consumption**	
					$\left(\frac{\text{g HNO3}}{\text{g Alloy}}\right)$	**(%)**
0.0	0.00	0	0	69.50	0.000	0.0
1.0	14	4634	8	64.84	0.066	99.8

*Average value from duplicate corrosion tests or solution analyses conducted with errors captured in the graphs discussed.

HF acid consumption for the mild steel, stainless steel and nickel alloy coupons tested in pure 70% HF did not exceed 2%, after 11 days. These acid consumptions for CT tests were significantly lower than for PICTs (comparing after pre-passivated in Figure 5.46 to 0% HNO_3 in Figure 5.14) even though the PICTs were 3 days shorter. This was because the methods used for the PICTs differed from the CTs in that after 4 days, a fresh (pre-passivated) coupon was introduced to the corrosion solution, whereas in the CT tests, coupons were only introduced on the first day of the experiment. Introducing a new coupon into a corrosion tests encourages acid consumption because the newly introduced coupon reacted more vigorously in the first 24 hours of exposure to the HF solution (established in Section 5.1.2). For this reason, the acid consumption data of Sections 5.1 and 5.2 were not comparable.

Spiking up to 1% HNO_3 into the corrosion solution doubled the HF acid consumption for the nickel alloy while causing HF consumed by mild steel coupons to rise six-fold, compared to corrosion tests where pure 70% HF was used (Figure 5.46). Enhanced corrosion, experienced by mild steel and the nickel alloys measured in terms of acid consumption, was further supported

by nearly all the HNO_3 acid spiked (>99.98%) being consumed after 11 days. Unlike mild steel, the nickel alloy did not have a scale layer to protect it from corrosive attack by HNO_3. Therefore, the ~3% HF consumption experienced by the nickel alloy, compared to the ~6% of mild steel, was not a true reflection of the harsh corrosive attack experienced by the Monel 400 alloy. Here, the HNO_3 attacked the nickel alloy coupons directly, so that acid consumption measured was not a reflection of the combined attack on the scale layer and substrate, but only of the cleaned coupon surfaces.

Stainless steel behaved completely opposite to mild steel and the nickel alloy, since HF acid consumption was lower in the CTs where 1% HNO_3 was spiked (Figure 5.46). HF acid consumption was below 0.4% after 11 days, with HNO_3 consumption at the lowest levels for any corrosion tests conducted in this study (>64% HNO_3 consumed). The stainless steel formed an oxide-fluoride scale during pre-passivation (Figure 5.46); and after exposure to a 70% HF corrosion solution spiked with 1% HNO_3, this scale was completely dissolved (Figure 5.45: Row c). Therefore, the little acid consumed during the corrosion tests was a result of the combined attack of HF and HNO_3 on the scale layer left behind after the pre-passivation step. Oxygen in the HNO_3 then formed an oxide film on the stainless steel to prevent further corrosion by HF in solution. This in turn resulted in the low acid consumptions measured for SS 904 L coupons when compared to mild steel and Monel 400.

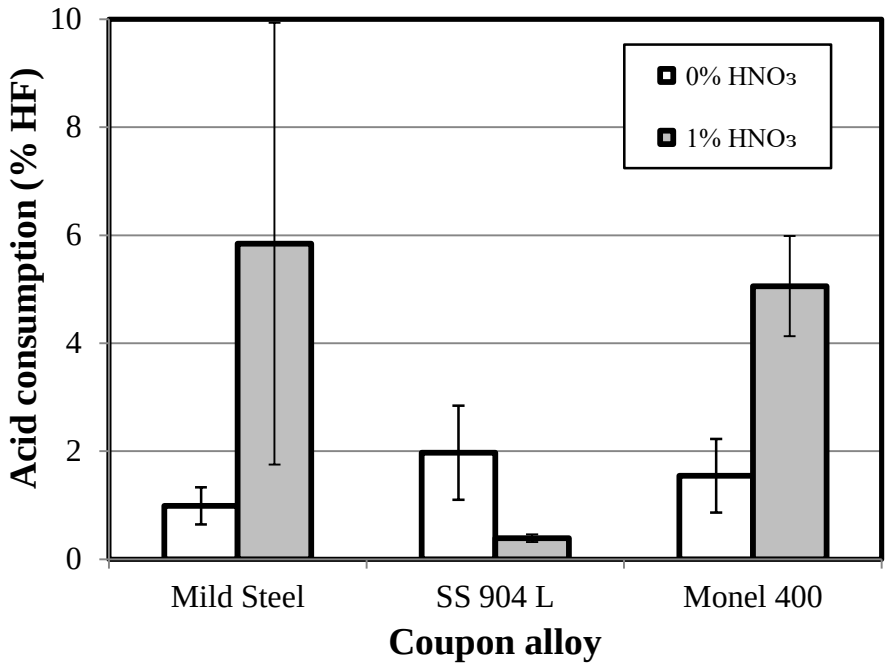

Figure 5.46: Percentage HF acid consumption after 11 days of mild steel, stainless steel and nickel alloy corrosion, at 25ºC. Error bars obscured by markers in some instances.

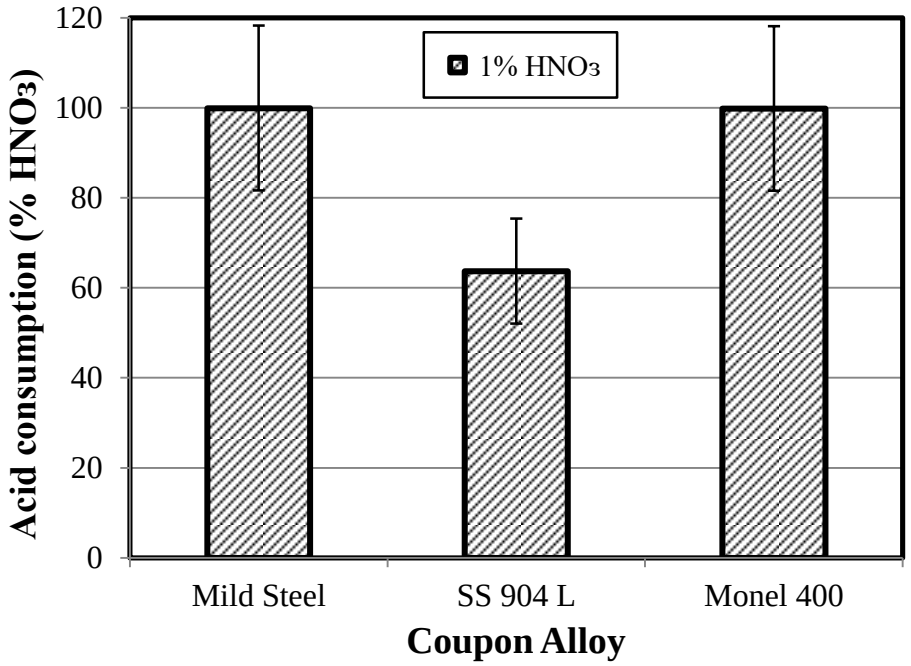

Figure 5.47: Effect of percentage HNO_3 acid consumption after 11 days of mild steel, stainless steel and nickel alloy corrosion, at 25ºC. Error bars obscured by markers in some instances.

Observations of photographs of corroded coupons

Conversely to the steels tested (Tables 5.34 and 5.42), the nickel alloy was observed to not produce an oxide or fluoride scale during the pre-passivation step (Table 5.47). Exposure to HF acted as a cleaning step giving in the nickel alloy coupons a clean appearance while maintaining the matt surface finish produced by sand-blasting (Figure 5.48: Row c). The surface finishes of the coupons after 11 days were the same as the original coupons introduce to the 70% HF corrosion test, and the mass losses were well below 0.1% for each coupon. Hence, the corrosion at these conditions was deemed negligible.

When 1% HNO_3 was spiked into the corrosion solution, the nickel alloy coupons corroded significantly more. The coupons removed from the corrosion solution were covered with a black oxide, which effectively hid the corrosion damage underneath (Figure 5.49: Row c). After cleaning, the coupons had a bright metallic lustre with visible pits covering the surfaces.

Table 5.47: Observations of corrosion products from a nickel alloy in HF with lowest to highest HNO_3 contamination, over an 11 day corrosion test (Figures 5.48 and 5.49: Row c and d).

	0% HNO_3	**1% HNO_3**
Appearance of coupons before cleaning	Metallic lustre not comparable to grey matt colour of original sand-blasted coupons. Light brown tint evident of some scale formation on the surface.	Black, mottled with dark brown scale. Exposed silver grey portions were also visible on coupons removed after 4 days.
Appearance of coupons after cleaning	No visible corrosion. Clean surface.	The black scale was easily removed from all coupons, leaving behind a light brown scale with the metal substrate exposed having a clean metallic lustre. Severe attack of entire coupon surface over entire test period. Pitting corrosion was visible over most of the coupon surfaces inspected.
Composition of final corrosion solution	68.6% HF <2 mg/kg HNO_3 7 ppm Fe <1 ppm Cr 3 ppm Mn 168 ppm Cu 191 ppm Ni 5 ppm Si	65.7% HF 14 mg/kg HNO_3 417 ppm Fe 5 ppm Cr 268 ppm Mn 8249 ppm Cu 17389 ppm Ni 42 ppm Si

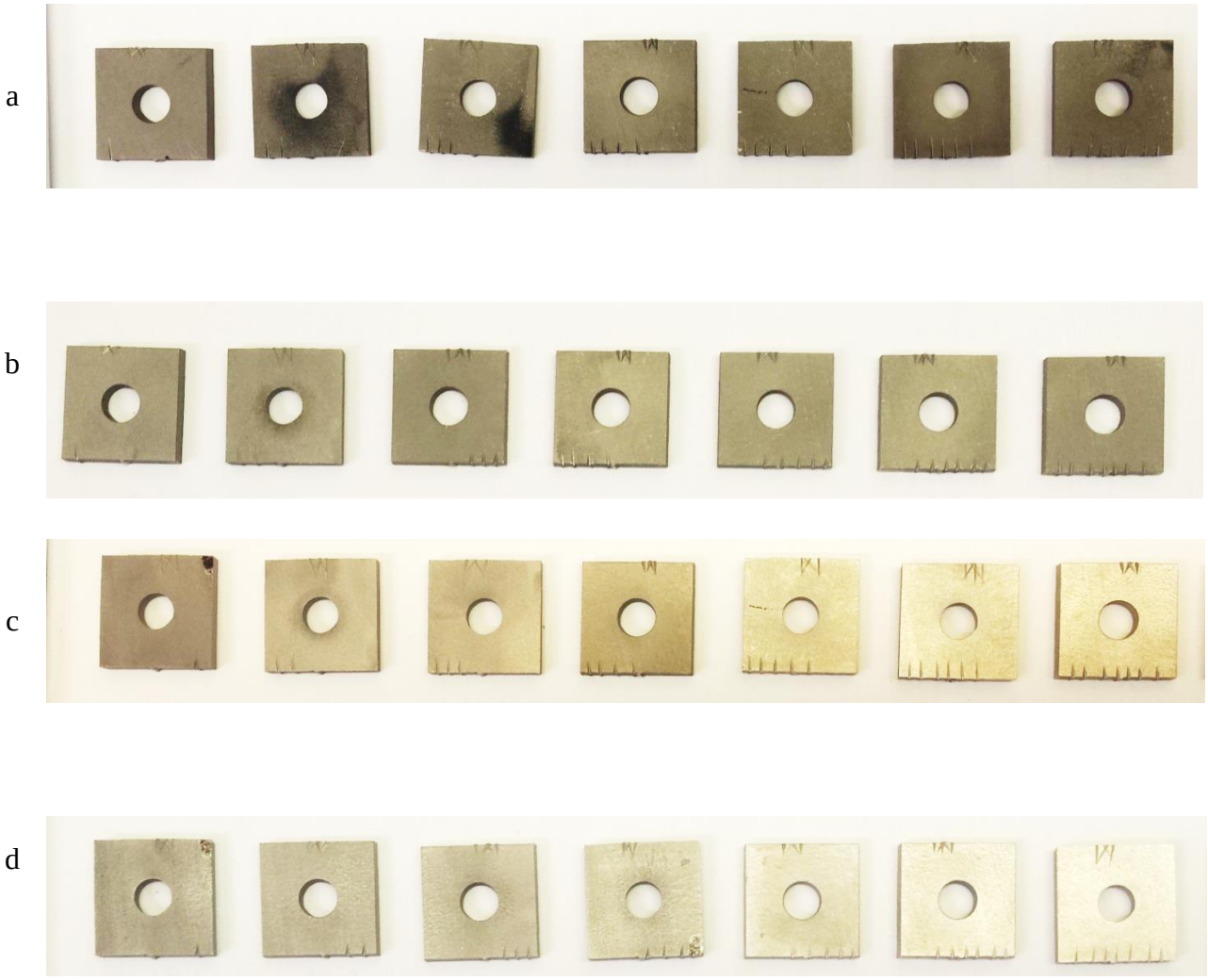

Figure 5.48: CT 17: Nickel alloy (Monel 400) coupons (1-7): Row a; before exposure, Row b; after pre-passivation step, Row c; after exposure to 70% HF, and Row d; after removal of the scale layer, at 25ºC.

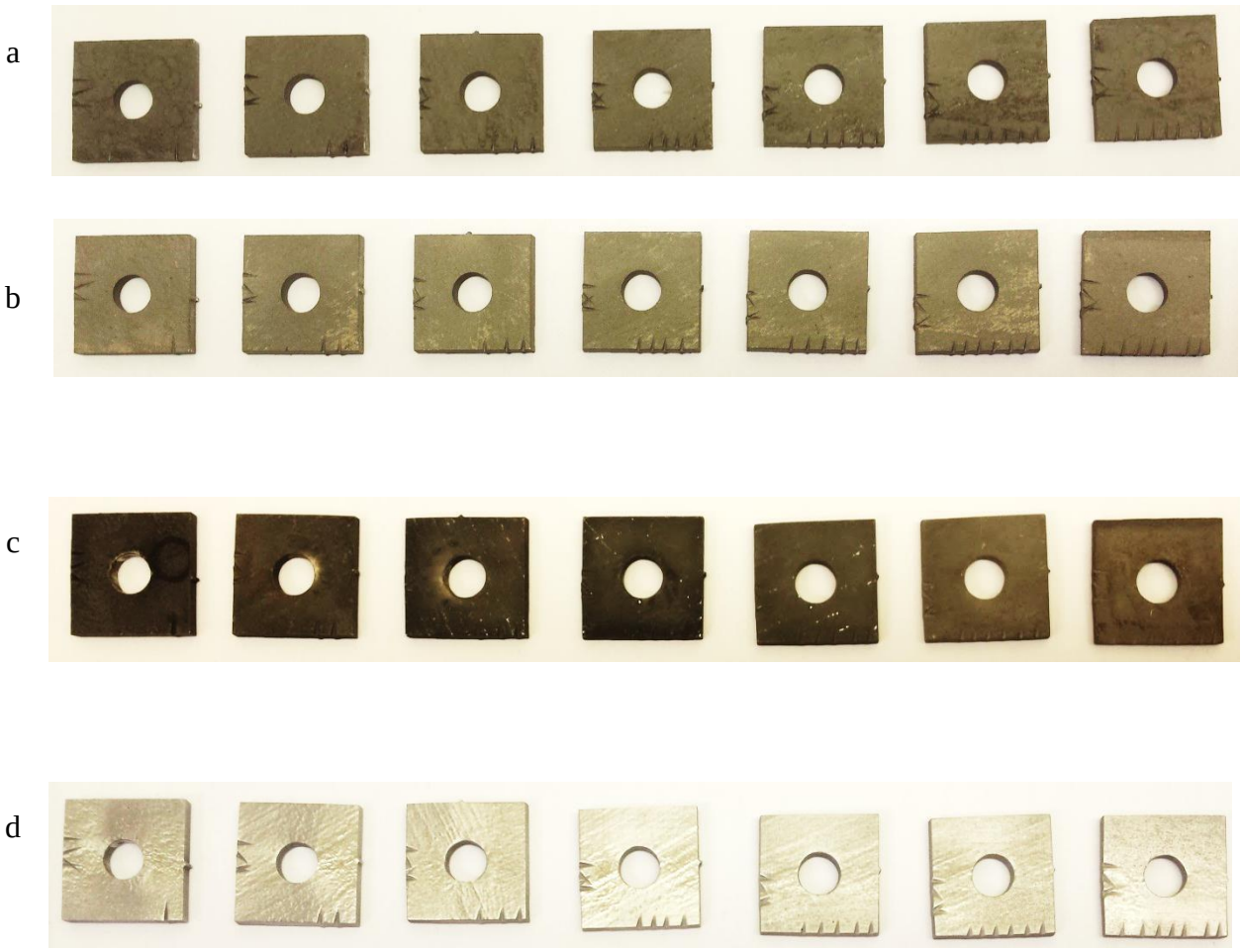

Figure 5.49: CT 18: Nickel alloy (Monel 400) coupons (1-7): (row a) before exposure, Row b; after pre-passivation step, Row c; after exposure to 70% HF spiked with 1% HNO_3, and Row d; after removal of the scale layer, at 25ºC.

CHAPTER 6

DISCUSSION

6.1. PLANNED INTERVAL CORROSION TESTS

6.1.1. Introduction

Raw data and findings from corrosion tests, given in the results sections, are discussed here to derive the reason for the underlying trends. Firstly, the need for a 24 hour pre-passivation step in pure HF, determined through mass loss and apparent corrosion rate data from PICTs was discussed. The discussions started off with briefly summarizing results from the PICTs, then moving on to the CTs and ending off with corrosion kinetics.

6.1.2. Effect of pre-passivation on mild steel

Mass loss and apparent corrosion rates

To investigate the effect of acid concentration on mild steel corrosion and the role of pre-passivation, all mass loss measurements are compared in a single graph (Figure 6.2). When no pre-passivation was involved, the percentage mass losses experienced in 40% and 48% HF concentration were approximately equal (nearly 37%), although more than 36% higher than iron mass loss by any of the mild steel coupons tested in 70% HF (nearly 1%).

The ineffectiveness of the pre-passivation steps in the 40% (Figure 5.5) and 48% HF (Figure 5.6) tests was evident when compared to the lower mass loss experienced by the untreated coupons over the duration of the PICTs (Figures 5.2 and 5.3). The percentage mass loss determined for PICTs with pre-passivation was calculated using the mass of the coupon after the pre-passivation step (coupon covered with the fluoride scale layer formed by exposure to fresh HF for 24 h). During the pre-passivation step, the coupon was exposed to the corrosive solution for 24 hours prior to the actual tests, which resulted in a mass loss. When pre-passivation was conducted in 70% HF (Figure 5.7), the percentage mass loss during that 24 h was consistently measured at nearly 0.2% of the coupon, which was negligible. However, in tests where pre-passivation step was conducted with 40% and 48% HF, the mass loss over this period was nearly 22% and 34% respectively.

Accordingly, the influence of these prior mass losses sustained during the pre-passivation step were not incorporated into Figure 6.2. This explains why the 40% HF tests consistently had a higher percent mass loss (>8%) than the PICT, when pre-passivation was involved. During the pre-passivation step (Section 4.4.1), the coupons in the 40% HF tests lost around 34% of their mass, and therefore were approximately 12% lighter going into the PICT, compared to the coupons pre-passivated in 48% HF. The reduced mass and relatively poor scale formation on these pre-passivated coupons (Figure 5.5 and 5.6: Row b) made them more susceptible to corrosive attack during PICTs that followed, Figure 6.1. The weight discrepancies of the coupons, which were pre-passivated in 40%, 48% or 70% HF before going into their respective PICTs, thus made the mass losses determined at the end of each PICT, incomparable.

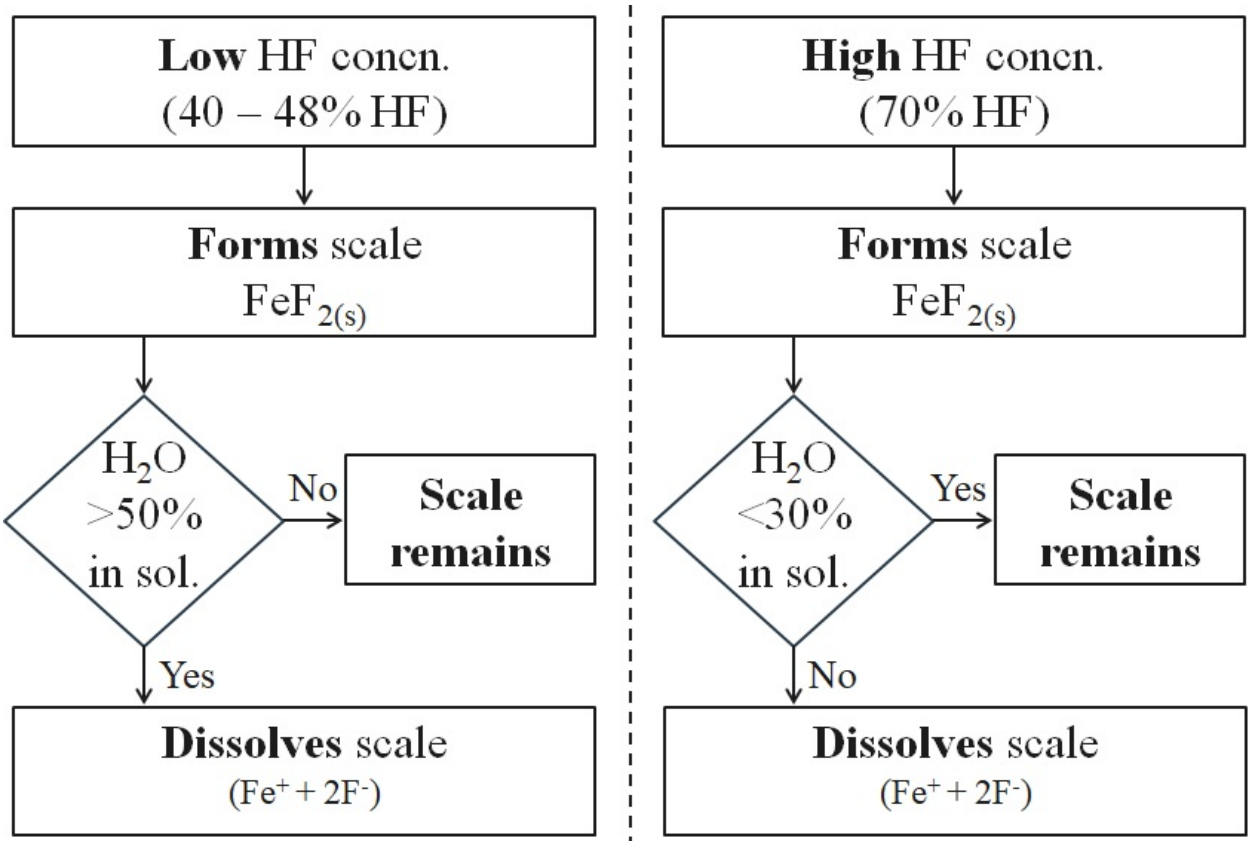

Figure 6.1: Flow chart to demonstrate how a change in HF concentration affects scale formation on mild steel.

Figure 6.2 shows that the mass losses by coupons during the 70% HF PICTs were very close (1 – 2% mass loss), especially after the initial day spent in solutions (both at ~0.5% mass loss). However, after the first day in the test solution, the untreated coupons lost nearly 1.7 times more iron than their

pre-passivated counterparts. This demonstrated the benefit of a pre-passivation step for the succeeding corrosion tests.

a

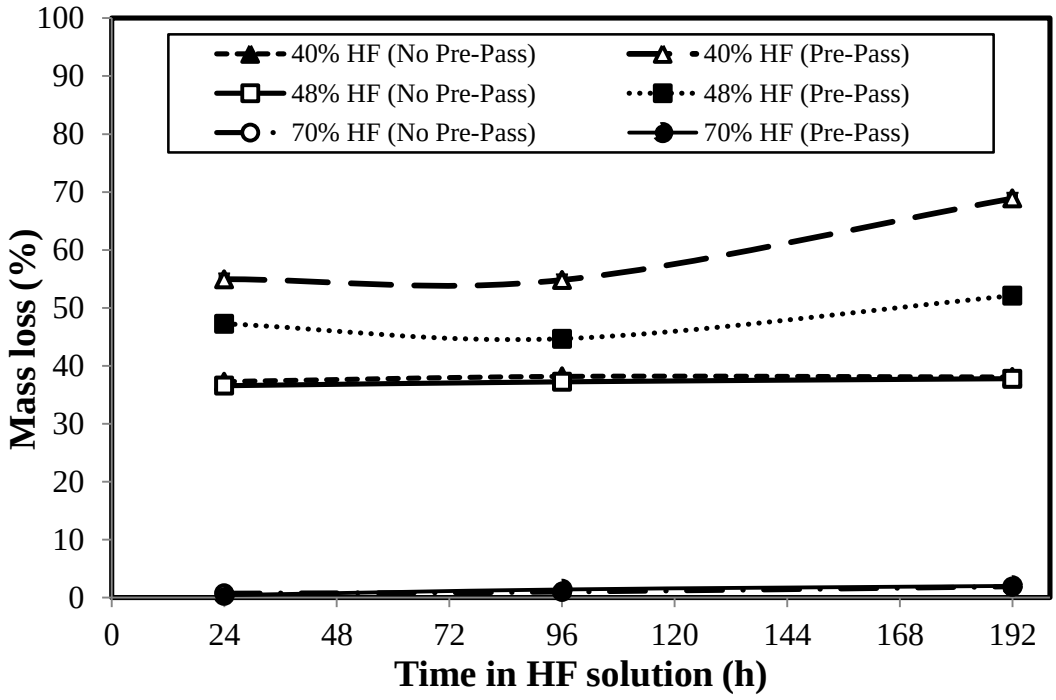

b

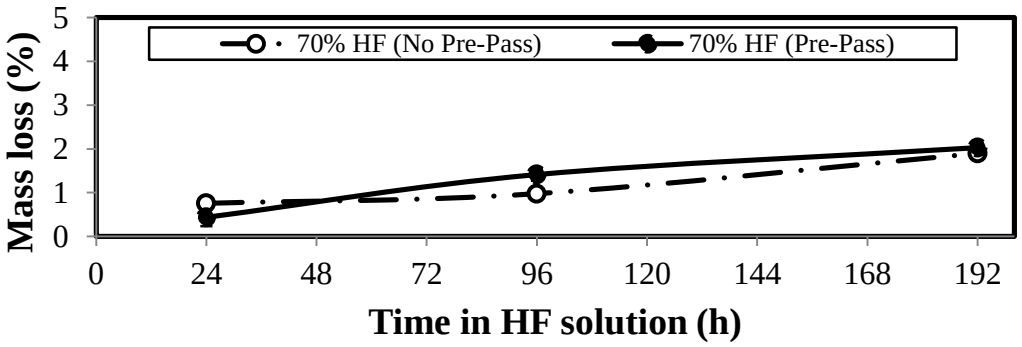

Figure 6.2: Effect of a pre-passivation step on mass loss with increase in percentage HF in the corrosion solution, at 25ºC. Error bars obscured by markers in some instances: (a) whole range of the mass losses, and (b) lower mass losses.

Higher HF concentrations tend to be associated with lower corrosion rates (Honeywell International Inc, 2014). Pre-passivation for the 48% HF PICTs produced a similar result to the 40% HF test (Figure 6.3), with the protective scale having even less resistance to corrosion and this test, even producing the highest corrosion rate measured for mild steel in this entire study (A_1 value in Table 5.4). This proves just how highly susceptible mild steel is to corrosion in an HF environment,

even when the concentration of relatively pure HF solutions (HNO_3 contamination >5 ppm) are slightly altered.

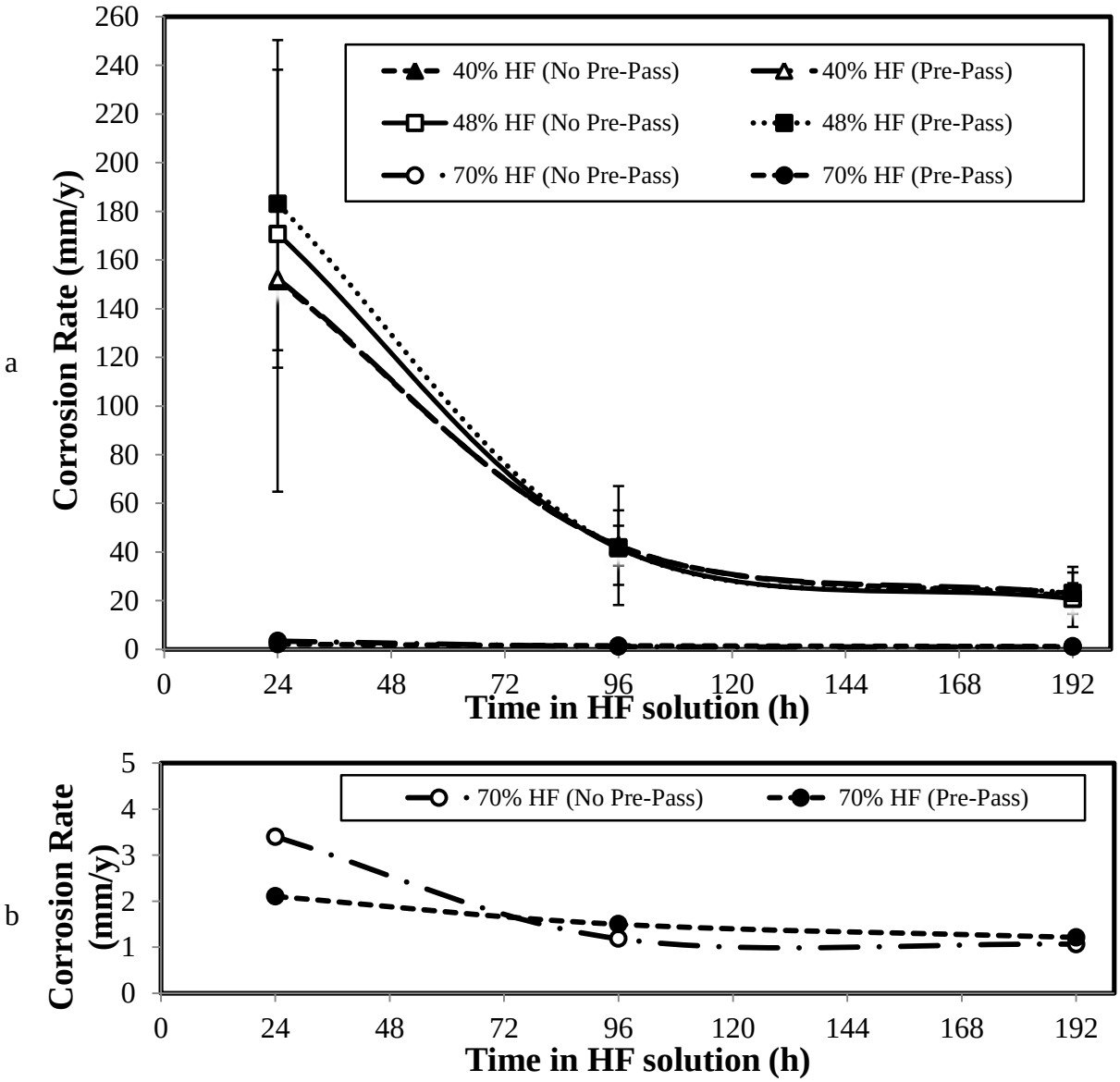

Figure 6.3: Effect of a pre-passivation step on apparent corrosion rate with increase in percentage HF in the corrosion solution, at 25ºC. Error bars obscured by markers in some instances: a) whole range of the mass losses, and b) lower mass losses.

In these tests, pre-passivation proved to have no measurable effect on the susceptibility of the metal to corrosion, as the corrosion rates determined in both instances remained approximately the same. However, the apparent corrosion rate determined for the PICT test conducted with no prior pre-

passivation step was approximately 1.6 times lower than that of the untreated coupons, indicating that the corrosiveness of the acid decreased faster. Thus, within the first 24 hours, more HF was consumed to produce the fluoride scale on the raw coupons, which then served to protect the steel over the rest of the test. Conversely, in the test where a pre-passivation step was included, the protective scale had already formed during that pre-passivation step, and therefore a slower apparent corrosion rate was measured within the first 24 hours. Therefore, pre-passivation is not only an operative step in the commissioning of HF storage tanks, but also an effective step when working with 70% HF, as it effectively maintains a slower diminution in the corrosiveness of the liquid (Figure 6.3)

Observations of photographs of corroded coupons

Mass loss measurements were considered the most important variable in the study and therefore the coupons needed to be cleaned after each corrosion test. Unlike with the dry scale collected during the post-mortem corrosion study (Figure 3.6), scale collected from the corroded coupons was significantly less, because it was from the collected wash water. Since the scale collected was a dried precipitate from the wash water, the precipitated substances and crystals formed when evaporating the wash water off, would not produce crystallographic information comparable to the unwashed scale which used to be attached to the coupon. Characterization of the washed scale using SEM-EDS analyses was also inconclusive due to the limitations of the super ultra-thin windows (SUTW) on the AppolloX EDS detectors used in light elemental quantification (EDAX, 2013), which included oxygen and fluorine in the scale. However, EDS scans did assist in confirming that there was more oxygen present in the black scale, while the grey and yellow-brown scales contained more fluorine (F). Thus, the visual colour of the precipitated substances on the corroded coupon surfaces, from photographs taken before washing, was considered as a reliable alternative means of characterizing the corrosion and scale.

According to (Haynes, 2016), iron fluoride (FeF_2) has a grey colour, while the ferric hydroxide ($FeF_3.3H_2O$) has a distinct yellow-brown colour. Therefore, in instances where coupons surfaces were observed to have a black scale, it was characteristic of oxidation (iron II/III) on the coupon surfaces and was considered plausible as the corrosion reaction was allowed to take place in a well ventilated bottle (Tables 5.8 and 5.9). The mixture of all these coloured substances, which formed on a coupon surface during each corrosion test, comprised the scale on each coupon surface and produced colours visibly distinct on the photographs (Figures 5.2 – 5.4).

The iron concentration analysed in the corrosion products from the 70% HF tests was less than 0.02% (Table 5.9). Therefore, the scale layer formed during the pre-passivation step succeeded in protecting the mild steel from further corrosion and produced a surface visibly free from corrosion, once the scale had been washed off (Figures 5.4 and 5.7). After cleaning, corrosion was hardly visible. Lack of corrosion was further confirmed by pit depth measurements, made using high magnification optical microscopy, on the original sand-blasted coupons (Figure 5.11) which had larger holes (deepest ~57 µm) than the coupon surfaces from 70% HF PICT (deepest ~43 µm in Figure 5.8). Significantly more pit measurements (>100) over a larger surface area (entire coupon) of more corroded coupons would have produced statically comprehensive pit classification results that would better support determining the effect of HF concentration on pitting corrosion of mild steel. However, the few measurements conducted and correlated succeeded in qualifying the pitting corrosion and the degree of pitting associated with HF concentration in the corrosion. Therefore, 70% HF had a more cleaning effect on the coupon surfaces than a corrosive one (Table 5.8), while the addition of a pre-passivation step only improved corrosion resistance when further exposure to the corrosive solution was involved.

6.1.3. Effect of steel and alloy composition

Mass loss and apparent corrosion rates

With and without pre-passivation, the mild steel, stainless steel and the nickel alloy coupons did not lose more than 2% of their total mass within 24 h of exposure to pure 70% HF (Figure 6.4). Of the three metals tested, only the stainless steel lost more than 2% of its mass over the eight day PICTs. Steel coupons that were pre-passivated lost slightly more mass than untreated coupons at 48 hours: ~0.4% for mild steel and ~0.2% for SS 904 L. Mass loss by pre-passivated mild steel coupons caught up to the untreated coupons after eight days, which indicated that mass loss was due to continuing scale formation on the coupons (after 24 h) until adequately formed to mitigate further HF corrosion. However, the reducing environment created by the pure 70% HF did not support formation of the oxide layer needed for corrosion resistance by the stainless steel coupons. This was because, unlike mild steel (99 wt% Fe) which forms scale (FeF_2) during its passivation, the chromium component in SS 904 L stainless steel (46 wt% Fe and 20 wt% Cr) needs oxygen in solution to form Cr_2O_3 on the steel surface for it to passivate. The pure HF used did not contain enough oxygen or HNO_3 for the stainless steel to passivate in solution. Thus, mass loss by SS 904 L

remained steady at approximately 0.05% per hour as the steel continued to corrode unrestricted. The only reason why the pre-passivated coupons had a higher mass loss (~0.7% more after eight days) was due to pre-passivation step cleaning the coupon surface to produce weakly bonded oxide scale on the surface (Figure 5.15; Row b) which could not mitigate corrosion by HF. Mass loss by nickel alloy coupons remained below 0.5% throughout each of the PICTs conducted, and thus the effect of pre-passivation was not conclusive. Therefore, pre-passivation for all coupons was done, since it either produced a protective scale or a cleaned surface suitable for the following corrosion tests.

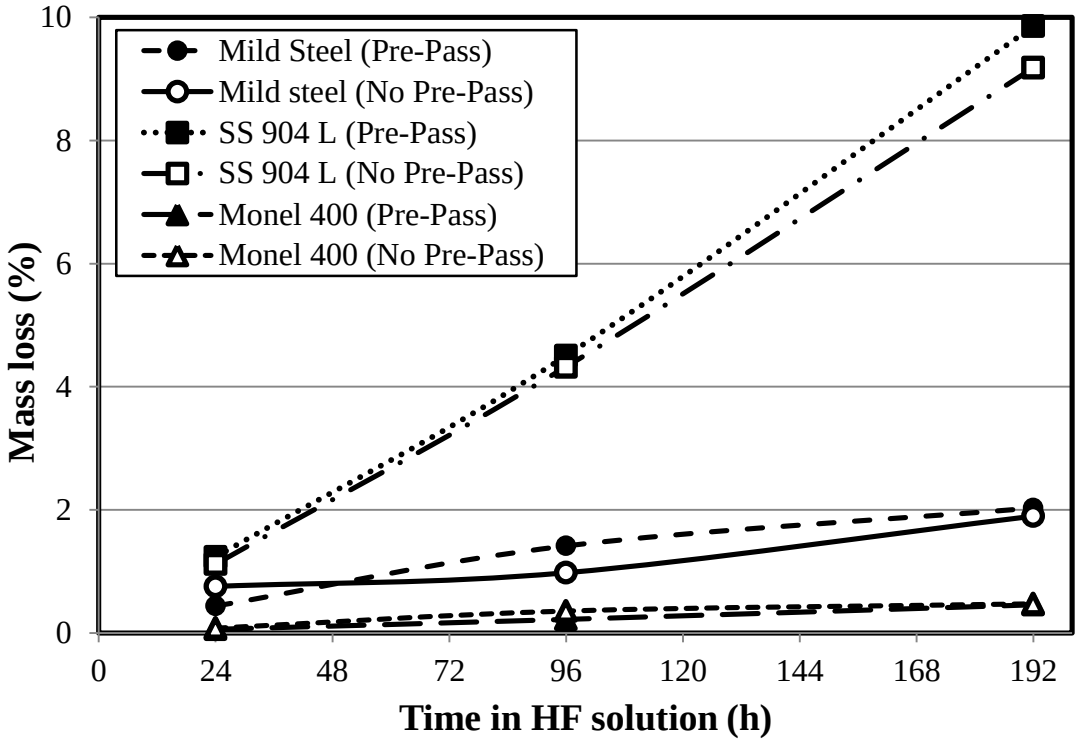

Figure 6.4: Effect of a pre-passivation step on mass loss of mild steel, stainless steel and nickel alloy during a PICT, at 25ºC in 70% HF. Error bars obscured by markers in some instances.

The apparent corrosion rates for mild steel, stainless steel and nickel alloy, with and without pre-passivation, over the 8 day PICTs are compared in Figure 6.5. The nickel alloy coupons corroded at less than 0.4 mm\y over the corrosion test period. Corrosion rates of these coupons slowed down (>0.4 mm/y) after 48 h, which indicated that there was a slight initial reaction which then subsided. This was due to surface mill scale or residue (SiO_2) which was dissolved by the HF and subsequently the exposed nickel alloy showed superior corrosion resistance (<0.3 mm/y after eight days). Conversely, stainless steel coupons corroded at a constant rate of between 4.2 and 4.6 mm/y, providing inferior corrosion resistance to the 70% HF. Even after pre-passivation, stainless steel

corrosion did lessen somewhat and the reduced coupon surfaces corroded slightly faster (>4.8 mm/y after 8 days). Scale formation was not as effective in slowing the corrosion rate in stainless steel coupons as for mild steel coupons (Figure 6.5). Compared to the pre-passivated mild steel coupons, the higher corrosion rate of the untreated coupons, seen at 24 h, demonstrated how the increase in corrosion rate was due to scale formation. The pre-passivated coupons already had strongly bonded scale (Figure 5.7; Row b), slowing corrosion to below 2 mm/y, measured at 24 h. Corrosion rates slowed down to below 1 mm/y, measured after 192 h, as the oxide-fluoride scale stabilized further to mitigate corrosion.

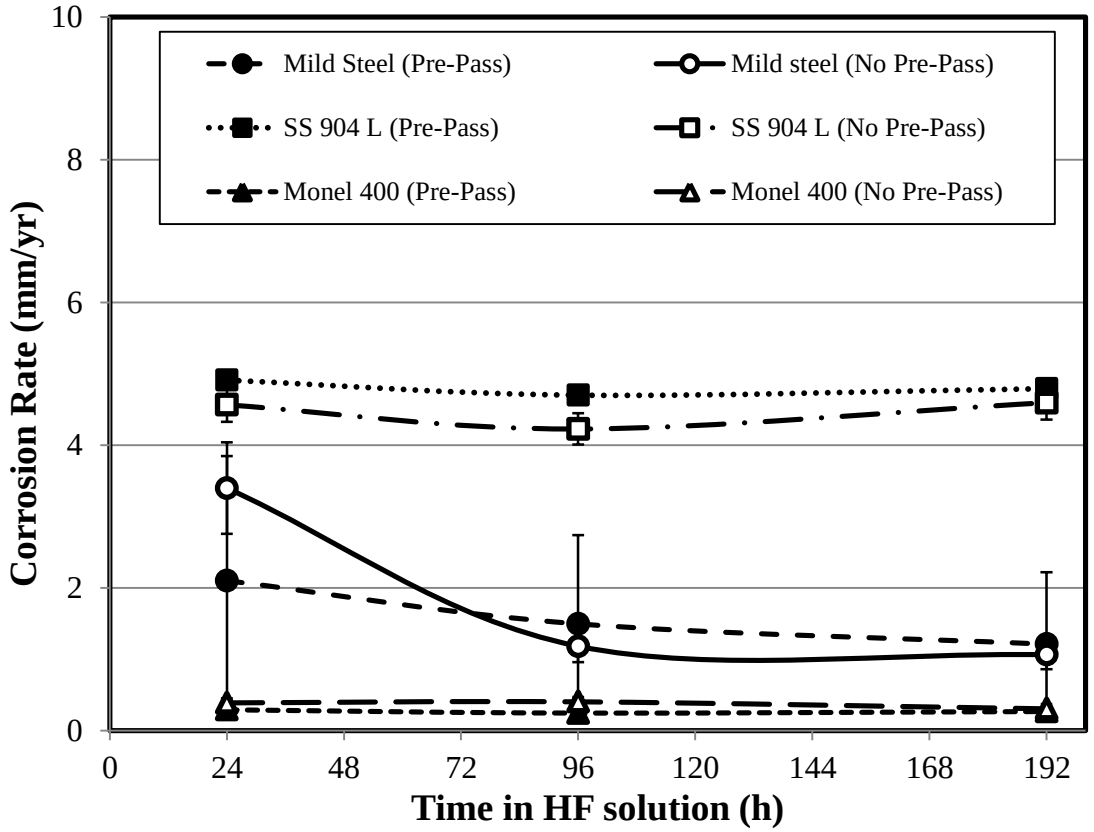

Figure 6.5: Effect of a pre-passivation step on the apparent corrosion rate of mild steel, stainless steel and nickel alloy during a PICT, at 25ºC in 70% HF. Error bars obscured by markers in some instances.

6.2. CONTINUOUS CORROSION TESTS

6.2.1. Introduction

Findings made on mass losses and corrosion rates of steels and metallic alloys, as affected by the change in HNO_3 concentration and temperature in an HF mother solution, were compared. Mass losses for the coupons over time frequently showed linear tendencies, which made it possible to define corrosion rates in terms of reaction kinetics. This allowed the comparison of activation energies from Arrhenius plots to demonstrate the effect of HNO_3 concentration and solution temperature on the corrosion of mild steel.

6.2.2. Mild steel corrosion

6.2.2.1. Effect of nitic acid concentration

Mass loss and apparent corrosion rates

The effects of HNO_3 concentration in the 70% HF solutions on the mass loss of mild steel coupons during corrosion are clearly discernible in Figure 6.6. Higher concentrations of HNO_3 spiked into a 70% HF corrosion solution, gave higher mass losses from the pre-passivated coupons over an 11 day CT. The relationship between mass loss and HNO_3 concentration was linear (Figure 6.7). Thus the gradient "m" represents the corrosion rate defined as percent mass loss / time (as an alternative to conventional mm/y) and increased for higher HNO_3 concentrations (0.0076 in pure HF compared to 0.013 in HF spiked with 1% HNO_3). Based on these proportional relationships, it was determined that increasing the HNO_3 to 0.1% in 70% HF nearly doubled the mass loss compared (at any point in time) to mass losses experienced by corrosion tests conducted in pure HF. Increasing the spiked dosage to 0.5% HNO_3 produced a mass loss that was nearly seven times more than in tests where no HNO_3 was spiked in. This value doubled when the spiked HNO_3 concentration was doubled (from 0.5% to 1%). Therefore, considering the *y*–intercepts on the regression line functions (Figure 6.7), an increase of 0.1% HNO_3 in HF resulted in increased mass loss by a mild steel coupon of approximately 1.22% ($y = 7.5x + 0.47$). Since the linear trend lines were not parallel (different gradients), this relationship was only valid between 0 and 24 h in the corrosion solutions. Increasing HNO_3 concentration (0.5% – 1%) gave relatively higher mass losses than the lower HNO_3 concentrations (≤0.1%), which showed that even though HNO_3 was consumed early on in the corrosion reaction (Figure 5.19), its dissolution of the fluoride scale (Equation 6.1) allowed HF to

corrode the exposed steel substrate at a higher rate (higher "m" values at higher HNO_3 concentrations in HF, Figure 6.7).

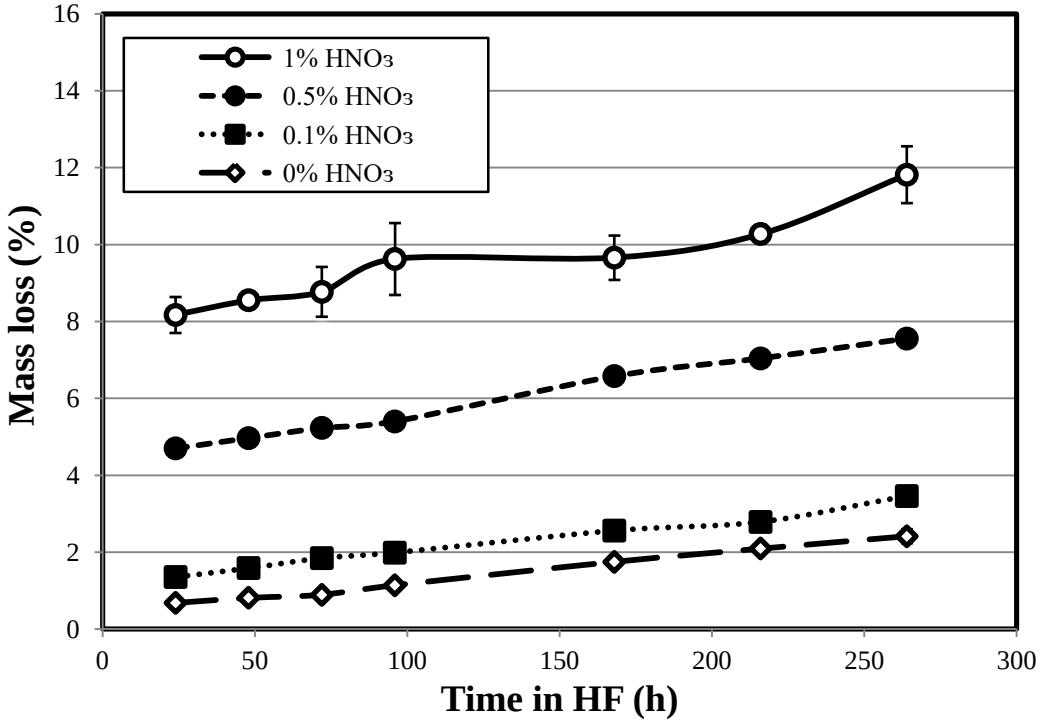

Figure 6.6: Effect of HNO_3 concentration on mass loss of mild steel when corroded in HF at 25ºC in 70% HF. Error bars obscured by markers in some instances.

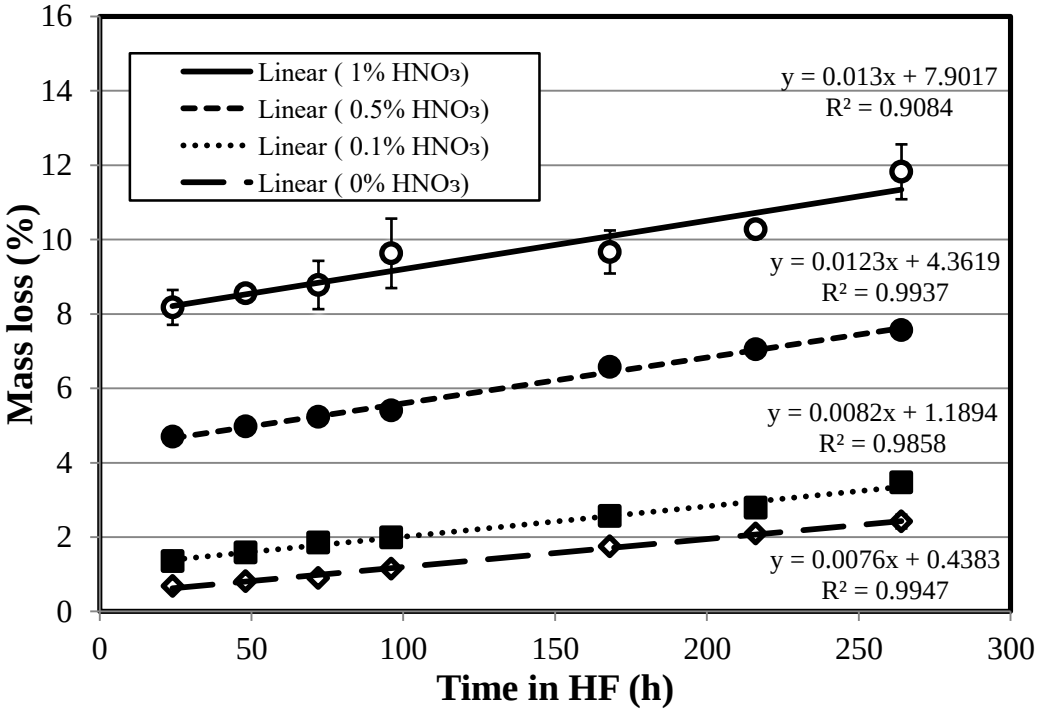

Figure 6.7: Effect of HNO_3 concentration on mass loss of mild steel when corroded in HF (linear trends), at 25ºC in 70% HF. Error bars obscured by markers in some instances.

In pure 70% HF, pre-passivated mild steel was found to corrode at an apparent corrosion rate of 1.0 mm/y and lost nearly 0.18% of its mass per day when tested at ambient temperature (25ºC). This was nearly double the typical rate at which mild steel HF storage tanks were recognized (Valkenburgh, 2012a) to corrode per year under normal operating conditions (0.5 mm/y) while in contact with the technical grade HF product for up to 6 months (Valkenburgh, 2012d), with negligible water evaporation as indicated by the relatively stationary liquid level visible in Figure 3.3a (in Section 3.5). Thus, both the plant and experimental environments were virtually closed environments. This discrepancy between corrosion rates measured in the laboratory simulated corrosion tests and the HF storage tanks on site was due to the time over which the corrosion measurement took place, and not the influence of a slight increase in HF concentration brought on by minor water evaporation during experiments (< 2.5 ml HF per day, Section 4.5.2.2). In the laboratory corrosion tests, mild steel was determined to initially (after 24 h) corrode at 3 mm/y, and this was attributed to the scale formation reaction, since to the pre-passivation time was not long enough. This is because the scale in the steel tanks thickens and densifies on the steel surfaces with time, and therefore offers more corrosion protection to the steel with time spent in a pure 70% HF solution. This was verified in the 70% HF laboratory corrosion tests, since the apparent corrosion was estimated to slow down to the required 0.5 mm/y, if the corrosion test was allowed to continue an additional 21 days in pure 70% HF.

Regardless of HNO_3 concentration in the 70% HF corrosion solutions, initial apparent corrosion rates for mild steel were faster (measured at 24 h) and then slowed down considerably as time in solutions continued (Figure 6.8). Apparent corrosion rates did not exceed 6 mm/y in CTs where low HNO_3 concentrations ($\leq$ 0.1% HNO_3) were used. Therefore, the initial peak in corrosion rate was due to HF still reacting with exposed mild steel, which did not form scale during the pre-passivation step. Conversely, in CTs where more HNO_3 was spiked (0.5% and 1% HNO_3), initial corrosion rates were in excess of 20 mm/y. This was due to more HNO_3 being available, having a larger impact on the protective fluoride scale formed during pre-passivation. In HF with higher HNO_3, the fluoride layer was attacked, as shown in Equation 6.1, and became porous (Figure 5.42), which allowed HF access to the steel substrate again. The newly-exposed steel reacted repeatedly with fresh HF to form a succession of scale layers, which explains the high initial corrosion rates (~36 mm/y measured for 1% HNO_3 at 24 h).

$$FeF_2 + 2HNO_3 \rightarrow Fe(NO_3)_2 + 2HF \qquad \text{Equation 6.1}$$

All corrosion rates subsided to below 5 mm/y after 7 days (Figure 6.8), which was a result of complete nitric acid consumption (>99% for all tests shown in Figure 5.19). As HNO_3 was nearly depleted (<13ppm, Table 5.33) and HF concentration only slightly reduced (>65% HF left, Table 5.32), scale formed again, unhindered by the presence of HNO_3, to mitigate HF corrosion, which in turn slowed down the apparent corrosion rate. It was estimated, by following the trends in the corrosion rates measured after seven days, that if corrosion tests continued for longer (between 19 and 23 days), corrosion rates experienced in industry (<0.5 mm/y) would be reached.

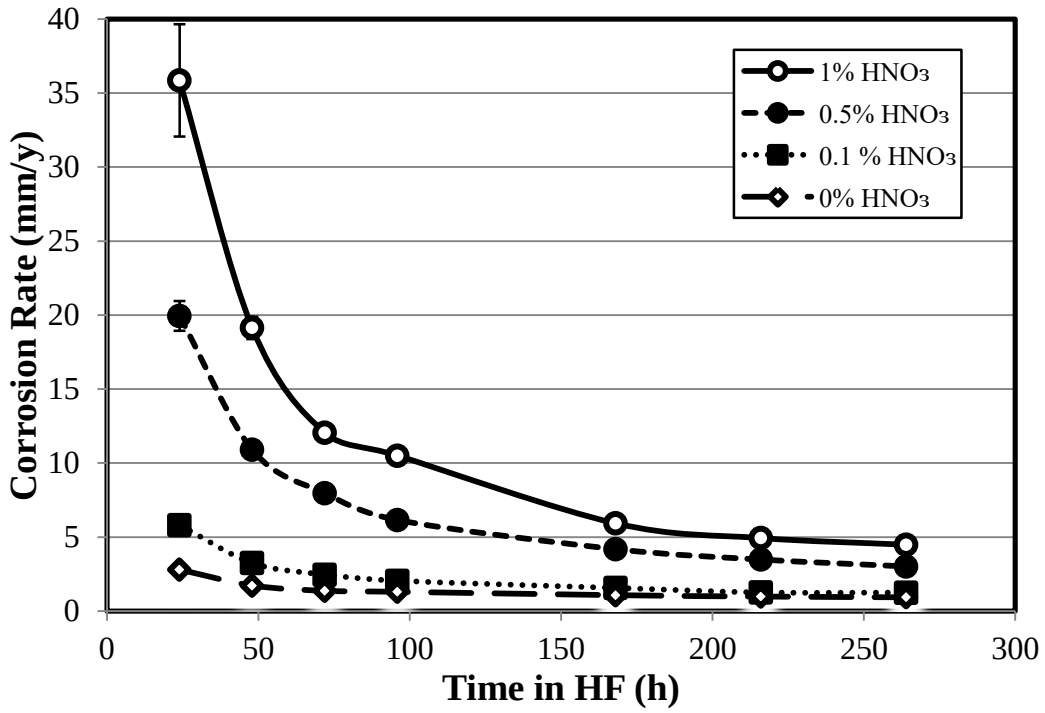

Figure 6.8: Effect of HNO_3 concentration on the apparent corrosion rate of mild steel in HF, at 25ºC in 70% HF. Error bars obscured by markers in some instances.

6.2.2.2. Effect of temperature

Mass loss and apparent corrosion rates

The same corrosion tests conducted at 25ºC in Section 6.2.2.1 were repeated at lower temperatures (0ºC and 15ºC) to determine the effect of temperature on the mass loss by mild steel coupons, when corroded in 70% HF solutions spiked with varying concentrations of HNO_3. In each instance, corrosion tests conducted at lower temperatures resulted in less mass being lost when corroded by HF and HNO_3 in solution (Figures 6.8, 6.9, 6.10 and 6.11). Irrespective of initial HNO_3

concentration spiked, coupons collected after 11 days from the 25ºC CTs consistently had nearly 1% higher mass losses than coupons removed from 0ºC CTs and nearly 0.5% higher mass losses than coupons removed from 15ºC CTs.

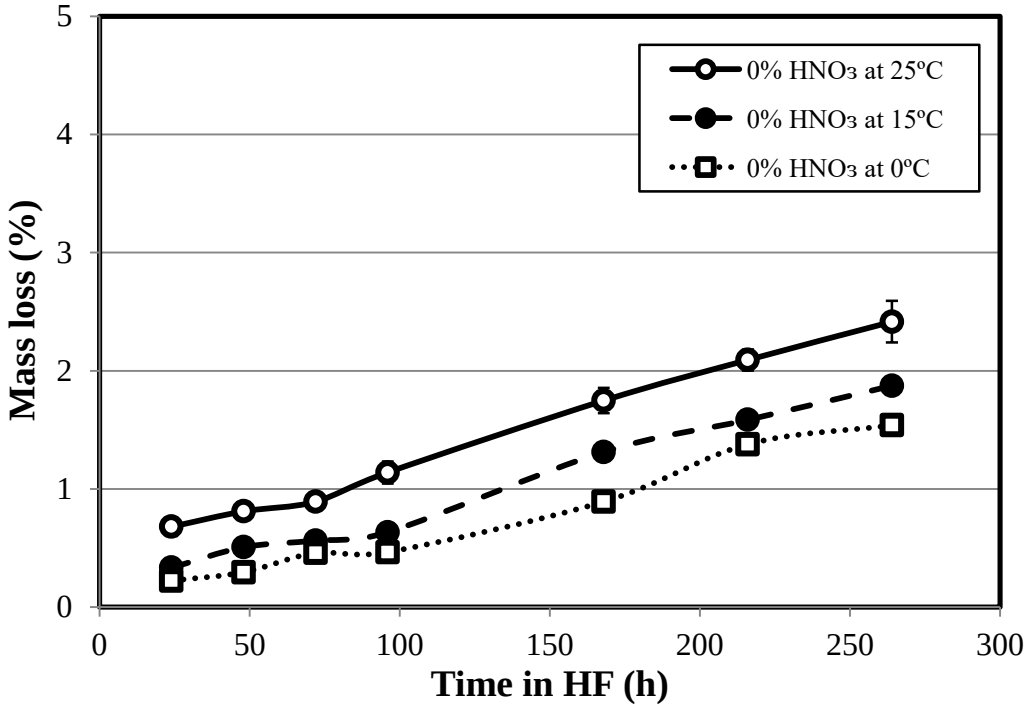

Figure 6.9: Effect of temperature on mass loss of mild steel when corroded in pure HF. Error bars obscured by markers in some instances.

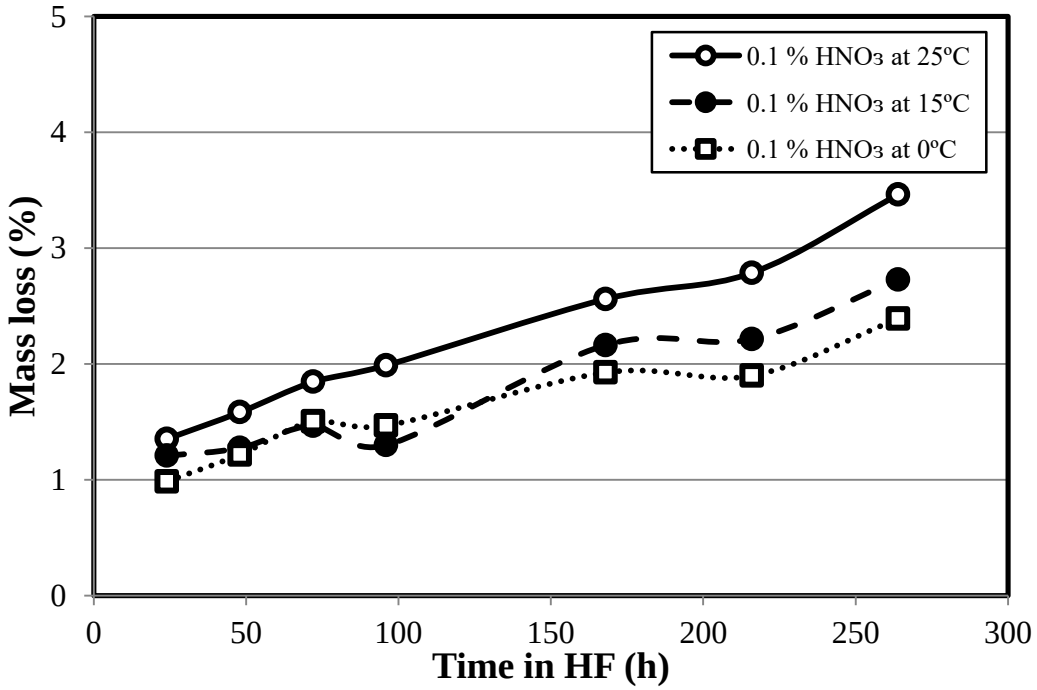

Figure 6.10: Effect of temperature on mass loss of mild steel when corroded in 70% HF spiked with 0.1% HNO_3. Error bars obscured by markers in some instances.

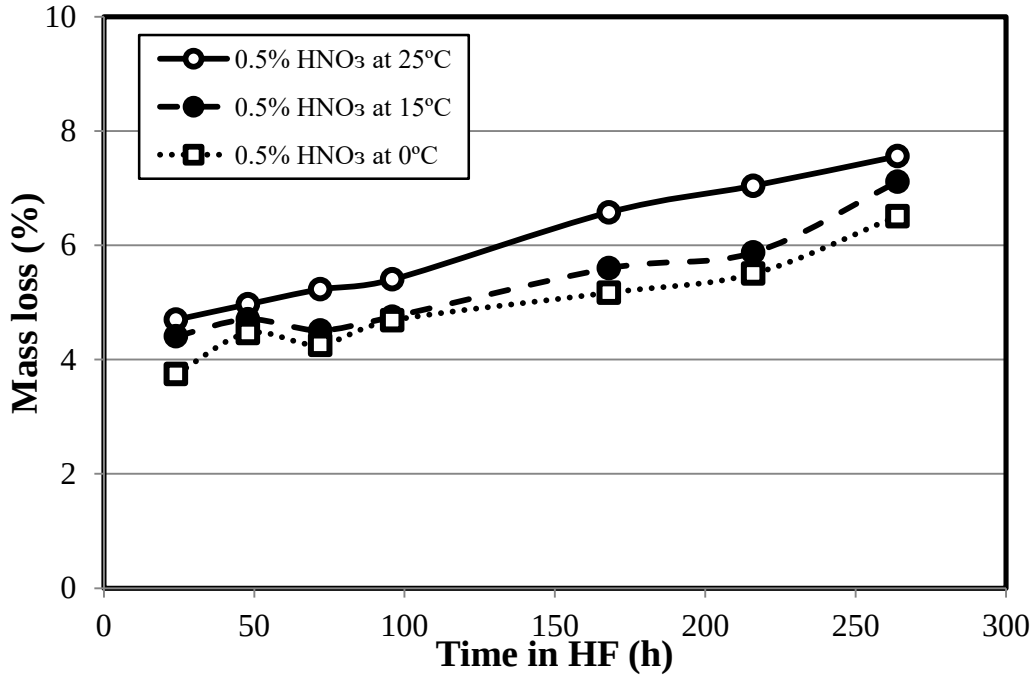

Figure 6.11: Effect of temperature on mass loss of mild steel when corroded in 70% HF spiked with 0.5% HNO_3. Error bars obscured by markers in some instances.

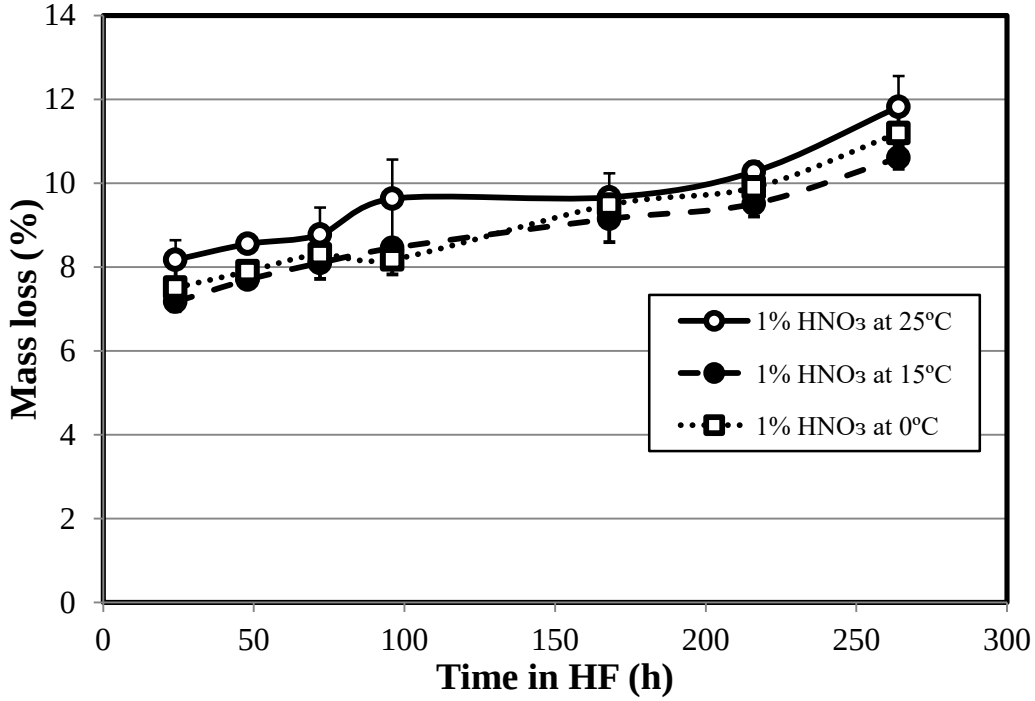

Figure 6.12: Effect of temperature on mass loss of mild steel when corroded in 70% HF spiked with 1% HNO_3. Error bars obscured by markers in some instances.

Monitoring the effect of temperature on apparent corrosion rates of mild steel coupons in HF solutions spiked with varying concentrations of HNO_3 (Figures 6.12 – 6.15) revealed a little more than monitoring percentage mass loss. As also seen in percentage mass loss profiles (Figures 6.8 – 6.11), in each instance, corrosion tests conducted at lower temperatures resulted in lower apparent corrosion rates. However, in apparent corrosion rate profiles, it was possible to demonstrate that higher concentrations of HNO_3 spiked into the corrosion solution reduced the effect of temperature. For instance, CTs conducted at 25ºC, spiked with 0% and 0.1% HNO_3 had approximately 0.1 to 0.2 mm/y faster corrosion rates than the same tests conducted at 15ºC and 0ºC (264 h in Figures 6.12 and 6.13). Conversely, in CTs conducted at 25ºC, 15ºC and 0ºC, spiked with 0.5% (Figure 6.15) and 1% HNO_3 (Figure 6.16), showed no discernible difference in corrosion rates measured at 11 days (all at 2.7 mm/y and 4.6 mm/y respectively). Therefore, at higher HNO_3 concentrations (≥0.5%), apparent corrosion rates were more influenced by HNO_3 in solution than solution temperature. This is counterintuitive, and was because the corrosion reaction of the HNO_3 component, in the predominantly HF solution, with the fluoride scale (Equation 6.1) and the steel substrate (Equation 5.2) was faster at higher temperatures than the HF component, which made the HF corrosion reactions (Equation 1) appear slower. This phenomenon is further explained in the section on kinetics and rate constants (Section 6.2.5) where the effect in temperature and HNO_3 concentration in a 70% HF solution was examined as a whole (e.g. Arrhenius plot, Figure 6.27).

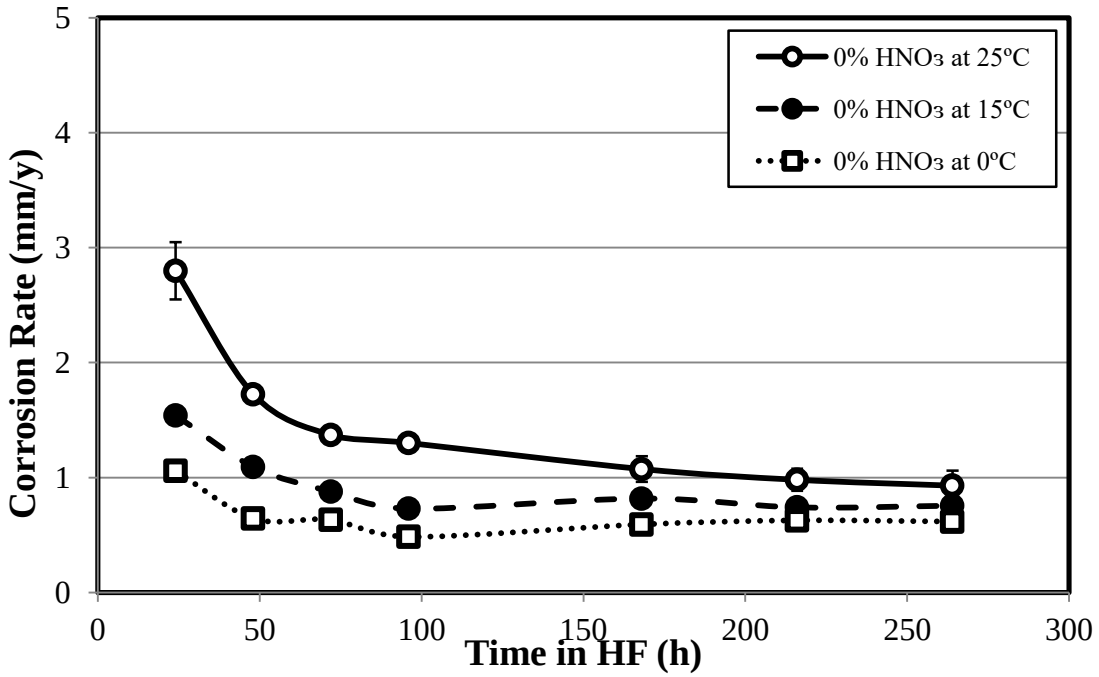

Figure 6.13: Effect of temperature on apparent corrosion rates of mild steel in pure HF (<50 ppm HNO_3). Error bars obscured by markers in some instances.

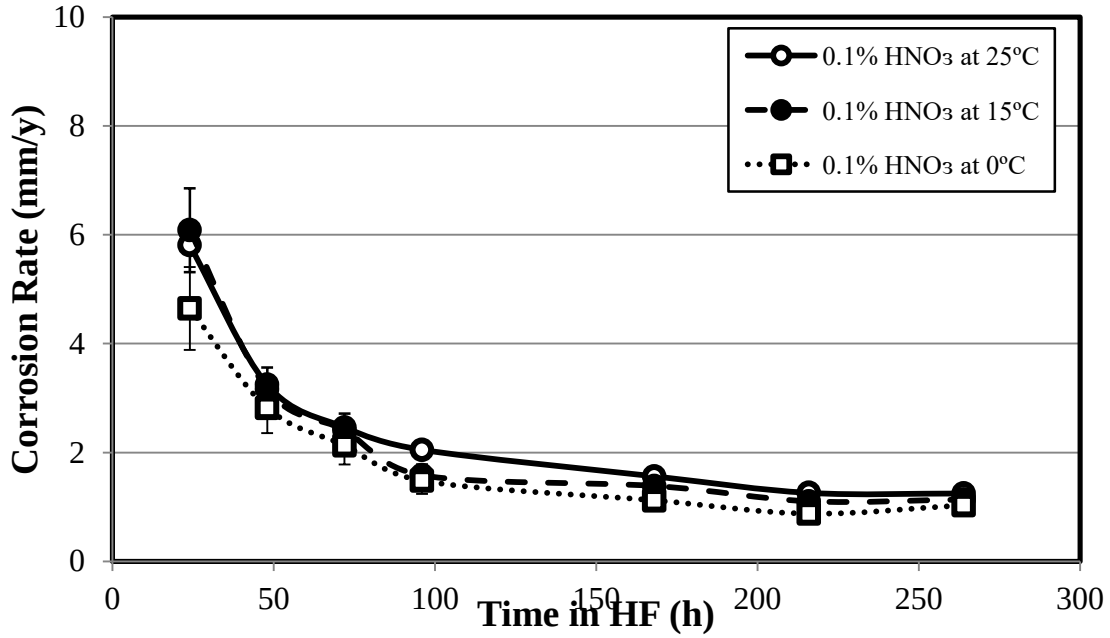

Figure 6.14: Effect of temperature on apparent corrosion rates of mild steel in 70% HF spiked with 0.1% HNO_3. Error bars obscured by markers in some instances.

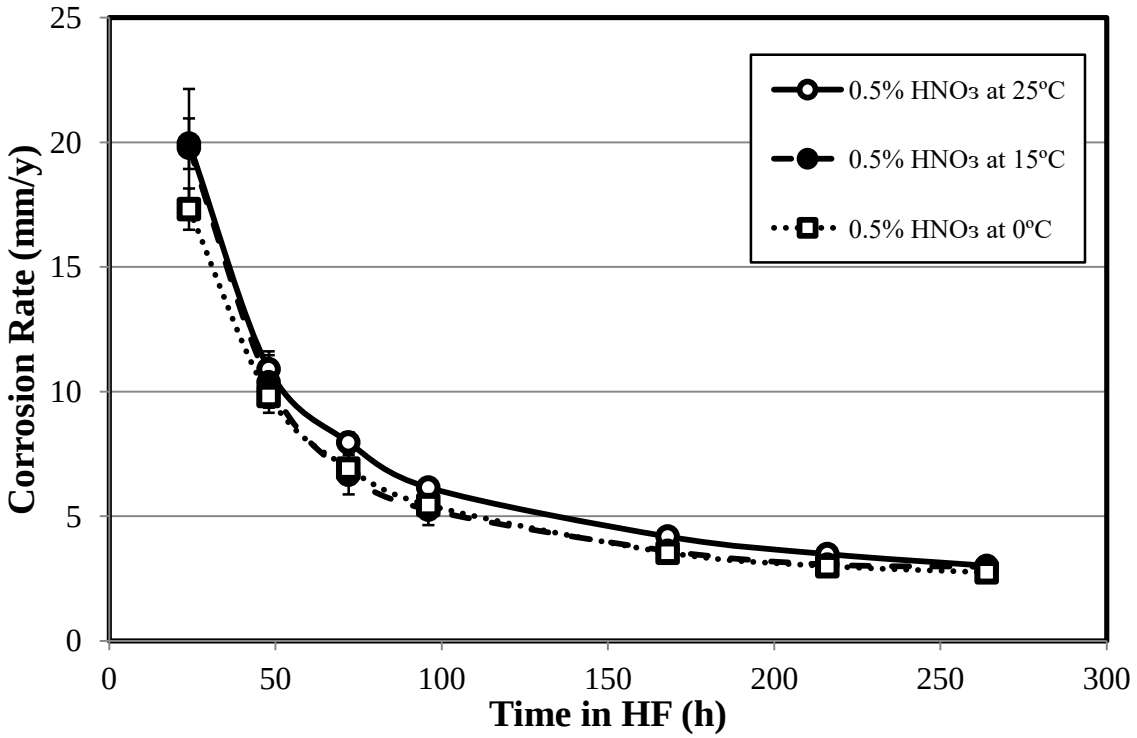

Figure 6.15: Effect of temperature on apparent corrosion rates of mild steel in 70% HF spiked with 0.5% HNO_3. Error bars obscured by markers in some instances.

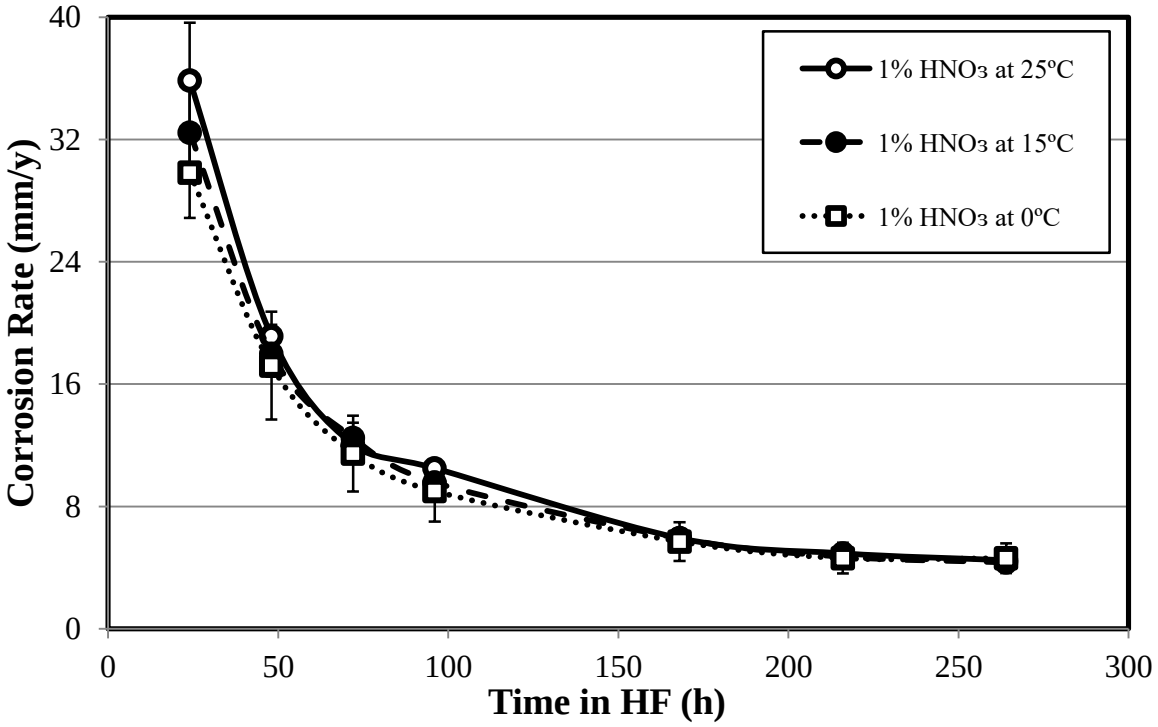

Figure 6.16: Effect of temperature on apparent corrosion rates of mild steel in 70% HF spiked with 1% HNO_3. Error bars obscured by markers in some instances.

Acid consumption

The lowest concentration of HNO_3 spiked into the corrosion solution was 0.1% which produced the lowest HF corrosion rate (>0.2%) at the lowest temperature tested (0ºC). However, conducting corrosion tests at 15ºC drastically increased the HF acid consumption to ~2%, and this acid consumption more than doubled at 25ºC. Similar corrosion tests where 0.5% HNO_3 was spiked also showed a slight increase with increased temperature (>0.02% HF consumed per 1ºC rise in temperature), but it was not as severe as for corrosion tests spiked with 0.1% HNO_3. Corrosion tests where HF was spiked with 1% HNO_3 produced the highest HF acid consumptions at all temperatures (Figure 5.20). In the presence of 1% HNO_3 in the corrosion solution, HF consumption increased with approximately 0.1% HF consumed per 1ºC increase in temperature. This was still half the HF consumed per 1ºC increase measured for HF spiked with 0.1% HNO_3 (at a gradient of 0.2% HF consumed / ºC). Thus, when the HNO_3 concentration in solution was low (up to 0.1%), the HF acid consumption was mostly dependent on temperature change, while at high HNO_3 concentrations (1% HNO_3) higher HF acid consumption was more a result of HNO_3 corrosion than temperature. This was because the HNO_3 is consumed when taking part in the reaction with the fluoride scale (Equation 6.1) and dissolves it, which then exposes the underlying mild steel substrate

(99% Fe) to the HF acid in solution, whereby it is consumed in higher quantities (Figure 5.20) during the scale forming reaction (Equation 1.1).

6.2.3. Stainless steel corrosion

6.2.3.1. Effect of nitic acid concentration

Mass loss and apparent corrosion rates

Stainless steel 904 L reacted with pure 70% HF, as well as HF spiked with 1% HNO_3, in a completely opposite way to any of the other metals tested. Where scale formation on mild steel coupons mitigated attack by pure 70% HF (~0.0076% mass loss per hour, Figure 6.7), the oxide scale formed on stainless steel (Figure 5.44; Row b and c) did not protect against corrosion, since the mass loss by SS 904 L continued to be high (~0.052% mass loss per hour, Figure 6.17). Moreover, contradictory to mild steel and nickel alloy tested (Figures 6.6 and 6.19) in 70% HF spiked with a maximum of 1% HNO_3, exceptionally low percentage mass losses (<1.6%) were recorded for SS 904 L under the same corrosive conditions. This was because mild steels and nickel alloys are different from stainless steels, which depend on the formation of a passive oxide layer for its corrosion resistance in a corrosive environment (Singh & Gupta, 2001; Olsson & Landolt, 2003). Therefore, the large difference between mass losses recorded for stainless steel in pure 70% HF and HF containing 1% HNO_3 reinforced the necessity of an oxidizing acid in a corrosive solution, if SS 904 L is to be used for construction materials in plants exposed to HF.

No considerable change in apparent corrosion rate for stainless steel in pure 70% HF was observed (0% HNO_3 trend in Figure 6.18). SS 904 L coupons continued corroding at a rate of nearly 5 mm/y for the entire duration of the corrosion tests. It was estimated that at a constant corrosion rate of 5 mm/y, if corrosion tests were to continue for a further 70 days, the stainless steel coupons would have been dissolved completely. Therefore, without the presence of an oxidizing acid in the corrosion solution, stainless steel would provide no corrosion resistance to 70% HF. Thus, in an HF solution containing HNO_3, the oxygen required by the chromium component in stainless steel to form the passive oxide film (Cr_2O_3) can be supplied by the oxygen component of HNO_3 by following Equation 6.2, acquired from Davenport (2016):

$$4Cr + 2HNO_3 \rightarrow 2Cr_2O_3 + H_2 + N_2 \qquad \text{Equation 6.2}$$

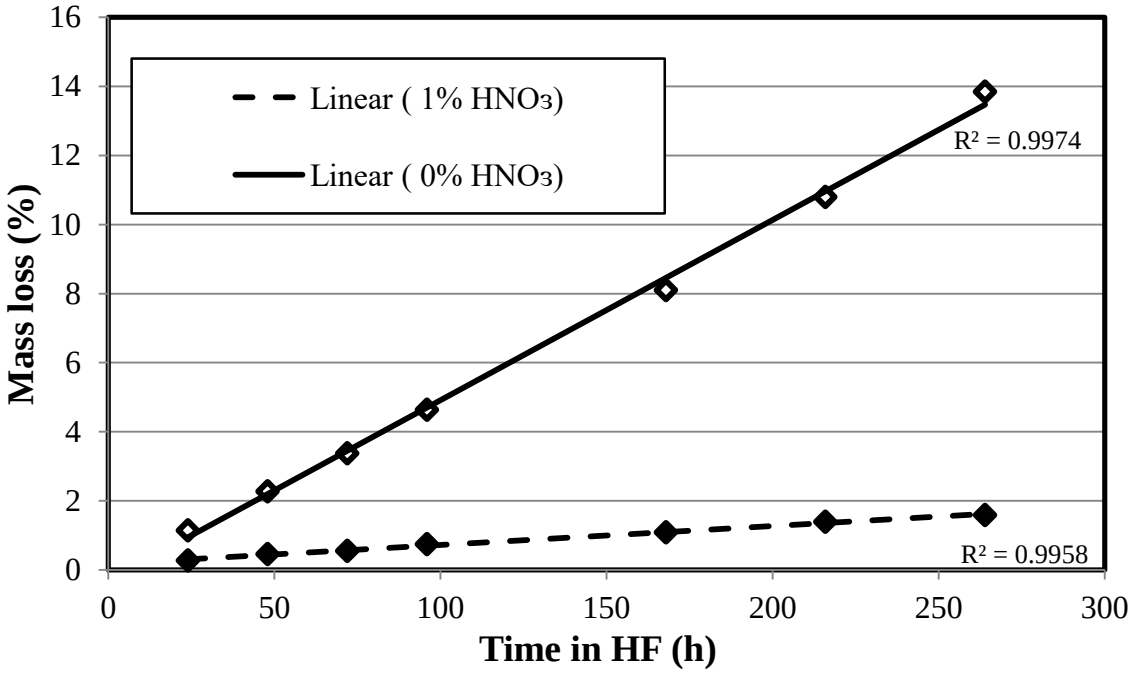

Figure 6.17: Effect of HNO_3 concentration on mass loss of stainless steel when corroded in 70% HF at 25ºC. Error bars obscured by markers in some instances.

Conversely, in CTs where 1% HNO_3 was spiked, SS 904 started with a higher corrosion rate (2.3 mm/y) that quickly slowed down at a rate of ~0.014 mm/y for every hour spent in solution (gradient of initial rate in Figure 6.19) for the first 72 h. After 96 hours, the apparent corrosion rate slowed down evenly at a rate of ~0.0021 mm/y for every hour spent in solution (gradient of proceeding rate in Figure 6.19) and it was estimated that if that deceleration in the corrosion rate would remain constant, the stainless steel coupons would cease to corrode under those test conditions after 24 days. The visible transition from an initially fast corrosion rate slowing down fast and proceeding to slow down more steadily (Figure 6.19) was indicative of passivation occurring on the surface of the coupons at this transition point (between 72 h and 96 h in solution). Once stainless steel was exposed to the HF containing HNO_3 for the first time, the formation of the passive oxide film initiated Under the corrosive conditions tested, this passive layer quickly formed (within ~72 h, according to Equation 6.2) to actively resist corrosive attack by HF, as it continued to attack the coupons surfaces at a high apparent corrosion rate. Subsequently, when the passive oxide film successfully formed, it continued to stabilize and then continued to resist corrosive attack more passively (slower rate). Nitric acid consumption in this CT supported these results (Figure 5.47) since it was the only test where all the nitric acid was not consumed after 11 days (~65% HNO_3 consumption). Therefore, HNO_3 was consumed up to a point, and then ceased once it stopped taking

part in the corrosion and passivation reactions, at around 72 h in solution (where initial and proceeding rates intersected, Figure 6.19). Thus, 1% HNO_3 in a 70% HF solution succeeded in completely passivating the mild steel coupons, with approximately 0.052 g of HNO_3 needed to passivate 1 g of stainless steel in a 70% HF solution (g_{Alloy}/g_{HNO3} recorded in Table 5.40).

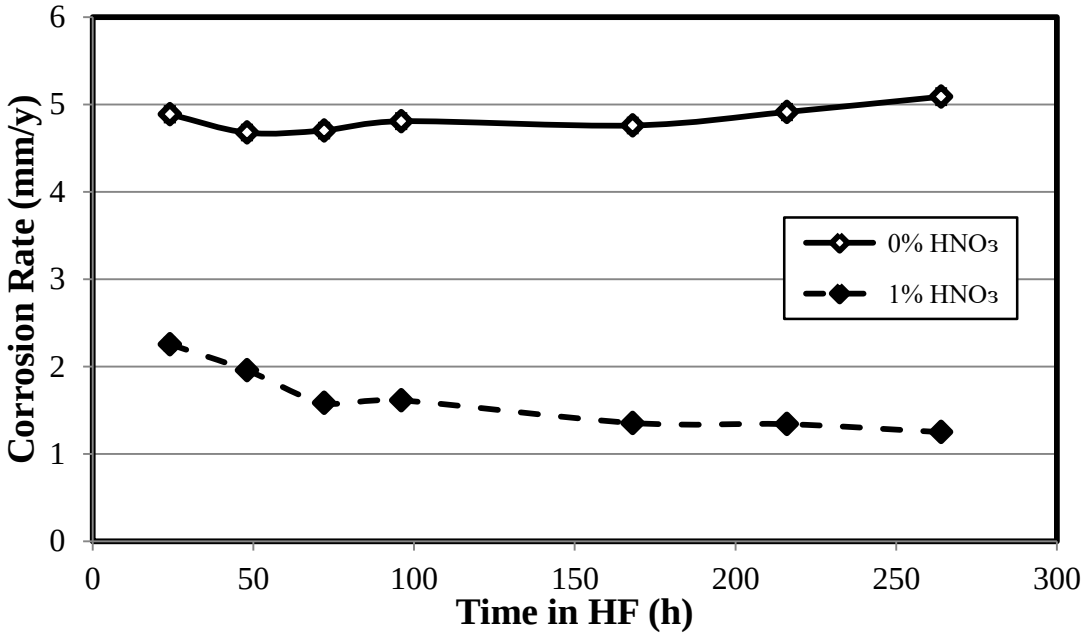

Figure 6.18: Effect of HNO_3 concentration on the apparent corrosion rate of stainless steel in 70% HF, at 25ºC. Error bars obscured by markers in some instances.

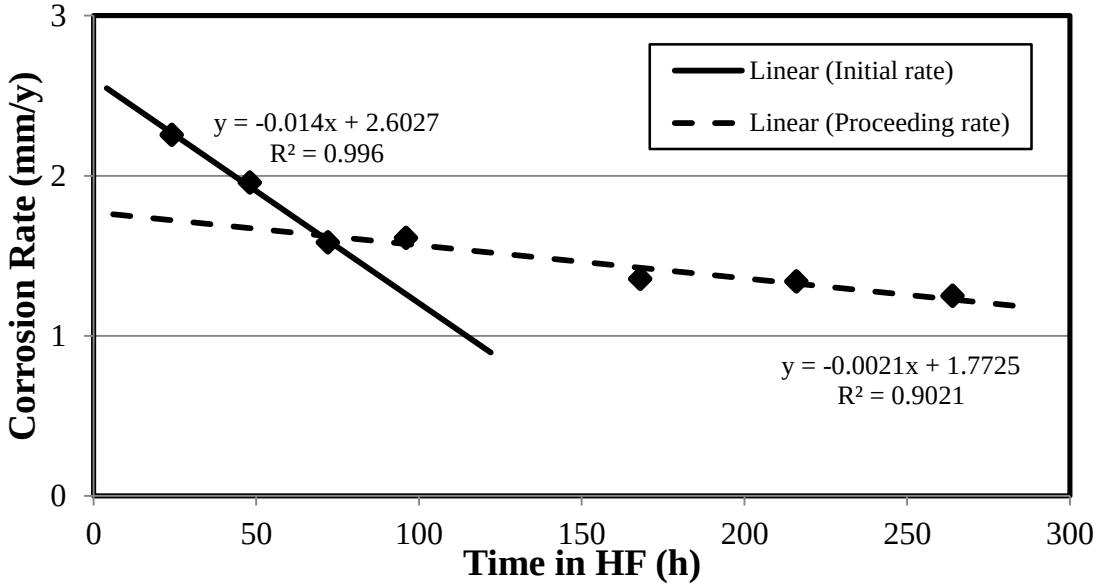

Figure 6.19: Transition from fast initial apparent corrosion rate to slower proceeding rates evident for stainless steel corrosion in 70% HF with 1% HNO_3, at 25ºC. Error bars obscured by markers in some instances.

6.2.4. Nickel alloy corrosion

6.2.4.1. Effect of nitric acid concentration

Mass loss and apparent corrosion rates

Monel 400 coupons maintained the lowest percentage mass loss in pure 70% HF (<50 ppm HNO_3) of all coupons tested in the 11 day CTs (<0.8%, Figure 6.20). Thus, in these tests, the superior corrosion resistance of nickel alloys to stainless and mild steels in relatively pure HF solutions was demonstrated. However, in CTs where 1% HNO_3 was spiked into the HF corrosion solution, the Monel 400 indicated signs of corroding away excessively after 11 days (~20% mass loss). Mass loss by the nickel alloys was initially the same as mild steel exposed to the same conditions (~9% at 24 h in solution). However, conversely to mild steel, the percentage mass loss rapidly increased, then decreased slightly after 7 days in solution (to ~0.02% mass loss per hour after 168 h). Contrary to the steels tested in 70% HF spiked with 1% HNO_3 (Figure 6.7 for mild steel and Figure 6.17 for stainless steel), the nickel alloy did not follow a linear trend with mass loss, but rather a logarithmic trend (Figure 6.20). Thus, if mass loss through HNO_3 in HF corrosion continued according to the logarithmic function, mass loss from the nickel alloy coupons would continue, but at an ever declining rate (>0.4% mass loss per day). Since HNO_3 was found to be nearly completely consumed after 264 hrs in solution (Figure 5.47), it was estimated that the corrosion rate would fall below 0.3 mm/y if the corrosion tests were allowed to run over 15 days (Figure 6.24). However, due to the short time of the CTs, it could not be established if the nickel alloy returned to its superior corrosion resistance (loosing no further mass) after all the HNO_3 was consumed when leaving only HF behind. This is particularly true since the excessive mass loss by Monel 400 dip tubes, when exposed to a 70% HF environment contaminated with up to 1% HNO_3, showed failure (Figure 2.4).

For nickel alloy coupons in 70% HF the corrosion product solutions analysed had very low traces of nickel, copper and iron (Table 5.47). Thus, less than 0.4% of each metal present in the coupons reported to the final corrosion solution. This supports previous observations (PICTs on Monel 400 summarized in Table 5.19) that the surface of the nickel alloy was only cleaned and underwent no further corrosion afterwards. However, when 1% HNO_3 was spiked into the HF corrosion solution, the metals in the solutions were the highest of any corrosion tests (Ni measured at ~13460 ppm). Copper was removed most from the coupons (>17%), with iron and nickel removal at approximately

the same proportions (~15%). Therefore, copper in the nickel alloys were slightly more susceptible to corrosive attack by the HF and HNO_3 combination (Table 5.47).

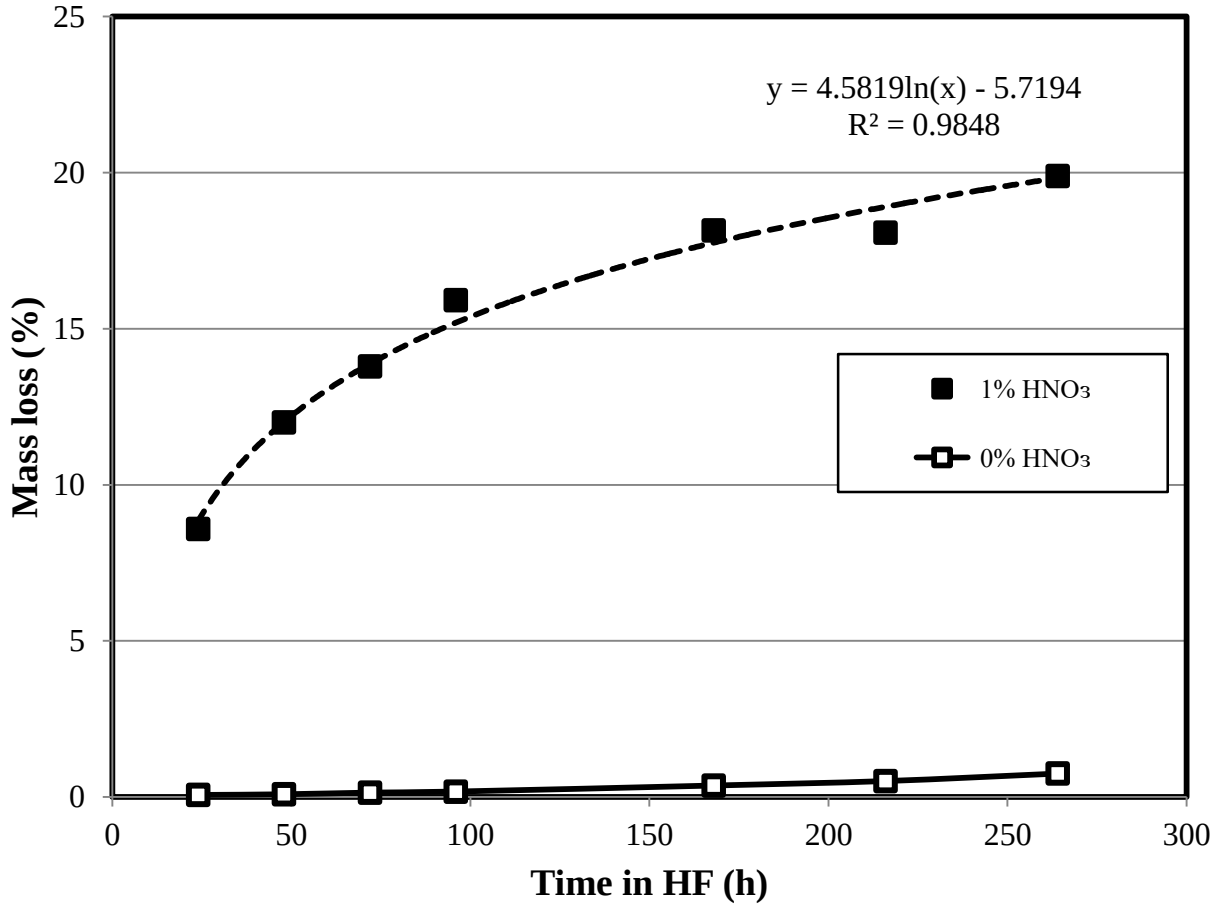

Figure 6.20: Effect of HNO_3 concentration on mass loss of nickel alloy when corroded in 70% HF at 25ºC. Error bars obscured by markers in some instances.

As supported by mass loss profiles (Figure 6.20), the nickel alloy corroded negligibly in pure 70% HF, demonstrated by the apparent corrosion rate did not exceed 0.3 mm/y at any point in the CT. Whilst the nickel alloy maintained the lowest corrosion rate in 70% HF, it also held the record in the study for the highest apparent corrosion rate measured when 1% HNO_3 was present in the corrosion solution. Within the first 24 hours Monel 400 coupons corroded at a rate of nearly 40 mm/y, whilst the fastest apparent corrosion rate measured for mild steel under the same conditions reach its peak at 36 mm/y. However, the corrosion rate of Monel 400 decreased to less than ~22 mm/y within 72 h at a rate ~0.4 mm/y for every hour spent in solution (gradient of initial rate in Figure 6.24). Subsequently, a rate change took place after 72 h in solution and coupons corroded even slower as the inherent resistance of nickel alloy to HF attack appeared to be re-establishing. It was estimated,

from the declining in the apparent corrosion rate (proceeding rate in Figure 6.22), that the Monel coupons left in the pure HF solution (<1 ppm HNO_3, Table 5.46), would cease to corrode if the CT continued a further 4.5 days.

This same tendency occurred for stainless steel at 72 h (Figure 6.19), although stainless steel corroded significantly slower. This was explained by repeat GD-OES analysis of the original (sand-blasted and ultrasonically cleaned) stainless steel coupon surfaces, revealing that SS 904 L possessed an oxide layer of nearly 68 µm thick, whilst the original Monel 400 coupons possessed an oxide layer that was nearly half as thick (37 µm) when analysed using the same technique. Therefore, stainless steel had a thicker more, resilient oxide layer going into the contaminated HF, while the nickel alloy was at a disadvantage. The nickel alloy relied more on the intrinsic corrosion resistance of its nickel and copper components, while stainless steel relied more on the presence of chromium to regenerate its oxide layer (Schillmoller, 1995). The nickel and copper components in Monel 400 was not as effective in regenerating its relatively thin oxide layer in the presence of HNO_3 as SS 904 L was, and therefore corroded faster under the same conditions. These characteristics of the nickel alloy made it unsuitable for use in HF solutions contaminated with an oxidizing acid.

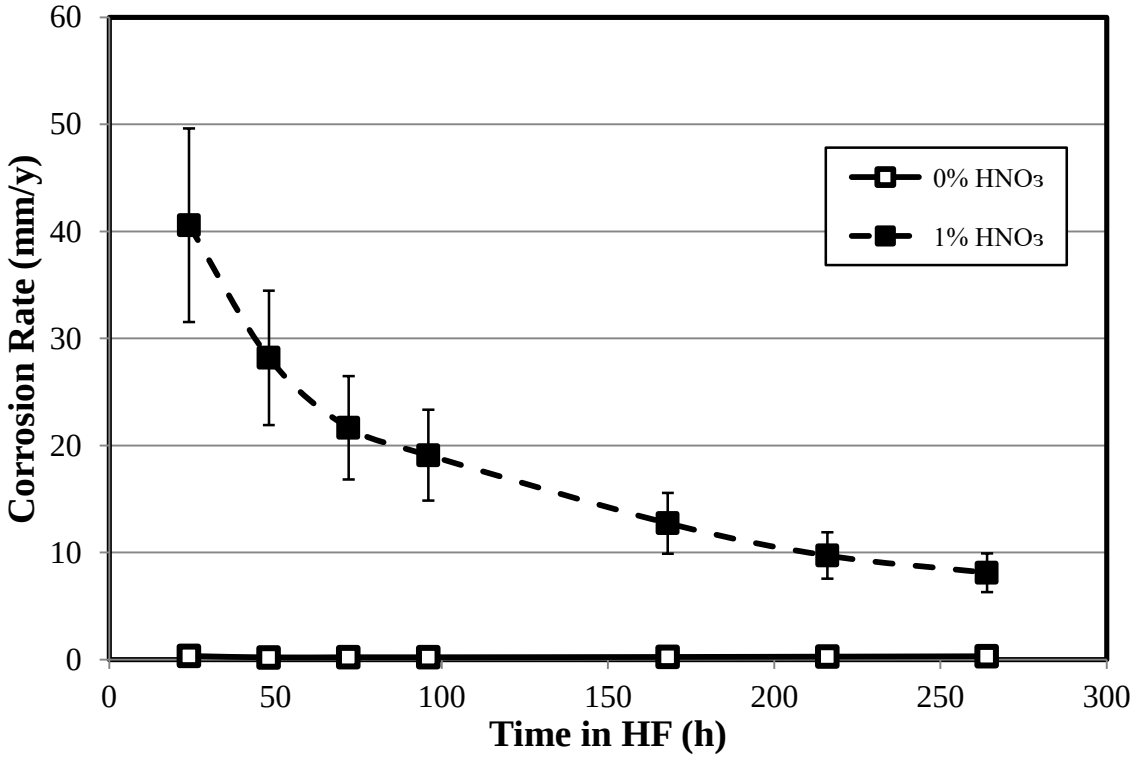

Figure 6.21: Effect of HNO_3 concentration on the apparent corrosion rate of nickel alloy in 70% HF at 25ºC. Error bars obscured by markers in some instances.

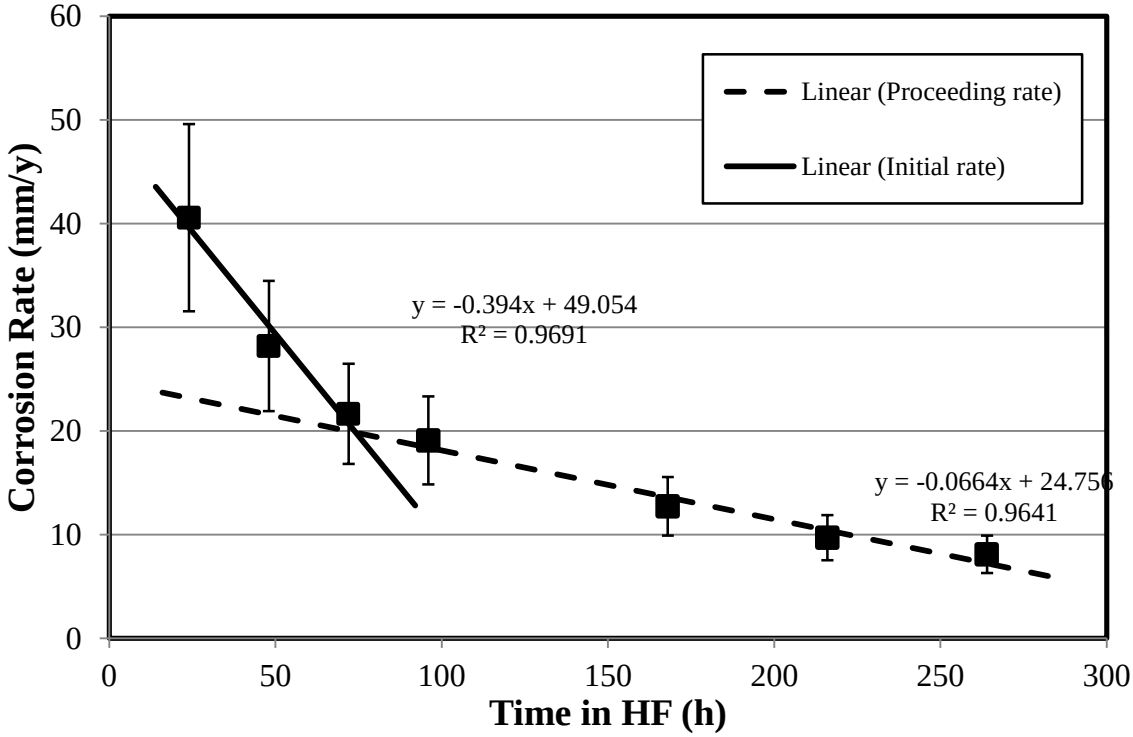

Figure 6.22: Effect of HNO_3 concentration on the apparent corrosion rate of nickel alloy in 70% HF at 25ºC. Error bars obscured by markers in some instances.

6.2.5. Kinetics and rate constants

6.2.5.1. Purpose of kinetic study

Chemical kinetics focusses on the quantitative determination of the rates of chemical reactions and the factors on which these rates depend (Khadom & Abdul-Hadi, 2014). This kinetics study was conducted as a physical chemical means of examining corrosion rates in HF solutions. It differs from the conventional means of examining corrosion rates in that the metal gained by the corrosion solution was the subject, instead of metal lost by the coupons from the corrosion reactions. During a corrosion test, the variables altered affected the rate of metal (iron, chromium, nickel, molybdenum, copper and manganese) extraction from the coupons, which led to an increase in metal concentration in corrosion solution. In all CTs conducted, there were no residues found after 11 days and therefore all metal remain in solution as ions. Therefore, collective metal lost by coupons was equal to metal gained by the corrosion solution. This was confirmed by analyses of the final solutions (Tables 5.34 – 5.37) which related well to the combined mass losses of all coupons recorded, for the CTs conducted.

The scope of the kinetic study was mostly concerned with the removal rates of iron from mild steel coupons (since mild steel is 99% Fe), or metals from stainless steel and the nickel alloy (combination of all metals ions in solution). Since the volume of the corrosion solution was known (and relatively constant throughout at 460 – 463 mL), the mass of metal lost by each coupon was used as the basis for determining the concentration of metal in solution (in g/L).

Quantification of the corrosion kinetics was carried out in terms of the reaction kinetics of metals extracted from the coupons, by comparison of rate constants (k) and activation energy (E_a).

6.2.5.2. Determining rate constants

The reaction kinetics of steel and metallic alloy coupons was described by means of rate constants (k), which were determined for each corrosion test. The suitability of a curve to fit a set of corrosion data was determined by means of linear graphs. Here, the correlation factor (R^2) was used to either reject the corrosion data from representing a rate family (Levenspiel, 1999; Perry, 2011) or offer evidence towards its suitability. The R^2 value was derived from a trend line on corrosion data plotted, which provided the measure of reliability of a linear relationship between the time in corrosion solution (x values) and metal concentration (y values). An R^2 value close to 1 indicated the linear reliability of a set of corrosion data and the degree to which the data fitted the rate family selected.

Already, during the first evaluation of mass loss trends (Figure 6.7), it was realized that mass loss by the coupons to the corrosion solution followed a linear trend. Converting metal removed from the coupons to metal concentration in a corrosion solution, and then plotting it against the same residence time did not affect this linear relationship. Therefore, the corrosion of steel and metallic alloy belonged to the first order rate family (Levenspiel, 1999), as metals were observed to typically corrode following a first order reaction. Thus, k could be obtained using the first order rate equation for mild steel:

$$\frac{d[\mathrm{Fe}]}{dt} = k \text{ and thus: } [\mathrm{Fe}] - [\mathrm{Fe}]_0 = kt \qquad \text{Equation 6.3}$$

as well as stainless steel and nickel alloy:

$$\frac{d[\mathrm{Metal}]}{dt} = k \text{ and thus: } [\mathrm{Metal}] - [\mathrm{Metal}]_0 = kt \qquad \text{Equation 6.4}$$

Combined effect of temperature and nitric acid concentration

The integrated rate method (Equation 6.3) was used to determine the rate constants (k) for each corrosion test on mild steel coupons in which temperature and HNO_3 concentration were varied (Figures 6.22 – 6.25). As seen with percentage mass loss from the coupons (Figures 6.8 – 6.11), corrosion tests ran at lower temperatures resulted in lower metal concentrations when coupons were corroded by HF contaminated with HNO_3. However, as seen with the apparent corrosion rate trends (Figures 6.12 – 6.15), the effect of higher HNO_3 concentration was more apparent. For instance, in corrosion tests where HNO_3 concentration was low (≤0.1% HNO_3), regression lines started parallel and then diverged with corrosion time (Figures 6.22 and 6.23). Conversly, corrosion tests with higher HNO_3 concentrations (≥0.5% HNO_3) had converging regression lines which started off in close proximity (Figures 6.24 and 6.25).The only factors influencing iron dissolution from mild steel in pure HF that could cause the diverging regression lines in Figure 6.23, in order of rate controlling action were:

1. Temperature,
2. Chemical reaction of the still exposed steel surface with HF in solution (Equation 1.1), and
3. Diffusion of HF through the fluoride scale to corrode the steel.

It was established in Section 5.12 that 24 h was not sufficient to completely passivate the mild steel in HF on a laboratory scale, and when comparing Figure 5.38 (~10 µm of scale formed after 24 h in pure HF) and Figure 5.39 (~60 µm of scale formed after 11 days in pure HF). The growth in scale demonstrated that scale kept growing in pure HF to confirm action 2 above. Thus, because temperature directly influenced the rate of mild steel corrosion by causing the rate controlling actions 2 and 3 to take place sooner, the lines diverged because action 2 went to completion quicker, and action 3 then initiated earlier at higher temperature (25ºC) compared to the lower temperature (0ºC). However, introducing a second oxidizing acid (0.1 – 1% HNO_3) added another factor, which affected the iron dissolution kinetics in the mother (70% HF) solution and caused the regression lines to change from being diverging (Figure 6.24) to being more parallel (Figure 6.25), and eventually converging (Figure 6.26) as directly related to the amount of HNO_3 spiked per test. Thus, as seen with apparent corrosion rate regressions, corrosion rates were more readily influenced by HNO_3 in solution than the solution temperature, so that the number of rate controlling actions in the spiked HF solutions increased:

1. Temperature,

2. Chemical reaction of the still exposed steel surface with HNO_3 (Equation 5.2),
3. Dissolution of fluoride scale formed in pure HF, during the passivation step (Equation 6.1),
4. Chemical reaction of the still exposed steel surface with HF in solution, and
5. Diffusion of HF through the fluoride scale to corrode the steel.

Since the higher temperature (25ºC) still increased the reaction rates of HNO_3 with the steel substrate and fluoride scale (actions 2 and 3 directly above), the higher HNO_3 concentration dissolved more iron from the steel substrate, as well as the scale, into the HF corrosion solution and was consumed more quickly. When HNO_3 was completely consumed, it could no longer take part in controlling the iron dissolution and thus all reactions converged to a point (Figure 6.26), after which they would be expected to diverge again (after 264 h) as dissolution and HF corrosion would continue as before (actions 4 and 5). Due to the relatively short length of the corrosion tests, this divergence could not be verified. Those regression lines which appeared to have closer gradients were just prolonged intervals where converging lines were transitioning to diverging, caused by one rate controlling reaction subsiding and another starting to dominate (Figure 6.25).

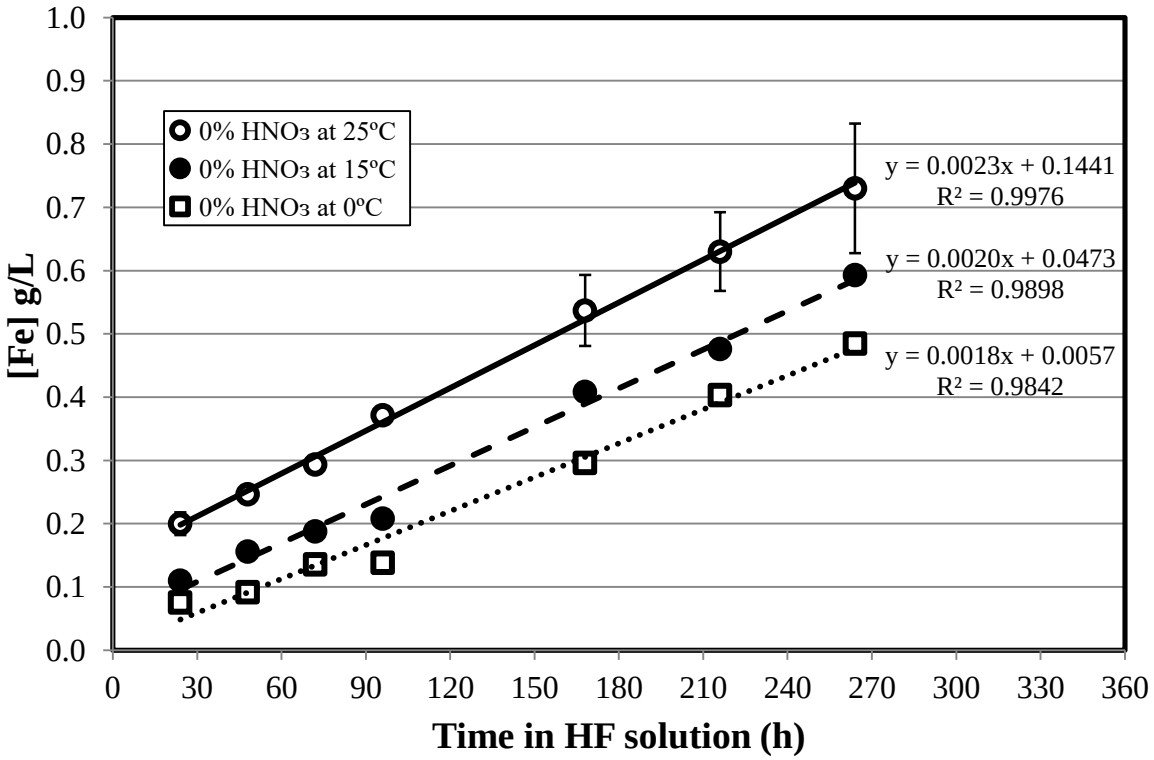

Figure 6.23: Effect of change in temperature on corrosion rates of mild steel in pure HF. Error bars obscured by markers in some instances.

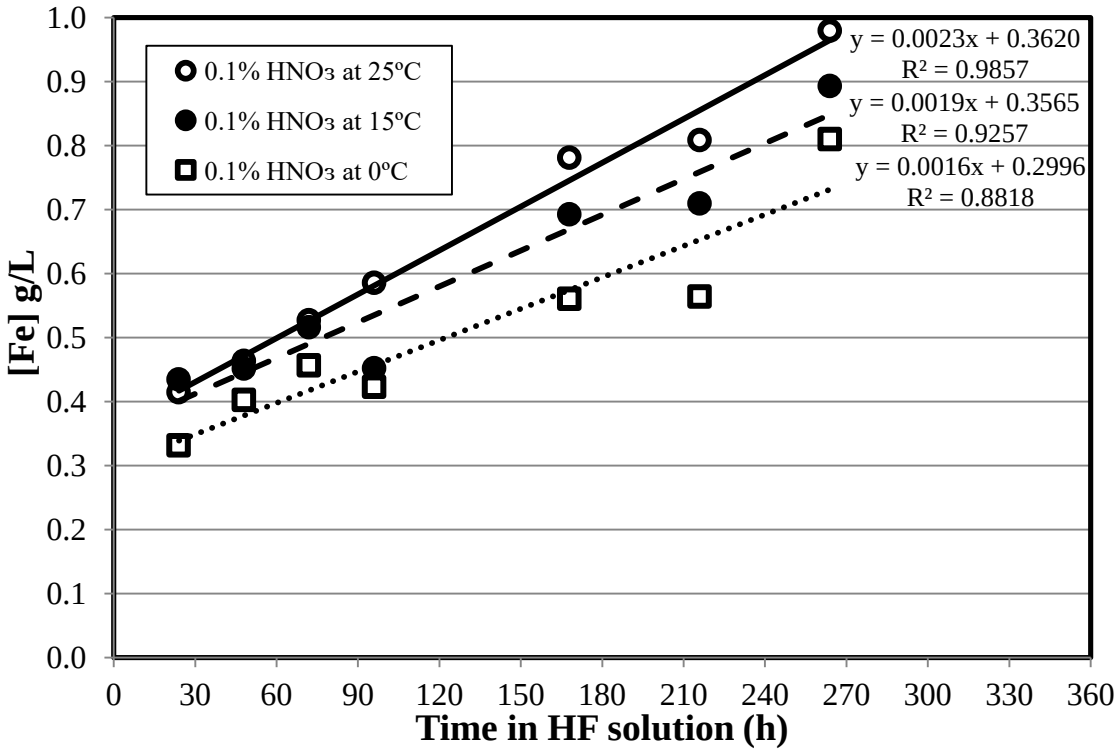

Figure 6.24: Effect of change in temperature on corrosion rates of mild steel in 70% HF spiked with 0.1% HNO_3. Error bars obscured by markers in some instances.

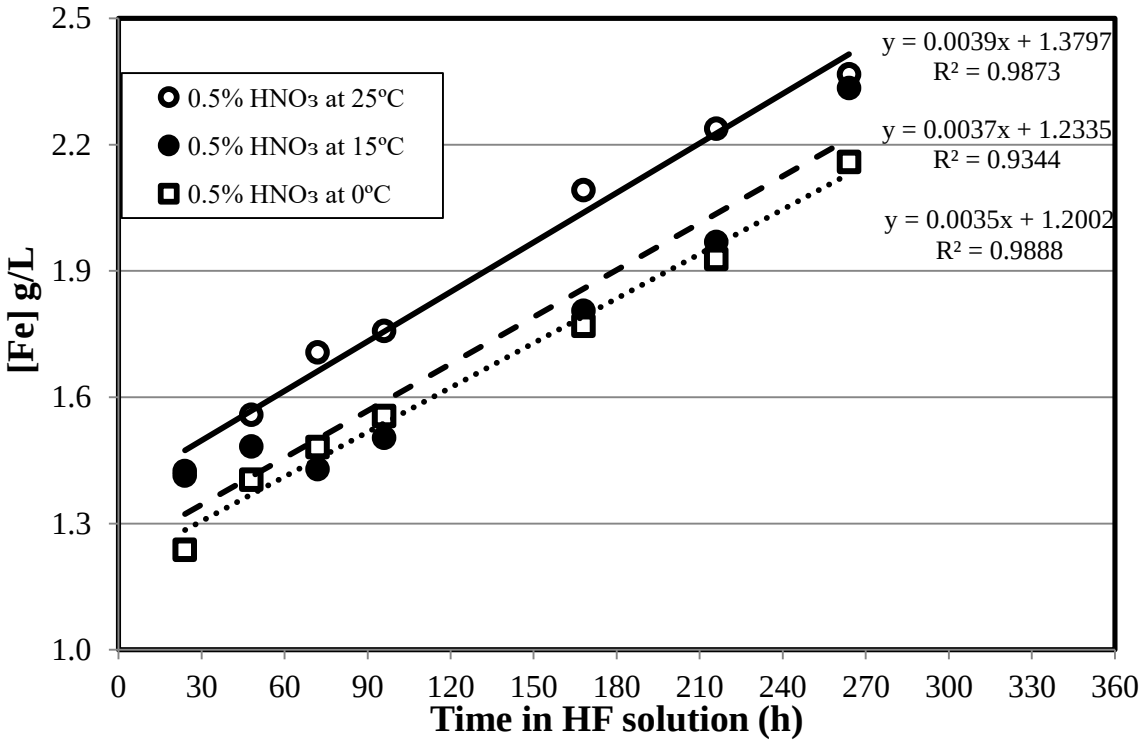

Figure 6.25: Effect of change in temperature on corrosion rates of mild steel in 70% HF spiked with 0.5% HNO_3. Error bars obscured by markers in some instances.

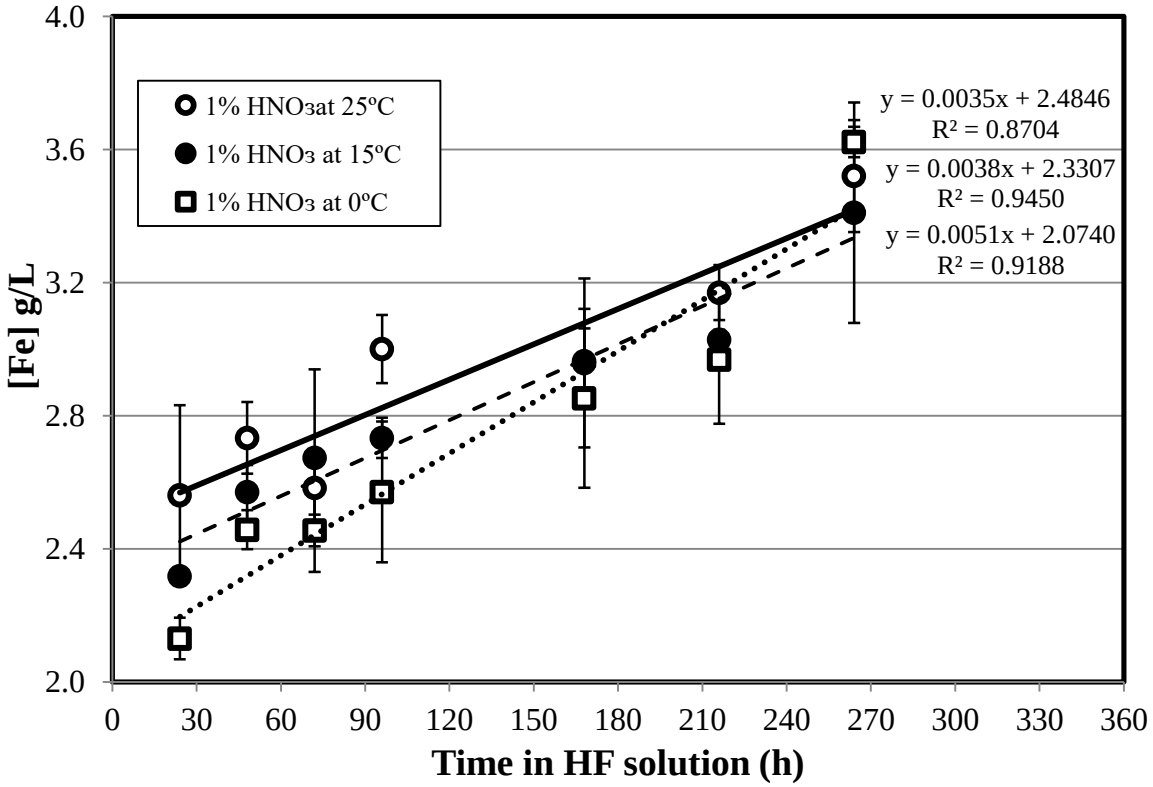

Figure 6.26: Effect of change in temperature on corrosion rates of mild steel in 70% HF spiked with 1% HNO_3. Error bars obscured by markers in some instances.

The corrosion rates of iron removed from mild steel coupons were highest at ~0.0023 g/L·h at the highest temperature tested (25ºC) when HNO_3 concentration in the corrosion tests were kept below 0.1% (Tables 6.1 and 6.2). The removal rates of iron from mild steel coupons in 70% HF with 0.5% HNO_3 had nearly double the amount of iron extracted at the same temperatures tested (Table 6.3). Therefore, in these tests, the combined corrosive effect of HNO_3 was observed, since an increase in temperature still produced the highest iron removal rates. Conversely, in corrosion tests where HNO_3 in solution was at 1%, the lowest temperature tested (0ºC) produced the highest iron removal rate (0.0512 g/L·h) of all tests conducted (Table 6.4). Thus, since lower temperatures slowed down HF reaction rates, it encouraged HNO_3 attack.

Table 6.1: Kinetics data from corrosion tests on mild steel in pure HF.

Temperature	**Rate constants from [Fe]**		**Activation Energy (E_a)**	
ºC	**(g/L·h)**	**(mol/L·sec)**	**ln(k)**	**1/T**
25	0.002252	1.12×10^{-8}	-18.31	0.00201
15	0.002037	1.01×10^{-8}	-18.41	0.00205
0	0.001786	8.88×10^{-9}	-18.54	0.00211
			E_a = 18.05 kJ/mol·K	

Table 6.2: Kinetics data from corrosion tests on mild steel in HF spiked with 0.1% HNO_3.

Temperature	**Rate constants from [Fe]**		**Activation Energy (E_a)**	
ºC	**(g/L·h)**	**(mol/L·sec)**	**ln(k)**	**1/T**
25	0.0023	1.14×10^{-8}	-18.29	0.00201
15	0.0019	9.45×10^{-9}	-18.48	0.00205
0	0.0016	7.96×10^{-9}	-18.65	0.00211
			E_a = 27.37 kJ/mol·K	

Table 6.3: Kinetics data from corrosion tests on mild steel in HF spiked with 0.5% HNO_3.

Temperature	**Rate constants from [Fe]**		**Activation Energy (E_a)**	
ºC	**(g/L·h)**	**(mol/L·sec)**	**ln(k)**	**1/T**
25	0.00392	1.95×10^{-8}	-17.75	0.00201
15	0.00372	1.85×10^{-8}	-17.81	0.00205
0	0.00353	1.75×10^{-8}	-17.86	0.00211
			E_a = 8.22 kJ/mol·K	

Table 6.4: Kinetics data from corrosion tests on mild steel in HF spiked with 1% HNO_3.

Temperature	**Rate constants from [Fe]**		**Activation Energy (E_a)**	
ºC	**(g/L·h)**	**(mol/L·sec)**	**ln(k)**	**1/T**
25	0.00354	1.76×10^{-8}	-17.86	0.00201
15	0.00380	1.89×10^{-8}	-17.78	0.00205
0	0.00512	2.54×10^{-8}	-17.49	0.00211
			E_a = -29.74 kJ/mol·K	

With the rate constants associated with each CT conducted on mild steel obtained (Tables 6.1 – 6.4), the Arrhenius relationship, within the temperature range of 0ºC to 25ºC (Ln *k* vs. 1/T) was plotted (Figure 6.27). From the Arrhenius plot, the activation energies (E_a) associated with each HNO_3 concentration in the corrosion solution, were determined and summarized in Tables 6.1 to 6.4.

The results indicated that the minimum energy required to remove iron from mild steel coupon surfaces in a pure 70% HF solution was approximately 18 kJ/mol·K. However, when spiking the HF with 0.1% HNO_3, the energy requirements increased by nearly 34% (to 27.37 kJ/mol·K). The increase in energy was due to increased scale formation by HF, attributed to the presence of HNO_3 ($\leq$0.1% HNO_3). The increase in scale formation, by the reaction of HF with the mild steel surface exposed by HNO_3 oxidation of the scale (Equation 1.1), was first identified in Figure 5.43.

Conversely, the energy required to corrode iron from mild steel coupons under same conditions dropped to below 10 kJ/mol·K, when the HNO_3 concentration increased five-fold (to 0.5%). This was indicative of high corrosion rates being a function of nitric acid attack, rather than thermal energy provided to the reactor. When HNO_3 concentration was at 1% in the corrosion reactor, the activation energy was nearly -30 kJ/mol·K. This specified that heat to the system had a negligible effect on the rate at which iron was extracted from the coupons under these conditions. Thus, at these high HNO_3 concentrations (≥1%), corrosion of the coupons was completely driven by oxidation of the steel surface by HNO_3 in the HF corrosion solution.

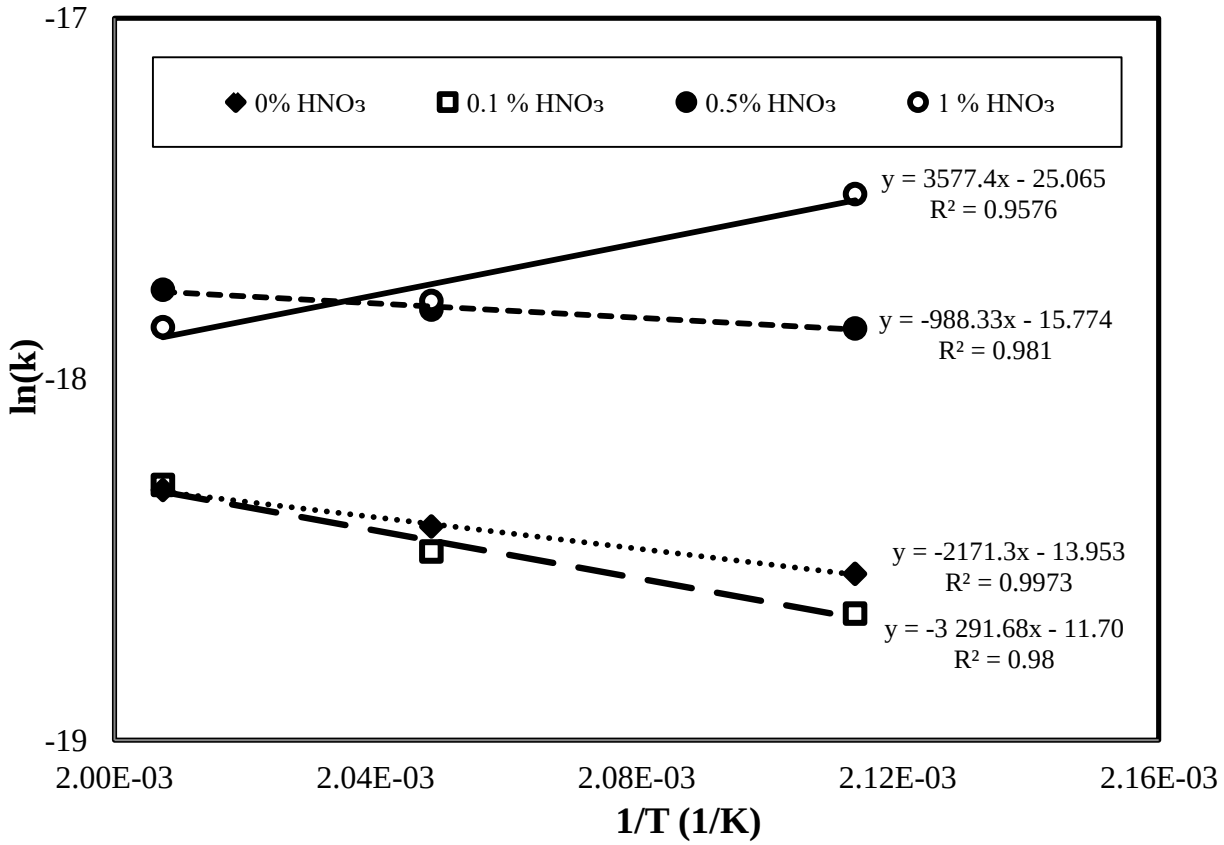

Figure 6.27: Effect of temperature and HNO_3 concentration on the corrosion reaction rate of mild steel in 70% HF, displayed on an Arrhenius plot.

The Arrhenius hypothesis states that when the temperature of a reaction is increased, the activation energy of the reactant molecules increases, thereby increasing the rate of the reaction (Levenspiel, 1999). Therefore, in an Arrhenius-type relationship, the concentration dependency of the corrosion reaction rate can be examined for the variation of the rate constant (ln k) with temperature (1/T), with the slope producing the activation energy (E_a) as seen for 0%, 0.1% and 0.5% HNO_3 in

Figure 6.27. Since Arrhenius hypothesis states that an increase in temperature will result in an increase in reaction rate, the convention is that the activation energy should be a positive value, and hence the negative sign $-Ea/\mathrm{R}$ in the Arrhenius-type relationship, shown in Equation 6.5:

$$k = k_0 e^{-\frac{Ea}{\mathrm{R}}} \text{ with } E_a = \left(-\frac{\mathrm{J}}{\mathrm{mol}}\right) \qquad \text{Equation 6.5}$$

Having a negative activation energy, as seen for the 1% HNO_3 CT in Figure 6.4, means that increasing the temperature decreased the corrosion reaction rate, which is thus in disagreement with the Arrhenius-type relationship. Activation energy was expected to always be positive, since the addition of heat provides energy to the iron atoms to move them from the steel surface into the solution. However, a negative activation energy does not necessary indicate an erroneous result (Revell & Williamson, 2013). The activation energy is a single representation of possible multiple, interplaying reactions (Vyazovkin, 2016). Each of these reactions has their own activation energy, which can either be positive or negative. The sum of these reactions combines into a single energy value, which is obtained from the Arrhenius curve. When HNO_3 was spiked into pure HF, removal of iron from the steel surface became a function of two corrosion reactions (HF and HNO_3), instead of one (HF only). Since HF was the bulk of the corrosion solution (>69%), it was considered to be the dominant corroding agent (in solutions with less than 0.5% HNO_3), and shown to be sensitive to temperature change (Figure 6.23). Hence, positive activation energies were prevalent where the HF was leading the corrosion reaction as an increase in temperature increased the corrosion rate (Tables 6.1 – 6.3). When HNO_3 in solution was more than 1%, the HF corrosion was replaced by HNO_3 as the dominant reaction and its dependence on temperature change reversed. Therefore, increased HNO_3 in solution produced the faster corrosion rates than increasing temperature and since the Arrhenius plot depends on rate change as a function of temperature, it was limited in explaining activation energy for these corrosion tests. Notwithstanding, the negative activation energy still indicated the high impact of HNO_3 concentration on the rate of mild steel corrosion in HF corrosion solutions.

The effect of nitric acid concentration on alloys tested

Dissimilar to mild steel (99% Fe), the SS 904 L and Monel 400 coupons used were alloys containing varying quantities of Ni, Cr, Mo, Fe, Cu and Mn (Tables 5.11 and 5.12), with each element present being susceptible to corrosion during corrosion tests. Thus, it was possible to quantify the corrosion rate of each alloy provided that the total metal (a function of the combined

mass of Ni, Cr, Mo, Fe, Cu and Mn lost by each coupon) by a coupon during a corrosion tests adhered to the same first order rate requirements as mild steel (Equation 6.4). This prerequisite was true for solutions where no HNO_3 was present. However, in 70% HF corrosion solutions containing up to 1% HNO_3, metals removed at a rate that did not follow a linear trend (Figure 6.29). Therefore, only rates from corrosion tests conducted in pure HF could effectively be compared (Figure 6.28).

In pure HF, metal was removed from Monel 400 coupons at a constant rate of 0.001 g/L·h (Table 6.5). This was nearly half the rate at which iron was removed from the pre-passivated mild steel coupon corroding under the same conditions. In the absence of an oxidizing agent present in pure 70% HF, stainless steel corroded nearly seven times faster than mild steel, indicating the significance of appropriate application of the steel in an HF plant.

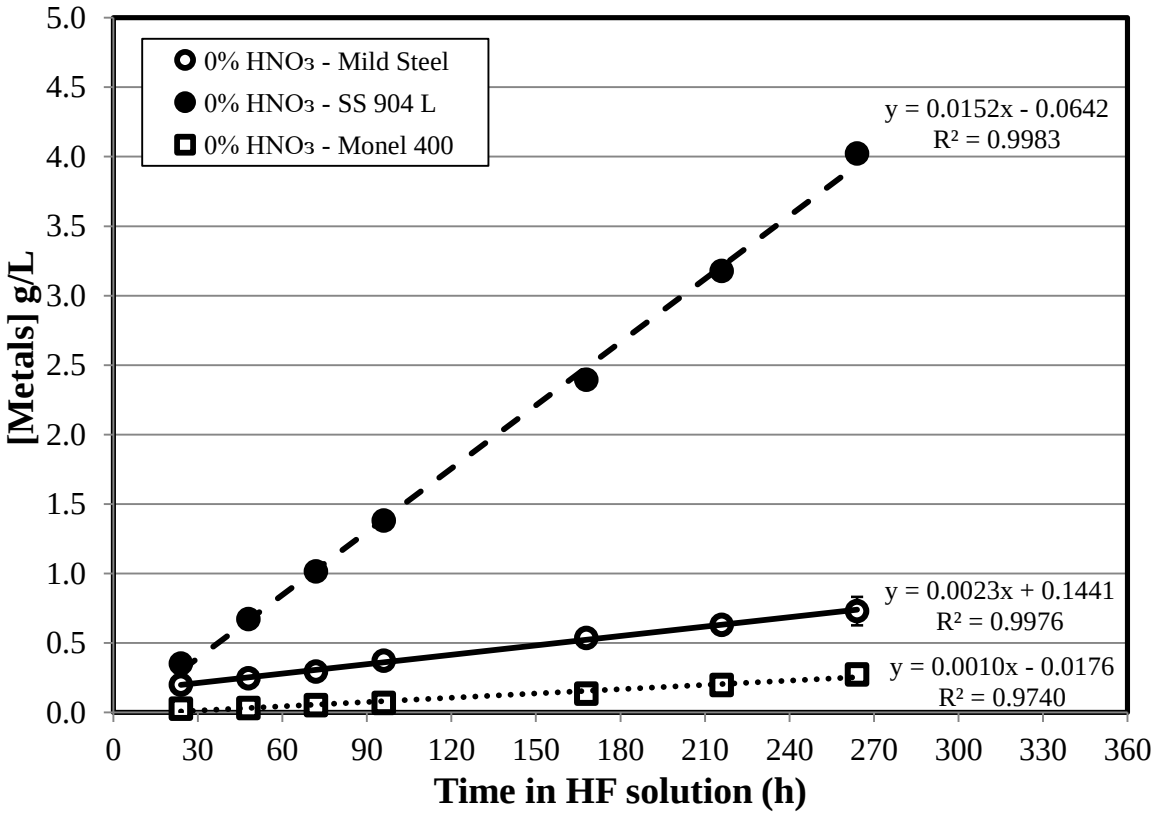

Figure 6.28: Dissolution rates of mild steel, stainless steel and nickel alloy in pure HF at 25ºC. Error bars obscured by markers in some instances.

Table 6.5: Kinetics data from corrosion tests on mild steel, stainless steel and nickel alloy in pure HF at 25ºC.

Metal	**Rate constants from [Metals] in solution (k) (g/L·h)**
Mild steel	0.0023
SS 904 L	0.0152
Monel 400	0.0010

Since all the steels and metallic alloys corroded in 70% HF spiked with 1% HNO_3 did not have linear relationships (R^2 <0.9), the corrosion rates using the first order rate equation could not be accurately derived (Figure 6.29). However, corrosion rates could loosely be compared to demonstrate the impact of HNO_3 in the corrosion solution on the metals used (Table 6.6). After 24 h, the concentration of the metals in solution, which resulted from mild steel corrosion, were approximately 13 times more than for stainless steel. Subsequently, metal was removed from the two steels at a rate of 0.003 g/L·h throughout the rest of their respective CTs. Thus, in both instances, after the initial corrosive attack, which resulted from the presence of HNO_3 in solution, both steels re-established their corrosive resistance and continued corroding at steady rate. For stainless steel, the presence of HNO_3 quickly regenerated the oxide layer needed by stainless steel to resist corrosive attack by HF. For mild steel, HNO_3 attacked the scale layer aggressively within the first 24 h, resulting in its early depletion, which in turn allowed HF corrosion to replenish the scale layer enough to resist further corrosive attack by HF. However, the nickel alloy did not re-establish its corrosion resistance in the same time as the two steels and continued corroding at a rate nearly double of what was determined for stainless steel in pure HF (~0.03 g/L·h). The exceptionally high rate at which metal was lost by the Monel coupons indicated that it reacted and consumed HNO_3 in solution within 168 h. After 168 h, a plateau was reached, since metal in solution remained at ~7 g/L for the remainder of the corrosion test (Figure 6.19). Thus, similar to mild steel, the corrosive reaction of HNO_3 in HF aggressively consumed HNO_3 and depleted it in the HF solution, after which it ceased to corrode the metal further.

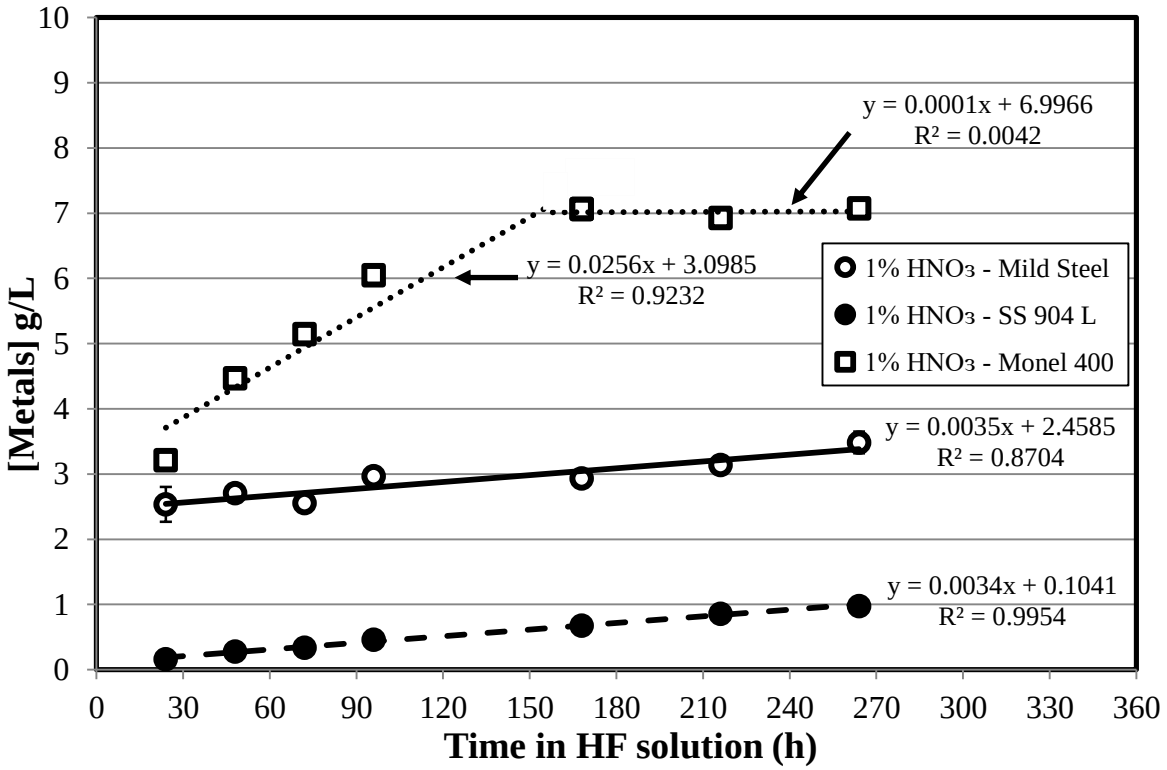

Figure 6.29: Dissolution rates of mild steel, stainless steel and nickel alloy in 70% HF spiked with 1% HNO_3 at 25ºC. Error bars obscured by markers in some instances.

Table 6.6: Kinetics data from corrosion tests on mild steel, stainless steel and nickel alloy in HF spiked with 1% HNO_3, at 25ºC.

Metal	**Rate constants from [Metals] in solution (k)**
	(g/L·h)
Mild steel	0.0034
SS 904 L	0.0035
Monel 400	0.0256

6.2.6. Summary

The corrosion rate and corrosion mechanism for mild steel (SA516 Grade 70 normalized), stainless steel (SS 904 L) and nickel alloy (Monel 400) in 70% HF contaminated with up to 1% HNO_3 were determined and are summarized in Table 6.7. A breakdown of the corrosion characteristics of each of these individual metals currently in service at the HF plant, as determined during the laboratory corrosion tests, is also provided. This section is intended to consolidate the findings made during this study prior to the conclusions.

Mild steel

HF product storage tanks are completely manufactured out of low cost carbon steels identical to the SA516 Grade 70 used in this study. This is because these steels form a dense oxide-fluoride scale when brought in contact with concentrated HF (>60%), which mitigates further corrosive attack from the HF present in the storage tanks. Thus, scale formation during a 24 hour pre-passivation step was essential to the corrosion resistance of mild steel coupons and implemented in all corrosion tests. Prolonged exposure of the pre-passivated mild steel to pure HF thickened the scale layer, causing a further deceleration in the corrosion of the steel (proceeding rate of 1 mm/y, Table 6.7). This explained the extended lifecycle of the HF storage tanks used in industry (~0.5 mm/y for the last 23 years).

Dosing a very low quantity of HNO_3 (0.1 – 0.5%) into a 70% HF corrosion solution attacked the scale layer and made it porous enough to allow fresh HF to contact the exposed substrate. The available HF reacted with the exposed steel and corrosion proceeded continuously, causing large unstable growths of scale which eventually weakened the steel. At the maximum HNO_3 concentration tested (1% HNO_3), the scale was nearly completely dissolved, with the steel loosing iron at a constant rate of 0.3 mass percent per day. As a result, the mild steel substrate was exposed and susceptible to continuous corrosive attack for as long as the oxidizing acid was in at concentrations close to 1% in the corrosion solution. However, HNO_3 was completely consumed during the 11 day corrosion tests and the re-establishment of the scale layer after the depletion of HNO_3 was not confirmed, due to the short length of the corrosion tests. Extreme pitting corrosion was observed on the surfaces of mild steel coupons corroded in HF corrosion solutions where the water content in the acid exceeded 50% mass concentration (40% and 48% HF with water mixtures). Compared to the very minor pitting observed on the surfaces of the cleaned corrosion coupons exposed to 1% HNO_3 in 70% HF, pitting corrosion which resulted from the oxidizing acid was not recognized as the dominant corrosion mechanism in the steel tanks. However, localized corrosion of the steel substrate by HF, at the bottom of the pores formed in the scale where HNO_3 selectively dissolved it, was visible after the scale was washed off. This observation made during the laboratory simulated corrosion tests compared well with the corrosion mechanism which resulted in the catastrophic failure of the original storage tanks.

The HF corrosion reaction was found to be dependent on temperature, as the apparent corrosion rate was at between 1.5 and 2.5 times slower at reduced temperatures measured (15ºC and 0ºC). Energy

requirements for removing iron from mild steel coupons rose by approximately 10 kJ/mol·K when 0.1% HNO_3 was added to the corrosion solution and then decreased by 20 kJ/mol·K (to below 9 kJ/mol·K) in corrosion tests where the initial HNO_3 concentration was increased to 0.5% HNO_3. This was indicative that lower concentrations of the oxidizing acid (0.1% HNO_3) stimulated corrosion by HF attack, while increased HNO_3 concentrations (>0.5% HNO_3) demonstrated the shift to HNO_3 as the dominant corroding agent in the solution. However, when the initial HNO_3 content in the HF solution was at 1% concentration, kinetics demonstrated that mild steel corrosion increased with decreasing temperature, as implied by the negative 29.74 kJ/mol·K determined. This unique phenomenon in the reaction kinetics were attributed to the HNO_3 corrosion (dissolution of the scale) dominating over the HF corrosion (scale formation) reactions, thus driving the iron removal process (corrosion) faster than heat supplied (0ºC – 25ºC) to the HF system.

A relationship between the discolorations of the scale on the coupons and the degree of corrosion, by oxidation (HNO_3) or reduction by (HF), was observed with varying quantities of HNO_3 in solution. Often, the yellow-brown ($FeF_3.3H_2O$) and grey (FeF_2) mottled scales were associated with fluorine in the scales and HF corrosion, while black (iron II oxide) or red-brown (iron III oxide) scales signified oxidation of the scale. Oxidation of the scale was mostly attributed to dissolved oxygen in solution, since the corrosion experiments were conducted in open air. However, in HF corrosion solutions where the oxidizing acid, HNO_3, was between 0.5% and 1% in solution, the scale turned black, mottled with dark red and brown, indicative of iron III oxide. Observation of these distinct discolorations associated with the degree of HF corrosion and oxidation of steel was found to be a useful method for distinguishing reducing HF corrosion of the steel substrate (scale formation) from oxidative attack (selective dissolution) of the scale. It could be a visual means of identifying the corrosive attack resulting from HNO_3 contamination of the HF feed stream, and can be made part of the mandatory inspections at the plant.

Stainless steel

A concentration of 1% HNO_3 in a 70% HF corrosion solution positively affected the formation of an oxide film on the surface of the SS 904 L coupons. During the initial stages of the corrosion tests where HF was spiked with 1% HNO_3, the stainless steel initially corroded at nearly 2 mm/y and this value decreased to below 1 mm/y once the oxide film stabilized in the HF solution. Of all metals tested, the SS 904 L coupons consumed the least HNO_3 per coupon tested (>0.05 g_{HF}/g_{Alloy}), which was associated with the 64% HNO_3 consumption determined after 11 days. All other corrosion tests

conducted with other steels and alloys had HNO_3 acid consumption in excess of 98%. An oxide scale did form on the stainless steel surface during the pre-passivation step, and was completely dissolved by the nitric acid present by the end of the corrosion test. Therefore, it was concluded that HNO_3 in the HF solution was firstly consumed during its reaction with the scale, and secondly utilized in forming the protective oxide film on the stainless steel coupons. Consequently, once HNO_3 formed and stabilized the oxide film in the HF solution, it took no further part in the corrosion process. Kinetics revealed that metal removed from stainless steel, in 70% HF spiked with 1% HNO_3, produced the slowest recorded rate of 0.03 g/L·h, which was comparable to the rate of iron removal from mild steel coupons in pure HF at 25ºC (Table 6.7).

In pure HF, stainless steel performed poorly compared to mild steel and the nickel alloy as mass losses, which resulted only from HF corrosion, kept constant at nearly 0.2% per day. The absence of an oxygen source in the HF corrosion solution caused SS 904 L coupons to corrode at a steady apparent corrosion rate of approximately 5 mm/y, with no signs of slowing down if the corrosion tests were to be extended. The corrosion rate of metals from the stainless steel coupons was the highest at 0.015 g/L·h, which was nearly seven times more than metal corroded from the pre-passivated mild steel coupons. Therefore, the oxide scale formed on the stainless steel did not serve the same protective function as the scale formed on the mild steel coupons. After cleaning the scale from the corroded coupons, no pitting was observed on the corroded surfaces, therefore uniform corrosion was the only corrosion mechanism under these circumstances.

Nickel alloys

Nickel alloys are frequently recommended for use in an HF environment due to their intrinsic corrosion resistance in a wide range of operating conditions (Jennings, 2007). The superior corrosion resistance of Monel 400 in pure 70% HF was confirmed in this study, with the nickel alloy coupons producing the lowest mass losses (>0.8%) and apparent corrosion rates (<0.4 mm/y) recorded (Table 6.7). Monel 400 is a reliable alloy used in the HF production plant, with its application only limited due to its high cost. As a result, mild steel is often favoured, and with good reason, as it was found to compete well with Monel based on its corrosion resistance in pure 70% HF, but at a fraction of the cost. Once the passive scale on mild steel coupons was stabilized, metal was found to corrode close to the 0.001 g/L·h set by Monel 400 coupons.

The only instance in which mild steel and stainless steel outperformed the nickel alloy in corrosion resistance was when the HF corrosion solution was contaminated with 1% HNO_3. Since Monel 400

could not rely on an oxide-fluoride scale barrier or a relatively large oxide film to mitigate the combined attack of HF and HNO_3 in a corrosive solution, it was vulnerable to prolonged corrosion. In the presence of HNO_3 in HF solution, the Monel 400 coupons corroded at the highest initial apparent corrosion rate (>40 mm/y). Not only was mass loss the highest in Monel 400 coupons under these conditions, it also followed a non-linear trend (logarithmic), which still made it possible to determine when it would cease to corrode as rapidly once HNO_3 in the corrosion solution was depleted. After cleaning, pitting corrosion was visible over a significant portion around the centre of the corroded coupons, which agrees with the rapid failure of the dip tube pipes used in the HF plant.

Table 6.7: Summary of corrosion type, corrosion rate and corrosion resistance data for all metals in service tested in 70% HF contaminated with up to 1% HNO_3 at 25ºC.

Type of Corrosion	Material	Acid Concentration		Corrosion Rate				Corrosion Type	Corrosion resistance*
		HF (%)	HNO_3 (%)	Initial (mm/y)	Proceeding (mm/y)	Mass loss / time (% / h)	Reaction rate (g/L·h)	Dominating mechanism, supporting mechanism	
PICT	Mild Steel	40	-	152.2	22.8	0.0863**	0.01270	Pitting corrosion, uniform corrosion	Inadequate
	Mild Steel	48	-	183.1	23.1	0.0314**	0.11710	Pitting corrosion, uniform corrosion	Inadequate
	Mild Steel	70	-	2.1	1.2	0.0015	0.00320	Uniform corrosion	Suitable
CT	Mild Steel	70	-	2.8	1.0	0.0076	0.00225	Uniform corrosion	Suitable
	Mild Steel	70	0.1	5.8	1.2	0.0082	0.00228	Uniform corrosion	Suitable
	Mild Steel	70	0.5	20	3.0	0.0123	0.00392	Uniform corrosion	Inadequate
	Mild Steel	70	1	36	4.5	0.0130	0.00354	Uniform corrosion, pitting corrosion	Inadequate
	SS 904 L	70	-	4.9	5.1	0.0522	0.0152	Uniform corrosion	Inadequate
	SS 904 L	70	1	2.3	1.2	0.0055	0.0034	Uniform corrosion	Suitable
	Monel 400	70	-	0.3	0.3	0.0028	0.0010	Uniform corrosion	Superior
	Monel 400	70	1	41	8.0	0.0408**	0.0256**	Uniform corrosion, pitting corrosion	Inadequate

* Corrosion resistance qualification from proceeding corrosion rate: >1mm/y = *Inadequate*, ~1mm/y = *suitable* and <1mm/y = s*uperior*.

** Results based on non-linear (R^2<0.9) trends to enable comparisons.

6.2.7. Inhibition strategies

After characterizing the corrosion of steels and metallic alloys used as construction materials in an HF plant where HNO_3 contamination was a problem, strategies in the prevention and inhibition of corrosion specific to each of the metals applicable on site were identified and listed here.

Reduction of nitrous compounds

The presence of an oxidizing acid such as HNO_3 produced a unique corrosive environment in an HF production plant. This led to unforeseen corrosion rates of construction materials used for manufacturing components and storage tanks in constant contact with technical grade HF at Necsa. The elimination of nitrous compounds from the HF product stream should be the first priority to extend the service life of the vessels.

The passive fluoride scale formed on mild steel during the pre-passivation step resisted HNO_3 attack in HF for no more than a day. If the HNO_3 concentration was kept high (0.1-1% HNO_3) through replenishment (i.e. continuous addition of fresh contaminated HF), the HF corrosion would continue to increase, and lead to failure of the HF storage tank linings at the level most frequently in contact with the fresh acid.

Change of construction materials

The only metal tested that provided superior corrosion resistance in the presence of up to 1% HNO_3 was stainless steel 904 L. Therefore, if nitrous acids in the product stream became unavoidable, one solution would be to manufacture the storage tank, or those sections mostly in contact with the contaminated HF, with SS 904 L. However, the use of this steel is only applicable when sufficient HNO_3 is available in the HF to sustain the oxide film on the steel surface, as the 904 L significantly corroded in HF corrosion solution which lacked a source of oxygen.

The nickel-based alloys, especially Monel 400, should be avoided as construction material when HNO_3 is present in the HF product stream. Monel 400 was found to excessively corrode in HF contaminated with HNO_3 with signs of excessive pitting corrosion on failed dip tubes collected on site (Valkenburgh, 2012e) as well as on coupons collected from laboratory tests. Uniform corrosion measured by mass loss measurements made it possible to estimate the service life of this metal when exposed to these unique conditions. However, since pitting corrosion was also found to deteriorate the metal surface, the failure of this metal in service occurred more rapidly and could be projected using laboratory immersion type corrosion tests.

Other methods

Other corrosion inhibition approaches identified in this study were changes in plant operating temperatures and selective HNO_3 acid consumption from the HF product streams. Throughout the study, mild steel was found to be capable of producing a comparable corrosion resistance to stainless steel in 70% HF contaminated up with up to 1% HNO_3 for a limited time. Therefore, since mild steel is the most economically feasible and preferred material of construction in the HF plant, the inhibition strategies formed were especially to the benefit of this alloy.

Decreasing the temperature at which contaminated HF is stored was not an effective means to control the corrosion rate of the mild steel used. Higher operating temperatures were associated with increased fuming of the HF solution with vapour/liquid corrosion, creating a new set of corrosion opportunities. Such conditions could not be undertaken in the laboratory due to safety restrictions. Lowering the temperature within the experimental scope (0ºC–25ºC) promoted HNO_3 corrosion, which was more detrimental to mild steel. Thus, the storage should be at least, 25ºC where possible when storing HF contaminated with HNO_3, since reaction equilibria were shifted slightly more towards the HF corrosion reaction (responsible for formation of the protective scale) at higher temperatures.

Acid consumption was determined to be a significant variable. In nearly all corrosion tests conducted on mild steel in 70% HF contaminated with HNO_3, the HNO_3 was nearly completely consumed (>98%), while HF acid consumption never reached above 5%. Therefore, there is the possibility to selectively consume HNO_3, while minimizing HF consumption. HF consumption was only due to the reaction of HF with the mild steel substrate, where HNO_3 preferentially dissolves the oxide-fluoride scales covering the coupons.

CHAPTER 7

CONCLUSIONS AND RECOMMENDATIONS

7.1. CONCLUSIONS

7.1.1. Evaluation of aims

The corrosion characteristics of steels and metallic alloys that made up the bulk of construction materials in an HF plant, which were in potential contact with HF contaminated with between 50 ppm and 10000 ppm HNO_3, were successfully established. After significantly reducing the safety risks associated with conducting corrosion experiments using concentrated hydrofluoric acid (≥40% HF), more than 30 laboratory scale immersion type corrosion tests were safely completed. These tests were effective in predicting the changes in corrosion mechanisms and corresponding corrosion rates of metals used within an HF production plant circuit affected by HNO_3 contamination in the downstream products.

The HF storage tanks were manufactured out of SA 516 Grade 70 normalized mild steel and thus the effect of reducing temperature as an alleviating measure was only investigated for this metal. Due to the fuming capacity of 70% HF, the safest temperature range in the corrosion test set-up conducted was at between 0ºC and 25ºC. The corrosion resistance of the stainless steel and nickel alloy used in service at the HF plant was also investigated in both pure 70% HF and 70% HF contaminated with up to 1% HNO_3.

7.1.2. Evaluation of objectives

7.1.2.1. Rates and mechanism of corrosion of steels and alloys

Uniform corrosion was the principal corrosion type for all steels and metal alloys exposed to 70% HF contaminated with up to 1% of HNO_3. The HNO_3 selectively attacked the protective oxide-fluoride scale layer formed on the coupons during the pre-passivation step. Partial dissolution of the scale layer by HNO_3 left it sufficiently porous to allow fresh HF to corrode the newly exposed steel substrate, and the steel reacted repeatedly with fresh HF to form a succession of scale layers in a localized area, which produced pitting corrosion.

Actual pitting corrosion was most prominent on cleaned coupons exposed to pure HF solutions below 50% concentration. Therefore, pitting corrosion was more a function of HF concentration (water content in the acid) than HNO_3 concentration. However, more regular pitting corrosion was observed on parts of mild steel and nickel alloy (Monel) coupons exposed to 1% HNO_3 in 70% HF and the high mass losses indicated that the dominant corrosion mechanism was uniform corrosion. Under these conditions, pitting corrosion was a supporting mechanism which significantly increased the corrosion rates and contributed greatly to the rapid failure. Since HNO_3 was consumed early in nearly the all corrosion tests, the extent to which these materials would also pit under a constant supply of the oxidizing acid was not established.

Decreasing the temperature slowed the corrosion rate of mild steel in pure 70% HF. However, between 0.1% and 1%, HNO_3, the corrosion rate increased, even at lower temperatures (15ºC and 0ºC), indicating a deceleration of the HF corrosion reaction rate, which promoted corrosive attack by HNO_3. Based on the activation energies determined, HNO_3 in solution accelerated the corrosion rate of mild steel in HF more than increased temperature.

Mild steel

Increased concentrations of HNO_3 (0.1%, 0.5% and 1%) in 70% HF on the corrosion of mild steel linearly increased the corrosion rate of the pre-passivated steel. The initial apparent corrosion rate increased with 3.3 mm/y for every 0.1% increase in HNO_3 concentration. Thus, pre-passivated mild steel corroded nearly 13 times faster in 70% HF contaminated with up to 1% HNO_3, and based on mass loss trends in the laboratory simulated environment would last a maximum of 295 days before it would completely corroded (100% mass loss).

However, since the HNO_3 concentration was not replenished in the laboratory tests after it had been entirely consumed during the reaction with the protective oxide-fluoride scale, the corrosion rate decreased to below 5 mm/y, which was attributed to the scale being re-established in the concentrated HF. Thus, if HF contaminated with up to 1% HNO_3 entered an HF storage tank, and the HNO_3 is quickly consumed, the service life of the vessels would ultimately be halved, since the protective scale would have an opportunity to re-establish.

Stainless steel

Stainless steel 904 L exhibited the best corrosion resistance of the three metals used in the HF production plant for 70% technical grade HF contaminated with up to 1% HNO_3. However, the corrosion resistance under these unique conditions was entirely dependent on the formation of an oxide film in the HF product stream and maintaining it through the continual addition of oxygen-

containing acid, such as HNO_3. The SS 904 L corroded at 0.3 mm/y in contaminated 70% HF, which was negligible compared to mild steel under the same conditions.

The reasons that stainless steel is not used as the main construction material for storage tanks in service the higher cost than mild steel, and its inadequate corrosion resistance to relatively pure 70% HF (<50 ppm). Stainless steel 904 L coupons corroded at approximately 5 mm/y, which is a mass loss of nearly 0.2% per day. The absence of an oxygen source (i.e. HNO_3 contamination) in the uncontaminated technical grade HF would have made SS 904 L highly unsuitable in storage tanks used under normal plant operating conditions, since it would corrode nearly seven times faster than mild steel used under the same circumstances. Therefore, HNO_3 was beneficial to the corrosion resistance of stainless steel, since it provided an oxygen source to the steel surface to form the Cr_2O_3 passive layer required to resist the corrosive HF operating environment.

Nickel alloys

Monel 400 coupons had the slowest apparent corrosion rates in pure 70% HF. However, in 70% HF contaminated with up to 1% HNO_3, this nickel alloy initially corroded at more than 40 mm/y and then subsequently corroded at 8 mm/y, even after HNO_3 had been completely consumed over the duration of the 11 day corrosion test. In service at the HF plant, nickel alloys relied predominantly on their inherent corrosion resistance provided by the nickel and copper contents and less on the formation of passive oxide layer, or fluoride scale layer. Due to the high mass losses and propensity to pit and subsequently fail (corrode through and leak) in HF contaminated with up to 1% HNO_3, Monel 400 was deemed unsuitable for use in this unique corrosive environment.

7.1.2.2. Inhibition strategies

The first inhibition strategies should be to reduce the amount of nitrous compounds entering the HF plant, else the construction material recommended for the HF storage tanks should be stainless steel SS 904 L. If mild steel is the preferred construction material, other methods to limit corrosion would be to increase the operating temperature of the plant to lower the corrosion rates from HNO_3 in HF. Alternatively, strategies around the selective consumption of HNO_3 within in the HF product stream by oxide and fluoride salts, which should be compatible with the protective oxide-fluoride scale already protecting the inside of the mild steel HF storage tanks, should be investigated.

7.2. RECOMMENDATIONS

Expansion of the corrosion study is recommended to include testing of alternative alloys (Table 2.1) more suited for to the unique corrosive environment experienced at the HF plant. Also, other corrosion prevention and inhibitions strategies need to be tested and implemented on site, if found suitable after extended laboratory tests.

An increase in the length of the corrosion tests is recommended, as the extent to which the HNO_3 consumption affected the re-establishment of the protective oxide-fluoride layer could not be established, and neither could its long-term influence on the corrosion resistance of mild steel in service. Corrosion tests where the HNO_3 concentration in the HF corrosion solution is maintained over the entire duration of the corrosion tests are also recommended to study this effect.

The selective consumption of HNO_3 from the contaminated HF solution, possibly using iron fluoride and iron oxide salts, needs to be examined. During the current study, HNO_3 selectively dissolved the passive oxide-fluoride scale before attacking the steel substrate. Therefore, an investigation into the degree to which nitrous compounds may be consumed and their effect on the corrosion resistance of pre-passivated mild steel in solution is suggested. Iron oxide and fluoride salts are recommended, rather than other salts, since they are unlikely to add additional complexes to the HF corrosive mix already present in the HF storage tanks in service.

REFERENCES

Ahmad, Z. 2006. Principles of corrosion engineering and corrosion control. 1st Edn. Elsevier/BH: Amsterdam ; Boston, USA.

Andersen, T.N., Vanorden, N., & Schlitt, W.J. 1980. Effects of Nitrogen Oxides, Sulfur Dioxide, and Ferric Ions on the Corrosion of Mild Steel in Concentrated Sulfuric Acid. Metall. Trans. A. 11(8):1421-1428.

Annual Book of ASTM Standards. 2009. Section 3, Vol. 03.04. ASTM International: West Conshohocken, USA.

ASM Handbook. 1987. Vol. 13, Corrosion. American Society for Metals International: Materials Park, Ohio, USA.

ASTM. 2009a. G 31 - 72, Standard Practice for Laboratory Immersion Corrosion Testing of Metals. Annual Book of ASTM Standards. ASTM International: West Conshohocken, USA.

ASTM. 2009b. G 161 - 00, Standard Guide for Corrosion-Related Failure Analysis. Annual Book of ASTM Standards. ASTM International: West Conshohocken, USA.

ASTM. 2009c. E 1459 - 92, Standard Guide for Physical Evidence Labelling and Related Documentation. Annual Book of ASTM Standards. ASTM International: West Conshohocken, USA.

ASTM. 2009d. G 1 - 03, Standard Practice for Preparing, Cleaning, and Evaluating Corrosion Test Specimens. Annual Book of ASTM Standards. ASTM International: West Conshohocken, USA.

ASTM. 2009e. G 46 - 94, Standard Guide for Examination and Evaluation of Pitting Corrosion. Annual Book of ASTM Standards. ASTM International: West Conshohocken, USA.

Baboian, R. 2005. Corrosion Tests and Standards: Application and Interpretation. ASTM International: West Conshohocken, USA.

Bingöl, D. & Canbazoğlu, M. 2004. Dissolution kinetics of malachite in sulphuric acid. Hydrometallurgy. 72(1–2):159–165.

Blanchard Jr., W.K. & Mack, N.C. 1992. Corrosion Results of Alloys and Welded Couples Over a Range of Hydrofluoric Acid Concentrations at 125ºF (CORROSION/2003 No. 452). NACE International. NACE: Houston, Texas, USA.

Campbell, F.C. (Ed.). 2008. Elements of Metallurgy and Engineering Alloys. ASM International: Materials Park, Ohio, USA.

Cleland, J.H. 1996. What does the pitting resistance equivalent really tell us? Eng. Fail. Anal. 3(1):65–69.

Craig, B.D. & Anderson, D.S. 1994. Handbook of Corrosion Data. ASM International: Materials Park, Ohio, USA.

Crookes, R. 2007. Pickling and passivating stainless steel. Euro Inox: Brussels.

Davenport, A. 2016. Shedding Light on Corrosion, AfriCORR 2016, Book of Abstracts, 27 – 29 July 2016, Midrand, South Africa.

Davis, J.R. (Ed.). 1994. Stainless steels. ASM Specialty Handbook. ASM International: Materials Park, Ohio, USA.

Davis, J.R. (Ed.). 2000. Corrosion: understanding the basics. 1st print Edn. ASM International: Materials Park, Ohio, USA.

Dillon, C.P. 1995. Corrosion Resistance of Stainless Steels. Corrosion Technology. M. Dekker: New York, USA.

EDAX. 2013. Extending Detector Window life [WWW Document]. Tech. Note - EDS. URL http://www.edax.com/mobile/literature/eds.aspx (Accessed: 4 April 2017).

El Hussaini, O.M. & Rice, N.M. 2004. Liquid–liquid extraction of niobium and tantalum from aqueous sulphate/fluoride solutions by a tertiary amine. Hydrometallurgy. 72(3):259–267.

Falkenberg, F., Raja, V.S., & Ahlberg, E. 2001. An Alternative Explanation for the Apparent Passivation of Molybdenum in 1 mol/L Hydrochloric Acid. J. Electrochem. Soc. 148(4):B132.

Garverick, L. (Ed.). 1994. Corrosion in the Petrochemical Industry. ASM International: Materials Park, Ohio, USA.

Genuino, H.C., Opembe, N.N., Njagi, E.C., McClain, S., & Suib, S.L. 2012. A review of hydrofluoric acid and its use in the car wash industry. J. Ind. Eng. Chem. 18(5):1529–1539.

Ghali, E. 2010. Corrosion Resistance of Aluminium and Magnesium Alloys: Understanding, Performance, and Testing. Wiley series in corrosion. John Wiley: Hoboken, New Jersey, USA.

Gildenpfennig, A., Gramberg, U., & Hohlneicher, G. 2003. Passivation and corrosion of the metallic high performance materials Alloy 33 and MC-Alloy in different environments. Corros. Sci. 45(3):575–595.

Gökelma, M., Birich, A., Stopic, S., & Friedrich, B. 2016. A review on alternative gold recovery re-agents to cyanide. J. Mater. Sci. Chem. Eng. 04(08):8–17.

Gysbers, A.C., Hashim, H.H., Clarida, D.R., Ghirinos, G., Marsh, J., & Palmer, J.W. 2003. Specification for Carbon Steel Materials for Hydrofluoric Acid Alkylation Units (No. 03651). NACE International. NACE: Houston, Texas, USA.

Han, J., Liu, W., Xue, K., Qin, W., Jiao, F., & Zhu, L. 2017. Influence of NH_4HF_2 activation on leaching of low-grade complex copper ore in NH_3-NH_4Cl solution. Sep. Purif. Technol. 181(Supplement C):29–36.

Hathaway, G.J. & Proctor, N.H. 2014. Proctor and Hughes' Chemical Hazards of the Workplace. 5th Edn. Wiley-Interscience: Hoboken, USA.

Haynes, W.M. 2016. CRC Handbook of Chemistry and Physics, 94th Edition. CRC Press: London, UK.

HF production-Eurofluor [WWW Document]. 2017. URL http://www.eurofluor.org/hf-production/ (Accessed: 3 August 2017).

HF applications-Eurofluor [WWW Document]. 2018. URL https://www.eurofluor.org/hf-applications/metallurgical-industry/ (Accessed: 27 July 2017).

Hill, K. & Knott, H. (Eds.). 1960. The Design of Plants for Handling Hydrofluoric Acid. Institution of Chemical Engineers: London, UK.

Honeywell International Inc. 2014. Literature | Honeywell Hydrofluoric Acid [WWW Document]. URL https://www.honeywell-hfacid.com/literature/ (Accessed: 3 July 2016).

Hore-Lacy, I. 2016. Uranium for Nuclear Power: Resources, Mining and Transformation to Fuel. Elsevier: Kidlington, UK.

Horn, E.-M., Manning, P., & Renner, M. 1992. Corrosion of stainless steels and nickel-based alloys in solutions of nitric acid and hydrofluoric acid. Werkst. Korros. 43:191–200.

McEwan, J.J. (Ed.). 2004. Corrosion Control In Southern Africa. 2nd Edn. Corrosion Institute of Southern Africa: Kelvin, South Africa.

Mohanty, J.N. (Ed.). 2003. Indian Chemical Engineering Congress, Indian Institute of Chemical Engineers, Council of Scientific & Industrial Research (India), & Regional Research Laboratory. Role of Chemical Engineering in Processing of Minerals and Materials. Allied Publishers Pvt. Limited: New Delhi.

Jackson, E. 1986. Hydrometallurgical Extraction and Reclamation. Ellis Horwood Series in Industrial Metals. Horwood: Chichester. UK.

Jennings, H. 2001. Materials for Hydrofluoric Acid Service in the New Millennium (No. 01345). NACE International. NACE: Houston, Texas, USA.

Jennings, H. 2007. Materials for Storing and Handling Commercial Grades of Aqueous Hydrofluoric Acid and Anhydrous Hydrogen Fluoride (No. 24057). NACE International Publication 5A171 (2007 Edition). NACE.

Jones, D.A. 1996. Principles and Prevention of Corrosion. 2nd Edn. Prentice Hall: Upper Saddle River, NJ, USA.

Jones, D.A. 2014. Principles and Prevention of Corrosion. Pearson Education: Harlow, Essex, UK.

Jones, D.S. & Pujadó, P.R. 2008. Handbook of Petroleum Processing. Springer: The Netherlands.

Kaesche, H. 2003. Corrosion of Metals: Physicochemical Principles and Current Problems. Engineering materials and processes. Springer: Berlin ; New York, USA.

Katsamas, A.I., Haidemenopoulos, G.N., Zervaki, A.D., & Melas, I. 2004. Stress-corrosion cracking of a monel 400 tube. J. Fail. Anal. Prev. 4(6):44–50.

Kennedy, B.A. (Ed.). 1990. Surface Mining. 2nd Edn. Society for Mining, Metallurgy, and Exploration (U.S.): Littleton, Colorado, USA.

Khadom, A.A. & Abdul-Hadi, A.A. 2014. Kinetic and mathematical approaches to the corrosion of mild steel in nitric acid. React. Kinet. Mech. Catal. 112(1):15–26.

Khanna, A.S. 2002. Introduction to High Temperature Oxidation and Corrosion. ASM International: Materials Park, Ohio, USA.

Lazzari, L. 2017. Engineering Tools for Corrosion: Design and Diagnosis. European Federation of Corrosion Publications. WP, Woodhead Publishing, an imprint of Elsevier: Duxford, UK.

Levenspiel, O. 1999. Chemical Reaction Engineering. 3rd Edn. Wiley: Hoboken, NJ, USA.

Li, J., Gao, X., Du, L., & Liu, Z. 2017. Relationship between microstructure and hydrogen induced cracking behaviour in a low alloy pipeline steel. J. Mater. Sci. Technol. Article in Press.

Li, J., Huang, J., Tian, Y., & Liu, C. 2009. Corrosion action and passivation mechanism of magnesium alloy in fluoride solution. Trans. Nonferrous Met. Soc. China. 19(1):50–54.

Li, Y., Xu, X., Hou, Y., Zhang, C., Wang, F., Omura, K., Koizumi, Y., & Chiba, A. 2015. Regulating the passive film of NiCoCrMo alloy in hydrofluoric acid solution by small addition of Cu. Corros. Sci. 98(Supplement C):119–127.

Liu, J., Zhang, T., Meng, G., Shao, Y., & Wang, F. 2015. Effect of pitting nucleation on critical pitting temperature of 316L stainless steel by nitric acid passivation. Corros. Sci. 91(Supplement C):232–244.

Louw, D.C. 2014. Safety Risk Evaluation Procedure for Projects. Internal report: Doc No: AC-BPMS-PRO-08006: Necsa, South Africa.

Lutton, K. & Scully, J.R. 2017. Kinetics of Oxide Growth of Passive Films on Transition Metals, in: Reference Module in Chemistry, Molecular Sciences and Chemical Engineering. Elsevier: Oxford, UK.

Lyons, W.C., Plisga, G.J., & Lorenz, M.D. 2016. Standard Handbook of Petroleum and Natural Gas Engineering. 3rd Edn. Elsevier: USA.

M. Woite GmbH. 2017. M.WOITE Sonderwerkstoffe Edelstähle [WWW Document]. Nirosta 4565S. URL www.m-woite.de (Accessed: 28 August 2015).

Mannan, S. & Lees, F.P. (Eds.). 2005. Lee's Loss Prevention in the Process Industries: Hazard Identification, Assessment, and Control. 3rd Edn. Elsevier Butterworth-Heinemann: Amsterdam, Netherlands.

McCafferty, E. 2010. Introduction to Corrosion Science. Springer: New York, USA.

McGuire, M.F. 2008. Stainless Steels for Design Engineers. ASM International: Materials Park, Ohio, USA.

Mular, A.L. (Eds.). 2002. Mineral Processing Plant Design, Practice, and Control Conference, & Society for Mining, Metallurgy, and Exploration. Proceedings, Vancouver, B.C., Canada, Oct. 20 - 24, 2002. Society for Mining, Metallurgy and Exploration: Littleton, Colorado, USA.

NACE International. 2003. Standard Test Method: Evaluation of Pipeline and Pressure Vessel Steels for Resistance to Hydrogen-induced Cracking. NACE International: Houston, Texas, USA.

Nage, D.D. & Raja, V.S. 2006. Effect of nitrogen addition on the stress corrosion cracking behaviour of 904L stainless steel welds in 288°C deaerated water. Corros. Sci. 48(8):2317–2331.

Nazri, G., Yeager, E., Cahan, B.D. 1981. Corrosion and Passivation Studies of Iron and Ferrous Alloys. Defence Technical Information Centre. Case Western Reserve University: Cleveland, Ohio. USA.

Nickel Development Institute. 2017. Literature | Corrosion resistance of nickel-containing alloys in hydrofluoric acid, hydrogen fluoride and fluorine [WWW Document]. URL https://www.nickelinstitute.org/KnowledgeBase/TechnicalLiterature.aspx (Accessed: 12 October 2017)

Noh, J.S., Laycock, N.J., Gao, W., & Wells, D.B. 2000. Effects of nitric acid passivation on the pitting resistance of 316 stainless steel. Corros. Sci. 42(12):2069–2084.

Oguzie, E.E. 2004. Influence of halide ions on the inhibitive effect of congo red dye on the corrosion of mild steel in sulphuric acid solution. Mater. Chem. Phys. 87(1):212–217.

Olsson, C.-O. & Landolt, D. 2003. Passive films on stainless steels—chemistry, structure and growth. Microsc. Nanoscopic Asp. Corros. Corros. Prot. 48(9):1093–1104.

Pelchem. 2015. Safety Awareness Training - Anhydrous Hydrogen Fluoride & Hydrofluoric Acid solutions. Pelchem (Pty) Ltd.

Pelchem. 2014. Pelchem SOC Ltd Overview February 2014. 2014. [WWW Document]. URL http://nwdc.co.za/wp-content/uploads/2015/02/Pelchem-Overview-August-2014.pdf (Accessed: 3 August 2017). Perry, D.L. 2011. Handbook of Inorganic Compounds, 2nd Edn. CRC Press: Sound Parkway, USA.

Philippe, H. 2001. Glow Discharge - A Modern Concept for Coating Analysis. Millenn. Steel. [WWW Document]. URL https://www.leco.com/index.php/component/edocman/?view=document&id=906&Itemid=906 (Accessed: 3 October 2017)

Pourbaix, M. 1974. Atlas of Electrochemical Equilibria in Aqueous Solutions. National Association of Corrosion Engineers. Houston, Texas.

Razygraev, V. & Lebedeva, M. 1982. On inhibition of corrosion and cathodic reactions on stainless steels in nitric-acid media by fluoride ion. Zashchita Met. 18(2):227–230.

Rebak. 2003. Corrosion Behaviour of Nickel Alloys in Wet Hydrofluoric Acid. American Society for Metals: Metals Park, Ohio, USA.

Rebak, R.B., Dillman, J.R., Crook, P., & Shawber, C.V.V. 2001. Corrosion behaviour of nickel alloys in wet hydrofluoric acid. Mater. Corros. 52(4):289–297.

Revell, L.E. & Williamson, B.E. 2013. Why are some reactions slower at higher temperatures? J. Chem. Educ. 90(8):1024–1027.

Richardson, T.J.A., Cottis, B.R.A., Lindsay, R., Lyon, S., Scantlebury, D.J.D., Stott, H., & Graham, M. 2009. Shreir's Corrosion. Elsevier Science: Burlington.

Riding, J.B. & Kyffin-Hughes, J.E. 2010. The use of pre-treatments in palynological processing. Rev. Palaeobot. Palynol. 158(3):281–290.

Rosenberg, G. & Sinaiova, I. 2017. Evaluation of hydrogen induced damage of steels by different test methods. Mater. Sci. Eng. A. 682 (Supplement C):410–422.

Saldanha, B. 2000. Denickelification of Cu-Ni Alloys. Houston, Texas, USA.

Sanderman, J., Farrell, M., Macreadie, P.I., Hayes, M., McGowan, J., & Baldock, J. 2017. Is demineralization with dilute hydrofluoric acid a viable method for isolating mineral stabilized soil organic matter? Geoderma, 5th International Symposium on Soil Organic Matter 2015. 304 (Supplement C):4–11.

Schillmoller, C. 1995. Selection and Use of Stainless Steels and Nickel-bearing Alloys in Nitric Acid. NiDI Technical Series. Nickel Development Institute: Toronto, Canada.

Singh, V.B. & Gupta, A. 2001. The electrochemical corrosion and passivation behaviour of Monel (400) in concentrated acids and their mixtures. J. Mater. Sci. 36(6):1433–1442.

Thyssenkrup VDM. 2013. VDM Metals | Home [WWW Document]. Nicrofer 3033 – Alloy 33 New Corros.-Resist. Austenitic Mater. Many Appl. Rep. No 24 Available From. URL http://www.vdm-metals.com/en/ (Accessed: 28 August 2015).

Valkenburgh, E.G. 2013. Interview with chief advisor for HF plant on involvements in the Pelchem corrosion study. South Africa.

Valkenburgh, E.G. 2012a. 70% HF Storage tank Corrosion (Confidential internal report: Part 5: No. PCM-OPSA60-REP-12007). Necsa: Pelchem SOC Ltd. South Africa.

Valkenburgh, E.G. 2012b. H_2SO_4 supplier investigation. Internal report: Part 4: PCM-OPSA60-REP-12007: Pelchem SOC Ltd. South Africa.

Valkenburgh, E.G. 2012c. H_2SO_4 Storage tank investigation. Internal Report: Part 3: PCM-OPSA60-REP-12007: Pelchem SOC Ltd. South Africa.

Valkenburgh, E.G. 2012d. HF ISO tanks Corrosion Evaluation. Confidential Internal report: Part 1: PCM-OPSA60-REP-12007: Pelchem SOC Ltd. South Africa.

Valkenburgh, E.G. 2012e. Dip tube failures on ISO tanks. Internal report: Part 2: PCM-OPSA60-REP-12007: Pelchem SOC Ltd. South Africa.

Van der Merwe, R. 2010. Leaching characteristics of copper refractory ore: Effect of pre-oxidation stage. Tshwane University of Technology: Pretoria, South Africa.

Van der Merwe, R., Cornish, L.A., & Van der Merwe, J.W. 2016. Corrosion Safety Risk Assessment for Testing in Hydrofluoric Acid. Afri. J. Corr. 2(1):28–36.

Van Der Merwe, R. & Kasaini, H. 2011. Leaching characteristics of copper refractory ore in sulfate media. Miner. Metall. Process. 28(4):208–214.

Vyazovkin, S. 2016. A time to search: finding the meaning of variable activation energy. Phys. Chem. Chem. Phys. PCCP. 18(28):18643–18656.

Wachter, A. & Treseder, R. 1947. Corrosion Testing Evaluation of Metals for Process Equipment. Chemical Engineering Progress.

Walter, S. 1937. Production of sodium aluminium fluoride. Patent no. US2075370 A. USA.

Whitaker, G.C. 1950. Corrosion of metals in fluorine and hydrofluoric acid. Corr. 6(9):283–285.

Young, C. (Ed.). 2008. Hydrometallurgy 2008: Proceedings of the Sixth International Symposium, honouring Robert S. Shoemaker. Society for Mining, Metallurgy, and Exploration (U.S.), Inc: Littleton, Colorado, USA.

Young, D.J. 2016. High Temperature Oxidation and Corrosion of Metals. Elsevier Science: San Diego, California, USA.

Zhang, B., Hao, S., Wu, J., Li, X., Li, C., Di, X., & Huang, Y. 2017. Direct evidence of passive film growth on 316 stainless steel in alkaline solution. Mater. Charact. 131 (Supplement C):168–174.

APPENDICES

APPENDIX A

ERROR CALCULATIONS

Errors were estimated in several ways throughout the corrosion study. As far possible, experiments were duplicated and then the standard deviation of identical tests calculated and used as the error. One example is Figure A.1 where the corrosion test for 70% HF spiked with 0% and 1% HNO_3 were the only tests that were duplicated and their error bars were represented by the standard deviation at each time interval. However, the standard deviation determined for 0% HNO_3 was so small (<0.2 mm/y) that the error bars were not visible behind the chart markers.

For corrosion tests that were not duplicated, the size of the measurement errors were assigned to random errors that occurred due to the sensitivity of the measuring instruments used. These errors arose from mass loss measurements using a mass balance (0.01 g) and the tolerance of the water-jet cutting instrument used to reproducibly cut out a designated area (±0.025 mm).

The error associated with feed and product solution analyses for HNO_3 and HF content were not known. Therefore, the errors associated with acid titrations (HF analyses) and ion chromatography (HNO_3 analyses) were determined through triplicate analyses of a sample solution spiked with known quantities of HF (69.2%) and HNO_3 (1%). The difference in concentration between the three identical samples analysed was used to determine the accuracy of the analytical techniques used at Pelchem Ltd. to analyse HF and HNO_3 at the desired concentration and the reproducibility of their techniques.

The standard deviations of the results of the three duplicate samples analysed and their relationship to the true value (known concentrations spiked) were used to determine the errors associated with acid consumptions during each corrosion test conducted. The error associated with analysing HNO_3 was much higher than HF, since the concentration of HNO_3 in solution was in the ppm range while HF was in the percentage range (e.g. Figure A.4). Therefore, the sensitivity of the IC to analyse for HNO_3 in such a low concentration required higher sensitivity of the analytical instrument and therefore was associated with a higher relative error (e.g. Figure A.5).

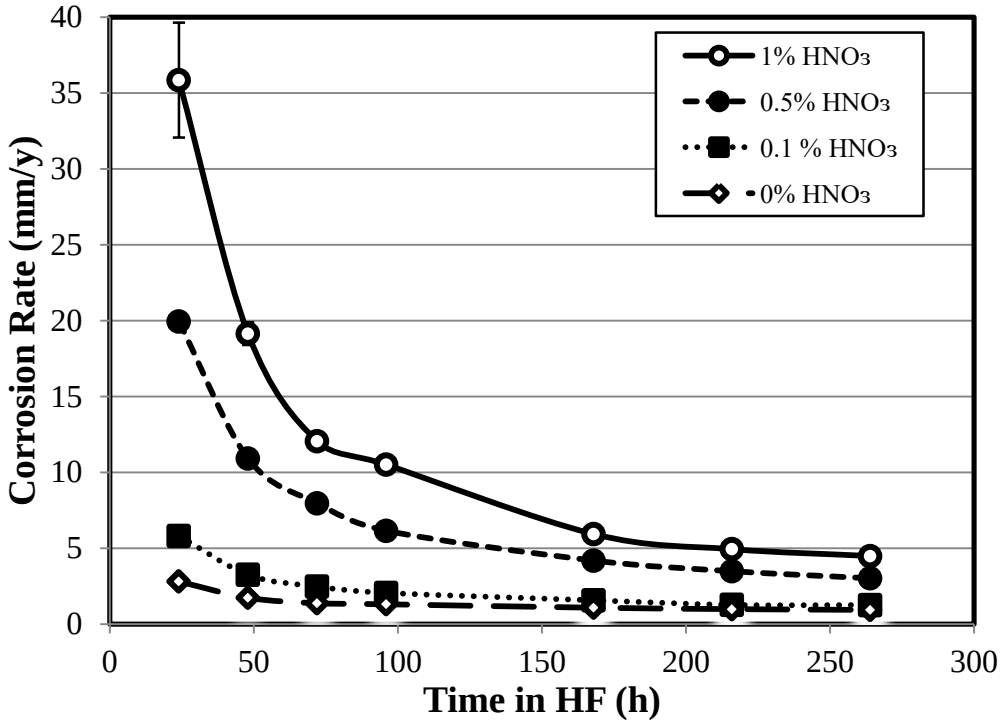

Figure A.1: Adaptation of Figure 6.8, to demonstrate the implementation of errors implemented in terms of standard deviations. Error bars obscured by markers in some instances.

Apparent corrosion rate

From Equation 4.4, CR = 87.6 × (W/ρAt) where W = weight loss (in mg), ρ = density (in g/cm^3), A = area (in cm^2) of the coupons exposed to HF over time (in hours).

Here follows the procedures for determining the error associated with apparent corrosion rate in the study:

87.6 and ρ (density of mild steel is given as 7.85) are constants. Therefore no errors were applicable.

Error of $\frac{W}{t}$ = the error in slope of a W vs. t plot (Figure A.2) was obtained from the Linest function when applied over the raw data in Excel (Table A.1).

Error of A = ±0.0025^2 (Area = l × l = 0.0025 cm× 0.0025cm)

$$\frac{\Delta CR}{CR} = \sqrt{\left\{\frac{\Delta\left(\frac{W}{t}\right)}{\frac{W}{t}}\right\}^2 + 2\left(\frac{\Delta l}{l}\right)^2}$$

$$\frac{\Delta CR}{CR} = \sqrt{\left\{\frac{\Delta\, slope}{slope}\right\}^2 + 2\left(\frac{0.025}{25}\right)^2}$$

Since $2\left(\frac{0.025}{25}\right) = 2 \times 10^{-3}$: the square is negligibly small then

$$\frac{\Delta CR}{CR} = \sqrt{\left\{\frac{\Delta\, slope}{slope}\right\}^2}$$

Absolute error: $\Delta CR = \sqrt{\left\{\frac{\Delta\, slope}{slope}\right\}^2} \times CR$

Example using experimental data:

As shown in the example graph (Figure A.3), error bars could then be added to the graphs to indicate the possible deviations due to the random errors that may have occurred during the corrosion experiments. In corrosion tests where the absolute errors fell below ±1 mm/y, the errors were rarely visible behind the markers used to represent the point measurements made. This was frequently the case in corrosion tests conducted in 70% HF, since the corrosion rates seldom exceeded 10 mm/y effectively resulting in an error less than ±0.5 mm/y.

Table A.1: Calculating absolute error using error in the y estimate from linear regression.

40% HF (Pre-Pass)				**Error calculations**		
Sample	**Interval**	**Mass loss**	**Apparent corrosion Rate**	**From Linest f(x) in Excel**		**Absolute Error**
	hours	mg	mm/y	6*	4961**	mm/y
A1	24	5039	152.2			29.3
At	96	5634	42.6	1***	141****	8.2
At + 1	192	6041	22.8			4.4

* Gradient (m) in x-y plot, ** Y intercept, *** standard deviation of the slope (used as the $\Delta\, slope$) and **** standard deviation of the Y intercept

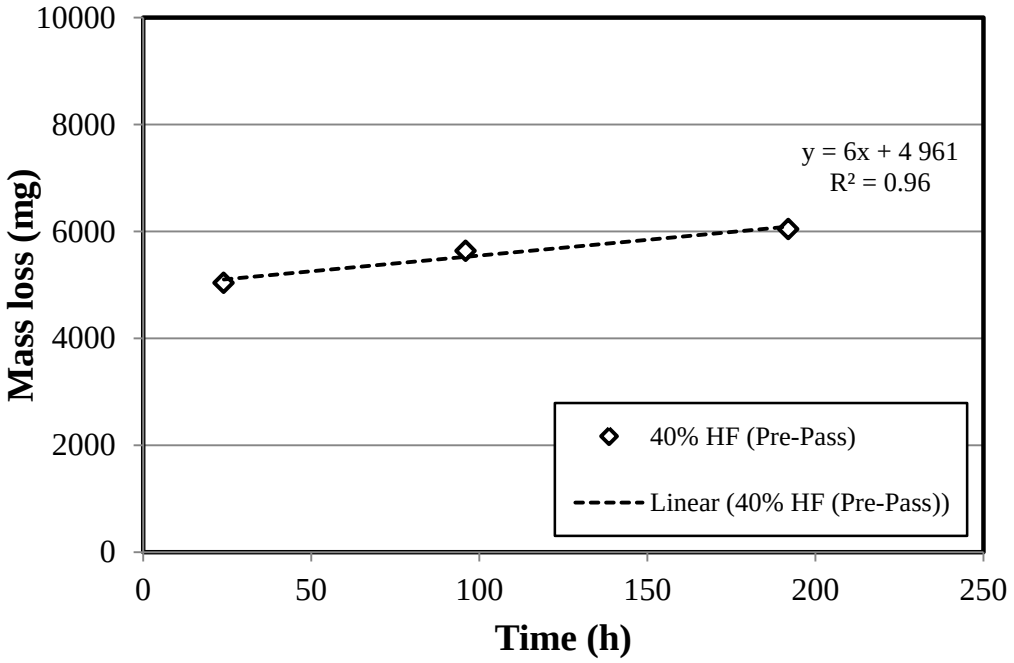

Figure A.2: Mass loss of mild steel coupons with time in 40% HF, at 25ºC.

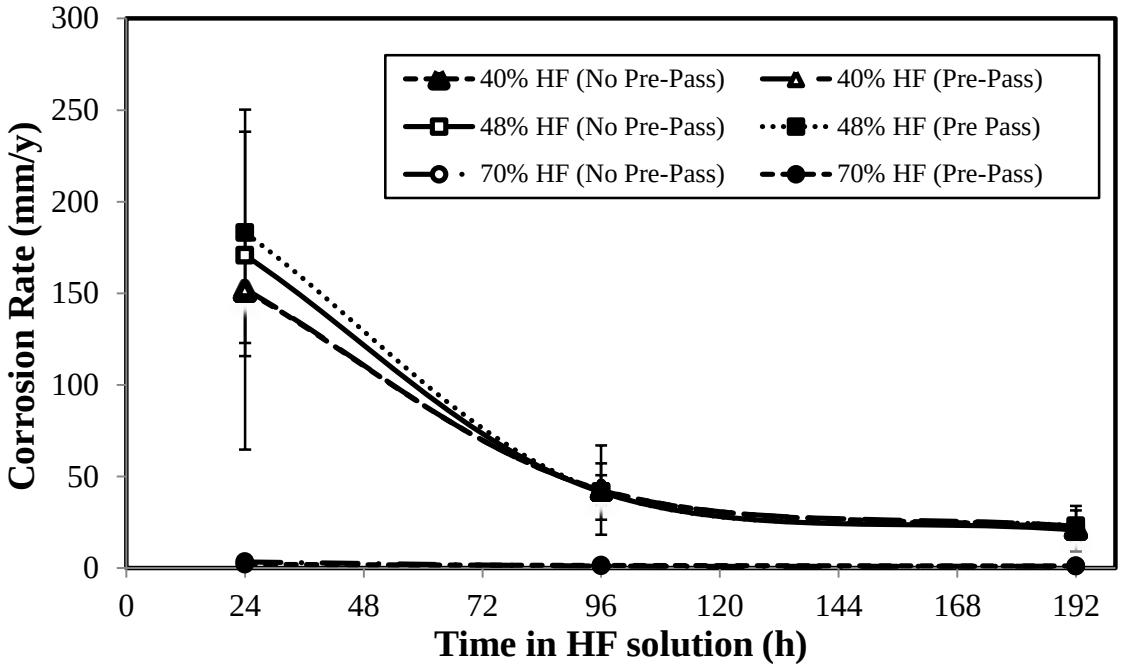

Figure A.3: Adaptation of Figure 6.3, to demonstrate the implementation of errors calculated. Error bars obscured by markers in some instances.

Hydrofluoric acid consumption

The formula for calculating HF acid consumption was adapted from Equation 4.1:

$$\text{HF consumption} = \frac{(\text{HF in Feed}) - (\text{HF in Product})}{\text{HF in Feed}} \times 100 \qquad \text{Equation A.1}$$

Here follows the procedure for determining the error associated HF consumption applicable to the study:

Three HF solution samples spiked with 1% HNO_3 was sent for HF concentration determined potentiometrically, by titrating an aliquot of the sample with 1M NaOH using an antimony electrode. Spiking analytical grade HNO_3 into 70% Analytical grade HF resulted in the HF being diluted to 69.21% HF.

The three identical samples analyses came back with a variation (68.74, 69.27 and 69.23% HF). Therefore the standard deviation was calculated to be ±0.175%.

$$HF_{consumed} = HF_{Feed} - HF_{product}$$

$$\Delta HF_{consumed} = \sqrt{\Delta(HF_{feed})^2 + \Delta(HF_{product})^2}$$

$$\Delta HF_{consumed} = \sqrt{2(\Delta HF_{measured})^2}$$

$$\Delta HF_{consumed} = \sqrt{2(0.175)^2} = 0.2475$$

$$\Delta HF_{consumed} = \sqrt{\left(\frac{0.25}{69.21}\right)^2 + \left(\frac{0.175}{69.21}\right)^2} = 0.00442$$

Absolute error: $\Delta HF_{consumed} = (0.00442) \times HF_{consumed}$

Example using experimental data:

Random errors associated with analyses of HF in solution were very small (Table A.2) and were seldom visible on the bar graphs constructed (Figure A.4). Since the HF concentrations of the samples sent for IC analyses was so high (>65% HF), and the method for analysing HF at Pelchem well established, the analyses could be done with high accuracy and precision, and were associated with the low errors determined.

Table A.2: HF consumption summarized from Table 5.7 to include absolute errors determined.

HF concentration (%)	**HF Consumed (%)**	**Absolute Error (%)**
40	7.0	0.031
48	3.7	0.016
70	1.7	0.008

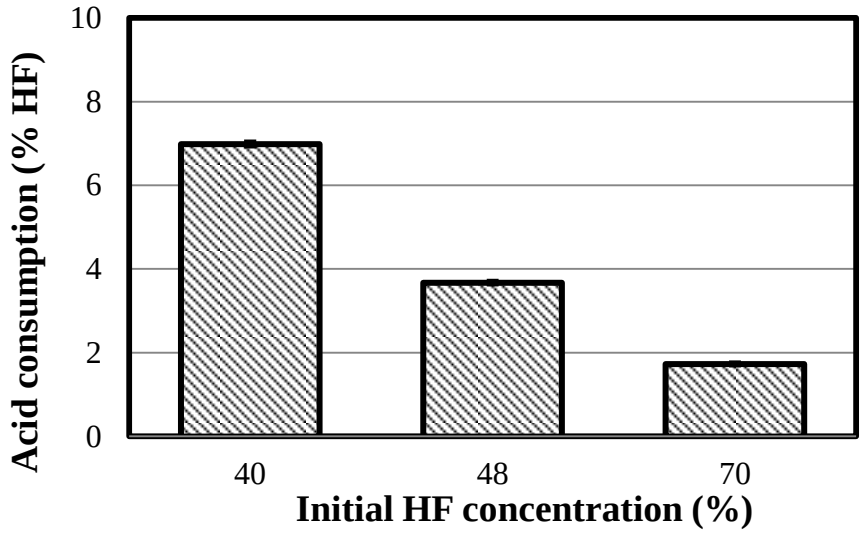

Figure A.4: Adaptation of Figure 5.1, to demonstrate the implementation of errors calculated into HF consumption results. Error bars obscured by markers in some instances.

Nitric acid consumption

The formula for calculating HNO_3 acid consumption was adapted from Equation 4.1:

$$\text{HNO3 consumption} = \frac{(\text{HNO3 in Feed}) - (\text{HNO3 in Product})}{\text{HNO3 in Feed}} \times 100 \qquad \text{Equation A.2}$$

Three HF solution samples spiked with 1% HNO_3 was sent for analyses IC (Ion chromatography). Spiking analytical grade HNO_3 into 70% Analytical grade HF resulted in the HNO_3 present in solution to be 4634.2 mg/kg.

The three identical samples analysed came back with a variation (4337, 4371 and 5202 mg/kg solution). Therefore the standard deviation was calculated to be ±489.9 mg/kg.

Then the relative standard deviation was calculated as follows:

$$\text{HNO3}_{consumed} = \text{HNO3}_{Feed} - HF_{product}$$

$$\Delta\text{HNO3}_{consumed} = \sqrt{\Delta(\text{HNO3}_{feed})^2 + \Delta(\text{HNO3}_{product})^2}$$

$$\Delta\text{HNO3}_{consumed} = \sqrt{2(\Delta H\text{HNO3}_{measured})^2}$$

$$\Delta\text{HNO3}_{consumed} = \sqrt{2(489.90)^2} = 692.82$$

$$\Delta\text{HNO3}_{consumed} = \sqrt{\left(\frac{692.8}{4634.2}\right)^2 + \left(\frac{489.9}{4634.2}\right)^2} = 0.183$$

Absolute error: $\Delta HNO3_{consumed} = (0.183) \times HNO3_{consumed}$

Example using experimental data:

Random errors associated with analyses of HNO_3 in solution were significantly large (Table A.3) and visible on the bar graphs constructed (Figure A.5). Since the HF concentrations of the samples sent for analyses was so low (≤1% HNO_3), and the method for analysing HNO_3 in concentrated HF solutions (70% HF) at Pelchem Ltd. was not well established, the analyses were not be done with high accuracy and precision. High acid consumptions (>99% HNO_3) implied that the very little HNO_3 (<70 ppm) was detected in the product corrosion solutions which added to the difficulty in analysing such low levels of HNO_3, further impacting the accuracy of analyses.

Table A.3: Percentage HNO_3 consumption with absolute errors – adapted from Table 5.33.

Temp. (ºC)	**0.1% HNO3 spiked in (%)**	**Absolute error (mg/kg)**	**0.5% HNO3 spiked in (%)**	**Absolute error (mg/kg)**	**1% HNO3 spiked in (%)**	**Absolute error (mg/kg)**
0	99.68	18.24	99.14	18.14	99.22	18.16
15	98.54	18.03	99.24	18.16	99.72	18.25
25	98.41	18.01	99.76	18.25	99.95	18.29

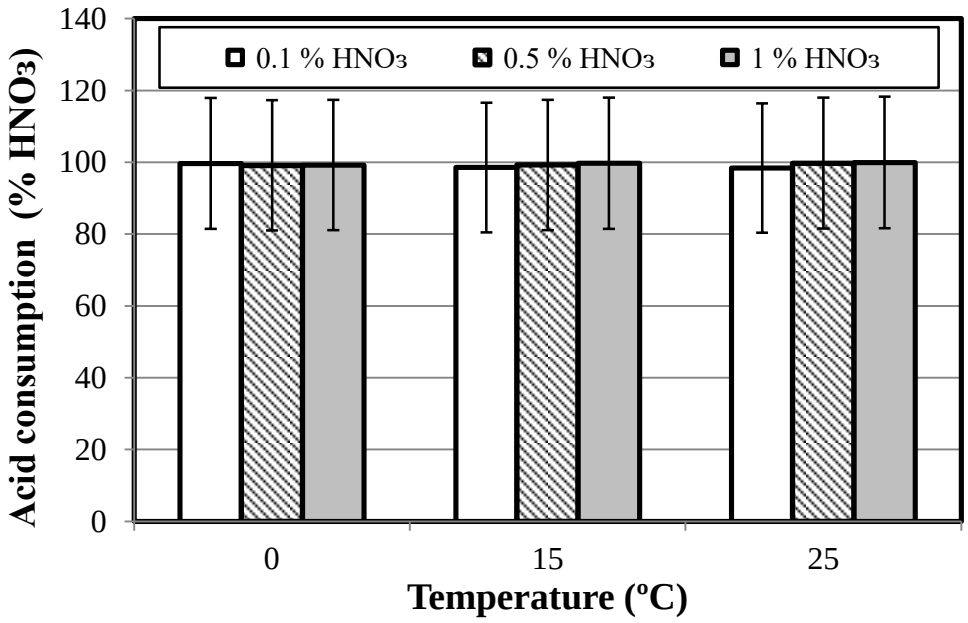

Figure A.5: Adaptation of Figure 5.21, to demonstrate the implementation of errors calculated into HNO_3 consumption results. Error bars obscured by markers in some instances.

APPENDIX B

CONSIDERATIONS FOR COUPON SIZES AND DOSING HYDROFLUORIC ACID CALCULATIONS

Coupon sizes

The dimensions of a typical test coupon, with its exposed surface area are illustrated in the isometric drawing presented in Figure B.1.

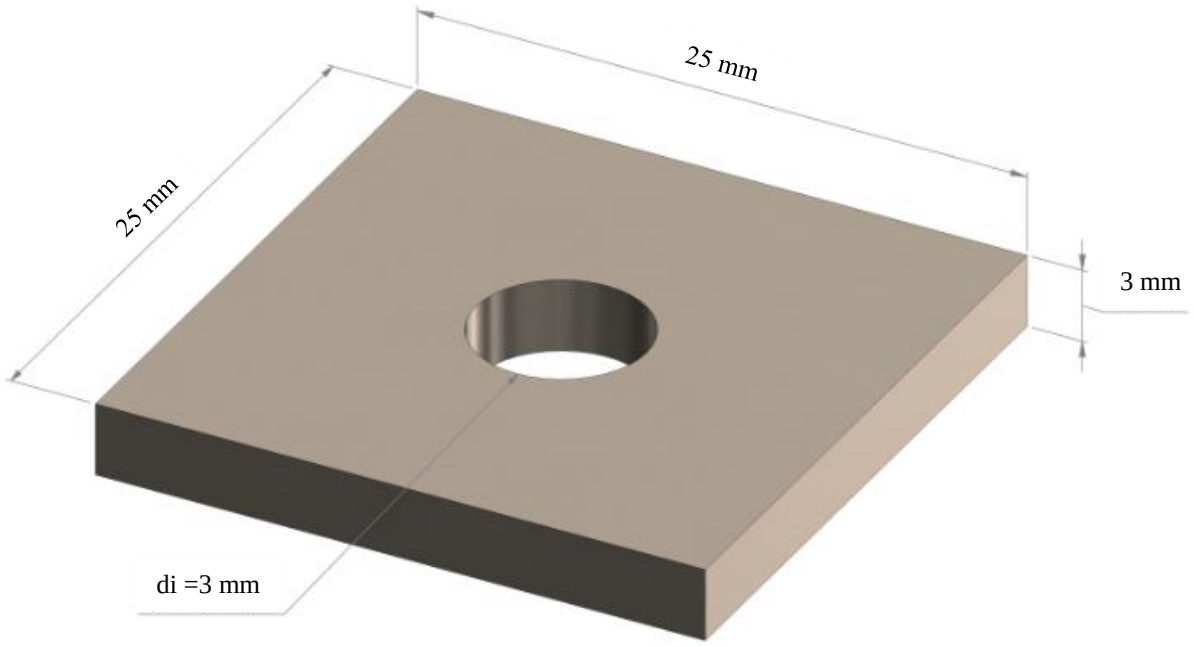

Figure B1: Dimensions of mild steel coupon used in surface area calculations.

Then the exposed surface area of a corrosion coupon was calculated by adding the surface area of a cylinder to the surface area of the front and side surfaces as follow:

(1) Surface area of a cylinder: $2\pi r \times \mathrm{h} = \times 2(\pi \times 3.5) \times 3$ = 65.97 mm^2

(2) Surface area of front faces: $2(l \times \mathrm{b}) - (2\pi r^2) = 2(25 \times 25) - 2(\pi \times 3.5^2)$ = 1173.03 mm^2

(3) Surface area of side faces: $4 \times (l \times \mathrm{b}) = 4 \times (3 \times 25)$ = 300 mm^2

Total coupon surface area: (1) + (2) + (3) = 1539 mm^2

Acid volume per coupon area ratio

The ratio of the solution volume (acid volume) to the coupon area exposed to the corrosion solution during a corrosion experiment was an essential parameter during the planning of an appropriate immersion type corrosion test. Maintaining a ratio equivalent to what was recommended in literature, as well as experienced in industry, within the laboratory set-up enabled the comparison of the corrosion test results to corrosion a larger scale. The volume of acid in a Teflon bottle in contact with coupons suspended in the HF corrosion solution was empirically determined to be 463 ml and hence the solution volume to surface area ratio on a laboratory scale was determined using Equation B.1:

$$\text{Solution volume to surface area ratio} = V/(N \times A_s) \qquad \text{Equation B.1}$$

where A_s = Exposed surface area of an individual test specimen (mm^2), N = the number of test specimens in the experiment and V = Volume of the corrosive solution used in the test vessel (mL) as per (Baboian, 2005). The total surface area of a coupon was determined to be 1539 mm^2, which made it possible to compare its surface area to acid volume in the Teflon bottle to other solution volume to surface area targets specified for corrosion tests as summarized in Table B.1.

Table B.1: Targets solution volume to surface area ratios for laboratory immersion tests.

No.	Source	Solution volume to surface area ratio (mL/mm^2)
1	Book: (Baboian, 2005)	0.30
2	ASTM practice G 31 (ASTM, 2009a)	0.20
3	HF storage tank (calculated)	0.45
4	Laboratory set-up: Coupon in Teflon bottle	0.30

Sources 1 and 2 were from recommendations made in literature, while source 3 was determined from the actual dimensions of the HF storage tanks used on site (A_s), with the solution volume (V) determined from the true measured quantity of HF in contact with the inner mild steel shells of the V1460 and V1461 storage tanks (Figure 3.1a), as measured from the liquid band (Figure 3.4). The solution volume to surface area ratio determined for the laboratory set-up compared well to recommendations made in literature (Baboian, 2005; ASTM, 2009a), but was 1.5 times lower that the acid volume to surface area actually experienced in the HF storage tanks used in industry (Table B.1).

Spiking HNO_3 into HF

Since the density of the 65% analytical grade HNO_3 (1.36 g/ml) and the specific gravity of 70% HF at 25ºC (1.22) was known, the volume of the analytical grade HNO_3 that needed to be pipetted to make up a 1 L stock solution of either 0, 0.1, 0.5 and 1% HNO_3 in 70% HF could be calculated. Since dosing in any volume of HNO_3 (65% HNO_3 and 35% H_2O) into the 70% HF dilutes it, this dilution was also recorded and incorporated into the acid consumption calculations (e.g. Table 5.32). To illustrate the considerations made in contaminating the 70% HF with a known concentration of HNO_3, and then how the HF corrosion solutions were spiked, values for preparing a 1% HNO_3 was provided in Table B.2.

Table B.2: Preparation of a 1 L, 70% HF stock solution spiked with 1% HNO_3.

Preparations	**Values and calculations**
1 L of 65% HNO_3	1360 g
Mass of HNO_3 in 1 L	884000 mg
HNO_3 concentration spike required	1% = 10000 mg/L
HNO_3 volume needed to spike 1 L	884000/10000 = 11.31 mL
65% HNO_3 pipette volume needed	11312 µL
HF volume to add	1000 mL – 11.31 mL = 988.69 mL
Dilution of HF due to spiking	69.21%

APPENDIX C

PUBLICATIONS AND CONFERENCE PROCEEDINGS

There were several publications from this work, which are given below. They were all written by the student with input from the supervisors.

R. van der Merwe, L.A. Cornish and J. van der Merwe, The Effect of Cutting on the Microstructure of Mild Steel for Corrosion Tests, 52nd Microscopy Society of southern Africa Conference Proceedings, Volume 44, p. 91, Stellenbosch, 2nd – 5th December 2014. ISBN 0-620-35056-3

R. van der Merwe, L.A. Cornish and J. Van der Merwe, Corrosion study of mild steel used in storage of fluorine containing acids, Proceedings of the Microscopy Society of Southern Africa Conference, Vol. 45, p. 45, Pretoria, 2nd – 4th December 2015. ISBN 978-0-620-68731-7

R. van der Merwe, L.A. Cornish and J.W. van der Merwe, Safety Risk Assessment for Corrosion Testing in Hydrofluoric Acid, African Journal of Corrosion, 2(1) (2016) 28- 36.

Ryno van der Merwe, Lesley A. Cornish and Josias W. van der Merwe, Corrosion safety risk assessment for testing in hydrofluoric acid, AfriCORR 2016, p. 31, Midrand, 25th – 29th July 2016, which was awarded the Best Student Poster, 28th July 2016.

Ryno van der Merwe, Josias W. van der Merwe, Lesley A. Cornish and E. Snyders, Post mortem corrosion study of mild steel used in storage of fluorine-containing acids, AfriCORR 2016, p. 64, Midrand, 25th – 29th July 2016.

R. van der Merwe, L.A. Cornish and J.W. van der Merwe, Corrosion characteristics of mild steel storage tanks in fluorine-containing acid, J. South African Institute of Mining and Metallurgy, 116 (2016) 921-926.

R. van der Merwe, L.A. Cornish and J.W. van der Merwe, Effect of nitric acid contamination on mild steel corrosion resistance in hydrofluoric acid Microscopy Society of Southern Africa Conference, Vol. 47, p. 21, Bela-Bela, 4th – 7th December 2017.

The following awards were given:

- The Ivan Ogilvie Research Scholarship, Corrosion Institute of South Africa, 17th October 2014, for 2015.
- AfriCORR 2016, Best Student Poster, 28th July 2016.
- Zeiss prize for the paper that uses microscopy to address an industrial problem, MSSA 2017, 8 December 2017.